Formation of Astrophysical Jets

Habilitationsschrift

zur Erlangung des akademischen Grades
Doktor rerum naturalium habilitatus
(Dr. rer. nat. habil.)
in der Wissenschaftsdisziplin Astrophysik

eingereicht an der
Mathematisch-Naturwissenschaftlichen Fakultät
der Universität Potsdam

von
Christian Fendt
geboren am 20. Dezember 1962

Potsdam im Juli 2002

Preface

In this Habilitation Thesis I discuss a selection of my scientific papers published in the years 1996 to 2002 (in *Astronomy & Astrophysics*) exploring the theory of astrophysical jet formation. The spatial region under consideration is the innermost – observationally not resolved – region of the jet origin. As the jet phenomenon is an universal feature observed in a variety of astronomical sources, a discussion should consider all these different astrophysical objects – young stars, microquasars and active galactic nuclei.

The puzzle of (magnetohydrodynamic) jet formation is rather complex and any theoretical approach to it requires certain simplifications. My papers on this topic can be divided into three categories,

- stationary magnetohydrodynamic relativistic jets,
- time-dependent magnetohydrodynamic simulations,
- observationally related theory, parameter studies.

Clearly, such a distinction cannot not be a strict one. Stationary models may used as initial condition for the simulations – and sometimes show up in the end of the long-term time-dependent evolution. Parameter estimates are essential in the case of a model setup which cannot (yet) be treated numerically. As a link between theory and observations this might help us to define proper model constraints for the numerical calculations, but may also prove the outcome of the numerical results. In the end, the long lasting question of astrophysical jet formation can only be answered from a combined effort in all the different approaches.

The research presented in this thesis has been carried out at several scientific institutes, namely the *Landessternwarte Heidelberg*, *Lund Observatory* and the *Astrophysikalisches Institut Potsdam*. I acknowledge the hospitality of all these institutions and the great friendship to some of my colleagues. I also like to thank all my collaborators for their help and support – those who appear as co-authors and also the others remaining probably invisible, but having contributed also a lot as technical and administrative staff.

Formation of astrophysical jets

Abstract

Highly collimated, high velocity streams of hot plasma – the jets – are observed as a general phenomenon being found in a variety of astrophysical objects regarding their size and energy output. Known as jet sources are protostellar objects (T Tauri stars, embedded IR sources), galactic high energy sources ("microquasars"), and active galactic nuclei (extragalactic radio sources and quasars).

Within the last two decades our knowledge regarding the processes involved in astrophysical jet formation has condensed in a kind of *standard model*. This is the scenario of a *magnetohydrodynamically* accelerated and collimated jet stream launched from the innermost part of an accretion disk close to the central object.

Traditionally, the problem of jet formation is divided in two categories. One is the question how to collimate and accelerate an uncollimated low velocity disk wind into a jet. The second is the question how to initiate that outflow from a disk, i.e. how to turn accretion of matter into an ejection as a disk wind. My own work is mainly related to the first question, the collimation and acceleration process.

Due to the complexity of both, the physical processes believed to be responsible for the jet launching and also the spatial configuration of the physical components of the jet source, the enigma of jet formation is not yet completely understood. On the theoretical side, there has been a substantial advancement during the last decade from purely stationary models to time-dependent simulations lead by the vast increase of computer power. Observers, on the other hand, do not yet have the instruments at hand in order to spatially resolve observe the very jet origin.

It can be expected that also the next years will yield a substantial improvement on both tracks of astrophysical research. Three-dimensional magnetohydrodynamic simulations will improve our understanding regarding the jet-disk interrelation and the time-dependent character of jet formation, the generation of the magnetic field in the jet source, and the interaction of the jet with the ambient medium. Another step will be the combination of radiation transfer computations and magnetohydrodynamic simulations providing a direct link to the observations. At the same time, a new generation of telescopes (VLT, NGST) in combination with new instrumental techniques (IR-interferometry) will lead to a "quantum leap" in jet observation, as the resolution will then be sufficient in order to zoom into the innermost region of jet formation.

Contents

Chapter 1
Introduction

Astrophysical jets are defined as highly collimated plasma streams of high velocity. These characteristics are observationally detected as *elongated image* of the outflow feature together with *Doppler shifted* emission lines or the *proper motion* of resolved jet substructures [1]. Jets are observed as a common phenomenon to be found among in rather different astronomical objects concerning their size and energy output – protostars, galactic high energy sources, active galactic nuclei and probably also in gamma ray bursts. Depending on the jet source, the observed jet velocity ranges from several 100 km/s to apparently superluminal speed.

Years of observations and theoretical investigations have lead to a kind of standard model for jet formation. Besides the conventional characteristics of collimation and high velocity, the crucial jet properties can be summarized as follows.

- Astrophysical jets emanate from *accretion disk* sources.
- Astrophysical jets are *magnetized*.
- Astrophysical jets are *huge* – with jet radii up to 1000 times the size of the central object.

The fact that jets are observed in different classes of astrophysical objects is an important constraint for any jet formation model. Certainly, one can suppose that the jet launching mechanism is the same in all these sources. Indeed, most of the theoretical models so far allow for a "scaling" of the parameters in order to apply the model to the different jet sources. Generally speaking, jets originate from the innermost part of a complex scenario consisting of the central body (the "star") and the surrounding accretion disk, coupled by magnetic fields. I like to point out the hypothesis that jets can only be formed when that star-disk-jet system is highly *axisymmetric*. This might explain why other highly magnetized stars surrounded by accretion disks as cataclysmic variables or some neutron stars do *not* have jets. The essential aspects involved in the jet formation mechanism can be summarized as follows.

[1] I suggest that both characteristic features – collimation *and* velocity – must be observationally indicated in order to announce a certain object as a jet

- A sufficiently strong *magnetic field* is provided by the "star"-disk system (either generated by a dynamo process or advected by the accretion disk).
- The "star"-disk system also drives an *electric current*.
- The material *accreted* within the disk is lifted from the disk surface, couples to the magnetic field and becomes ejected as a wind.
- The disk wind is initially accelerated *magneto-centrifugally*. *accelerated magnetically*, i.e. by conversion of Poynting flux to kinetic energy.
- Inertial forces in the wind flow will "bend" the poloidal magnetic field (i.e. the field along the meridional plane including the jet axis) in toroidal direction.
- The existence of a toroidal magnetic field component leads to Lorentz forces which further accelerate the wind and eventually collimate the flow into the narrow beam of a jet.
- The plasma velocity subsequently exceeds the speed of the magnetosonic waves. In the fast magnetosonic regime the flow is causally decoupled from outer boundary conditions.
- Where the jet meets the interstellar medium (ISM), a *shock* develops, thermalizing the jet energy. Also, the electric current is closed via the bow shock, and the jet net current returns to the source of the current via the ISM.

Although this scenario is accepted nowadays as the general picture of astrophysical jet formation, there are still many open questions which have not yet been able to proof theoretically as well as observationally.

The main difficulty concerning a theoretical approach is the fact that the presence of magnetic forces does not allow for a simple one-dimensional treatment of the equations (as e.g. for the case when only gravity and gas pressure would be important). Further, the complex geometry of the jet source consists of three rather different components – the (small) central body, the surrounding accretion disk and the jet itself – all connected by the magnetic field. The huge size of the jets compared to the central source does not allow for numerical simulations on the global scale together with, at the same time, considering also the inner region of jet formation with the required numerical resolution. With a stationary approach such a global treatment becomes feasible. However, other technical difficulties arise and all stationary solutions published so far rely on far-reaching simplifications as e.g. self-similarity, force-freeness or other. Obviously, they cannot explain any time-variable behavior.

As it is the accretion disk which is most probably the ultimate source of the jet, it would be desirable to consider also the disk evolution for the treatment of jet formation. However, since the time scales and physical properties in disk and jet are too different, a combined numerical treatment is not yet possible to do.

In this thesis I will summarize what I believe are the most important steps towards the current understanding of astrophysical jets. In particular, I will only discuss the issue of

jet *formation* – the acceleration of matter and the collimation of the mass flow. It is, of course, not possible to cover all topics which come along with the subject of astrophysical jets. Even for the specific subject of jet formation itself, a wealth of literature is waiting. There are observational and theoretical papers for various classes of objects and also for certain specific sources them self. I will not discuss the issue of radiation mechanisms in jets – shock models, forbidden line emission, radiation transport, synchrotron emission, Compton scattering, etc. These processes are expected to be not important for the jet dynamics in region close to the source (although there are probably important for the interpretation of the observed data). Nor will I discuss the problem of jet stability which is related to the already evolved, "asymptotic" region of the jet, i.e. for the already collimated and accelerated flow far away from its source. The presence of an accretion disk seems to be the fundamental ingredient for jet formation. However, this subject is an even more extensive topic in the literature and I will only discuss such work which is closely related to the jet formation. Not much is known about the interaction between the jet and the disk – the launching mechanism of the time-dependent jet ejection. It might well be that the final answer to the question of jet formation will come from accretion disk theory. The topic of this thesis, however, is the structure and evolution of the initial, collimating jet flow itself.

Chapter 2
Jet history – the early years

2.1 M87 – the first jet source detected

The first hint ever on an astrophysical jet has been reported in 1918. Observing the galaxy M87[1] among "*762 Nebulae and Clusters, photographed with the Crossley reflector*", H.D. Curtis (1918) recorded that a

> "*a curious straight ray lies in a gap in the nebulosity in p.a. 20deg, apparently connected with the nucleus by a thin line of matter. The ray is brightest at its inner end, which is 11″ from the nucleus....*".

This discovery remained somewhat un-noticed until the mid-1950s when Baade & Minkowski (1954a,b) identified M87 as the optical counterpart of a strong radio source. In their paper they mention "*several strong condensations in the outer part of the jet*" (see Fig. 2.1). Taking into account also the spectra observed by Humason, Baade and Minkowski delivered the correct interpretation of that jet feature:

[1] M87 = NGC 4486 = Vir A

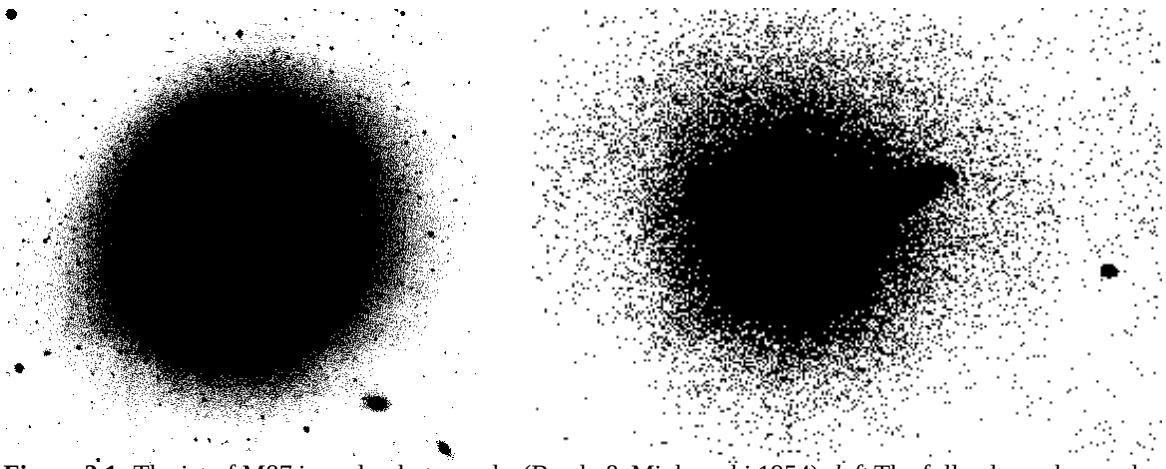

Figure 2.1. The jet of M87 in early photographs (Baade & Minkowski 1954). *left* The full galaxy observed in the $\lambda\lambda$ 3600-5000 band. The size of the saturated region is about $2'.2$. *right* The center of the galaxy observed in the UV ($\lambda < 4000$). The size of the saturated region is about $17''$. The jet extends about $20''$ from the center and has a width of about $2''$ ($\equiv 30$ pc). The scale of this picture is 3 times lower compared to the left picture.

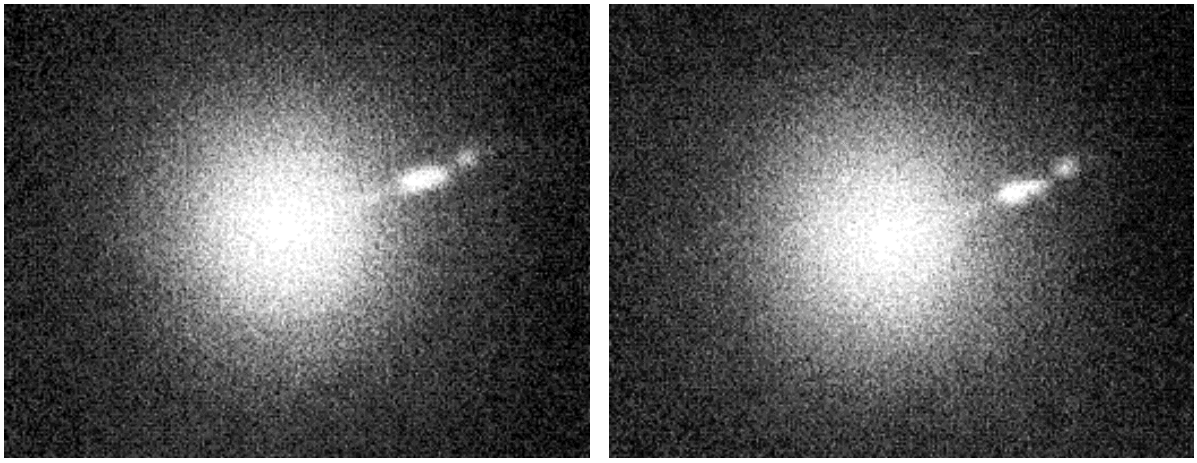

Figure 2.2. Optical polarization of the M87 jet. Two exposures with maximum transmission of the electric vector in 200° (left) and 290° (right) clearly indicating the polarization. Three strong condensations at the end of the jet can be identified (Baade 1956).

> "*The interpretation which suggests itself is that the jet was formed by ejection from the nucleus and that the [O II] line is emitted by a part of the material which forms the jet and is still very close to, if not still inside the nucleus.* "

Based on ad-hoc assumptions about the jet inclination and velocity they estimated period of jet formation of about 10^6 years. Although they give a correct interpretation of their data, at the same time they admit that

> "*no possibility exists at this time of forming any hypothesis on the formation of the jet, the physical state of its material, and the mechanism which connects the existence of the jet with the observed radio emission.* "

Baade and Minkowski were also the first who called this "*unique peculiarity*" a ***jet***, a term which has been adopted for this kind of phenomenon ever since.

Besides the interpretation of the M87 feature as a jet, the Baade and Minkowski discovery of optical counterparts of radio sources can also be considered as a big step towards what is nowadays known as the "unified model" for active galactic nuclei (Sanders et al. 1989). In fact, the identification made clear that most of the observed "radio stars" were actually radio *galaxies* with radio luminosities 10 to 10^6 times greater than that of the Milky Way (see Moffet 1966).

The next important observational discovery came with polarization measurements. It was Baade (1956) who detected optical polarization in the M87 jet resolving the inner jet in three separate condensations differing partly in the polarization angle (Fig. 2.2). The degree of polarization was estimated to about 30%. The interpretation of the polarized emission was *synchrotron radiation* (correctly, as we know today), as suggested by observations of the Crab Nebula together with a new theoretical understanding of the origin of the radio emission as synchrotron radiation from energetic electrons (Shklovskii 1953a,b). Presumably, Baade's detection of polarization was the very first hint on the *magnetic character of astrophysical jets*. Later observations by Hiltner (1959) presenting

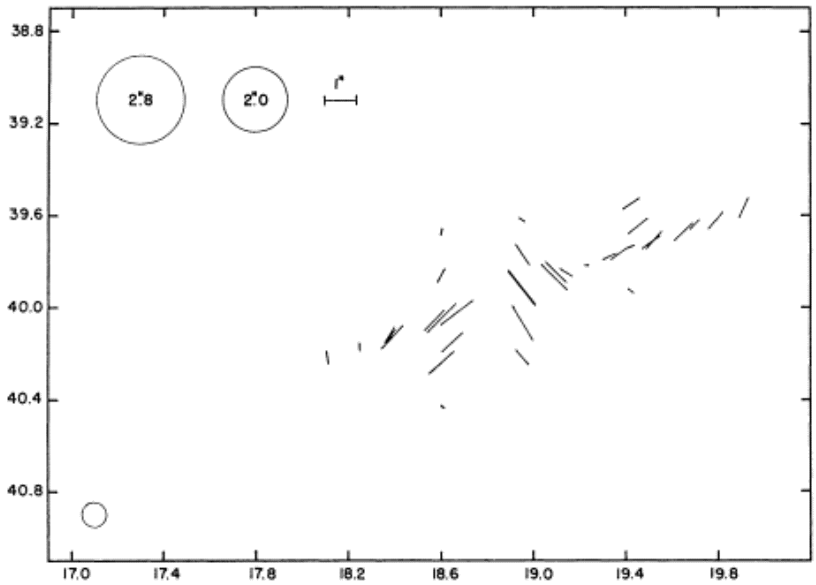

Figure 2.3. Optical polarization of the M87 jet. Map of optical polarization vectors obtained by photo electric observations. The M87 nucleus is located at the small open circle in the lower left corner (Hiltner 1959).

detailed polarization vector maps of the M87 jet (Fig. 2.3) confirmed these results. Hiltner concluded that "*no significant polarization was observed in M87 except in the jet*".

A first detailed theoretical treatment of the observed synchrotron radiation was made by Burbidge (1956) based on Baade's observations. He estimated a total jet energy in particles and magnetic field of about 10^{57}erg for a field strength of about 10^{-3} G. To explain such a "*tremendous amount of energy*" (Burbidge) involved in the jet motion was not a simple task. Burbidge argued that the potential energy of a galactic mass is about 10^{59} erg. Other preliminary ideas were supernova outbursts (a number of 10^7 required), collisions between globular clusters or even processes involving antimatter.

The model of Piddington (1964) discussed the presence of radio galaxies in the framework of a *unified galaxy formation* scenario. The basic idea is that the inclination between the galaxy rotation axis and the magnetic field axis is the key parameter for the evolution of the galaxies in different classes. Nowadays, such a model hypothesis can be ruled out. On the other hand, the sketch of the Piddington model looks remarkably similar to the modern scenario of jet formation (Blandford & Payne 1982).

X-ray emission from M87 jet was discovered by Byram et. al (1966) and Bradt et al. (1967). The latter also report a non-detection of X-ray emission from 3C 273, which is now known as another famous jet source.

Felten and co-workers (Felten 1968, Felten et al. 1970) investigated the physical properties in the M87 jet giving estimates on the jet density and magnetic field. The conclusion was that if the electrons responsible for the optical emission are produced at the nucleus and escape out to the end of the jet, the ambient plasma must also move with about the speed of light. However, local re-acceleration of electrons remained possible but the necessary theories were lacking, as Fermi acceleration seemed to be unlikely. If

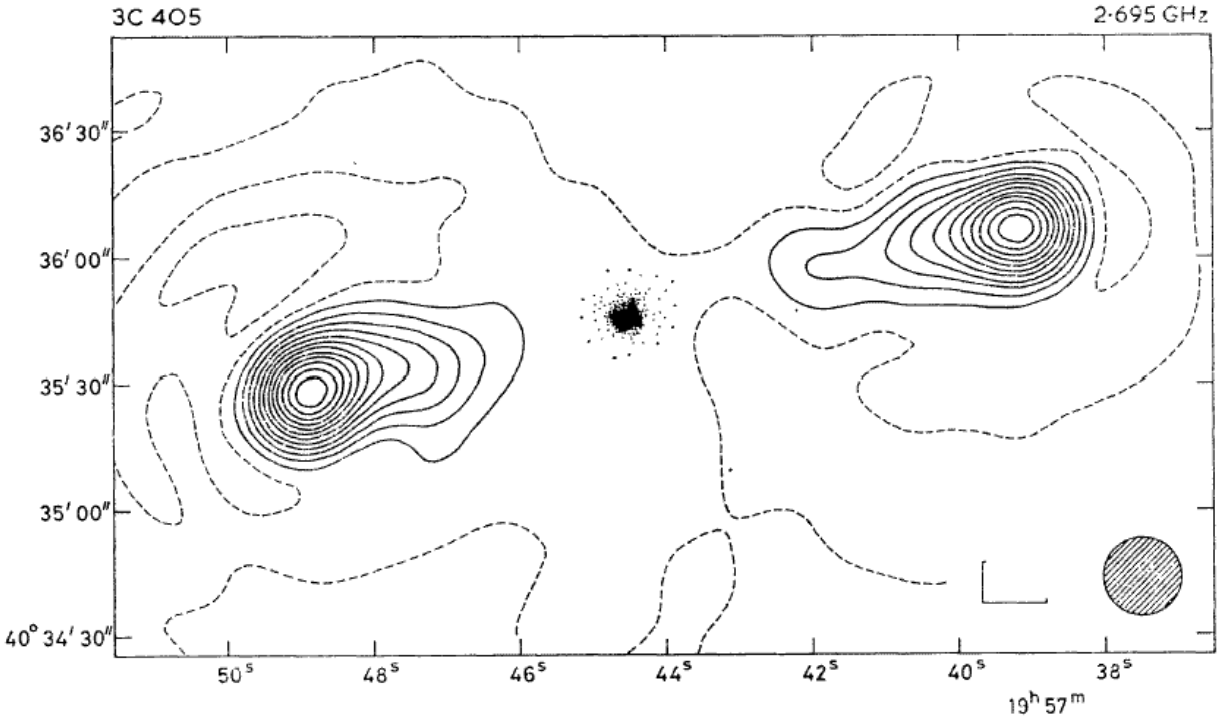

Figure 2.4. The radio double source 3C 405 (Cygnus A) observed by Mitton & Ryle (1969) at 2.696 GHz. The 'L' shape symbol indicates the compression of the scale in declination, and measures $10''$ for both arms.

heating by cosmic ray protons confined to the optical knots is considered as alternative, these knots, which have a time scale of about 10^5 years, should contain a large mass of $\sim 3 \times 10^7 \mathrm{M}_\odot$ wnd a particle density of about $400\,\mathrm{cm}^{-3}$ to maintain themselves against disruption by the cosmic ray pressure. A first analysis of the jet stability and confinement was given by e.g. Okoye (1973). The available observational data, however, did not allow for an unique desription of the M87 stability conditions. Thus, the optical knots may be either stabilized by their inertia or by an external medium, depending on the physical parameters of the jet.

2.2 Radio galaxies and radio lobes

In that time the M87 jet was still a unique astrophysical feature with no other "jets" observed and investigated to that extend.

A big step towards a more general picture of astrophysical jets came from observations of radio galaxies, being routinely observed since the beginning of the 50ies. In general, many of the observed sources showed a typical double lobe structure like 3C 452 (Ryle et al. 1965b) or the beautiful example of Cyg A (Fig. 2.4, Mitton & Ryle 1969). The first detection of radio emission from a *jet* has been reported by Schmidt (1963) who identified

"a star of about thirteenth magnitude and a faint wisp or jet"

near the position of the radio source 3C 273 (Hazard et al. 1963). Hogg et al. (1969) showed that a compact radio source at some distance from 3C 274 coincides with the brightest knot in the optical jet of M87 indicating that the radio emission comes directly from the optical feature. The first direct evidence for a radio jet in a powerful double radio source came by the observation of an "abbreviated jet" in the radio galaxy 3C 219 (Turland 1975).

Along with the discovery of radio galaxies and radio lobes came the detection of apparent superluminal motion in these sources. Cohen et al. (1971) find that the expansion rate of the brightness distribution in 3C 273 and 3C 279 is 2 and 3 times the speed of light, respectively. They called such a behavior a "*super-light expansion*", actually confirming confirmed earlier measurements by Gubbay et al. (1969), Moffet et al. (1971), Knight et al. (1971) and Whitney et al. (1971). These results fit also fits into the picture of a rapid radio variability of 3C 273 (Dent 1965) and the subsequent theoretical interpretation as a relativistic (superluminal) expansion (Rees 1966, 1967). Another superluminal source discovered in these years is 3C 120 with $v/c \simeq 2 - 3$ (Shaffer et al. 1972).

Finally, one must at least mention the very first ideas towards the modern "unified model" for active galactic nuclei by Gold (1967) who speculated that the extragalactic radio sources observed so far might be basically of one type, where quasi-stellar objects (QSO) just represent an "active phase" (Gold) in the life of radio galaxies.

2.3 A theoretical breakthrough – the model of Blandford & Rees

Motivated by the observational finding that the powerful extragalactic double radio sources are most probably fed continuously from the nuclear region of huge galaxies, Blandford & Rees (1974) suggested a scenario where the

> "*energy is supplied by a light fluid – composed of fast (possibly relativistic) particles, perhaps pervaded by electromagnetic fields – which is generated in the nuclear region and collimates into two oppositely directed beams..*".

This model – the so-called "twin-exhaust' model – describes how (i) the stream of particles, which flows within a channel bored into the interstellar medium surrounding the galactic nucleus, becomes accelerated to supersonic speed and collimated into a narrow beam by the action of a *de Laval* nozzle, and how (ii) the bulk energy of the beam is converted into radiation when it hits the interstellar medium.

The basic idea can be summarized as follows. In the center of the galactic nucleus a hot outflow is initiated. This process is not further specified and its details are not of great importance for the model. The only requirement is that the central active region is able to provide the power for at least $10^6 - 10^7$ years and is smaller than about 10 pc. The stream of particles is embedded in a cool gas cloud with decreasing gas pressure (with distance from the center). The stream is in pressure equilibrium with the surrounding gas and collimated by the external pressure. Therefore, the cross-section of the initially un-collimated flow decreases. At the same time the flow becomes accelerated. At the sonic point, the

location where the flow velocity equals the sound speed, a hydrodynamic "nozzle" forms[2] (see Fig. 2.5). After leaving the nozzle (i.e. after passing the sonic point) the stream propagates in a ballistic manner with supersonic speed and with a radius comparable to the minimum radius of the nozzle, $r_{\rm nz}$. The "jet radius" is about

$$r \simeq 0.6\,\gamma\,r_{\rm nz} \simeq 0.6(P_0/P)^{1/4} r_{\rm nz}$$

with the bulk flow Lorentz factor γ, and the gas pressure P of the ambient cloud normalized to its value at the nozzle. This is indicating a weak opening of the flow channel even if the external pressure may decrease drastically.

The head of the beam advances into the intergalactic medium and a shock will occur. At this "working surface" the kinetic energy of the flow is "randomized", i.e. converted into random energy with no traces left of the original energy distribution in the flow. The processes involved could be manifold. Adiabatic or radiative losses will randomize the flow energy giving rise to synchrotron emission in radio wavelength. A "strong" shock may accelerate relativistic particles to ultra-relativistic velocities. Some stochastic acceleration mechanism (e.g. Fermi acceleration) may change the energy distribution into a power law.

For the observed radio luminosity of Cyg A, Blandford & Rees estimated that the central engine must have maintained a power output of $\simeq 5 \times 10^{45}\,{\rm erg\,s^{-1}}$ for about 10^7 years. Collimation would have been occurred if the gas around the nucleus has a temperature of 3×10^8K, a central density of $300\,{\rm cm^{-3}}$. The collimation distance would be $\simeq 220$ pc with a minimum radius of the nozzle of about 10 pc. The beam diameter close to the working surface is about 1 - 3 kpc. The estimated Lorentz factor of the particles in the Cyg A jets is about 3.

So far, the "twin-exhaust" model is still up-to-date. Modifications were added in order to establish a *complete* self-consistent scenario of extragalactic jets. I just mention the ideas to generate the initial jet flow as a leptonic plasma driven electrodynamically by the black hole rotation (Blandford & Znajek 1977), or as a self-collimating magnetized disk wind (Blandford & Payne 1982, see below). The modern *unified model* of *active galactic nuclei* explains the observational appearance of "different" kinds of active galactic nuclei (AGN) as incarnations of just the same intrinsic setup which mainly depend on the viewing angle and the age of the object (see Blandford 1990).

2.4 A relativistic stellar jet – SS 433

Till the late 70ies the only jet sources known so far were the extragalactic jets observed in radio galaxies or other active galaxies, among them M87 and 3C 273.

Then, a new area started when Milgrom (1979) and Margon et al. (1979a,b) detected time-dependent shifts of emission lines in the emission line star SS 433[3]. The "*bizarre spectral features*" of this "*unusual object*" (Margon et al. 1979a) were soon interpreted as

[2] Such a scenario is similar to the physics of jet engines in an aircraft except the fact that in that case the size of the nozzle is fixed, while in the Blandford&Rees exhaust model the interface between outflow and ambient medium is adjusted by the pressure equilibrium.

[3] SS = Stephenson-Sanduleak

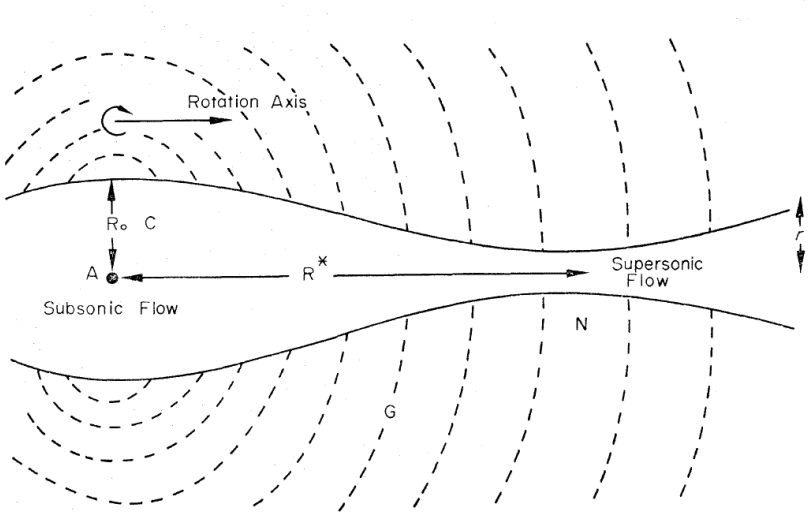

Figure 2.5. The model of Blandford & Rees (1974) – a "twin-exhaust" engine.

Doppler shifted lines and related to a physical configuration consisting of "*two regions, symmetrically situated about a central object with velocities equal in absolute value and opposite in sign* (Milgrom 1979). Three broad emission line features seen in green, red and infrared colors vary strongly in intensity, profile and frequency in an – apparently – aperiodic manner. In the beginning, these peculiar lines were not immediately identified and, at the very early stage of observation, the nature of the object was completely unknown.

Later, Margon et al. (1979b) identified these lines with two sets of Doppler shifted Balmer and He I emission. The derived velocities were found to vary cyclically repeating in both the blue shifted and the red shifted systems with a period of 164 days. The velocities reach maximum values of about $+50\,000$ km/s and $-35\,000$ km/s, respectively (see also Liebert et al. 1979).

Fabian & Rees (1979) proposed a double-jet scenario for SS 433. The model explains the origin of the emission lines in cool knots accelerated in the jet and counter-jet. The jet beam itself was considered to be steady in time or variable in velocity. Both possibilities could have been verified with better spectra. The authors further mention the point that the derived velocities are high enough to render the *transverse* Doppler effect significantly. Martin & Rees (1979) further developed the jet model for SS 433. The jet source should now be located in a binary system, giving rise to precession of the jets with a period of 160 days. Although they proposed a central black hole as jet source (which is not the case), the idea of precession is the key point to what nowadays is accepted as the standard kinematic model of SS 433.

Many other publications followed and already two years after the discovery of the "bizarre features", the SS 433 jets were very well investigated, now being even considered "*as a prototype of astrophysical jets*" (Davidson & McCray 1980). Indeed, the fact that this source is much closer to the observer compared to extragalactic jets and that, due to the scaled down size and energy output, the time-scales of the system is much shorter, made SS 433 the favorite source in order to investigate the process of astrophysical jet

formation. For a more detailed discussion, I refer to the review papers by Margon (1984) and Eikenberry et al. (2001).

Some other interesting points concerning SS 433 should be mentioned. That is (i) the fact that, as we know today, the jets of SS 433 originate in an accretion disk, similar to the jets from AGN and protostars, (ii) that, on the other hand, SS 433 seems to be unique among the jet sources as it is part of a binary system, and (iii) it is yet the only known jet source where the central object is a neutron star. All these aspects impose important constraints for the theory of jet formation.

2.5 Protostellar jets and Herbig-Haro objects

After SS 433 has been established as a jet source, this *unique example* of a stellar jet, together with the numerous class of jets from the nuclei of active galaxies remained the only known sample of astrophysical jet sources for a couple of years. Jets were then known as relativistic high energy phenomena, most probably caused by the presence of a collapsed object and an accretion disk. A new point of view came up with the discovery of jets originating in young stellar objects (YSOs) observed in our Galaxy.

The first examples of protostellar jets have been discovered by Mundt & Fried (1983) when observing the close environment of T Tauri stars in the forbidden line emission. They resolved an elongated feature extending from the young star DG Tau and other T Tauri stars (see Fig. 2.6). With other observations following this discovery, the number of jet sources drastically increased. Moreover, a *new class* of jet sources has been established on a completely different energy scale.

The essential point recognized especially from stellar jet detections is the fact that stellar jets are observed only from *accretion disk* sources. If the jet source itself is visible (which is not the case fro e.g. embedded infrared sources), it always shows also the signature of an accretion disk. In particular, jets are observed only from classical T Tauri stars, not from their disk-less brothers, the weak line T Tauri stars.

Forbidden line emission (eg. the lines [SII], [OII], [OIII] or [NII]) has been known already as signature of stellar winds. In particular, Appenzeller et al. (1983) applied this technique to investigate the geometry of winds in T Tauri stars. What they found were only blue shifted emission line components and no red shifted emission. This could be explained by the presence of an *accretion disk* around these stars, absorbing the red shifted lines emitted by the wind “behind” the star.

Substantial insight in the protostellar jets came from observations of Herbig Haro (HH) objects. It was found that many Herbig Haro objects are actually parts of jets. Some of the HH objects are aligned over some parsecs tracing the jet motion, others represent just the head of the jet. The idea is that a HH object may be a signature of shocked gas resulting from interaction of a jet with its ambient medium or from internal shocks within the jet. In both cases, the shocks give rise to forbidden emission lines. Today, many of the extended jet sources are just named as HH objects – among them the most well known being HH 30, HH 34, HH 212 (see Fig. 2.6).

The presence of magnetics field in young stellar objects is indicated only indirectly. Early Zeeman measurements gave only upper limits for magnetic field strengths in T Tauri

stars (Brown & Landstreet 1983, Johnstone & Penston 1986, 1987). On the other hand, the strong X-ray luminosity (related to the coronal magnetic field) of T Tauri stars together with their relatively slow rotation (in comparison with the magnetic field via the dynamo mechanism) implies an enhanced magnetic activity (Bouvier 1990). In the same direction goes the detection of flare activity in the radio band of some young stars which can be fitted by a $100 - 2000$ G dipolar field structure with an radio emitting size of ~ 5 stellar radii (André et al. 1988, 1991, Bieging & Cohen 1989).

Also, the presence of cold stellar spots on T Tauri stars and their derived large size indicate a enhanced magnetic activity (Bouvier et al. 1993). Recent Zeeman observations (Günther et al. 1999) support this scenario of a magnetized T Tauri star. Direct indication for a protostellar jet magnetic field comes from circularly polarized radio emission observed as elongated structure extending from the jet source T Tauri S (Ray et al. 1997). The derived field strength of about 1 G is much higher than a dipolar stellar field at this distance ($B \sim r^{-3}$). However, the derived field strength is also much above the theoretically expected value for a jet magnetic field of about μG to mG fields. On the other hand, the observations clearly show that large-scale magnetic fields with substantial strength must be present around that object.

The observational characteristics of protostellar jets can be summarized as follows. Jets from YSOs typically show a *"knotty" structure* with knots of emission aligned along the jet axis. These knots are interpreted as *shocks* – internal shocks in the jet flow or shocks arising from the interaction with the ambient medium. The emission from the knots is found predominantly *in forbidden emission* lines or H_α. Many jet knots are spatially resolved indicating a jet diameter of about 100 AU. Many jets show *perfect collimation*, even to a distance of about 2 pc from the central source. Typically, the jet flow terminates in a *bow shock*, often connected to the Herbig-Haro objects. In many cases, only one jet can be seen while the signature of a counter jet is missing. The *jet velocity* derived from the Doppler shifted emission lines proper motion measurements is about 300-500 km/s. Protostellar jets are heavy enough to drive massive molecular outflows. The region of jet formation in YSOs is magnetized. A direct indication for a protostellar jet magnetic field is shown only for one example so far. Protostellar jets originate in young stellar objects which also have a surrounding accretion disk. They are observed in classical T Tauri stars and not in weak line T Tauri stars.

If it is correct that all astrophysical jets are generated by the same process, then the presence of protostellar jets tells us that relativity cannot be the essential ingredient for jet formation (as maybe thought previously when only relativistic jet sources were known). Indeed, the present jet formation theory assumes the same principal scenario for all astrophysical jet sources and the results of the numerical calculation may just be scaled according to the mass of the central object.

Due to their proximity, protostellar jets are an ideal target to investigate innermost part the jet formation region. With the availability of optical and IR interferometric devices the resolution required to zoom into the jet formation region will become feasible.

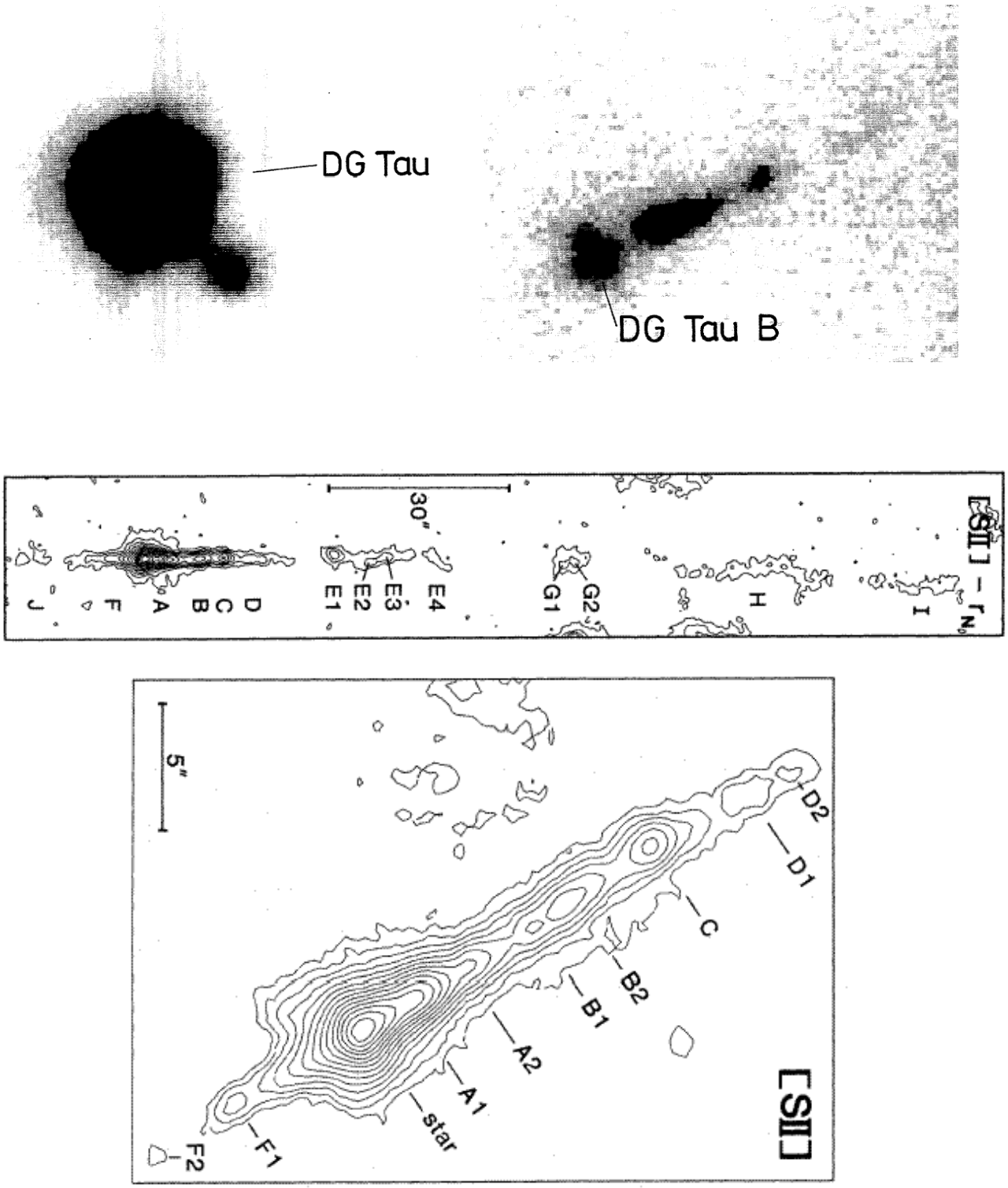

Figure 2.6. The discovery of protostellar jets. *Above:* Two T Tauri stars as jet sources. DG Tauri with its "micro jet" and DG Tau B showing an extended jet feature (Mundt & Fried 1983). *Middle* and *below:* The jet HH30, extending perfectly collimated over more than 2 pc. Note the slight bending of the jet in the upper picture. The lower picture shows the inner part of the jet with higher resolution (Mundt et al. 1990).

2.6 Microquasars

I conclude this introduction to the "history" of astrophysical jets with only briefly mentioning the class of microquasars. Essentially, these are sources of *superluminal* motion located within our Galaxy (Mirabel & Rodriguez 1994, 1999; Tingay et al. 1995). The current understanding is that Galactic relativistic jets emanate from high energy sources like high mass X-ray binaries with a black hole as a central object.

As for the other jet sources, there exists clear observational evidence for the existence of an accretion disk. So far, the observed superluminal radio blobs indicate that a magnetic field is also present.

Thus, the astrophysical scenario is similar to other jets, in particular to the (semi-)relativistic case of SS 433. Consequently, SS 433, once representing the unique class of a stellar jet, is now considered to be a small-scale version of a microquasar. As typical jet velocity one observes 0.9 c - 0.95 c (Mirabel & Rodriguez 1999). A recent measurement of the central mass in GRS 1915+105 gives 14 ± 4 solar masses (Greiner et al. 2001). Interestingly, if one assumes symmetry between jet and counter jet, the derived Doppler boosting enables us to determine the *distance* to the source. For the example of GRS 1915+105 Mirabel & Rodriguez (1994) obtain a distance of about 12 kpc.

Microquasars are of particular importance as they are supposed to undergo similar physical processes as quasars (AGN), but, due to the lower central mass, on a much shorter time scale. This provides a great advantage concerning the observational access to these processes.

Chapter 3
The model of magnetically driven jets

Observations of astrophysical jet sources have established the general idea that the formation of jets is connected to the presence of an accretion disk and strong magnetic fields. This holds for various scales of energy output, jet velocity and spatial scale of the jet – jets are ejected from AGN, Galactic high energy sources, and protostars (see Zensus et al. 1995; Mirabel & Rodriguez 1995; Mundt et al. 1990; Ray et al. 1996). Astrophysical jets are believed to originate very close to the central object in the interaction region with the accretion disk. Beside observational arguments also theoretical considerations have shown that magnetic fields must play an important role in jet formation and propagation (Blandford & Payne 1982; Pudritz & Norman 1983, 1986; Shibata & Uchida 1985; Sakurai 1985; Camenzind 1986, 1987; Lovelace et al. 1991).

In case of extragalactic jets the presence of magnetic fields is rather obvious. Polarized synchrotron emission at radio wavelengths (in radio galaxies) but also in the optical band (see the example of M87) give direct evidence for magnetic fields. Many observations deal with the *asymptotic* jet, the already accelerated and collimated plasma beam on kpc-scale and its interaction with the ambient interstellar (or intergalactic) medium. Yet, the region of the very jet origin can hardly be resolved observationally, although radio interferometry may resolve the mas scale equivalent to some pc (Cyg A, Krichbaum et al. 1998) depending on the distance of the source. An exceptional case is (again...) M 87 where the resolution achieved is fractions of mas corresponding to about 30 Schwarzschild radii of a $3 \times 10^9 \mathrm{M}_\odot$ central black hole (Junor et al. 1999). Another interesting (and again exceptional) example is the accretion disk in NGC 4258 where VLBI water maser observations find (i) direct evidence for a cool and thin Keplerian disk between 0.13 and 0.26 pc (Miyoshi et al. 1995) and (ii) also a disk magnetic field strength in the toroidal component of less then 300 mG (Herrnstein et al. 1998). Besides this information, any further clues about magnetic field structure and field strength in this area is in general provided by theoretical estimates and models.

Indication for a magnetic character of stellar jets is rather indirect. The "standard model" of protostellar jet formation is the scenario of a central protostar carrying a dipolar magnetic field of kG strength surrounded by an accretion disk launching the jet. However, as a fact, the observational proof for such a field distribution is not very strong and convincing arguments are risen against such a scenario (Safier 1998, 1999). Theoretical investigations based on this standard model for young stellar objects has been performed by Camenzind (1990) and co-workers (Fendt et al. 1995, Paatz & Camenzind 1996) and

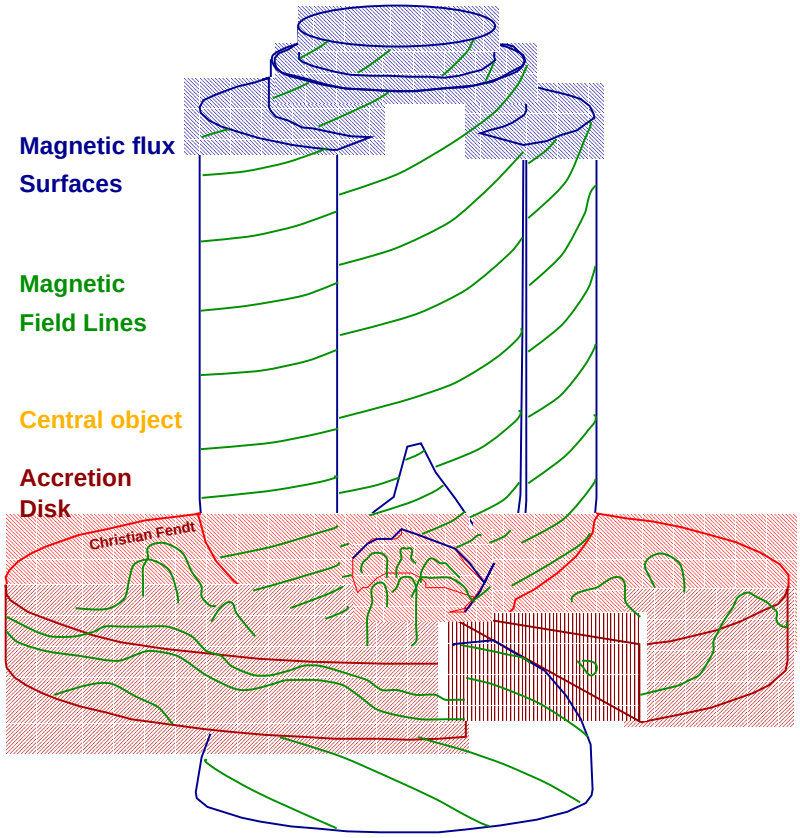

Figure 3.1. Model of a magnetohydrodynamic jet. The jet is launched from the accretion disk surrounding a central object – which can be a young star for protostellar jets, a stellar mass or a super massive black hole for relativistic jets in the Galaxy or AGN, respectively. The jet flow consists of axisymmetric magnetic flux surfaces defined by layers of helical magnetic field lines. The matter flows along these surfaces. The initial disk wind is launched from by magnetohydrodynamic effects and then accelerated magneto-centrifugally in almost radial direction. Magnetic tension of the toroidal magnetic field component which is induced by inertial forces of the matter leads to a collimation of the stream. The Lorentz force may accelerate the matter even further.

Shu and co-workers (1994, 1995).

However, despite the uncertainties with the structure of the central region in protostars and AGN it can be shown that neither radiative nor thermal forces are able to power the jets. So far, only magnetic forces remain as a driver for astrophysical jets, a scenario which is comparable to the well understood solar wind. Theoretical investigations have also shown that strong magnetic fields may easily accelerate the matter to relativistic velocities (Michel 1969, Fendt & Camenzind 1996), with the flow magnetization as the chief parameter determining the jet velocity.

Therefore, the main task for the theoretical modeling is “just” to solve the magnetohydrodynamic (MHD) equations with appropriate astrophysical boundary conditions – i.e. for a model scenario of the three components central object, accretion disk and jet, interacting with each other and being connected by a magnetic field. Traditionally, the approach to the problem of jet formation and propagation is disentangled in the following

sub-problems where each of these subjects are treated *separately*.

- The question how to **collimate** and **accelerate** an uncollimated low velocity disk wind into a jet (which is the topic of this thesis).
- The question how to launch that outflow from a disk, i.e. how to turn **accretion** of matter **ejection** into the disk wind.
- The question how to **generate** the **magnetic field** responsible for jet formation. Is it that magnetic field a disk field or the field of the central object? Is it dynamo-generated within the disk or advected from the ambient medium?
- The question of **stability** of the asymptotic jet and **radiation** processes.

It seems to be obvious that these processes, which play their role at different spatial locations in the jet system, are interrelated and not independent. However, due to the complexity of both the governing magnetohydrodynamic equations and the geometry of the jet source, a general solution taking into account such an interaction is not yet feasible. The main reason for the separate approach is just the necessity of simplification (coming along with a further simplified treatment of the single problems ...).

As discussed above, the current understanding of astrophysical jets is that of a stream of plasma which is accelerated and collimated by magnetic forces and which is launched within the innermost region around a central object surrounded by an accretion disk (Fig. 3.1). The general believe is that the basic mechanism of jet formation is the same in all jet sources, i.e. it is the same for relativistic and non-relativistic jets. These ideas – which I will call the *standard* model of jet formation – result from decades of observations and theoretical investigations.

Before I summarize the relevant equations and the present status of the jet formation theory in the next chapters, I will now discuss the principal features of magnetic jet formation with elementary examples. While the mathematical and numerical formalism of MHD is quite complex, and, yet, impossible to solve in general, the basic processes can be explained simply. For example, some characteristic properties of MHD jets can be derived just by manipulating the expression for the Lorentz force $\vec{F}_{\rm L}$.

3.1 Ideal MHD and magnetic flux surfaces

The very first point to stress is the fact that we are dealing with a *MHD model*. That means that the matter is treated as a single fluid (or gas) with *averaged* properties of the particles species (e.g. ions and electrons)[1]. As for a two-component plasma, also the MHD fluid is *neutral* with the Coulomb forces canceling on small scale. Thus, in MHD we do not deal with the behavior of single particles, but treat the interaction of ionized, neutral "gas clouds" with the magnetic field.

[1]For example, the mass velocity is the mean value of the ion velocity times the ion particle density and the electron velocity times the ion particle density, and similar for the mass density, forces, electric currents etc. Certain approximations can be made for the averaging procedure such as the electron mass is much less then the ion mass

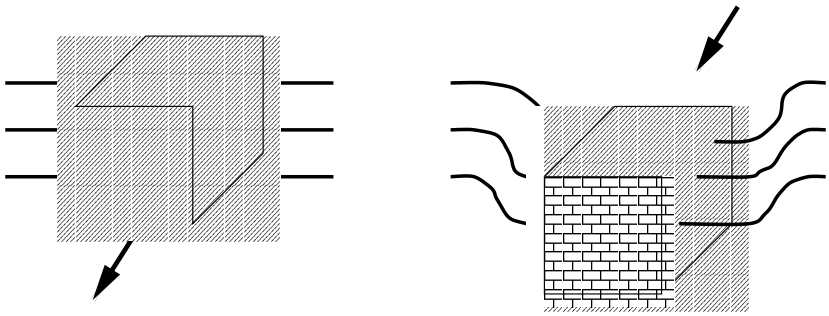

Figure 3.2. The model of ideal MHD. For a infinite conductivity, the magnetic field is "frozen-in" into the plasma. Motion of the fluid will advect the magnetic field and vice versa.

The classical way to understand how jet formation works, is to study the *stationary axisymmetric ideal* MHD equations in cylindrical coordinates (R, ϕ, Z). In this case, a de-composition of vector fields in *poloidal* and *toroidal* components simply gives to the field components in the meridional (R, Z) plane (subscript p) and a "ring" component (subscript ϕ) in ϕ-direction. With that, the total magnetic field $\vec{B} = \vec{B}_{\rm p} + \vec{B}_{\phi}$ has a helical structure with a pitch angle of the field defined by the ratio $B_{\phi}/B_{\rm p}$. The helical magnetic field lines follow (and define) *magnetic flux surfaces* Ψ, axisymmetric surfaces of constant magnetic flux,

$$\Psi(R, Z) \equiv \frac{1}{2\pi} \int \vec{B}_{\rm P} \cdot d\vec{A}, \tag{3.1}$$

where $d\vec{A}$ is the area element of a circular area perpendicular to the symmetry axis. The ideal MHD assumption, i.e. the assumption of a very high plasma conductivity implies the concept of *frozen-in* magnetic field lines. The field lines are considered to be "locked" into the plasma fluid and the advection of matter will automatically transport magnetic flux (Fig 3.2). If we would allow for a resistivity or for a certain amount of non-ionized material in the fluid, diffusive effects will play a role (magnetic diffusivity or ambipolar diffusion) leading to a drift motion between field and matter.

Under the assumptions prescribed above it follows that the poloidal plasma velocity is always parallel (or anti-parallel) to the poloidal magnetic field, $\vec{v}_p || \vec{B}_p$. However, the total velocity vector $\vec{v}$ is not parallel to the total magnetic field vector – *the plasma moves along the field but not parallel to the field*. This is possible due to the presence of a toroidal field component allowing the plasma to slide along the field in toroidal direction,

$$\vec{v} = \frac{\eta(\Psi)}{\rho} \vec{B} + R\,\Omega_{\rm F}(\Psi)\,\vec{e}_{\phi}, \tag{3.2}$$

where η is the mass flow rate along the flux surfaces, ρ the (rest frame) mass density and $\Omega_{\rm F}$ the iso-rotation parameter (Ferraro 1937). For illustrative purposes, the latter quantity can be interpreted as the "angular velocity of the magnetic field lines". For a stationary flow one can show that $\eta = \eta(\Psi)$ and $\Omega_{\rm F} = \Omega_{\rm F}(\Psi)$ are conserved along the field line or flux surface. The same is valid for the total specific energy $E(\Psi)$ and angular momentum $L(\Psi)$.

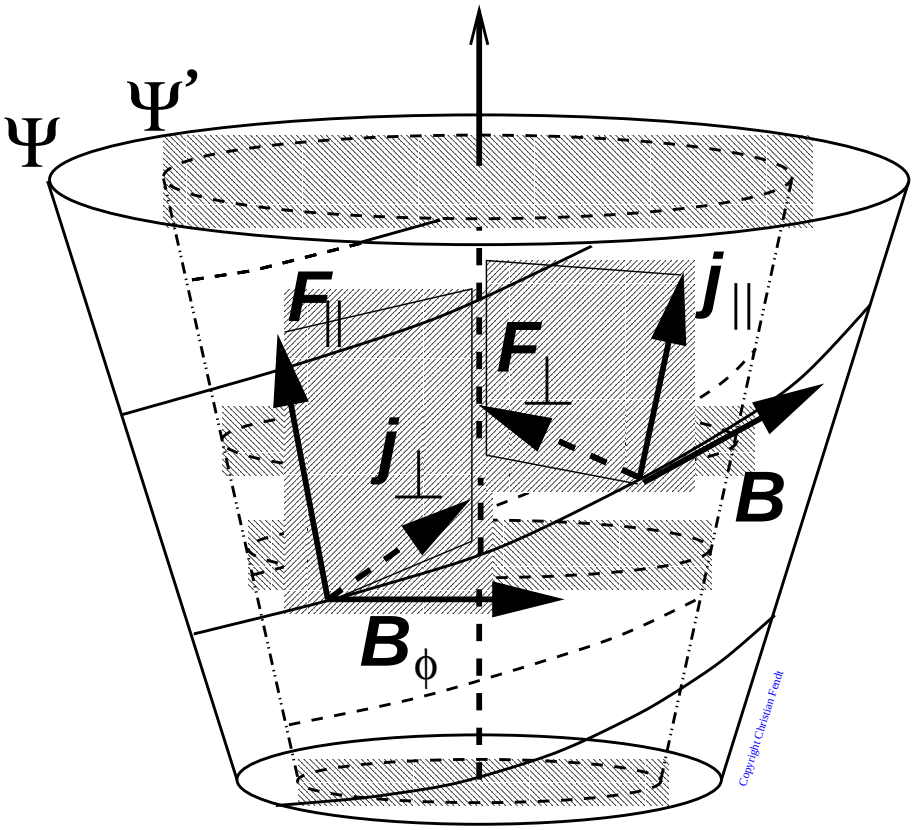

Figure 3.3. The Lorentz force components projected with respect to the magnetic flux surfaces $\Psi(R,Z)$. The parallel component $\vec{F}_{L,||} \sim \vec{j}_\perp \times \vec{B}_\phi$ is the accelerating (or decelerating) component. The perpendicular component $\vec{F}_{L,\perp} \sim \vec{j}_{||} \times \vec{B}$ is the collimating (or de-collimating) component.

3.2 The Lorentz force

The *magnetic* character of astrophysical jets is taken into account by considering the *Lorentz force* $\vec{F}_L \sim \vec{j} \times \vec{B}$ in the equation of motion[2] . A simple decomposition of the Lorentz force vector visualizes the role of magnetic forces for the jet collimation and acceleration. For example, we can rewrite the Lorentz force using Ampére's law, $\vec{F}_L \sim (\nabla \times \vec{B}) \times \vec{B}$, and the well known vector identities,

$$\vec{F}_L = \nabla \left(\frac{|\vec{B}|^2}{8\pi} \right) + \frac{1}{4\pi} \left(\vec{B} \cdot \nabla \right) \vec{B}. \tag{3.3}$$

[2]Note that in MHD the electric current density $\vec{j}$ defines the Lorentz force. This is different from the equation of motion of single particles where we have $\vec{F}_L \sim q(\vec{E} + \vec{v} \times \vec{B})$. In MHD, electric fields are negligible small in the rest frame of the fluid. The electric current density follows from the average value of the charged particles in the plasma, $\vec{j} \equiv q_e \vec{v}_e \rho_e + q_i \vec{v}_i \rho_i$, with the ion velocity $\vec{v}_i$ and electron velocity $\vec{v}_e$ and the charges q of the particles. Also, $\vec{v}$ represents the averaged velocity of the particles. (see also footnote [1]).

The first term on the right hand side is the gradient of the "*magnetic pressure*", the second one represents the *magnetic tension* due to the field curvature.

The decomposition shows several properties of the magnetic forces. First, a diverging field distribution like a monopole-type poloidal field with a gradient in field strength will generally accelerate the plasma outwards. In such a field with straight field lines pointing radially outwards, magnetic tension plays no role. A gradient in the magnetic field strength across the cylindrically collimated, asymptotic jet will also decollimate the jet. Magnetic tension of the collimating poloidal field lines may also accelerate the plasma. Essential for a jet, it is the tension force of the toroidal magnetic field which is responsible for the jet collimation. In the end, the jet collimation is determined by the total force balance between the gas pressure plus magnetic pressure plus the tension of the toroidal magnetic field of the jet and the pressure from the surrounding medium.

Another way to illustrate the Lorentz force is a decomposition in the components parallel and perpendicular to the *magnetic flux surfaces*, $\vec{F}_L \equiv \vec{F}_{L,||} + \vec{F}_{L,\perp}$ with

$$\vec{F}_{L,||} \equiv \vec{j}_\perp \times \vec{B}_\phi \quad \text{and} \quad \vec{F}_{L,\perp} \equiv \vec{j}_{||} \times \vec{B}. \tag{3.4}$$

This implies that a certain configuration of electric current and magnetic field distribution can accelerate the matter along the field (parallel force component) and collimate the flow across the poloidal field (perpendicular force component). Of course, also the opposite might be true, a decollimation or deceleration. In the cylindrical poloidal field distribution of a fully collimated jet accelerating Lorentz forces will be present. The magnetic field structure of the wind close to the disk/star will always have a kind of monopole-like distribution with the field lines in radial direction. The jet collimation region is the transition region between these two cases where the poloidal field lines turn from the radial outflow into a collimated stream.

In a fundamental paper Heyvearts & Norman (1989) have demonstrated that axisymmetric MHD flows have an intrinsic *self-collimating* property. A jet carrying a net poloidal electric current will always collimate into a cylinder. However, recently a discussion about the validity of such models has started (Okamoto 1999). In the literature, the jet self-collimation mechanism is often taken for granted. however, an "experimental proof" by MHD simulations about the question whether such a process really works on astrophysical scales is yet missing. Time-dependent MHD simulations (e.g. Ouyed & Pudritz 1997) seem to demonstrate such a behavior, but the influence of numerical constraints like the shape of the numerical grid (Ustyugova et al. 1999) or astrophysical boundary conditions as the accretion disk magnetic field distribution (Fendt & Elstner 2000) is not yet clear.

Finally, it should be noted that already a simple experiment usually shown in the high school physics course demonstrates the basic idea of the jet collimation. Two wires carrying an electric current in the some direction do attract each other.

3.3 The force-free limit

For some astrophysical applications the *force-free* limit is a suitable approximation of MHD. There are two ways to illustrate the force-free character of a magnetic field. The first is to imagine a magnetic field configuration such that the terms of magnetic tension and magnetic pressure gradient exactly cancel. In this case, there is no net Lorentz force disturbing the hydrodynamic equilibrium. Since in the equation of motion the Lorentz force vanishes, only the hydrodynamic part is left. The second way is to imagine a very strong magnetic field, or, respectively, a very small plasma density. In this case, the inertial terms in the equation of motion can be neglected. This equation is then equivalent to the condition that the total Lorentz force must vanish too.

The first viewpoint is appropriate in the case of dipolar accretion. If, the accretion stream follows a pure dipolar magnetic field geometry, the flow dynamics is equivalent to the case of free-fall. Of course, the force-free dipolar geometry will only be sustained if the field is strong, i.e. the plasma inertial forces (as the matter follows a curved trajectory) too weak in order to distort the field structure. The other viewpoint may be applied for highly relativistic jets. A high jet velocity can be obtained only in the case of a high plasma magnetization Therefore, for calculating the magnetic field structure, the inertial terms may be neglected. Clearly, a force-free field cannot accelerate the plasma. In order to answer the question of the plasma dynamics or for a fully self-consistent MHD solution, inertial terms must be included. However, since the low plasma density, only a small deviation from the force-free field structure can accelerate the matter to high velocities.

3.4 Magneto-sonic surfaces

One characteristic property of astrophysical jets is their high velocity. The asymptotic velocity of MHD jets is indeed higher than the speed of the magneto-sonic waves. Jets are therefore really *dynamic* bodies perturbed by magneto-sonic waves and shock waves.

In the region of jet formation, matter is lifted from the accretion disk with comparatively low velocity. The material is then accelerated by magneto-centrifugal or magnetic forces (see below). With increasing velocity of the matter, the speed of the slow magneto-sonic waves, the Alfvén waves and the fast magneto-sonic waves are succeedingly exceeded. The positions where this happens define the slow magneto-sonic surface, the Alfvén surface and the fast magneto-sonic surface of the jet flow. The super magneto-sonic character of the jet implies some interesting aspects.

The first point concerns the *causal interaction* of different parts of the jet. In MHD the fastest mode to exchange information is by fast magneto-sonic waves. Therefore, if some part of the jet becomes super fast magneto-sonic, this part jet causally decouples from the sub fast magneto-sonic part. This implies for example that any disturbance resulting from the interaction process of the asymptotic jet with the ambient medium cannot influence the region where the jet has been launched. On the other hand, the sub fast magneto-sonic jet region is determined by by the conditions at the jet foot point.

The Alfvén surface is interesting because this is the region where the jet kinetic energy become comparable to the magnetic energy. Therefore, until the matter reaches the

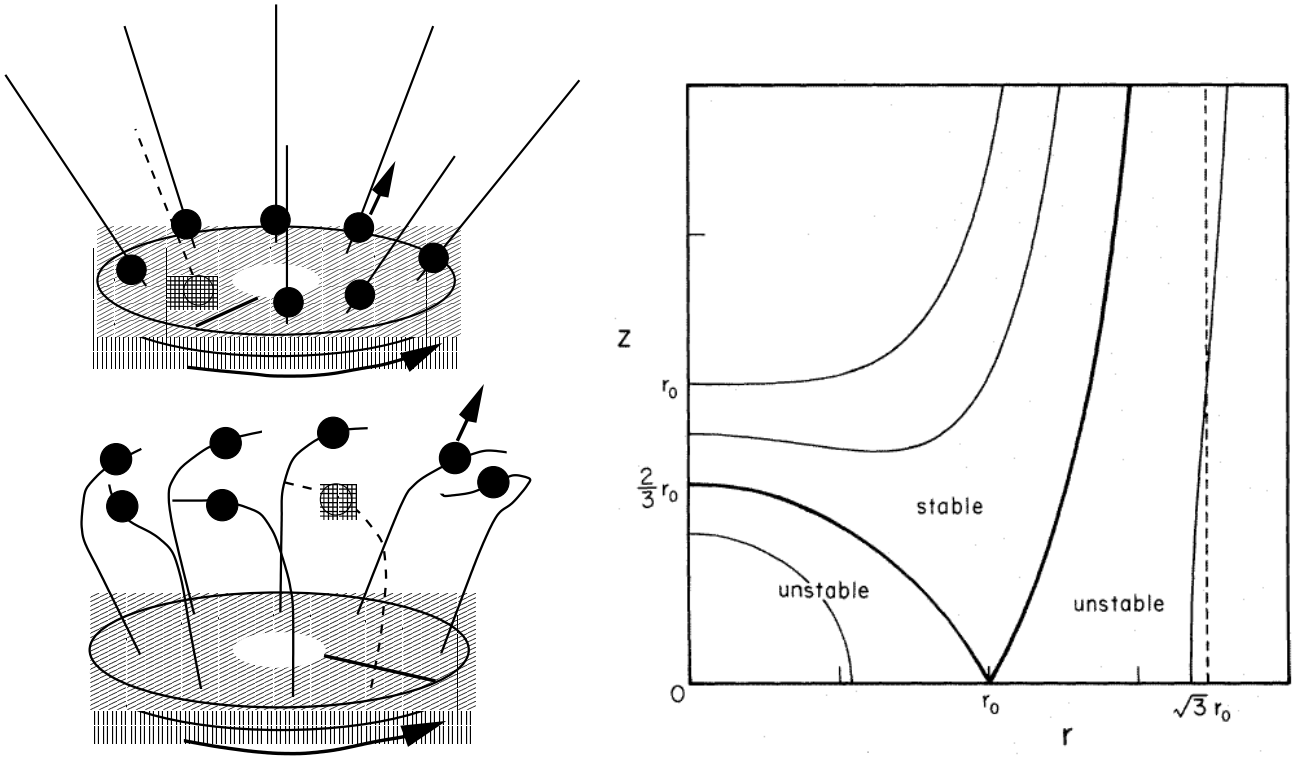

Figure 3.4. The idea of magneto-centrifugal acceleration. The gas fluid elements can be taught to represent beads on a wire anchored to a rotating body (*left*). For a magnetic field (wire) inclination of more then 30° to the rotational axis, the fluid elements (beads) are centrifugally unstable. The effective potential (Eq. 3.5) along such a field line (wire) with a foot point radius r_0 is shown in the *right* (from Blandford & Payne 1982). Disturbance of the unstable equilibrium leads to ejection of matter (beads) along the magnetic field lines (wire). After substantial acceleration the inertia of the mass flow (beads) bends the field line (wire) in toroidal direction.

Alfvén surface it is basically guided by the poloidal magnetic field and is co-rotating with the foot points of the field lines. Beyond the Alfvén surface, the field cannot control the plasma anymore. Instead, the plasma motion affects the magnetic field structure. The matter is moving radially outwards with constant kinetic angular momentum and decreasing toroidal velocity. A toroidal magnetic field is induced and will finally dominate the poloidal field component for large radii.

In the stationary MHD approach, the magneto-sonic surfaces represent singular surfaces in the equations (Grad-Shafranov equation and wind equation, see below). Certain boundary conditions must be defined along these surfaces, however, their location is not known from the beginning. This is the most important difficulty for the solution of the stationary MHD equations and limits this approach.

This problem is overcome with time-dependent MHD simulations. However, in this case care has to be taken in the definition of the numerical time step in order to allow for appropriate propagation of magneto-sonic waves across the grid. As a real difficulty,

current MHD codes cannot properly handle open boundary conditions in the sub-Alfvénic or sub-slow magneto-sonic regime of the flow and tend to reflect such waves.

3.5 The light cylinder of the magnetosphere

A term which is sometime cause of confusion is the *light cylinder* of a rotating magnetosphere. The light cylinder is a characteristic feature of relativistic MHD. Although a *rapid rotation* is the essential factor for the existence of a close light cylinder, such rotation is also necessary in order to launch a powerful jet. Therefore, jets moving with relativistic speed always enclose a narrow light cylinder.

What is the light cylinder? Imagine a rapidly rotating object with magnetic field lines anchored in the surface. This could be a stellar body or the surrounding accretion disk. As the magnetic field lines are considered to rotate *rigidly*[3] (like every part of a wire rotates with the same angular velocity), at a certain radius the rotational velocity of the field line reaches the speed of light. This location is called the light cylinder of that field line. If the angular velocity of all field lines Ω_F in a magnetosphere is the same, they will have the light cylinder radius $R_L = c/\Omega_F$ If the field line foot points rotate with different speed, the light *cylinder* deforms to a *surface*. An example of such a configuration would be the jet magnetosphere above a differentially rotating disk.

The light cylinder has no direct physical consequences for the flow (provided that, a relativistic treatment of such problems has been made). The foremost question which comes to mind is surely how, outside the light cylinder, the flow of matter can adjust to stay at velocities below the speed of light, while, seemingly, being frozen-in to field lines "rotating" faster than that. From a phenomenological point of view, in order to keep the matter velocity $\vec{v} = \frac{\eta}{\rho}\vec{B} + R\,\Omega_F < c$ the magnetic field structure has to change to a *toroidally dominated* field configuration. This will allow the plasma to *slide along* the magnetic field in toroidal direction while moving outwards. Therefore, the correct physical interpretation of the iso-rotation parameter Ω_F is the angular velocity of the plasma subtracted the slide motion along the field. As we know from analytical models in simple cases (Michel 1969) and also from numerically calculations for more complex geometries (Fendt & Camenzind 1996), the matter crosses the light cylinder smoothly without any particular incidents.

For Newtonian objects the light cylinder is far away from the foot points of the magnetosphere. For example, the Sun has a light cylinder of about 700 AU. It can be only of interest if there are field lines which in fact reach that radius. In rapidly rotating neutron stars the light cylinder may be located as close as 10 stellar radii to the stellar surface. For jets AGN a typical estimate of the light cylinder radius (derived from the rotation rate at the marginally stable orbit) is about some tens of gravitational radii.

It must be noted that in relativistic magnetohydrodynamics poloidal electric fields are induced which are not present in Newtonian MHD. The electric field (which is perpendicular to the poloidal magnetic field) scales with the light cylinder radius, $E_\perp =$

[3] It should probably be emphasized that in the picture used here for illustrative purposes we deal with the rotational velocity of field *lines* and not with a velocity of the *field* itself. The essential point is that field lines are no real physical objects and, therefore, any velocity may be attributed to these fiducial objects.

$(R/R_L)B_P$. Thus, the relativistic character of MHD manifests itself in the presence of poloidal electric fields.

3.6 The model of Blandford & Payne (1982)

The basic idea which is still behind most of the work on jet formation theory has been introduced some 20 years ago in a paper by Blandford and Payne (1982). It is perhaps the most influential publication on the topic of jet formation.

The main achievement of this paper is the finding that the observationally motivated ingredients of astrophysical jet sources – the accretion disk and a magnetic field – can be combined into a self-consistent model in which the interaction of these components is responsible for the formation of collimated high velocity streams. The physical mechanisms introduced with the new model – acceleration and collimation of the MHD jet – has been investigated by detailed numerical calculations.

The concept of Blandford & Payne had its precursors in the literature. The acceleration of matter and transport of angular momentum by the magnetic field has been calculated by Weber & Davis (1967) for the *solar wind*. Piddington (1970) proposed a model for double radio sources and quasars in which the twisting-up of magnetic field lines in a rotating galactic gas cloud is responsible for the ejection of jet knots. Lovelace (1976) and Blandford (1976) came up with a purely electro-magnetic model of *jet formation from accretion disks*. In both models, energy extraction from the disk into the jet is established continuously by the electro-magnetic torque. In the Lovelace model, the magnetized accretion disk around a massive black hole acts as an electric dynamo. The electric field created by the rotating disk accelerates collimated beams of protons to ultra-relativistic velocities. Blandford (1976) proposes the existence of a magnetosphere above the magnetized accretion disk in which the electro-magnetic momentum is focused towards the rotational axis as a mechanism for a continuous and aligned jet flow from parsec to megaparsec scale. An exact solution for a force-free disk magnetosphere is presented considering also the effects of an electro-magnetic wind, the electro-magnetic torque and inertial forces. Blandford & Payne (1982) extend this picture to a self-consistent MHD model taking fully into account the inertia forces of the jet mass flow. I will now briefly discuss the main results of this work.

3.6.1 Magneto-centrifugal acceleration

The first point to mention is the possibility to accelerate matter *magneto-centrifugally* along the magnetic field. Blandford & Payne were first to recognize that matter, attached to magnetic field lines with an inclination towards the equatorial plane, is in unstable gravito-centrifugal equilibrium. In the case of ideal MHD the field lines are frozen into the plasma (Ferraro's law of iso-rotation). The jet magnetic field is anchored in the accretion disk and therefore follows the disk rotation. The plasma moving along the poloidal field can be compared to beads on the wire. This analogy between a hydrodynamic description of a fluid and a kinematic toy-model has been suggested first by Henriksen & Rayburn (1971). Note that the matter moves along the field but not necessarily parallel to the field

(see Eq. 3.2). The effective equipotential surfaces for such a configuration follow from gravity and the centrifugal forces both acting on the 'beads' (plasma) rotating with the 'wire' (magnetic field lines). For a Keplerian disk one obtains

$$\Phi(r,z) = -\frac{G\,M}{r_0}\left(0.5\left(\frac{r}{r_0}\right)^2 + \frac{r_0}{\sqrt{r^2+z^2}}\right), \tag{3.5}$$

where the subscript 0 indicates the radius at the foot point of the field line. For an angle angle between the equatorial plane and the poloidal magnetic field less than the critical angle [4] of 60° the centrifugal equilibrium becomes unstable (Fig. 3.4 right). If the field lines are inclined away from the rotational axis, any small disturbance leads to a sling-shot effect, flinging the matter outwards by centrifugal forces and initiating the disk wind (Fig. 3.4 left).

What is also interesting but sometimes disregarded, is the fact that a similar instability works when the field lines are inclined *towards* the rotational axis (see also Fig. 3.4 right). In this case gravity wins and the gas is accelerated towards the origin.

3.6.2 The large-scale structure of a collimating self-similar MHD jet

The major achievement of Blandford & Payne (1982) is the self-consistent solution of the magnetohydrodynamic equations demonstrating the *self-collimating* character of the MHD disk wind.

In their approach, the essential assumption for the solution of the relevant MHD equations is *self-similarity* in the spherical radius. This means that all variables scale with a power law in the spherical radius. Radial self-similarity ignores boundary conditions at the jet axis and the jet radius (which is moved to infinity). Also the asymptotic jet collimated into cylindrical shape, is not self-similar in spherical radius. Nevertheless, for the region close to the disk, where the major jet acceleration and collimation takes place, the Blandford & Payne approach is valid in order to overcome the many difficulties involved in the solution of the MHD equations.

The poloidal field configuration derived by Blandford & Payne clearly indicates the collimation of the jet flow. Figure 3.5 shows the distribution of the poloidal field lines for different field line foot point radii. If we go along the jet, the toroidal magnetic field becomes stronger and the pitch angle $\alpha \equiv \arctan|B_\phi/B_p|$ becomes larger. At large distance from the disk (beyond the Alfvén surface), the magnetic field structure is increasingly dominated by its *toroidal* component (see the B_ϕ/B_p-curve in Fig. 3.5). This can be understood from the frozen-in concept and the fact that the plasma inertia disturbs the initial magnetic field structure. Beyond the Alfvén point the kinetic energy of the matter dominates the magnetic energy. The mass flow, which tends to conserve its momentum and thus its direction of propagation radially outwards, "bends" the magnetic field frozen into the matter.

[4] This angle has been derived for the assumption of a "cold" wind neglecting thermal pressure corresponding to a super slow-magneto-sonic flow. If thermal pressure is taken into account, the critical angle increases to 72° (Pelletier & Pudritz 1992)

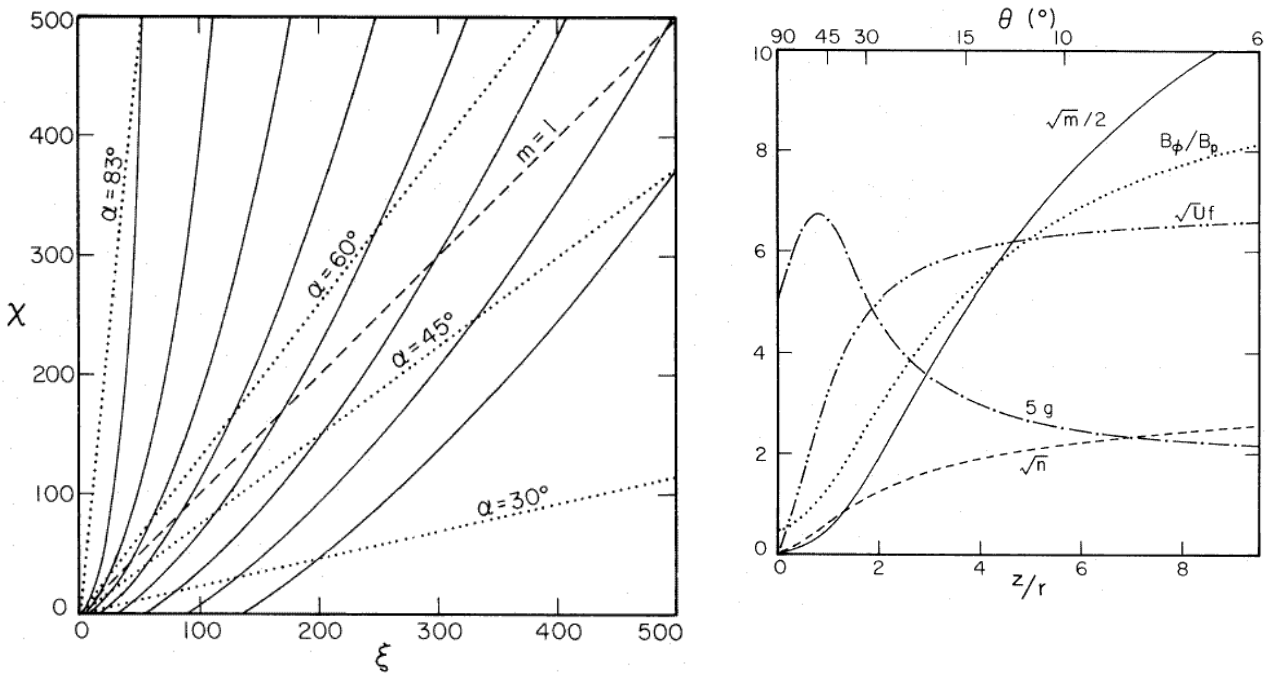

Figure 3.5. Stationary, self-similar MHD solution of jet formation (Blandford & Payne 1982). (*Left*) Magnetic field structure. Shown are poloidal magnetic field lines (*solid*), the pitch angle of the field lines (*dotted*), and the location of the Alfvén surface in normalized coordinates (ξ, χ). (*Right*) Dynamical parameters of the plasma flow. Poloidal (U) and toroidal (u) velocity, Alfvén Mach number (m) and fast magneto-sonic Mach number (n) and the ration of toroidal to poloidal magnetic field.

As the flow of matter becomes accelerated along the field lines, it passes the magneto-sonic points subsequently (see Sect. 3.4). Figure 3.5 show the velocities as function of the spherical distance from the foot point radius r_0. The poloidal velocity (here denoted with $\sqrt{U}f$) reaches the speed of the magneto-sonic waves where the Alfvén Mach number (denoted with $\sqrt{m}$) and the fast magneto-sonic Mach number (denoted with $\sqrt{n}$) become unity.

The toroidal velocity (denoted with g) of the jet matter decreases with radius while the matter moves radially outwards with constant kinematic angular momentum. Consequently, for the most part of the jet, the super-Alfvénic part, the jet must be considered as *non-rotating*. In the Blandford & Payne solution, the ratio of poloidal to toroidal velocity is about 20 for large distances. The toroidal speed in this region is also lower by a factor of 2.5 compared to the rotation at the foot point of the field line. The Alfvén surface in these self-similar solution follows the curve $z = r$ (Fig. 3.5 *left*), whereas the fast magneto-sonic point is reached at $(z/r) \simeq 1.5$ (Fig. 3.5 *right*).

The Blandford & Payne solution has the property that most of the power is concentrated in the central core region along the jet axis, whereas the angular momentum and magnetic flux is transported in the outer jet layers. The core-envelope structure of magnetic jets is a intrinsic feature of many jet models (e.g. Appl & Camenzind 1993a,b).

3.7 From accretion to ejection

The "holy grail" of jet formation theory is still the fundamental question of how the matter, which accretes within the disk towards the central object, is diverted in vertical direction and finally becomes injected in the jet.

To answer this question is again a difficult task (too difficult in some respects ...). As we have large gradients in the physical parameters in the jet forming region above the disk, we have even larger gradients in the transition region between disk and jet. The density varies drastically over several orders of magnitude on very short length scales. Also the (effective) electric resistivity changes by similar magnitudes. Since the accretion disk is turbulent, the magnetic diffusivity is high. In contrary, for the jet, ideal MHD is quite a good assumption.

So far, time-dependent numerical simulations have failed in investigating the jet-disk interaction for a reasonable period of time. Typical simulations run for not more then several orbital periods of the inner part of the disk.

A thorough investigation of this region has been made by Ferreira and collaborators (see Ferreira 1997) using a stationary, self-similar approach. They find that the important terms responsible for lifting the plasma off the disk in vertical direction, are (i) the turbulent magnetic diffusivity ν_m which allows the matter to cross the field lines and (ii) the magnetic torque $F_\phi = j_z B_r - j_r B_z$ establishing the hydrostatic equilibrium with in the disk. Essentially, the lifting mechanism is completely *magnetohydrodynamic* and can be understood by examining the Lorentz force components. If we denote the total poloidal electric current by $I(r,z) = -\frac{c}{2} r B_\phi$, we can write the Lorentz force components as follows. The Lorentz force in toroidal direction is

$$F_\phi = \frac{B_p}{2\pi r} \nabla_{||} I,$$

the poloidal force along the magnetic flux surfaces is

$$F_{||} = -\frac{B_\phi}{2\pi r} \nabla_{||} I,$$

and the poloidal force perpendicular to the magnetic flux surfaces is

$$F_\perp = B_p j_\phi - \frac{B_\phi}{2\pi r} \nabla_\perp I.$$

Ejection of matter from the disk into the jet occurs naturally, if the poloidal electric current density in radial direction, j_r, decreases vertically. Two processes may lift the plasma from the disk. (i) The *gas pressure gradient*, if the $F_\perp$ decreases, or (ii) the radial centrifugal acceleration of plasma, if F_ϕ increases. Figure 3.6 shows the stationary MHD calculation of the self-consistent disk-jet connection (Ferreira 1997). In the diffusive disk the matter accretes across the poloidal magnetic field lines, but then couples to the field and becomes ejected as a disk wind similar to the Blandford & Payne mechanism.

Numerical simulations of the accretion disk structure with a boundary condition allowing for a jet outflow are essential in order to understand the jet launching. They will

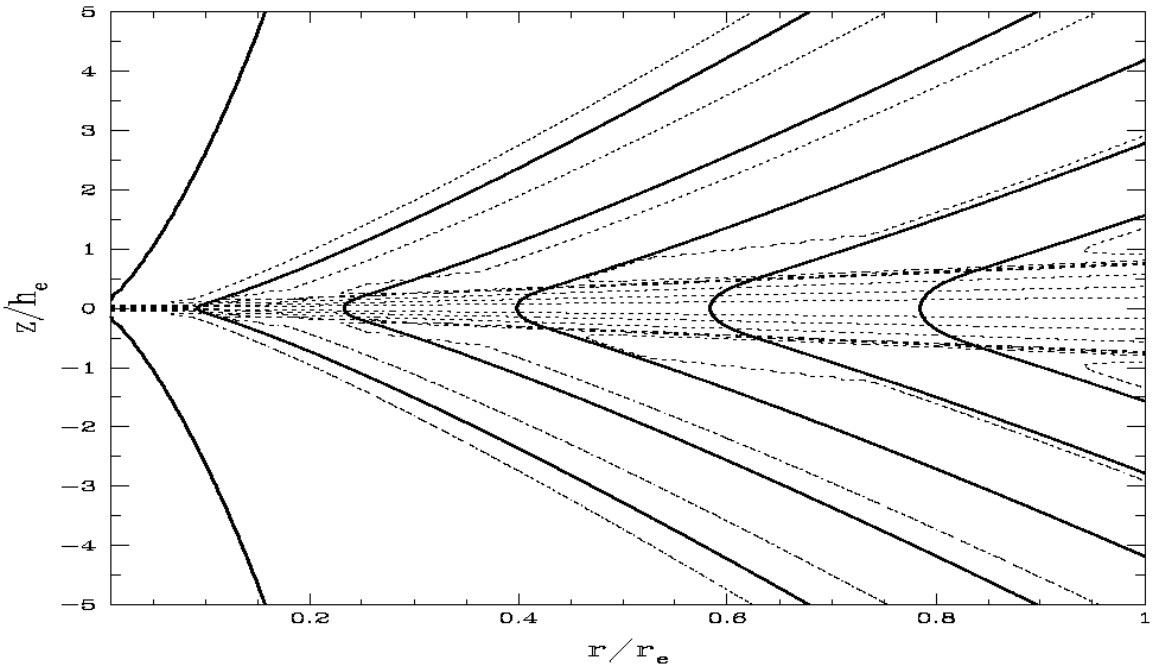

Figure 3.6. Magnetic field and plasma velocity in a accretion-ejection structure (Ferreira 1997). Shown are poloidal magnetic field lines (*solid*) and poloidal stream lines of the flow (*dashed*). Resistivity allows the accreting matter to cross the magnetic field lines. If the electric current decreases with disk height, matter is lifted from the disk surface into the corona. At larger heights the matter couples to the field line and becomes accelerated to higher velocities.

finally give an answer to the questions what kind of disks can generate jets and which do cannot and what the time scale of the jet ejecting mechanism is. They will also help to understand the magnetic field generating dynamo process in the disk providing the required field strength and field distribution for the jet launching (see v. Rekowski et al. 2000, Bardou et al. 2001).

Chapter 4
Magnetohydrodynamics of jet formation

In this chapter I will summarize the theoretical background of magnetohydrodynamic (MHD) jet formation. After a brief introduction to MHD itself and just presenting the well known MHD equations, I will go in more detail and discuss these equations in the limiting case of ideal, stationary and axisymmetric MHD. This is an essential step concerning the understanding of the physics of MHD jet formation. The discussion is further extended to the specific equations governing the force-balance in the MHD jet, the jet collimation and acceleration – the Grad-Shafranov equation and the wind equation.

4.1 The model of magnetohydrodynamics

Before a discussion of the basic MHD equations, it is maybe helpful to introduce in brief the essentials of *magnetohydrodynamics* itself. For somebody, who is not working in the field of MHD, some confusion may arise about the different ways how to describe the interaction between matter and the electro-magnetic field and about what the MHD concept actually implies in this respect.

The *microscopic* point of view is that a single charged particle is moving in the electro-magnetic field under the action of Lorentz and Coulomb forces. A statistical average over many particles of several species leads to the view point of *plasma physics*. Now there is a "fluid" (or "gas") of (partly) ionized matter with averaged properties (density, velocity, ...) for all species. For length scales above a certain limit (the Debye length), however, the charges cancel and the fluid in total is neutral. The plasma particles collide, exchange energy and charge. The collision frequency depends mainly on density and temperature. Also the electric conductivity is determined by the collision frequency. Due to the collisions, also the neutral component of a partly ionized fluid couples to the ionized components. Thus, it might be affected also by a large scale electro-magnetic field.

In plasma physics the different species (ions/electrons or electrons/positrons) are treated as separate components. The fluid equations are examined for each species separately, i.e. one has a equation of motion for electrons and for ions, and similar for the other moments of the Fokker-Planck equation. The *model of magnetohydrodynamics* averages over the properties of the different plasma species resulting in a *single fluid model*. For example, the momentum density of the single fluid is the sum of the velocities of the electrons and ions weightened with the particle mass and particle density, $\rho\vec{v} = n_e m_e \vec{v}_e + n_i m_i \vec{v}_i$ (with the particle number densities $n_{e,i}$ and the mass density ρ). Certain approximations are

taken into account, e.g. the much larger mass of the ions compared to the electrons. In the end, instead of describing charges (q_i, q_e) moving with velocities (v_i, v_e), one deals with the electric current density as the *net* motion of charges $\vec{j} \equiv Zen_i\vec{v}_i - en_e\vec{v}_e$, and similar for mass density, velocity, temperature etc.

The MHD concept is valid only for certain approximations. Velocities in the rest frame of the fluid must be small, charge neutrality must be conserved on global scales and friction between the components must be strong enough so that accelerating forces can act on both species simultaneously.

If the ideal MHD condition $\vec{E} = -\vec{v}/c \times \vec{B}$ is applied to the relativistically covariant equation of motion, the concept of relativistic MHD can be developed.

4.2 The MHD equations

The concept of magnetohydrodynamics delivers a set of equations which describe the state of an ionized fluid (or gas) under the influence of a magnetic field. With that the general task in order to model the magnetohydrodynamic jet formation is to solve these time-dependent, (resistive) MHD equations considering conservation of mass, momentum, and energy, the induction of magnetic field, and the non-existence of magnetic monopoles for astrophysical boundary conditions. In their non-relativistic version these equations are the following,

$$\frac{\partial \rho}{\partial t} + \nabla \cdot (\rho \vec{v}) = 0\,, \tag{4.1}$$

$$\rho \left[\frac{\partial \vec{v}}{\partial t} + (\vec{v} \cdot \nabla)\, \vec{v} \right] + \nabla P + \rho \nabla \Phi - \vec{j} \times \vec{B} = 0\,, \tag{4.2}$$

$$\rho \left[\frac{e}{\partial t} + (\vec{v} \cdot \nabla)\, e \right] + P(\nabla \cdot \vec{v}) - \frac{\eta_{\rm D} |\vec{j}|^2}{c^2} = 0 \tag{4.3}$$

$$\frac{\partial \vec{B}}{\partial t} - \nabla \times \left[\vec{v} \times \vec{B} - \frac{\eta_{\rm D} \vec{j}}{c} \right] = 0\,, \tag{4.4}$$

$$\nabla \cdot \vec{B} = 0\,. \tag{4.5}$$

Here, $\vec{B}$ is the magnetic field, $\vec{v}$ the velocity, ρ the mass density, P the gas pressure, e the internal energy, and Φ the gravitational potential. The electric current density $\vec{j}$ is given by Ampere's law, $\nabla \times \vec{B} = (4\pi/c)\vec{j}$. The magnetic diffusivity $\eta_{\rm D}$ measures the efficiency of magnetic diffusion and is determined by the physical processes leading to diffusion. In the astrophysical context the microscopic diffusivity (due to collisions and/or electric resistivity) is too small by orders of magnitude in order to have any influence and usually the effect of a turbulent motion is taken into account. Additional to the above equations, an equation of state is necessary to close the system of equations. This can be a polytropic gas law, as often used in jet models, or any other specification of the gas pressure.

The solution of the time-dependent MHD equations requests a lot of computational power and became feasible only during the last decade. Still, time-dependent simulations of the jet formation may cover only about some percent of the region where the jet

collimation is actually achieved.

4.3 Stationary, axisymmetric, ideal MHD

The limit of stationarity, axisymmetric and ideal MHD may give some fundamental insight into the jet physics. In this case, the time derivative and the derivative in toroidal (ϕ-) direction is neglected and the conductivity of the matter is assumed to be infinite. This is the *classical approach* to the jet problem, but still provides the best introduction to the ideas behind the model of jets as magnetohydrodynamic engines.

Here, I will briefly summarize the essential points implied by the assumptions introduced above. An early derivation has been presented by Chandrasekhar (1956). In the axisymmetric case it is appropriate to use cylindrical coordinates (R, ϕ, Z) and to distinguish between the *poloidal* components of a vector (the components in the meridional plane, i.e. the R and Z-components) and the *toroidal* component (the ϕ-component)[1]. From *stationary* Faraday's law, $\nabla \times \vec{E} = 0$, it follows that the electric field is the gradient of a potential, $\vec{E} = \nabla U$. Because of *axisymmetry* the ϕ-derivative vanishes and $E_\phi = 0$. For *infinite conductivity* Ohm's law implies the MHD condition,

$$\vec{E} = -\frac{1}{c}\,\vec{v} \times \vec{B}. \tag{4.6}$$

Since $E_\phi = 0$, it follows that

$$\vec{v}_p \times \vec{B}_p = 0, \qquad \text{or} \qquad \vec{v}_p \,||\vec{B}_p \qquad \rightarrow \vec{v}_p = \kappa(R,Z)\vec{B}_p. \tag{4.7}$$

Thus, the poloidal plasma velocity is parallel to the poloidal magnetic field. Because of mass conservation and stationarity we have $\nabla(\rho\vec{v}_p) = 0$ and for the scalar function $\kappa(R,Z)$ it follows that $0 = \nabla(\rho\kappa\vec{B}_p) = \vec{B}_p \cdot \nabla(\rho\kappa)$. Therefore, $\eta \equiv \rho\kappa$ is a conserved quantity along the field line. With the assumption of axisymmetry, a magnetic flux function can be defined,

$$\Psi(R,Z) = \frac{1}{2\pi}\int \vec{B}_p \cdot d\vec{A} = \frac{1}{2\pi}\int B_z\, R\, d\phi\, dR, \tag{4.8}$$

which measures the magnetic flux through a circle with radius R around the symmetry axis. Similar, the total poloidal electric current is $I(R,Z) = \int j_Z R d\phi dR = -(c/2)\, RB_\phi$. The axisymmetric magnetic field lines $\vec{B} = \vec{B}_p + \vec{B}_\phi$ enclose corresponding flux surfaces. Thus, $\eta(\Psi) \equiv \rho\kappa$ is conserved along the magnetic flux surface. From Eq. (4.7) it follows that

$$\vec{v} \times \vec{B} = \vec{v}_\phi \times \vec{B}_p + \vec{v}_p \times \vec{B}_\phi = \frac{1}{R}\left(v_\phi - \frac{\eta}{\rho}B_\phi\right)\nabla\Psi, \tag{4.9}$$

[1]The poloidal and toroidal components of a vector field can be defined in a more general way for other coordinate systems. See Lüst & Schl"uter (1954) or Chandrasekhar (1956, 1961) for a general introduction

and, using the MHD condition and Faraday's law, we obtain

$$0 = \nabla \times \vec{E} = \nabla\Psi \times \nabla \left(\frac{1}{R} \left(v_\phi - \frac{\eta}{\rho} B_\phi \right) \right). \tag{4.10}$$

This implies that the quantity $\Omega_F \equiv \left(v_\phi - \frac{\eta}{\rho} B_\phi \right) / R$ is conserved along the field line, $\Omega_F = \Omega_F(\Psi)$ (Ferraro's law of iso-rotation).

From Eq. (4.9) and the MHD condition it can be derived that the electric field is always perpendicular to the the flux surfaces, $\vec{E} = -(1/c)\Omega_F \nabla\Psi$, or $E_\perp = (R/R_L)B_p$ where $R_L = c/\Omega_F$ is the *light cylinder* radius. Thus, the poloidal electric field component is important only if the light cylinder is close to the central object. In fact, the presence of strong poloidal electric fields is the signature of relativistic MHD. For Newtonian MHD, electric fields can be neglected.

4.4 Conservation laws of stationary MHD

The assumption of stationarity implies conservation laws for certain physical quantities. With a more extended derivation one can proof that in stationary, axisymmetric MHD there are *four* physical quantities which are conserved along the magnetic flux surface. Here, I briefly discuss the expressions for these quantities in the Newtonian limit. The first conserved quantity, which has been already introduced above, is

$$\eta(\Psi) \equiv \rho \frac{v_p}{B_p} \mathrm{sgn}(\vec{v}_p \cdot \vec{B}_p) \tag{4.11}$$

It has has the meaning of a mass flow rate $\dot{M}$ per flux surface,

$$\dot{M}(\Psi + \Delta\Psi) - \dot{M}(\Psi) = \int_\Psi^{\Psi+\Delta\Psi} \rho \vec{v}_p \cdot d\vec{A} = \int_\Psi^{\Psi+\Delta\Psi} \eta \vec{B}_p \cdot d\vec{A}. \tag{4.12}$$

The iso-rotation parameter

$$\Omega_F(\Psi) \equiv \frac{1}{R} \left(v_\phi - \frac{\eta(\Psi)}{\rho} B_\phi \right) \tag{4.13}$$

is the second conserved quantity. In the MHD jet theory, Ω_F is sometimes considered as "angular velocity of the field line", a notation which is somewhat comprehensive but also misleading (see also discussion above). In the following, Ω_F will be denoted as *iso-rotation parameter* of a flux surface. The third quantity is the total angular momentum per unit density,

$$L(\Psi) = R^2 \Omega_F(\Psi) - \frac{R B_\phi}{4\pi\eta(\Psi)} \tag{4.14}$$

consisting of two contributions, the kinetic and the magnetic part. At the Alfvén radius R_A, this expression reduces to $L(\Psi) = \Omega_F(\Psi) R_A^2$ which guarantees that the stationary MHD flow remains regular at this point. Thus, only a certain combination of angular

momentum and iso-rotation parameter is possible. The Alfvén radius corresponds to the lever arm for the torque acting at the foot point of the jet (usually one finds an Alfvén radius 10 times larger than the foot point radius of the field line). It can be important for the evolution of the accretion disk that jets or winds may carry away angular momentum very efficiently due to the large lever arm. Beyond the Alfvén point, the plasma moves more or less with constant kinetic angular momentum and the angular velocity decreases with radius as $\Omega \sim R^{-2}$.

The fourth conserved quantity is the total energy. If we, for simplicity, neglect thermal pressure and gravity, also the total energy per unit density consists of two contributions – kinetic energy and magnetic energy (Poynting flux),

$$E(\Psi) = \frac{v^2}{2} - \frac{RB_\phi \Omega_F(\Psi)}{4\pi\eta(\Psi)}. \tag{4.15}$$

The essential point of considering a *magneto*hydrodynamic jets is the conversion of magnetic energy into kinetic energy of the bulk flow. This conversion process can be understood as driven by Lorentz forces (see above). The contribution of gravity and thermal pressure will modify the expression (4.15) (see Sect. 4.6). Usually, an adiabatic or polytropic gas law is assumed for the jet and the additional term in the energy equation (4.15) is $\sim \left(\frac{\Gamma}{\Gamma-1}\,\rho^{\Gamma-1}\right)$. However, it has been shown that jets are typically *cold*, and, consequently, gas pressure can be neglected in the region of collimation and acceleration. This is not true for the transition region between disk and jet where the the flow is accelerated from sub to super slow magneto-sonic velocity. In stationary MHD the regularity condition at the slow magneto-sonic point determines the mass flow rate $\eta(\Psi)$.

In the case of relativistic jets the Newtonian expressions discussed above have to be generalized. For special relativity, the main addition is to consider the fact that the jet's kinetic energy might be comparable to the rest mass energy of the jet flow while the role of gravity is usually neglected. In general, jets move with velocities faster than the escape velocity and therefore, for most the cases, the special relativistic approximation is sufficient. Only if processes close to the central black hole are investigated, maybe the jet formation process in the innermost accretion disk itself, the general relativistic effects may become important. The curvature of space time and the 'rotation of space' around a rotating black hole might influence the energy balance of such jets.

4.5 The Grad-Shafranov equation – the force-balance across the field

Under the assumptions of stationarity, axisymmetry, and high conductivity, the local force-balance of MHD can be split in two governing equations (see e.g. Camenzind 1987; Okamoto 1992). The *Grad-Shafranov equation* (GSE) describes the local two-dimensional force-balance across the field. The *wind equation* describes the force-balance along the field lines. Both equations are coupled due to inertial back reaction of the plasma on the structure of the magnetic field. A clever iterative procedure would be needed in order to solve this system of equations self-consistently. As a matter of fact, the problem

of a self-consistent solution is so complicated that is has not yet been solved without any further simplifying assumptions. If inertial forces can be neglected, the magnetic field structure follows solely from the electromagnetic force-balance (force-free field).

With the magnetic flux function (4.8) the toroidal component of Ampère's law can be re-written as

$$R\nabla\cdot\left(\frac{1}{R^2}\nabla\Psi\right)=-\frac{4\pi}{c}j_\phi\,. \tag{4.16}$$

This is the general version of the *Grad-Shafranov equation*. The source term of the GSE, the r.h.s. of Eq. (4.16), must be derived from the component of the equation of motion which is perpendicular to the flux surface.

Maxwell's equations and thus Eq. (4.16) are covariant concerning special relativity (and are therefore 'relativistic' by definition). Special relativistic effects for the *matter* are taken into account, if the relativistic equation of motion is considered for a derivation of the GSE source term. General relativity requires to consider the red-shift and time-lapse in the vicinity of a black hole and also the rotation of space (frame-dragging) around a rotating black hole. Thus, depending on the astrophysical jet source, different versions of the GSE may apply. For most cases of relativistic jets the special relativistic GSE (Camenzind 1987) is sufficient, whereas close to the black hole the general relativistic GSE (Nitta et al. 1991; Beskin & Pariev 1993) must be considered. Here, I show the special relativistic source term of the GSE,

$$\begin{aligned} j_\phi \;=\; & \frac{\mu\,\gamma\,\rho\,c\,R}{1-M_{\rm A}^2-R^2/R_L^2(\Psi)}\left(\frac{1}{\mu}\left(\,\partial_\Psi E(\Psi)-\Omega\,\partial_\Psi L(\Psi)\right)-\frac{u_{\rm p}^2}{\gamma}\partial_\Psi \ln\frac{\eta(\Psi)}{\rho}\right) \\ & +c\,R\,\frac{B_\phi^2}{4\pi}\,\partial_\Psi \ln\eta(\Psi)-\frac{c}{4\pi\,c\,R^2}\frac{R}{R_L(\Psi)}\left(\nabla\Psi\cdot\nabla\right)\left(R^2\Omega_{\rm F}(\Psi)\right), \end{aligned} \tag{4.17}$$

with the Lorentz factor γ, the poloidal component of the 4-velocity $u_{\rm p}$, and the Alfvén Mach number squared $M_{\rm A}^2=4\pi\gamma\rho u_{\rm p}^2/B_{\rm p}^2$. The GSE is a partial differential equation of second order. It can be considered as "highly" non-linear as the source term shows a very complicated (and *a priori* unknown) dependency on the flux function Ψ. The GSE source term also includes singular surfaces where $(1-M_{\rm A}^2-R^2/R_L^2)=0$. These are the *magneto-sonic surfaces* where the plasma velocity equals the speed of the magneto-sonic waves. As already mentioned, due to the complexity of this equation, it has not yet been possible to find two-dimensional fully self-consistent solutions in general. The single example of a rotating monopole-type field configuration (Sakurai 1985) is obtained in the limit of slow rotation (and thus does not show substantial collimation).

A special case is the *force-free* (relativistic) GSE where inertial terms in the source term are neglected. This is equivalent to the assumption that magnetic forces dominate over inertial forces. This version of the GSE equation is also known as *pulsar equation*. It considers the projection of the force-free equation of motion, $0=\rho_{\rm e}\,\vec{E}+\frac{1}{c}\vec{}\times\vec{B}$ (with the charge density $\rho_{\rm e}$), perpendicular to the magnetic flux surfaces.

The trans-field force-balance can eventually be written as the *modified* relativistic

GSE, in the force-free case we have

$$x\nabla\cdot\left(\frac{1-x^2\Omega_{\rm F}^2(\Psi)}{x^2}\nabla\Psi\right)=-g_I\frac{1}{x}\frac{1}{2}\frac{d}{d\Psi}I^2(\Psi)-x|\nabla\Psi|^2\frac{1}{2}\frac{d}{d\Psi}\Omega_{\rm F}^2(\Psi) \qquad (4.18)$$

(see e.g. Camenzind 1987), where we have normalized with $(R,Z)\rightarrow(x\,R_{\rm o},z\,R_{\rm o})$; $\Omega_{\rm F}\rightarrow\Omega_{\rm F}\,(c/R_{\rm o})$; $\Psi\rightarrow\Psi\,\Psi_{\rm mx}$; $I\rightarrow I\,I_{\rm mx}$. The radius $R_{\rm o}$ is the location of the *asymptotic* light cylinder, i.e. the asymptotic branch of the light surface $R_L(\Psi)$ for $z>>1$. At the light surface, where $R=R_{\rm L}(\Psi)\equiv c/\Omega_{\rm F}(\Psi)$, the source term of the force-free GSE becomes singular. The term "modified" refers to the fact the the singularity of the source term has been incorporated into the l.h.s. of Eq. (4.18). For differentially rotating magnetospheres the shape of this surface is not known *a priori* while for constant field rotation the light surface is of cylindrical shape. The normalization is chosen such that $\Omega_{\rm F}=1$ at $x=1$. Note that in the force-free case also the total poloidal electric current is conserved along the field line, $I(R,Z)=I(\Psi)$. Both the current distribution, $I(\Psi)$, and the rotation law of the field, $\Omega_{\rm F}(\Psi)$, determine the source term of the GSE and govern the structure of the magnetosphere. The constant g_I describes the strength of the first source term in the GSE. A usual estimate for active galactic nuclei is

$$g_I=\frac{4I_{\rm mx}^2R_{\rm o}^2}{c^2\Psi_{\rm mx}^2}\simeq 4\,\left(\frac{I_{\rm mx}}{10^{18}{\rm A}}\right)^2\left(\frac{R_{\rm o}}{10^{16}{\rm cm}}\right)^2\left(\frac{\Psi_{\rm mx}}{10^{33}\,{\rm Gcm}^2}\right)^{-2}.$$

Close to a rotating black hole, general relativistic effects must be taken into account. Using the 3+1 split of space-time (Thorne et al. 1986), the general relativistic expressions become similar to the special relativistic equations. The modifications concern a red-shift factor α in order to transform the local field and velocities to the global reference frame, and the differential rotation of space ω (frame dragging of a rotating black hole). With that, Ampère's law is modified to $\nabla\times\alpha\vec{B}=(4\pi/c)\alpha\vec{j}-(1/c)(\vec{E}\cdot\nabla\omega)\vec{m}$, with the Killing vector $\vec{m}=\tilde{\omega}^2\nabla\phi$. The force-free GSE in Kerr metric is

$$\tilde{\omega}\nabla\cdot\left(\alpha\,\frac{1-(\tilde{\omega}/\tilde{\omega}_{\rm L})^2}{\tilde{\omega}^2}\nabla\Psi\right)=-g_I\frac{1}{\alpha\tilde{\omega}}\frac{d}{d\Psi}I^2(\Psi)-\tilde{\omega}\,\frac{\Omega_{\rm F}-\omega}{\alpha}|\nabla\Psi|^2\frac{1}{2}\frac{d}{d\Psi}\Omega_{\rm F}^2(\Psi), \qquad (4.19)$$

in Boyer-Lindquist coordinates (Blandford & Znajek 1977; Thorne et al. 1986; Okamoto 1992) and with a normalization similar to Eq. (4.18). Here, $\tilde{\omega}$ corresponds to the cylindrical radius and $\tilde{\omega}_{\rm L}$ denote the position of the two light surfaces, $\tilde{\omega}_{\rm L}^2=\left(\pm\alpha/(\Omega_{\rm F}-\omega)\right)^2$. The $+/-$ signs hold for the outer ($\Omega_{\rm F}>\omega$) and inner ($\Omega_{\rm F}<\omega$) light surface, respectively.

Finally, I discuss the GSE in another form which is probably more transparent in showing the mechanisms determining the jet structure in the collimation region,

$$\tilde{\kappa}\left(1-M_{\rm A}^2-x^2\Omega_{\rm F}^2\right)\;=$$
$$\left(1-x^2\Omega_{\rm F}^2\right)\frac{\nabla_\perp B_{\rm p}^2}{8\pi}+\frac{\nabla_\perp B_\phi^2}{8\pi}+\nabla_\perp P+\left(\frac{B_\phi^2}{4\pi}-\rho u_\phi^2\right)\frac{\nabla_\perp x}{x}-\frac{B_{\rm p}^2\Omega_{\rm F}}{4\pi}\nabla_\perp(x^2\Omega_{\rm F}).$$

Here, $\nabla_\perp$ indicates the gradient perpendicular to Ψ, $\tilde{\kappa}\equiv\kappa B_{\rm p}^2/4\pi=\vec{n}\cdot(\vec{B}_p\cdot\nabla)\vec{B}_p/4\pi$

the poloidal field curvature, ρ the mass density and u_ϕ the toroidal speed (Chiueh et al. 1991; Appl & Camenzind 1993a). With this representation of the GSE one can easily identify the forces contributing to the stationary jet equilibrium. The first term considers the curvature of the poloidal field ($\tilde{\kappa}$) leading to a tension force, but takes into account also the de-collimating centrifugal force due to the motion of the matter along the curved poloidal field line $-\tilde{\kappa}(M_{\rm A}^2 + x^2\Omega_{\rm F}^2)$. The first term on the r.h.s. is the poloidal magnetic field pressure gradient reduced by the pressure gradient of the electric field $\sim x^2\Omega_{\rm F}^2\nabla_\perp B_{\rm p}^2$. The next term is the toroidal magnetic field pressure gradient. The terms in the parenthesis after the gas pressure gradient consider the collimating force of the toroidal field tension and the de-collimation due to centrifugal forces of the rotating plasma. The last term combines the tension of the curved poloidal field and the (relativistic) effect of the space charge density.

4.6 The wind equation – the force-balance along the field

The wind equation considers the force-balance along the field line or flux surface, governing the dynamics of the MHD flow. Also known as Bernoulli equation, the wind equation represents the integrated stationary MHD energy equation. Basically, the wind equation / energy equation can be obtained by combining the expressions for the conserved quantities. In the Newtonian limit and for a polytropic gas law the energy equation is

$$E = \frac{v_p^2}{2} + \frac{\Omega_{\rm F}^2}{2}\left(\frac{M_{\rm A}^2 R_{\rm A}^2 - R^2}{R(M_{\rm A}^2-1)}\right)^2 + \frac{c_{\rm s\star}^2}{\Gamma-1}\left(\frac{M_{\rm A\star}^2}{M_{\rm A}^2}\right)^{\Gamma-1} - \frac{GM}{\sqrt{R^2+Z^2}} - \Omega_{\rm F}^2\frac{R_{\rm A}^2-R^2}{M_{\rm A}^2-1}, \tag{4.20}$$

where M is the central mass, $c_{\rm s}$ the sound speed, Γ the polytropic index in the gas law, and $M_{\rm A}$ the Alfvén Mach number. The asterix denotes a value at the foot point of the field line. Note that in Eq. (4.20) there are conserved quantities along the considered flux surface, $E(\Psi)$, $\Omega_{\rm F}(\Psi)$, $R_{\rm A}^2(\Psi) = L(\Psi)/\Omega_{\rm F}(\Psi)$, and other quantities, which vary along the field line, e.g. $B(R)$, $\rho(R)$, $v(R)$. The typical approach is that one prescribes the shape of the poloidal magnetic field surfaces given by $Z = Z(R)$, and the poloidal field strength defined by the flow magnetization (see below) and then solves the wind equation at each radius and for the certain boundary conditions. In general, the combination of the solutions for each radius gives several solution *branches* for $v_{\rm p}(R)$. From these one have to find out the *physical* solution branch of the wind solution.

The location where the plasma velocity equals the speed of the magneto-sonic waves are called the magneto-sonic point (see also Sect. 3.4). At the slow and fast magneto-sonic point the wind equation may become singular. At the Alfvén point the wind equation is regular, i.e. for all solutions the Alfvén Mach number is $M_{\rm A} = 1$ at the Alfvén radius $R = R_{\rm A}$ (see last term of Eq. 4.20). Therefore the angular momentum $L = \Omega_{\rm F}R_{\rm A}^2$ is determined. The requirement of regularity of the solution at the other two magneto-sonic points determines the other two parameters of the flow. The mass flow rate $\eta(Psi)$ (or the flow magnetization $\sigma(\Psi)$) is fixed by the regularity condition at the slow magneto-sonic point while the energy $E(\Psi)$ is fixed by the fast magneto-sonic point.

The most general version of the stationary wind equation is that of a general relativistic

MHD flow. In this case the wind equation for the relativistically defined poloidal velocity $u_{\rm p} \equiv \gamma v_{\rm p}/c$ is

$$u_{\rm p}^2 + 1 = -\sigma_{\rm m} \left(\frac{E}{\mu}\right)^2 \frac{k_0 k_2 + \sigma_{\rm m} 2 k_2 M_{\rm A}^2 - k_4 M_{\rm A}^4}{(k_0 + \sigma_{\rm m} M_{\rm A}^2)^2}\,, \tag{4.21}$$

where

$$k_0 = g_{33}\Omega_{\rm F}^2 + 2g_{03}\Omega_{\rm F} + g_{00}, \quad k_2 = 1 - \Omega_{\rm F}\frac{L}{E}, \quad k_4 = -\frac{g_{33} + 2g_{03}\,L/E + g_{00}\,L^2/E^2}{g_{03}^2 - g_{00}g_{33}}.$$

(Camenzind 1986, Takahashi et al. 1990). Here, the Alfvén Mach number is defined by $M_{\rm A}^2 = 4\mu n u_{\rm p}^2/\tilde{B}_{\rm p}^2$, with the proper particle density n, the specific enthalpy μ, and a poloidal magnetic field $\tilde{B}_{\rm p} = B_{\rm p}/(g_{00)} + g_{03}\Omega_{\rm F})$, rescaled for mathematical convenience. The $\sigma_{\rm m}$ stands for the sign of the metric defined by the components of the metric tensor g_{ij}

In general, for a polytropic gas law (polytropic index $\Gamma \equiv n/m$), the wind equation (for example Eq. 4.21) can be converted into a polynomial equation,

$$\sum_{i=0}^{2n+2m} A_i(x;\Psi,\Phi;\Omega_{\rm F};E,L,\sigma_\star)\; u_{\rm P}^{i/m} = 0\,, \tag{4.22}$$

where the coefficients A_i are now functions of the normalized cylindrical radius x. The shape of the axisymmetric magnetic flux surface $\Psi(x,z)$ is prescribed as function $z(x;\Psi)$. The flux function $\Phi = B_{\rm p}x^2$ describes the opening of the flux tube. The faster Φ decreases the more rapidly the magnetic energy is be converted into kinetic energy. This behavior is similar to a hydrodynamic de Laval *nozzle*.

The essential parameter for the magnetic jet is the *magnetization* parameter (Michel 1967). We define the dimensionless magnetization parameter at the "injection" point of the matter into the jet $x_\star$,

$$\sigma_\star = \frac{\Phi_\star^2}{4\pi m_{\rm p} I_{\rm p\star}}. \tag{4.23}$$

The magnetization parameter measures or the Poynting flux in terms of particle flux $I_{\rm p} \equiv n u_{\rm p} x^2$ where $m_{\rm p}$ is the particle mass (here the proton mass). Equivalently, it determines the strength of the magnetic forces in terms of inertial forces or the magnetic energy in terms of kinetic energy, The magnetization determines the maximum energy available for plasma acceleration and thus determines also the asymptotic poloidal velocity.

In the case of a hot relativistic proton-electron plasma the polytropic index is $\Gamma = 5/3$ (a hot electron-positron plasma would imply $\Gamma = 4/3$). Then, at each radius x the polynomial equation (4.22) has $2n + 2m = 16$ solutions. Some of these mathematical solution branches have no physical meaning, e.g. because $u_{\rm p}^2$ is negative. The remaining physical solutions form a bunch (typically 2-3) of different curves in the $u_{\rm p}(x)$-diagram representing different solution branches[2]. The unique branch of *the* wind solution starts

[2]This is similar to the case of a stationary hydrodynamic accretion or wind flow (Parker wind), where the wind

at small radius with small velocity continuing outwards with increasing velocity. For an other parameter choice also 'accretion' branches can be found, starting from a large radius with small velocity and continuing inwards with increasing velocity.

As already discussed, not for all parameters E, L, σ there exist *physical* solutions which are continuous for all radii x. The *critical* parameters are just fixed by the regularity condition of having a smooth transition of the flow across the magneto-sonic points. In order to match astrophysical boundary conditions one can thus use the following free parameters,

- *the 'injection' radius,* $x_\star$, the location where the matter couples to the magnetic field. This radius also determines the iso-rotation parameter Ω_F.
- *the 'injection' velocity* $u_{\mathrm{p}\star} = u_\mathrm{p}(x_\star)$, defining the initial kinetic energy.
- *the Alfvén radius* x_A, which fixes the total angular momentum of the flow.

The critical wind solution for a given flux surface can then be found by varying the flow parameters E and $\sigma_\star$ in Eq. (4.22). Due to numerical convenience, one may instead vary

- *the sound speed* $c_{\mathrm{s}\star}$ at the injection radius, defining the initial density (or gas pressure and temperature),
- *the magnetization* parameter at the injection point $\sigma_\star(\Psi) = \Phi_\star^2/(4\pi m_\mathrm{p} I_{\mathrm{p}\star})$.

In turn, the condition of a regular flow at the magneto-sonic points fixes the sound speed and magnetization and, thus, jet mass flow rate and temperature.

equation gives two solution branches depending on the mass flow rate. Only one of those branches, i.e. the solution for the critical mass flow rate, is the 'true' stationary wind solution

Chapter 5
Formation of magnetic jets – the present state of theoretical studies

The majority of theoretical work on magnetohydrodynamic jets were initiated by the authoritative paper by Blandford & Payne (1982). Many of these first papers were considering *stationary* MHD models with only few exceptions of *MHD simulations* presented. In the mid 90ies the computational power became sufficient enough to carry out also time-dependent MHD simulations of the jet formation process with reasonable numerical resolution.

In the following the recent development in the theoretical understanding of the formation of magnetic jets – acceleration and collimation – will be summarized. There are good reasons to follow the traditional way and separate the topic in two parts – stationary MHD and MHD simulations. With the exception of just a few examples where analytical solutions to the MHD jet equations are feasible, all MHD solutions so far are the result of a *numerical* computation.

It is of course not possible to discuss or even mention every single paper published on this topic. I will try to give a fair reference to the most influential work done so far and discuss this in respect to my own work during the last years.

5.1 Stationary MHD models

If time-dependent processes are neglected for the solution of the MHD equations, the computational task is considerably reduced. The main advantage of the stationary approach is the possibility to obtain a *global* solution for the magnetic field structure, i.e. the field distribution from the inner boundary of a star or disk up to the asymptotic jet at distances of several thousand times the radius of the central object. Such a spatial resolution cannot yet be achieved by time-dependent MHD simulations. It should also be mentioned that the calculated stationary solution is *exactly defined* by the *regularity condition* at the magneto-sonic surfaces[1]. In the case of time-dependent computations, it is sometimes difficult to decide whether certain features of the simulation are numerical artifacts or indeed represent physical effects.

Due to the fact that extragalactic jets have been discovered earlier then protostellar jets, the early theoretical models were mostly concerned with the formation of *relativistic* jets

[1]However, in the stationary approach the magneto-sonic surfaces become *singular surfaces* of the governing equations. and, as a matter of fact, it is just these singularities, which causes the most serious difficulties for the stationary treatment

(however, not always treating the relativistic equations). In fact, in the case of stationary MHD, relativity is *not* the major difficulty in solving the MHD equations. The difficult part is the inter-action between matter and field, in particular the back-reaction of the plasma inertial forces on the magnetic field structure. Relativistic jets can be considered as almost force-free, and considerable understanding concerning the jet magnetic field structure could derived from solutions of the *force-free* MHD equations. Protostellar jets have a much higher mass load and the force-free approach can hardly be applied.

5.1.1 The self-similar ansatz and related approaches

The before mentioned mathematical complications of MHD have led many authors to look for special types of separable solutions which avoid the problems of the general two-dimensional integration. It was one of the basic ideas of Blandford & Payne to assume a *self-similar* geometry for the MHD jet structure. Self-similarity provides quite a powerful simplification for the MHD equations. In particular, this approach reduces the partial differential equation of second order (the Grad-Shafranov equation) to a set of ordinary differential equations. Self-similarity can be motivated by the power law distribution of certain physical quantities within the accretion disk which is (in these models) the origin of the jet. For a standard accretion disk model with Keplerian rotation, the power law distribution holds e.g. for the density, pressure, and magnetic field distribution. While a self-similar jet geometry can be expected close to the disk, it is clear that the far-disk jet structure cannot be self-similar. Some important features[2] which actually do constrain the solution but are not be included in a self-similar model, are the *jet axis* and the outer *jet radius* being almost of cylindrical shape and at finite distance from the axis (self-similar models extend to infinity). Also the light cylinder of relativistic jets is not self-similar.

The major outcome of the BP82 paper is the self-consistent calculation of the self-similar force-balance of collimating, cold (pressure-less) wind flows from a Keplerian accretion disk. Some limitations in this model were taken care of by other authors. For example, Li et al. (1992) generalized the Blandford-Payne self-similarity ansatz to *relativistic* jet solutions. Pelletier & Pudritz (1992) extended the BP82 approach taking into account gas pressure and a more general ansatz for the field structure. This is especially interesting close to the accretion disk where the jet is launched because in the stationary wind theory the slow magneto-sonic point (which is defined only when gas pressure is taken into account) defines the *mass flow rate* in the jet. As the vertical gas pressure gradient supports the launching of a jet, the critical launching angle for the disk magnetic field is decreased from 30° (Blandford & Payne) to about 18°. The ansatz by Pelletier & Pudritz (1992) also drops the assumption of self-similarity. The flux geometry is fully two-dimensional, however, the authors consider the separate MHD domains (sub slow to super fast magneto-sonic) separately. Under the assumption of a power law disk magnetic field distribution they reduce the GS equation in the asymptotic domain to a *linear* partial differential equation obtaining a cylindrical flow structure there, but with a re-collimating property in the case of high fast magneto-sonic Mach numbers.

[2] We discuss here the assumption of r-self-similarity, i.e. self-similarity in the cylindrical or spherical radius. Some other models use a θ-self-similarity and can be applied to stellar magnetospheres (Sauty & Tsinganos 1994).

There are also other MHD jet solutions available which apply a *non* self-similar ansatz. However, not all of these models cannot be considered as a fully self-consistent two-dimensional approach. One example is the self-consistent relativistic solution of the GS equation presented by Li (1993). In this case the self-similar assumption is not used. However, the author prescribes the position of the "first" magnetic flux surface close to the jet axis and then calculates the force-balance outside of this flux surface till a finite jet radius (Fig. 5.1). The other example is Lovelace et al. (1991, 1993) who proposed a general theory of MHD jets not underlying the self-similar scaling. Instead, a parameterization of the cylindrical radius in terms of the jet radius was chosen together with a separation of variables. The jet solution was than obtained by solving the conservation laws of ideal, stationary, axisymmetric MHD. This is a unique and clever approach as the stationary MHD conservation laws are conserved by definition. However, it does not consider the (more difficult) problem of the *local* force-balance described by the GS equation. In Contopoulos & Lovelace (1994) the authors return to the self-similar *ansatz* presenting "exact" (numerical) solutions. The term "exact" indicates that now the local force-balance is taken into account. This approach has been extended later to the special relativistic case (Contopoulos 1994, 1995a).

Contopoulos (1995b) proposed an alternative model for jet formation in the absence of large poloidal magnetic fields. In this case the Blandford-Payne magneto-centrifugal sling-shot mechanism cannot work and the matter is instead accelerated by the pressure gradient of strong toroidal fields provided by the accretion disk. In particular Contopoulos applied this model to explain the time-dependent ejection of knots in the jet.

I will discuss the work on self-similar jet models by Tsinganos and collaborators in Sect. 5.1.6.

5.1.2 Asymptotic jet collimation

Another way to simplify the jet MHD equations is the approach to obtain *asymptotic* solutions at large distance away from the origin of the jet flow. In a fundamental paper, Heyvaerts & Norman (1989) analytically derive that axisymmetric MHD flows enclosing a *net* poloidal current will always collimate to a cylindrical shape asymptotically. A vanishing electric current will lead to an un-collimated conical jet structure. This important result, obtained for the Newtonian case, has been extended later also for the case of relativistic jets (Chiueh et al. 1991)

The force-balance within such an asymptotically cylindrical jet can be described by the one-dimensional GS equation (with the radius as only variable). For this limit and for the case of relativistic jets Appl & Camenzind (1993a,b) obtained an analytical solutions of the local force-balance. In their solutions the jet equilibrium is characterized by the existence of a *core radius*. Magnetic flux and electric current is concentrated predominantly within the core radius. If the jet radius changes, for example by a change in the external pressure, the core of the jet remains more or less the same and only the outer region of the jet – the envelope – are affected. These analytical solutions of the asymptotic force-free jet equilibrium can be used e.g. as a boundary condition for the two-dimensional approach. These asymptotic solutions was also extended for differential rotation (Fendt 1997b).

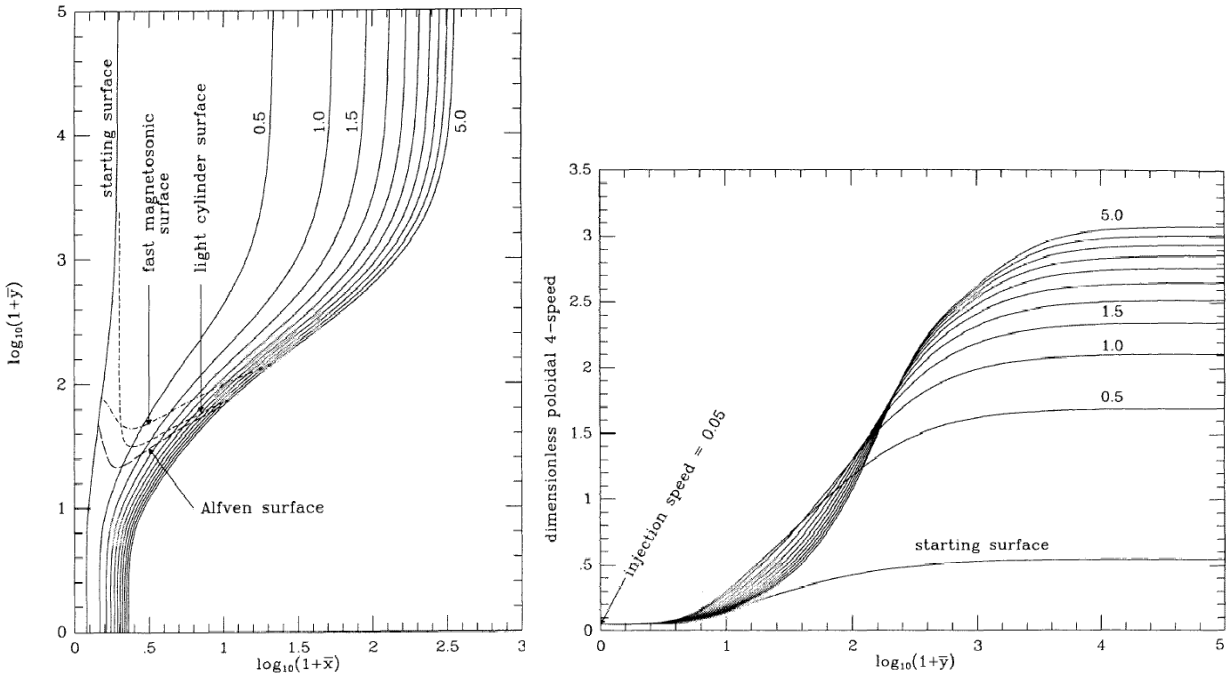

Figure 5.1. Solution of the relativistic GS equation (Li 1993). *Left* Shape of magnetic flux surfaces (dimensionless flux Ψ spaced by 0.5). *Right* Flow acceleration curves on these flux surfaces.

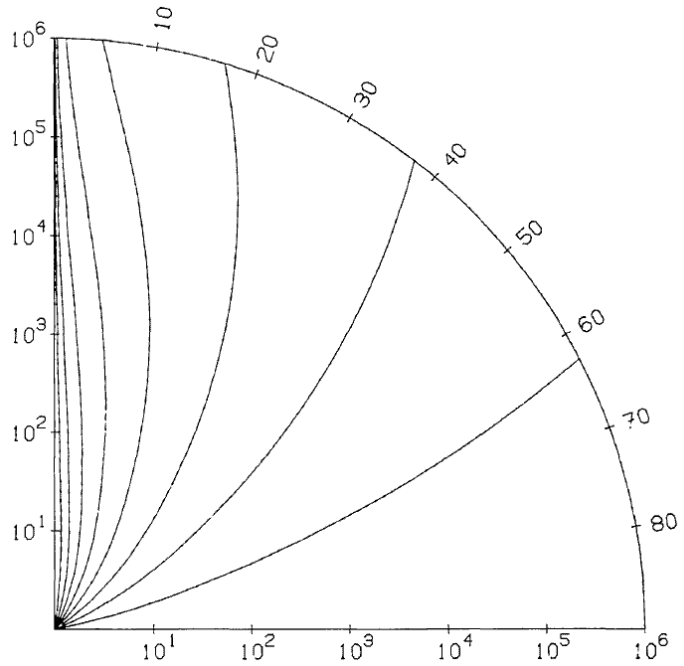

Figure 5.2. Self-consistent two-dimensional solution of the GS equation (Sakurai 1985). Structure of poloidal field lines at large distance plotted in logarithmic scale in spherical radius r. The Alfvén radius is located from about $r = 1$ (equator) to $r = 3$ (pole).

5.1.3 A self-consistent truly two-dimensional solution

This subsection is to give a reference to the unique case of a truly two-dimensional, self-consistent solution to the GS equation. Sakurai presented non-relativistic solutions of the GS equation for a stellar wind (an initially radial outflow, Sakurai 1985) and for a disk wind (a so-called split-monopole setup as initial configuration, Sakurai 1987). The remarkable fact is that these results from almost two decades ago are still the only fully two-dimensional, non force-free stationary MHD solutions available in the literature. However, due to the slow rotation, Sakurai's solutions essentially show a low degree of collimation, with the flow collimating only on a logarithmic scale (Fig. 5.2). This is in contrast to the observations indicating a rapid collimation of the protostellar jet within 100 AU.

5.1.4 Special relativistic MHD jets in the two-dimensional approach

Camenzind (1986, 1987) developed a fully two-dimensional, relativistic formalism for stationary magnetohydrodynamic jets. The method of *finite elements* has been introduced in order to solve the GS equation numerically for any choice of boundary conditions. Some example solutions for the relativistic jet magnetosphere and the wind dynamics in these jets were presented. These solutions were fully two-dimensional, however, not really global solutions since the inner and outer solutions (separated by the light cylinder) were obtained separately and did not satisfy the *same* regularity condition along the light cylinder. However, as an essential point in the understanding of MHD jets, it became clear that the diverging magnetic field structure acts just in the same way as the hydrodynamic de-Naval *nozzle*.

The relativistic wind equation as applied for MHD jets has also its progenitor in the stellar wind theory in particular in the subject of pulsar winds. The relativistic GS equation in its force-free version is also known as *pulsar equation* and has been examined by a number of authors. In order just to mention the most well known of these pulsar models, we cite Michel (1969, 1973a,b), Goldreich & Julian (1969, 1970), Okamoto (1974a,b; 1975a,b, 1978), Ghosh et al. (1977), Ghosh & Lamb (1978, 1979a,b). The Michel (1969) reference is of particular importance, as it introduces the *Michel magnetization parameter* σ and clarifies its role as *the* essential parameter concerning the acceleration of the MHD flow. The σ-parameter couples the three important ingredients for the launching of a MHD wind – the magnetic flux, the mass flux and the rotation of the wind launching object (a star or a disk).

As an extension of the classical pulsar magnetosphere models Sulkanen & Lovelace (1990) presented two-dimensional force-free solutions of the GS equation where the pulsar magnetosphere asymptotically collimates into a jet. However, also for these solutions the light cylinder regularity condition has not been treated properly and the derived field structure cannot be considered as a *global* two-dimensional solution.

Global numerical solutions to the two-dimensional relativistic force-free force-balance were presented for collimating jet magnetospheres from highly magnetized stars (Fendt et al. 1995), and for rotating black holes taking into account Kerr metric (Fendt 1997a). Essentially, these solutions take advantage from the analytical asymptotic (one-dimensional)

solution of Appl & Camenzind (1993b). Using asymptotic solution including also differential rotation (Fendt 1997b), Fendt & Memola (2001) derived the structure of two-dimensional relativistic magnetospheres with differentially rotating foot points of the field lines (e.g. an accretion disk). This allows actually for a scaling of the special relativistic magnetosphere (normalized to the light cylinder radius) in terms of the size/mass of the central source, as the Keplerian rotation of the disk is related to the central mass.

The field distributions calculated by Fendt and collaborators represent *global* solutions to the *local* cross-field force-balance equation. Essentially, these papers also presented a method to solve the *matching problem* of relativistic force-free magnetospheres, a well known feature in the context of pulsar magnetospheres. It became clear that a mismatch at the light cylinder could be removed by a proper adjustment of the current distribution and the outer boundary condition. Such a procedure can be interpreted as an adjustment of the "magnetic pressure equilibrium" between the regions inside and outside the light cylinder.

Another approach to the problem of relativistic MHD outflows was undertaken by Bogovalov (1997), who, obtaining stationary relativistic MHD solutions by solving the time-dependent problem, found indication for instabilities in the case of high magnetization. However, it is not clear (to me), whether the cause of these instabilities is numerical or really physical. Interestingly, Bogovalov finds solutions only with a weak degree of collimation.

So far, the force-free solutions presented by Fendt et al. are yet the only truly global, two dimensional stationary MHD solutions for relativistic jets available in the literature. The drawback of the force-free approach is the point that inertial forces in the jet are neglected. These, however, might especially be important in the collimation region of the jet, although convincing arguments were given that for highly relativistic jets the plasma inertial back reaction may indeed be neglected (Contopoulos & Lovelace 1994, Fendt 1997a, Fendt & Memola 2001).

5.1.5 Jet magnetospheres around black holes

Stationary axisymmetric vacuum electro-magnetic fields around a Kerr black hole have been investigated first by Petterson (1975) and King et al. (1975). Blandford & Znajek (1977) and Znajek (1977, 1978a,b) recognized the possibility that force-free magnetic fields coupled to a fast rotating black hole may lead to the extraction of rotational energy and angular momentum from the hole by a pure electro-magnetic process – a process which is now called Blandford-Znajek mechanism. In a simplified picture this may happen if the rotational velocity of the black hole $\Omega_{\rm H}$ differs from that of the magnetic field lines $\Omega_{\rm F}$ (the iso-rotation parameter). Considering these field lines as rigid wires they may just break the black hole rotation. The field lines may either be anchored in the surrounding accretion disk or in a Poynting flux dominated jet from the black hole. The mass flux in the jet is sustained by $\mathrm{e}^+ - \mathrm{e}^-$ pair production in the close magnetosphere and also provides the particles to drive electric currents. Interestingly, the Blandford-Znajek mechanism of energy extraction can be related to *Ohmic dissipation* corresponding to an internal effective resistance of the black hole of 30 Ohm (Znajek 1978b).

With the development of the 3+1 split of Kerr space-time (Thorne & Macdonald 1984,

Macdonald & Thorne 1982, Thorne et al. 1986) the interpretation of electrodynamic processes around rotating black holes becomes more transparent. For a chosen global time, the tensor description may be split up in the usual fields vectors $\vec{B}$, $\vec{E}$, the usual current density $\vec{j}$, and a scalar charge density. With that, the MHD equations can be formulated very similar to their version in flat Minkowski space. Using this powerful tool, Macdonald (1984) calculated numerical solutions for the magnetic field force-balance around rotating black holes. Three models (magnetic field distribution roughly radial, uniform, or paraboidal) of differentially rotating magnetospheres were investigated, however, the integration region was limited to $\lesssim 10$ horizon radii.

Okamoto (1992) investigates the evolution of a force-free black hole magnetosphere and the possibility of energy and angular momentum extraction due to a wind. Also, by examining the fast magneto-sonic point for the outgoing wind and for the wind directed towards the black hole, he derived an analytical expression for the poloidal current $I(\psi)$ and the field rotation law $\Omega_{\rm F}(\Psi)$ along a single magnetic field line. This work has been further extended to non-degenerate magnetospheres under the assumption of a split-monopole field structure (Horiuchi et al. 1995).

The general relativistic expression for the stationary trans-field equation including inertial effects is derived by Nitta et al. (1991) and Beskin & Pariev (1993). This is the *most general version of the Grad-Shafranov equation*.

In Fendt (1997a) the general relativistic Grad-Shafranov equation is solved in the limit of force-free MHD (see Fig. 5.3). Truly two-dimensional solutions were obtained for collimating jet magnetospheres from disks around rotation black holes. The solutions extend from the inner light surface close to the black hole horizon through the outer light surface to the asymptotically cylindrical jet. For the asymptotic jet the one-dimensional analytical jet solution of Appl & Camenzind (1993b) could be used, as in this region general relativistic effects are unimportant. Again, taking into account a proper treatment of the regularity condition along the light cylinder, the resulting field structure is a truly global solution of axisymmetric MHD.

Solutions of the so-called wind equation in Kerr geometry considering the stationary plasma motion along the magnetic field were obtained by Takahashi et al. (1990), however, mainly discussing the accretion flow onto the black hole. Fendt & Greiner (2001) extended this work to the outflow regime discussing various specifications for the field line shape and magnetic field distribution. In particular, the influence of the leading parameters of Kerr metric $M = 0$ and $a = 0$ on the flow acceleration has been investigated. In general, the wind flow for a smaller angular momentum parameters a is faster. The interpretation is that the effective potential of a black hole weakens for increasing values of a. Therefore, less magnetic energy is necessary to overcome the effective potential. The results have been be applied to the case of microquasars with moderate asymptotic Lorentz factors of about 2.5 (e.g. GRS 1915+105). Taking in to account these magnetohydrodynamic wind solutions, Memola et al. (2002) were able to derive a thermal, optically thin X-ray spectrum of the jet flow very close to its origin (Fig. 5.4).

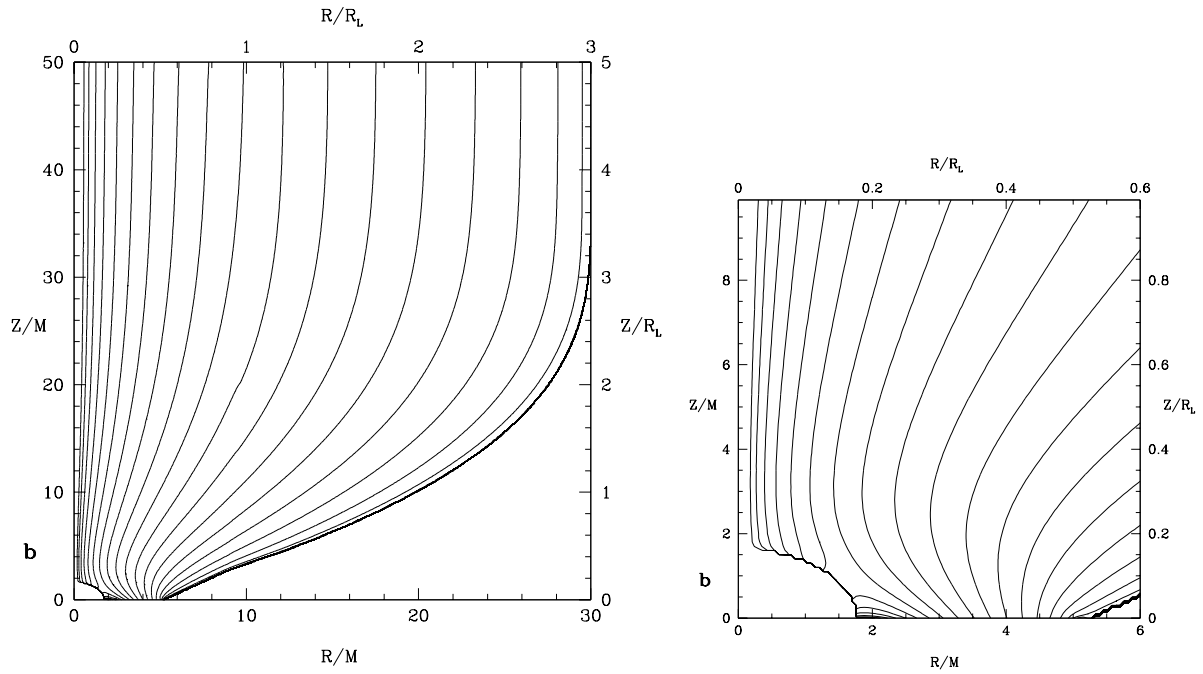

Figure 5.3. Two-dimensional magnetic field structure of a jet from a rotating black hole. Solution of the GS equation in Kerr metric (Fendt 1997a) Shown is the distribution of poloidal magnetic field lines (flux surfaces) on the global scale (*left*) and close to the black hole (*right*). The length scale is normalized to the asymptotic light cylinder radius (upper / right boundary) or to the gravitational radius (lower / left boundary), respectively. The ellipsoidal sphere close to the origin indicates the inner light surface and is also the inner boundary for the calculation.

5.1.6 Protostellar jets – high mass load and complex internal geometry

Most of the theoretical work discussed above was originally related to the issue of *extragalactic* jets. Pudritz & Norman (1983, 1986) were first to suggest that bipolar outflows from young stellar objects are centrifugally driven hydromagnetic winds from rotating disks. Here, the important point is that in jets from young stars the same mechanism as in the relativistic jets – the magnetic forces – is also responsible for the flow *collimation*. That magnetic fields play an essential role in accelerating plasma from rotating stars and affecting their angular momentum evolution has already been a subject for many years in the context of stellar winds (e.g. Parker 1958, Weber & Davis 1967, Mestel 1968, Goldreich & Julian 1970, Pneuman & Kopp 1971, Belcher & MacGregor 1976, Hartmann & MacGregor 1982). However, it now became clear that astrophysical jets from different kind of sources are generated by a similar process. These models of protostellar jet formation applying stationary MHD were accompanied by the first models of the time-dependent protostellar jet formation (Shibata & Uchida 1985, 1986; Uchida & Shibata 1985, see below).

The early models of protostellar jet formation were essentially *disk jet models* – with the jet being launched from the accretion disk surrounding the central star. However, from the observations it became clear that also the protostar may carry a magnetosphere. Such

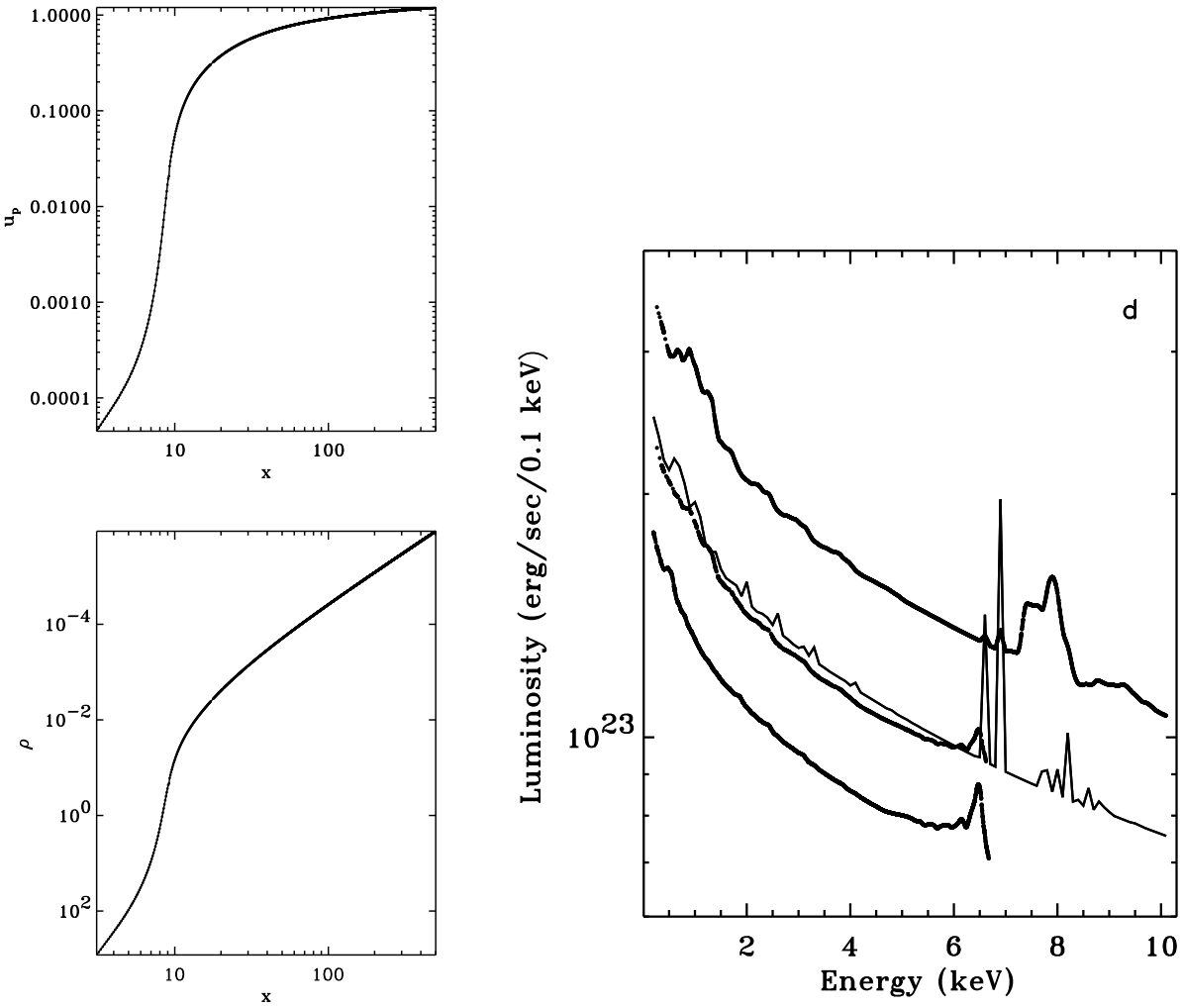

Figure 5.4. Thermal X-ray emission from highly relativistic MHD jets (Memola et al. 2002). *Left* Solution of the MHD wind equation in Kerr metric. Shown is the poloidal velocity $u_{\rm p} = \gamma v_{\rm p}/c$ and the density along a slowly collimating magnetic flux surface (see Fendt & Greiner 2001). The length scale (cylindrical radius x) is normalized to the gravitational radius $r_{\rm g}$, the density to the density at the jet injection radius $8.3\,r_{\rm g}$. *Right* Optically thin thermal X-ray spectrum from the innermost hot regions of the expanding jet. The total spectrum is calculated from the emission of each fluid element of the jet considering its actual velocity, density and temperature. Shown are the total spectra combined of the rest frame spectra (*thin line*) of the flow elements, the Doppler boosted and shifted spectra of the jet elements moving towards (*upper thick line*) and away from (*lower thick line*) the observer, and the combined spectrum of these two components (*middle thick line*). The jet inclination is 20°.

a star-disk-jet magnetosphere has a complex structure where the simplifying assumption of self-similarity cannot be applied anymore.

At the same time it has been recognized that the mass flow rates of stellar jets are relatively high. These can actually be measured by applying shock models to the observed

knots in forbidden emission lines. This is in difference to the case of relativistic jets where the debate about the matter content in these jets (hadronic or leptonic) still continues. The task, therefore, in solving the MHD equations for protostellar jet formation is to find the most general solutions to the GS equation – non self-similar, because of the complex geometry of the YSO, and also non force-free, since stellar jets have a high mass flow rate. So far, this problem has not been solved in general.

It was the model setup of Camenzind (1990) which first combined these features of protostellar jet formation in a self-consistent way. However, while giving estimates for important jet parameters, a solution to the MHD equations was not yet presented. As an interesting aspect, Camenzind (1990) raised the question whether protostellar jets may be explained also in a relativistic context. Due to the fast rotation of the protostar (periods of the order of days), the (hypothetical) light cylinder of the stellar magnetosphere would be located *inside* the observed jet radius. Note that a relativistic treatment of MHD cannot be wrong also for non-relativistic objects, as long as the parameters are chosen properly. Following the approach of Camenzind, global solutions of the GS equation (Fendt et al. 1995) as well as for the wind equation (Fendt & Camenzind 1996) were obtained. These are still they only global, fully two-dimensional solutions treating the scenario of a star-disk-jet magnetosphere. The drawback, however, is the force-free character of the magnetic field.

In a series of papers Shu and collaborators presented an alternative model of a protostellar jet driven by the mass outflow from the *X-point* between the stellar magnetosphere and the accretion disk (Shu et al. 1994a, 1994b). The model solutions so far are not *global*, i.e. the authors present separate solutions for the sub-Alfvénic region (Najita & Shu 1994), the accretion funnel and the "dead zone" (Ostriker & Shu 1995) and also for the asymptotic region of collimation (Shu et al. 1995, Ostriker 1997). The main point of their approach, the proposed existence of an X-point and its ability to launch a jet is under debate (see Ferreira et al. 2000), however the derived model solutions are complete in the sense that they cover the whole spatial range from the central star to the asymptotic jet. They are also self-consistent in the sense that they do not assume in general a self-similar or force-free jet structure.

Yet another self-similar approach was undertaken by Tsinganos and Sauty searching for analytical MHD solutions to the jet problem (Tsinganos & Sauty 1992a,b, Sauty & Tsinganos 1994, Sauty et al. 1999). The approach is that of a so-called meridionally self-similarity, i.e. a self-similarity not in the spherical radius r but in the angle θ. Another new issue here is to consider also a *non polytropic* gas law for the outflow. Some basic assumption which has been made here is to prescribe a spherical shape of the Alfvén surface. These automatically implies that the gas density should be taken as a separable form (Sauty & Tsinganos 1994). Further, only the first order terms of a multipole expansion for the magnetic flux function are taken into account. In the end, the calculations give a (spatially) *oscillating* asymptotic jet structure. As a condition for jet collimation they require an excess of the Bernoulli energy along non-polar stream lines. A similar approach was undertaken by Trussoni and co-authors (Trussoni et al. 1997), however, using an ansatz which *prescribes* the general structure of the field lines.

In the same direction goes the approach by Lery and co-authors who looked for MHD

jet solution prescribing the shape of the magnetic surfaces within the fast magneto-sonic surface (Lery et al. 1998,1999a). With that assumption, the solution could be integrated also in the super magneto-sonic regime.

Kudoh and co-authors investigated in particular the region of the jet launching close to the disk applying one-dimensional stationary MHD models (Kudoh & Shibata (1997a), 1D time-dependent (Kudoh & Shibata (1997b) and two-dimensional time-dependent models (Kudoh et al. 1998) to derive the mass loading from the disk into the jet and, e.g. its dependence from the actual iso-rotation parameter which could be sub-Keplerian. The time-dependent results confirm the stationary solutions in one dimension as well in two-dimensional.

The model of Lovelace et al. (1995, 1999) discusses an essential alternative to the classical Blandford-Payne centrifugal slingshot launching mechanism for jets. They investigate the evolution of a stellar dipolar magnetosphere surrounded by an accretion disk and the associated spin-up/down of the central star. Differential rotation between the star and the disk leads to winding-up the poloidal magnetic field. The magnetic pressure gradient in the induced toroidal field component finally inflates the magnetic field in vertical direction, leaving the possibility of magnetically driven outflows in the region of open field lines. Thus, in difference to the Blandford-Payne magneto-centrifugal acceleration, these outflows are driven by the magnetic pressure gradient in the toroidal magnetic field. These ideas were later confirmed by the MHD simulations (Hayashi et al. 1996, Miller & Stone 1997, Goodson et al. 1997, Fendt & Elstner 2000).

A recent addition to the theory of stationary MHD flows has been presented by Beskin & Kuznetsova (2000) deriving the most general form of the non-relativistic Grad-Shafranov equation where anisotropic pressure effects are formulated within the double adiabatic approximation.

In summary, one must state that the theoretical problem of protostellar jet formation is not yet solved. There is a general agreement about the basic processes. However, there is so far no self-consistent, two-dimensional solution of the stationary MHD equation published which covers all the important features known from the observations – the high mass flux (the plasma inertia), the high degree of collimation, and the complex magnetospheric structure of the star-disk-jet system.

5.1.7 Is there really a MHD self-collimation ?

Recently, there have been a number of papers arguing against the existence of a general self-collimating property of MHD flows. In fact, although such a property has been suggested by Heyvaerts & Norman (1989) and Chiueh et al. (1991) by analytical means, a direct *numerical proof* following the time-dependent evolution of the MHD flow was missing for a long time.

Self-similar models do not include the jet axis and also extend to infinity. They can therefore hardly describe the global structure of the flow. Some of these models show actually a super efficient collimation leading to a re-collimation to the flow towards the jet axis. This, however, has been proven to be indeed an artifact introduced just by the self-similar assumption (Ferreira 1997). The two-dimensional solution by Sakurai does not substantially collimate (note the logarithmic scale in Fig. 5.2). The truly two-dimensional

global force-free relativistic solutions (Fendt et al. 1995, Fendt 1997, Fendt & Memola 2001) do not consider inertial forces which may possibly de-collimate the jet. Further, as a general characteristic, the stationary approach can never tell whether the derived solutions are stable and really stationary in time. One might find that a certain solution exists, but does not know whether it can evolve from some initial state, nor whether it will stay like that if it could evolve further from the stationary state.

In particular, Okamoto and co-workers have raised objections against the self-collimation mechanism as a natural property of any rotating MHD flow (Okamoto 1997, 2000, 2001; Beskin & Okamoto 2000). Okamoto argues that almost all previously developed models of MHD jet collimation or processes claiming magnetic collimation are unsatisfactory with respect to causality and the current-closure condition. He concludes that magnetized winds as a whole will not collimate to the rotation axis without any external help, such as channeling effects of a thick accretion disk and/or confinement by the ambient medium (Okamoto 1997, 1999). Taking into account these constraints, the MHD flows discussed so far in the literature are likely to be asymptotically of "quasi-conically" structure (Okamoto 2000, Beskin & Okamoto 2000, Okamoto 2001).

So far, the question of a self-collimation of MHD jets has not yet been answered definitely. I think that with the numerical simulations, we now have a rather good argument for the existence of the MHD jet self-collimation as a generic property. Though, one must note that even if the time-dependent simulations (e.g. Ouyed & Pudritz 1997a) show the flow self-collimation for particular cases, the spatial scales investigated with that simulations is far below the observed global jet structure (see also next section).

5.2 MHD simulations of jet formation

As it is most clearly visible in the moving jet knots, a jet is not a steady state feature. On the other hand, we know that the large-scale jet structure of the jet remains stable for a long time as we see the knots moving in the same direction. Therefore, we might distinguish between the "almost stationary" jet "back-bone", probably consisting of an aligned large-scale magnetic field, and the time-dependent, yet unknown "knot generator". Thus, the formation of knots as a short-time phenomenon might not be directly connected to the large-scale jet structure itself. Indeed, the observed, highly symmetric structure of the protostellar jet HH 212 (Zinnecker et al. 1998) strongly suggest that the generation of knots must triggered by some process intrinsic to the accretion disk.

Thus, one major issue of the simulation of jet *formation* is to prove the feasibility of the MHD self-collimation. With axisymmetric simulations one may prove whether such a mechanism exists at all. Additional three-dimensional simulations can prove the stability of the two-dimensional results. In order to investigate the time-dependent jet *launching*, the accretion disk structure must be included in the treatment. As we will see, this approach is yet limited either by the computational resources or by the choice of the accretion disk model.

The first numerical MHD simulations of jet formation were performed by Shibata & Uchida (1985, 1986) and Uchida & Shibata (1985). Their model consists of a rotation gas disk penetrated by the magnetic field. In general, the rotation of the accretion disk winds

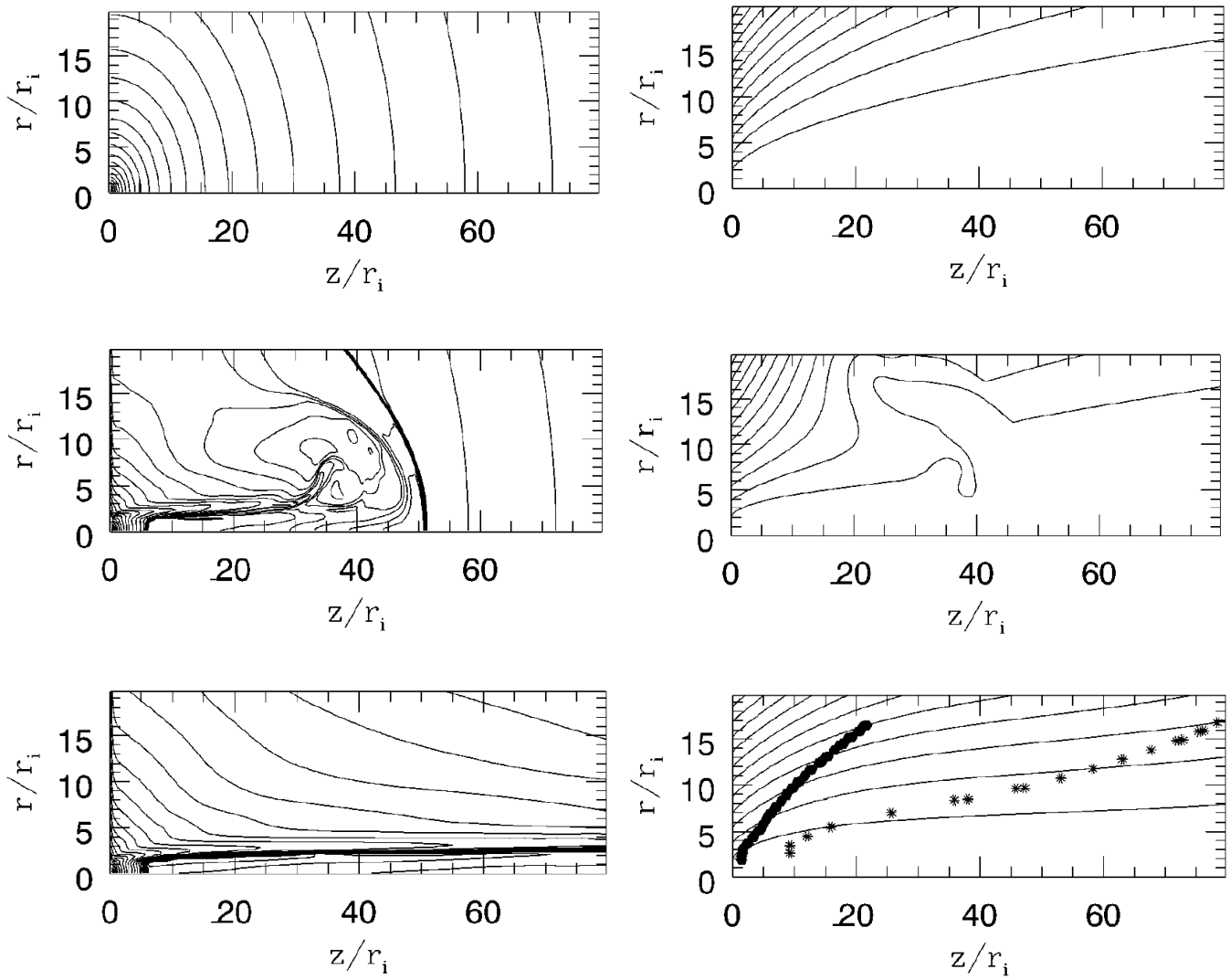

Figure 5.5. MHD simulation of the jet formation from an accretion disk (Ouyed & Pudritz 1997). Shown are the density and poloidal magnetic field distribution at $t = 0, 100, 400$ rotations of the inner accretion disk. The simulations starts with a force-free potential magnetic field in a hydrostatic density distribution. The accretion disk boundary condition is located along the r-axis. The Alfvén surface and the fast magneto-sonic surface is indicated by the asterix.

up the initial poloidal magnetic field. The resulting helically twisted field pushes the gas in polar direction by the Lorentz force. This model is, however, different from the classical approach of Blandford& Payne as it works mainly with the magnetic pressure gradient and not with the magneto-centrifugal acceleration. The removal of disk angular momentum by the magnetic field, also leads to an enhanced accretion. As the disk contracts, the magnetic field becomes advected both in radial and azimuthal direction.

After this early approach towards the numerical jet launching, most of the numerical jet simulations were concentrating on the “simpler” case investigating the evolution of the

asymptotic, collimated jet and its interaction with the interstellar matter. These simulations demonstrate how the jet propagates through the ambient interstellar medium, how the bow shock forms and how the jet can maintain the collimation along the its trajectory (Kössl & Müller 1988; Kössl et al. 1990a,b; Lind et al. 1989; Wiita et al. 1990; Blondin et al. 1990; de Gouveia dal Pino & Benz 1993). Such simulations assume as an "inflow" boundary condition an already collimated flow of high velocity. They do not treat the question, how such a jet can actually be launched.

The topic of modeling the jet *formation* process was again introduced by Ustyugova et al. (1995). The basic idea of this paper is that for a jet formation MHD simulation one may consider the accretion disk "only" as a *boundary condition* for the mass inflow into the corona and the magnetic flux distribution. The evolution of the disk structure is not considered, which allows for a numerical simulation for hundreds of Keplerian periods. With the same ansatz, Romanova et al. (1997) find steady state solutions as a final state of a time-dependent simulation of an initially split-monopole type disk magnetic field. The stationary state has been reached after about 100 Keplerian periods with a clear indication of a flow collimation.

Ouyed & Pudritz (1997a) presented time-dependent simulations of the jet formation from a Keplerian disk. This paper was first to demonstrated numerically the self-collimating property of rotating MHD flows predicted by Heyvaerts & Norman (1989). Essentially, Ouyed and Pudritz start their simulation from a stable hydrostatic initial condition, namely a force-free potential field and a hydrostatic density distribution. During the first evolutionary stages a disk wind evolves and the poloidal magnetic field becomes wound-up due to the differential rotation between the disk and the corona. The disk wind becomes super-Alfénic and super magneto-sonic and collimates to almost cylindrical shape. The jet stream sweeps out the initial corona and after 400 disk rotations a stationary state of a collimated disk wind evolves (Fig. 5.5). The existence of such stationary states, however, depends on the inflow boundary condition along the disk surface. In a follow-up paper Ouyed & Pudritz (1997b) investigated an initially cylindrical magnetic flux distribution. What is interesting here is the fact that an outflow develops at all. The disk wind inertia turns the initially cylindrical poloidal field into a field distribution with an inclination angle satisfying the Blandford& Payne (1982) condition for magneto-centrifugally driven outflows. In the long term evolution, however, these kind of boundary conditions do not lead to a stationary equilibrium state. Instead, this setup works as a *knot generator* emitting the knots from a region along the jet axis (on a spatial scale, however, which is not comparable to the size of the observed jet knots). Ouyed & Pudritz (1999) further investigated the influence of the mass flow rates on the jet collimation. For small mass loads in the jet, they observe the onset of an episodic behavior (instabilities and shocks) of the jet, independent from the initial magnetic configuration.

The paper of Ustyugova et al. (1999) gives a detailed analysis of the stationary state MHD jet solutions obtained from the time-dependent simulations. They claim the that the shape of the computational box may influence the collimation of the flow. In particular, an elongated numerical grid may lead to an artificial collimation of the flow, an effect which does not occur in the case of a grid of spherical or square shape.

The ansatz of a fixed disk boundary condition developed by Ustyugova et al. (1995)

and Ouyed & Pudritz (1997a) has been generalized by Krasnopolsky et al. (1999). In this approach, only the disk magnetic flux is conserved during the simulation, but not the magnetic field direction. The results, however, look quite similar, as they obtain a stationary super fast magneto-sonic jet after some 100 periods. One should note that in difference to Ouyed & Pudritz a smoothed gravitational potential has been used.

Fendt & Elstner (1999, 2000) have also used the approach of a time-independent disk boundary condition, however applying a central stellar *dipolar magnetic field* as initial condition. The main difference is that such a field decreases rapidly along the disk. As the disk magnetic field distribution is preserved during the simulation, this is an important constraint for the jet formation formation – it is basically connected to the question whether the jet originates as a stellar or a disk wind. Fendt & Elstner (2000) also find that the outflow can evolve into a final stationary state, in this case a two component outflow from the stellar surface and from the disk. However, the outflow remain un-collimated on the spatial scales considered. Two potentially important conclusions might be drawn from this results. First, the stellar dipolar field might not be strong enough to drive a collimated jet from the disk surface. Or, alternatively, the collimation of the jet will just happen at larger radii, out of the computational box considered. This would be also consistent with the observations showing a rapid collimation in direction of the jet axis, but, at the same time, a jet radius many time larger than the computational box. If the latter interpretation is correct, the question arises, what actually collimates the jet in the outer regions. External pressure seems to be the only answer.

So far, the jet formation simulations considering the disk as a fixed boundary condition have shown that a MHD self-collimation process seems feasible, although the outcome of the simulation seems to be sensitive to the choice of the disk magnetic flux distribution.

The other class of jet formation simulations considers the disk not only as a boundary condition, but also treats the disk structure together with the launching of the disk wind. Such simulations have been performed for young stellar objects as well as for systems containing a central black hole. The general problem here, and this has not changed since the early work by Uchida and Shibata, is that such simulations can be performed only for a few rotations of the inner disk. The reason seems to be the lack of an appropriate disk model. I will discuss this models in the next section.

5.3 Disk-jet interaction

The ultimate goal for the jet formation theoretician is the simulation of jet formation *out of the accretion disk*. However, so far no general theoretical model exists explaining the onset of jet formation from the accretion disk. The main reason for this “failure” is that several simplifying assumptions usually made when considering the disk or the jet alone are not valid in the case of a combined treatment of both components. The widely used assumption of ideal MHD, for example, is in clear contradiction with a highly turbulent accretion disk. On the other hand, turbulence seems to be an important ingredient in disk physics providing the angular momentum transport as well as the source for a magnetic field generating dynamo. Then, the large contrast between disk in jet in several physical properties, in particular the density, require a very high grid and time resolution.

Here, I will not go into a detailed discussion of this topic since the main subject of this thesis is the question of how to collimate and accelerate a magnetohydrodynamic outflow. However, it is interesting and also necessary, to discuss at least a few models considering the disk-jet connection. In the end, the jet is launched from the accretion disk and, thus, the jet formation being governed by the properties and the evolution of the accretion disk. The basic task is to connect a low velocity, low temperature, magnetized stream of matter of high density (the disk) with another one with "opposite" properties (the jet) moving in perpendicular direction.

5.3.1 Stationary MHD

In the *stationary case* a number of such models have been worked out. All of them take advantage from the assumption of a self-similar structure of the Keplerian accretion disk. In these models, the disk physics is not always considered in fully self-consistent way. The numerical difficulties which are already present when dealing with the jet formation only (acceleration and collimation) become even worse if one includes the accretion disk in the treatment. As a consequence, some models neglect "essential" features of accretion disks when considers the disk-jet connection. Some neglect, for example, radiation transport as an important aspect for the energy balance of accretion disk. Others, ignore the presence of a turbulent pattern which are essential both for the angular momentum transport and for the excitation of a magnetic field generating dynamo. Ambipolar diffusion is prominent in the weakly ionized, cool regions of a disk, a point which is especially important for protostellar disks.

Stationary models of the disk-jet interaction have been presented e.g. by Lovelace and collaborators discussing the the global electrodynamics of a viscous resistive accretion disk around a Schwarzschild black hole (Lovelace et al. 1987, Wang et al. 1990). Their solutions of the disk fluid dynamics include a self-collimated electromagnetic relativistic jet.

The most comprehensive study of the stationary jet launching has been performed by Ferreira and co-authors in the non-relativistic limit (see Sect. 3.7; Ferreira & Pelletier 1993a,b, 1995; Ferreira 1997, Casse & Ferreira 2000a,b). The strength of this approach is that the disk-jet connection itself is calculated in a self-consistent way with a continuous transition from the disk accretion to the jet ejection. In particular, the mechanism of how to launch the jet perpendicular to the accretion flow becomes transparent as purely due to magnetic forces. These forces either accelerate the matter in toroidal direction leading to a centrifugal force along the disk coronal magnetic field or, due to a decrease of the vertical Lorentz force in the disk, result in lifting-up the disk material into the jet due to gas pressure. The jets can be mostly described by the parameter of the ejection index, which is a local measure of how efficient the accretion stream is converted into the jet ejection. The injection index is found to lie in a very narrow range and is constrained by the disk vertical structure and also the angular momentum transfer. Ferreira (1997) further pointed out the following important results. First, the investigation of the disk vertical equilibrium implies a *minimum mass* for the jet ejected. Second, the asymptotic behavior of the jet flow depends critically on the ratio of the iso-rotation parameter to the poloidal Alfvén speed at the Alfvén surface. This ratio must be larger than, but of the

order of, unity. Another general result is that self-similar jets from Keplerian disks, after widening up to a maximum jet radius, always *re-collimate* towards the jet axis, until the fast magneto-sonic critical point is reached. Ferreira doubts that such solutions can cross this critical point maintaining stationarity, the jet either ending there or re-bouncing (a similar effect has been observed by Fendt & Camenzind 1996 for two-dimensional solutions). The re-collimation happens due to the increasing effect of magnetic constriction and most probably caused by the large opening of the magnetic surfaces which is a result of assuming a constant ejection efficiency across all surfaces.

In other models, the structure of the turbulent, magnetized accretion disk is derived together with the disk magnetic field distribution. In Shalybkov & Rüdiger (2000) it is shown that in the case of a strong vertical field the disk rotation can depart from a Keplerian law. The poloidal magnetic field inclination angle above the disk satisfies the Blandford & Payne condition for jet launching for a wide range of the turbulent magnetic Prantl number. These studies were extended including a self-consistent nonlinear dynamo model (v. Rekowski et al. 2000), assuming either a positive or negative sign of the alpha-effect. Besides changing certain disk properties as temperature or density distribution, the different sign essentially leads to a different topology of the global disk magnetic field – a quadrupolar field geometry (positive alpha-effect) and an open dipolar field geometry (negative alpha-effect). Only the latter is well suited for jet launching.

5.3.2 MHD simulations

In the recent years, more and more *time-dependent simulations* of accretion disks have been performed, which also include a possible outflow from their corona.

There are several papers considering the evolution of a stellar magnetic dipole in interaction with a diffusive accretion disk taking into account also the evolution of that disk (Hayashi et al. 1996, Miller & Stone 1997), Goodson et al. 1997, 1999a,b). In these papers a collapse of the inner disk is indicated depending on the magnetic field strength and distribution. The results of Goodson et al. (1997, 1999) and Goodson & Winglee (1999) are especially interesting since combining a huge spatial scale (2 AU) with a high spatial resolution near the star ($0.1\mathrm{R}_{\odot}$).

The main problem is that in general these time-dependent simulations last only for a short time scale of several to tens of inner disk rotations. However, it is essential to follow the evolution of such a magnetosphere over *many* rotational periods[3]. This is of particular importance if the initial condition of the simulation is not in a steady equilibrium.

Koide et al. (1998) were first to perform general relativistic MHD simulations of jet formation close to the black hole. In their model, the interaction of an initially cylindrical magnetic field with a Keplerian accretion disk results first in an inflow of matter towards the black hole. This accretion stream interacts with the hydrostatic corona around the black hole giving rise to a relativistic gas pressure driven jet. At larger radii a magnetically

[3]At this point, we emphasize that the observed kinematic time scale of protostellar jets can be as large as $10^3 - 10^4$ yrs, corresponding to $5 \times 10^4 - 5 \times 10^5$ stellar rotational periods (and inner disk rotations)! For example, proper motion measurements for the HH30 jet (Burrows et al. 1996) give a knot velocity of about $100 - 300\,\mathrm{km\,s^{-1}}$ and a knot production rate of about 0.4 knot per year. Assuming a similar jet velocity along the whole jet extending along 0.25 pc (Lopez et al. 1995), the kinematic age is about 1000 yrs.

driven wind is initiated from the accretion disk. The simulations were performed for less than two rotations of the inner disk (corresponding to less than 0.02 rotations of the disk at the outer edge of the grid). Although these results of the first fully general relativistic MHD simulations look indeed very exciting, some objections can be raised about the underlying model. The initial condition applied is that of a hydrostatic corona around a black hole, an assumption which is not compatible with the boundary of a black hole horizon. Such a configuration is not stable and will immediately collapse.

Recently, the authors extended their work applying an initial coronal structure in steady in-fall surrounding a non-rotating black hole (Koide et al. 1999) and also considered the quasi-steady in-fall of the corona around a Kerr black hole (Koide et al. 2000). Again, the computations were lasting over a few inner disk orbits. Therefore, the observed events of mass ejection could still be a relict of the initial condition and may not be present in the long-term evolution.

So far, all numerical simulations of jet formation including the treatment of the disk structure could be performed only for a few Keplerian periods of the inner disk (and a fraction of that for the outer disk). The main point is here that in all cases the disk-jet interaction has not been treated in a fully self-consistent way. For example, some authors treat the disk physics in the ideal MHD approach. Others assume a standard α-disk model as initial condition, but then neglecting the viscous terms for the time evolution. Or they prescribe sharp edges between the disk and jet and not a smooth transition. Clearly, the simulation of the long-term evolution of the disk-jet interaction requires to combine fully self-consistent models of disk and jet physics.

In summary, a future, complete understanding of the MHD jet launching can be only expected from such kind of model simulations. The formation of a jet outflow perpendicular the accreting stream of matter will remain the basic task for the jet formation theoretician over the next decades.

Chapter 6
Summary of the publications appended below

In the following, I summarize specific aspects of my publications in connection with the topic of this habilitation thesis. I will distinguish the publications between papers following the approach of stationary MHD, the papers dealing with time-dependent MHD simulations and the papers which are more connected to observationally related issues.

6.1 Stationary models of relativistic MHD jets

As explained in Sect. 4.5, 4.6 the stationary relativistic MHD equations can be reduced to the two issues of *collimation* and *acceleration,* thus, to the problem (i) dealing the *structure* of the jet magnetic field (the GS solution) and (ii) the problem considering with the dynamics of the flow of matter along the magnetic jet (the wind equation).

In a first step, the finite element code for relativistic MHD developed previously has been extended to relativistic jet sources where the jet source encloses a rotating black hole.

There is common believe that superluminal jet motion from active galactic nuclei and from galactic high energy sources originates in the magnetized environment of a rotating black hole surrounded by an accretion disk. The structure of these jet magnetospheres follows from solutions of the Grad-Shafranov equation for the force-balance between axisymmetric magnetic surfaces. In Fendt (1997a) two-dimensional force-free solutions of the stream equation are numerically obtained in a general relativistic context (3+1 formalism on Kerr geometry). In order to solve the GS equation (also called stream equation), the numerical method of finite elements has been applied. In this approach, the regularity conditions along the light surfaces are automatically satisfied. After iteratively adjusting the poloidal current distribution and the shape of the jet boundary, one finds a magnetic field configuration (*the* field configuration) without kinks at the outer light surface. The solutions obtained are *global* solutions extending from the inner light surface of the Kerr black hole to the asymptotic regime of a cylindrically collimated jet with a finite radius. Depending on the accretion disk magnetic field boundary condition, some of the solutions strongly indicate on a hollow jet structure. The magnetic field distribution of the jet shows a fast collimation beyond a distance of about one light cylinder away from the central source. The asymptotic jet radius is about 3-5 light cylinder radii with a jet expansion factor (asymptotic jet radius to jet foot point radius) of about 10-100.

In the next papers the differential rotation of the jet launching accretion disk is considered.

As first step towards a two-dimensional solution of the GS equation the asymptotic regime of a cylindrically collimated jet is investigated. This is necessary in order to provide the proper boundary conditions for the two-dimensional solution. In Fendt (1997b), the asymptotic field structure of differentially rotating magnetic jets is investigated, widening the study by Appl & Camenzind (1993a,b). In general, the results show that, with the same current distribution, differentially rotating jets are collimated to smaller jet radii as compared with jets with rigidly rotating field. In turn, differentially rotating jets need a stronger net poloidal current in order to collimate to the same asymptotic radius. Current-free solutions are not possible for differentially rotating *disk*-jet magnetospheres with cylindrical asymptotic. The paper presents a simple analytical relation between the poloidal current distribution and magnetic field rotation law. Also a general relation is derived for the current strength for jets with maximum differential rotation and minimum differential rotation. Analytical solutions are also given in the case of a field rotation leading to a degeneration of the light cylinder. Because field rotation and electric current are conserved quantities along the force-free field lines, one is enabled to connect the asymptotic solution to a Keplerian accretion disk. This allows to derive the total expansion rate for the jet, and also the flux distribution at the foot points of the flux surfaces are derived. Large poloidal currents imply a strong opening of flux surfaces, a stronger gradient of field rotation leads to smaller expansion rates. There is indication that extragalactic jet expansion rates are less than in the case of protostellar jets. High mass AGN seem to have larger jet expansion rates than low mass AGN.

Having now at hand the proper asymptotic boundary condition (Fendt 1997b), the full two-dimensional field structure of these source can be obtained. In Fendt & Memola (2001) the axisymmetric structure of collimating, relativistic, strongly magnetized (force-free) jets has been investigated. Essentially, the differential rotation of the foot points of the field lines is included in the treatment. The magnetic flux distribution is determined by the solution of the Grad-Shafranov equation and the regularity condition along the light surface. As the main difficulty, with differential rotation the shape of the light surface is not known a priori and must be calculated in an iterative way. For the first time, the force-free magnetic structure of truly two-dimensional, relativistic jets, anchored in a differentially rotating disk has been calculated. This approach allows for a direct connection between parameters of the central source (mass, rotation) and the extension of the radio jet. In particular, this can provide a direct scaling of the location of the asymptotic jet light cylinder in terms of the central mass and the accretion disk magnetic flux distribution. The paper demonstrates that differentially rotating jets must be collimated to a smaller radius in terms of the light cylinder if compared to jets with rigid rotation. Also, the opening angle is smaller. In general, differential rotation of the iso-rotation parameter leads to an increase of the jet opening angle. These results are applicable for highly magnetized, highly collimated, relativistic jets from active galactic nuclei and Galactic superluminal jet sources. Comparison to the M87 jet shows agreement in the collimation distance. A light cylinder radius of the M87 jet of 50 Schwarzschild radii can be derived.

So far, the papers consider the force-free magnetic field structure of a collimating rel-

ativistic jet. What is also interesting, and has even more observational implications, is the flow dynamics along the jet magnetic field. In Fendt & Greiner (2001) the dynamics of magnetically driven superluminal jets originating from rotating black holes has been investigated. For this, the stationary, general relativistic, magnetohydrodynamic wind equation along collimating magnetic flux surfaces has been solved numerically. The jet solutions are calculated on a global scale of spatial range from several to several 1000 gravitational radii and for different magnetic field geometries. For a given magnetic flux surface we obtain the complete set of physical parameters for the jet flow. The numerical results are applied to the Galactic superluminal sources GRS 1915+105 and GRO 1655-40. The observed speed of more than 0.9 c can be achieved in general by magnetohydrodynamic acceleration. The velocity distribution along the magnetic field has a saturating profile. The asymptotic jet velocity depends either on the plasma magnetization (for a fixed field structure) or on the magnetic flux distribution (for fixed magnetization). The distance where the asymptotic velocity is reached, is below the observational resolution for GRS 1915+105 by several orders of magnitude. The plasma temperature rapidly decreases from about 10^{10}K at the foot point of the jet to about 10^6K at a distance of 5000 gravitational radii from the source. Temperature and the mass density follow a power law distribution with the radius. The jet magnetic field is dominated by the toroidal component, whereas the velocity field is dominated by the poloidal component.

Motivated by the high temperatures found in the wind solution close to the origin of the jet, the possibility of X-ray emission from this part of the jets been discussed. Indeed, applying the MHD wind solution of Fendt & Greiner (2001), Memola et al. (2002) were able to derive the optically thin thermal X-ray spectrum including iron emission lines in the jet (see below).

6.2 MHD simulations of jet formation

The self-collimation property of MHD jets has been demonstrated by Ouyed & Pudritz (1997). However, these simulations were carried out for a certain initial field distribution of a potential field of “paraboidal” shape anchored in the disk. However, we know that in the case of protostellar jets the central star may also carry a magnetosphere, most probably much stronger than the disk magnetic field. It is therefore essential to investigate the jet formation process also for such a model setup.

In Fendt & Elstner (1999) the evolution of a stellar dipolar-type magnetosphere interacting with a Keplerian disk is investigated numerically using the ideal MHD ZEUS-3D code in the axisymmetry option. The evolution of the innermost region around the stellar object has been computed using a non-smoothed gravitational potential. The disk is taken as a boundary condition prescribing the mass inflow into the corona. Depending mainly on the magnetic field strength, our simulations last several hundred Keplerian periods of the inner disk. The main result is that the dipolar structure of the magnetic field almost completely disappears. An expanding bubble of hot gas of low density forms disrupting the initial dipolar field structure. A disk wind accelerates within the time limit of the simulation to velocities of about 0.5 the Keplerian speed and potentially may develop into a stationary collimated jet. Simulations with a rotating and a non-rotating star show signifi-

cant differences. In the case of a rotating star during the very first time steps a high speed outflow along the axis is initiated which does not exist in the case of a non-rotating star.

This model setup was further investigated in Fendt & Elstner (2000). Indeed, the stationary state solutions suggested by the earlier results were found. Depending mainly on the magnetic field strength, the simulations were lasting for several thousands of Keplerian periods of the inner disk. As before, a Keplerian disk is assumed as a boundary condition prescribing a mass inflow into the corona. Additionally, a stellar wind from a rotating central star is prescribed. The major result is that the initially dipole type field develops into a spherically radial outflow pattern with two main components, a disk wind and a stellar wind component. These components evolve into a quasi-stationary final state. The poloidal field lines follow a conical distribution. As a consequence of the initial dipole, the field direction in the stellar wind is opposite to that in the disk wind. The half opening angle of the stellar wind cone varies from 30° to 55° depending on the ratio of the mass flow rates of disk wind and stellar wind. The maximum speed of the outflow is about the Keplerian speed at the inner disk radius. An expanding bubble of hot, low density gas together with the winding-up process due to differential rotation between star and disk disrupts the initial dipole type field structure. An axial jet forms during the first tens of disk/star rotations, however, this feature does not survive on the very long time scale. A neutral field line divides the stellar wind from the disk wind. Depending on the numerical resolution, small plasmoids are ejected in irregular time intervals along this field line. Within a cone of 15° along the axis the formation of small knots can be observed if only a weak stellar wind is present. Essentially, with the chosen mass flow rates and field strength no indication for a flow self-collimation has been found. This is due to the small net poloidal electric current in the (reversed field) magnetosphere which is in difference to typical jet models.

Protostellar jets most probably originate in turbulent accretion disks surrounding the young stellar objects. In Fendt & Cemeljic (2002) the evolution of a disk wind into a collimated jet is investigated under the influence of magnetic diffusivity assuming that the turbulent pattern in the disk will also enter the disk corona and the jet. The ZEUS-3D code has been extended for magnetic diffusivity and used in the axisymmetry option to solve the time-dependent resistive MHD equations for a model setup of a central star surrounded by an accretion disk. The disk is taken as a time-independent boundary condition for the mass flow rate and the magnetic flux distribution. In the paper, analytical estimates for the magnitude of magnetic diffusion in a protostellar jet are derived connecting our results to earlier work in the limit of ideal MHD. It is found that diffusive jets propagate slower into the ambient medium, most probably due to the lower mass flow rate in axial direction. Close to the star a quasi stationary state evolves after several hundreds (weak diffusion) or thousands (strong diffusion) of disk rotations. Magnetic diffusivity affects the protostellar jet structure as follows. (i) The jet poloidal magnetic field becomes de-collimated. (ii) The jet velocity increases with increasing diffusivity, while the degree of collimation for the hydrodynamic flow remains more or less the same. (iii) The results suggest the mass flux as a proper tracer for the degree of jet collimation and find indication for a critical value for the magnetic diffusivity above which the jet collimation is only weak.

6.3 A link to observations – parameter studies and spectra

In this section I collect two jet papers which do not deal directly with the theory of MHD jet formation, but simply describe possible consequences for the observational detection of jets as well as for the interpretation of the observations.

In Fendt & Zinnecker (1998) a first example of this kind of research investigated protostellar jets with an observed slight misalignment between the jet and counter jet axis. Basically, a theoretical model explaining the formation of the such jets would require a fully three-dimensional MHD approach. Since this is hardly feasible, a first step is a parameter study of energies and forces involved.

Observations of several bipolar jet flows from young stellar objects reveal a slight difference in the apparent direction of propagation for jet and counter jet. The paper investigates possible mechanisms leading to such a jet deflection. Several reasons, which may be responsible for such a jet structure, are discussed. These are the motion of the jet source within a binary system, gravitational pull due to an asymmetric external mass distribution, dynamical pressure of the external medium, inertial effects due to proper motion of the jet source, an inclined interstellar magnetic field, and the coupling between a magnetic jet and an external magnetic field. What is found, is that for typical protostellar jet parameters the most likely mechanisms leading to a bent jet structure are *Lorentz forces* on the magnetic jet and/or motion of the jet source in a *binary system*. *Dynamical pressure* of a dense external medium or a stellar wind from a companion star cannot be excluded as source of jet bending.

The next paper considers the X-ray emission emitted from highly relativistic jets from microquasars. Having calculated the magnetic field structure (Fendt 1997a) and the plasma dynamics along the collimating relativistic magnetic jets (Fendt & Greiner 2001), the logical next step is to use these results to derive some spectral properties of these jet flows. Applying the jet dynamic parameters (velocity, density, temperature) calculated from the magnetohydrodynamic (MHD) equations, in Memola et al. (2002) the thermal X-ray luminosity along the inner jet flow in the energy range $0.2 - 10.1$ keV has been obtained. Note that the emitted radiation is considered as a *tracer* of the jet flow only. However, it can be shown afterwards that the emitted flux is weak compared to the kinetic energy flux of the jet and that, therefore, the polytropic MHD model applied is consistent with the calculated luminosity. The paper mainly concentrates on the case of Galactic microquasars emitting highly relativistic jets. For a $5\,\mathrm{M}_\odot$ central object and a jet mass flow rate of $\dot{M}_\mathrm{j} = 10^{-8}\,\mathrm{M}_\odot\mathrm{yr}^{-1}$ we obtain a jet X-ray luminosity $L_\mathrm{X} \approx 10^{33}\,\mathrm{erg\,s}^{-1}$. Emission lines of Fe XXV and Fe XXVI are clearly visible. Relativistic effects such as Doppler shift and boosting were considered for different inclinations of the jet axis. Due to the chosen geometry of the MHD jet the inner X-ray emitting part is not yet collimated. Therefore, depending on the viewing angle, the Doppler boosting does not play a major role in the total spectra.

Chapter 7
Future prospects – self-consistent disk-jet MHD simulations

So far, the basic mechanism behind the magnetohydrodynamic jet formation seems to be fairly understood. However, there are still some open points. The general problem of jet launching from an accretion disk has not yet been solved in a fully self-consistent way. In the following I will summarize some of these open questions. This list also represents a *what-to-do* list for the next years of jet theory. Only when these points will be clarified, one may continue to actually *model* certain jet sources calculating the emitted radiation from jets of different sources. This would allow to learn more about the detailed structure of the jet source, about intrinsic differences between individual jet sources and possibly about their different history.

7.1 The MHD model of jet formation – open questions

Magnetohydrodynamic self-collimation

At a first look, there seems to be clear indication from analytical studies of the asymptotic jet as well as from MHD simulations of the jet formation region that magnetohydrodynamic self-collimation should work (Heyvaerts & Norman 1989, Li et al. 1991, Ouyed & Pudritz 1997, Krasnopolsky et al. 1999).

However, a final theoretical confirmation of such a process is missing which, in particular, also considers the scales of astrophysical jets is still missing. The MHD simulations which actually support the idea of self-collimation clearly suffer from numerical constraints. The spatial numerical resolution available on current computers is too low resolving the jet formation region only of the order of just a few percent of the real jet dimensions. The collimation seen in the simulations therefore is on scales which are not comparable with the observed features. The jet radius derived from the simulations is far too small with the real jets being 100 times wider.

Concerning the stationary models, some principal arguments, mainly concerned about the current closure in jets, have been raised which doubt the self-collimation property of MHD flows.

A self-consistent astrophysical model scenario

So far, all time-dependent simulations as well as stationary solutions of the theoretical equations have been obtained under simplifying assumptions concerning the geometry of the jet source. However, it seems to be clear that an astrophysical jet source is a complex system consisting of several components – a star or a black hole, the disk and the jet. Beside their different shape (which actually constraints the numerical grid), these components differ substantially in their physical properties. As a consequence, a numerical code would have to deal with strong gradients in the dynamical parameters and quite different local time stepping time. These difficulties yet hinder a combined treatment of all these model constituents. Most important, the time-dependent ejection mechanism is not yet understood.

A consistent accretion disk model

While the physics of the star (or the black hole) and the jet is fairly understood, a fully consistent model of the accretion disk is yet missing. The difficulty here is that for the disk the complete set of physical equations must be solved and three-dimensional effects might be important. In particular, the disk structure is governed by the magnetohydrodynamic equations including *radiation transfer*. Needless to say that close to a black hole also relativistic effects will play an essential role. For the weakly ionized parts of a protostellar disk ambipolar diffusion might be considered as well as the influence of dust particles. Again, strong gradients are present in vertical and horizontal direction. Therefore the times scales vary not only along the disk radius but also in vertical direction limiting the numerical MHD simulation.

The intrinsic setup – the origin of magnetic field and jet

Two fundamental questions remain open partly as a consequence of the above mentioned difficulties.

The first one is whether some protostellar jets originates as a stellar jet, i.e. as a stellar wind from the stellar surface or whether jets are generally launched as a disk wind. Observations do not give a definitive answer (yet) and theoretical models are too simple (yet). The observed scale of the jet radius 100 - 1000 times larger than the central source indicates on jets being launched as disk winds. Also the time scale indicated for the emission of jet knots is in favor of being triggered by some process in the disk. For relativistic jets, the yet unknown matter content (baryonic or leptonic) may decide the question about the jet origin (Blandford & Payne or Blandford & Znajek).

The second is the question of the origin of the magnetic fields. So far, the models of jet formation assume that the magnetic field “is there”, has some topological structure (dipolar, quadrupole ...). However, the jet magnetic field can be generated by a dynamo process in the disk or the star (or both) or it can be advected with the accretion process from the surrounding interstellar medium. The resulting field structure might be quite different – a stellar dipole, possibly inclined, a disk magnetosphere with open (dipole) or closed (quadrupole) field lines or maybe some twisted, hour-glass shaped flux tubes anchored in the disk and the ambient medium. The time-scale of the dynamo process of

the advection will also influence the jet formation. In turn, the presence of the jet itself may have some impact on the magnetic field generating processes.

7.2 The future goal – model fits to observed jet sources

Due to the above mentioned incompleteness of the present MHD models – physics too simple, time scales too short, spatial scale too small – these cannot yet be applied to actually *fit* the observed data. These data, on the other hand, do not yet provide a look into the innermost regions of jet formation.

However, such comparative studies of jet formation are essential for the understanding of individual sources. Computers and instrumention might be ready for such a task in a couple of years.

From the theoretical point of view this would require first to answer or clarify all the open points summarized above. Time-dependent simulations taking into account the complex structure of the jet source consisting of three interacting components – the central object, its surrounding accretion disk, and the jet – all coupled by the magnetic field, but also the huge size of jet in respect to its origin will finally clarify the role of magneto-hydrodynamic self-collimation and the question of the jet origin.

Numerical simulations of the accretion disk evolution will tell us *why* jets are launched and how the magnetic field is established. It seems to be essential for such kind of simulations also to include a disk wind or a magnetized disk corona in the treatment, in order to allow for jets to be formed from the disk.

Having succeeded so far, the next step might be to calculate the radiative signatures emitted from the jet and its source. A first step in this direction has already been made (Goodson et al. 1997) who presented emission maps of forbidden emission lines in protostellar jets. Radio emission maps for relativistic extragalactic jets have been modeled in the hydrodynamic case (e.g. Aloy et al. 2000). Also the X-ray emission lines calculated from a relativistic MHD jet model of a microquasar (Memola et al. 2002) is along these lines.

By comparing individual sources of jets we will finally learn whether the present picture of jet formation is correct or whether some key process has been overlooked. We then also expect an answer to the questions why some disks have jets and some do not, and how the presence of a jet affects the evolution of the jet source.

Bibliography

[1] Aloy, M.-A., Gómez, J.-L., Ibanez, J.-M., Marti, J.-M., Müller, E., 2000, ApJ, 528, L85

[2] André, P., Montmerle, T., Stine, P.C., Feigelson, E.D., Klein K.L., 1988, ApJ, 335, 940

[3] André, P., Phillips, R.B., Lestrade, J.-F., Klein, K.L., 1991, ApJ, 376, 630

[4] Appenzeller, I., Krautter, J., Jankovics, I., 1983, A&AS, 53, 291

[5] Appl, S., Camenzind, M., 1993a, A&A, 270, 71

[6] Appl, S., Camenzind, M., 1993b, A&A, 274, 699

[7] Baade, W., 1956, ApJ, 123, 550

[8] Baade, W., Minkowski, R., 1954a, ApJ, 119, 206

[9] Baade, W., Minkowski, R., 1954b, ApJ, 119, 215

[10] Bardou, A., von Rekowski, B., Dobler, W., Brandenburg, A., Shukurov, A., 2001, A&A, 370, 635

[11] Belcher, J.W., MacGregor, K.B., 1976 ApJ 210, 498

[12] Beskin, V.S., 1997, Phys. Uspekhi, 40, 659

[13] Beskin, V.S., Pariev, V.I., 1993, Physics Uspekhi, 36, 529

[14] Beskin, V.S., Kuznetsova, I.V., 2000, ApJ 541, 257

[15] Beskin, V.S., Okamoto, I., 2000, MNRAS 313, 445

[16] Bieging, J.H., Cohen, M., 1989, AJ, 98, 1686

[17] Blandford, R.D., Rees, M.J., 1974, MNRAS, 169, 395

[18] Blandford, R.D., Znajek, R.L., 1977, MNRAS, 179, 433

[19] Blandford, R.D., Payne, D.G., 1982, MNRAS, 199, 883

[20] Blandford, R.D., 1990, in: T.J-L. Courvoisier, M. Mayor (eds) Active Galactic Nuclei, Lecture Notes, Saas-Fee Advanced Course 20, Springer, Heidelberg, p.242

[21] Blondin, J.M., Fryxell, B.A., Königl, A., 1990, ApJ, 360, 370

[22] Bogovalov, S., 1997, A&A 327, 662

[23] Bouvier, J., 1990, AJ, 99, 946

[24] Bouvier, J., Cabrit, S., Fernandez, M., Martin, E.L., Matthews, J.M., 1993, A&A, 272, 176

[25] Bradt, H., Mayer, W., Naranan, S., Rappaport, S., Spada, G., 1967, ApJ, 150, 199

[26] Brown, D.N., Landstreet, J.D., 1981, ApJ, 246, 899

[27] Burbidge, G.R., 1956 , ApJ 124, 416

[28] Burrows, C.J., Stapelfeldt, K.R., Watson, A.M., et al., 1996, ApJ 473, 437

[29] Byram, E.T., Chubb, T.B., Friedmann, H, 1966, AJ 71, 379

[30] Camenzind, M., 1986, A&A, 162, 32

[31] Camenzind, M., 1987, A&A, 184, 341

[32] Camenzind, M., 1990, in: G. Klare (ed.) Reviews of Modern Astronomy 3, Springer-Verlag (Heidelberg), p.234

[33] Casse, F., Ferreira, J., 2000a, 353, 1115

[34] Casse, F., Ferreira, J., 2000b, 361, 1178

[35] Chandrasekhar, S., 1956, ApJ, 124, 232

[36] Chandrasekhar, S., 1961, Hydrodynamic and hydromagnetic stability, Oxford, Clarendon

[37] Chiueh, T., Li, Z.-Y., Begelman, M.C., 1991, ApJ, 377, 462

[38] Cohen, M.H., Cannon, W., Purcell, G.H., Shaffer, D.B., Broderick, J.J., Kellermann, K.I., Jauncey, D.L., 1971, ApJ, 170, 207

[39] Contopoulos, J., 1994, ApJ 432, 508

[40] Contopoulos, J., 1995, ApJ 446, 67

[41] Contopoulos, J., 1995, ApJ 450, 616

[42] Contopoulos, J., Lovelace, R.V.E., 1994, ApJ 429, 139

[43] Curtis, H.D., 1918, Pub. Lick. Obs. 13, 11

[44] Davidson, K., McCray, R., 1980, ApJ, 241, 1082

[45] de Gouveia dal Pino, E.M., Benz, W., 1993, ApJ, 410, 686

[46] Dent, W.A., 1965, Science, 148, 1458

[47] Eikenberry, S.S., Cameron, P.B., Fierce, R.W., Kull, D.M., Dror, D.H., Houck, J.R., 2001, “Twenty Years of Timing SS433”, astro-ph/0107296

[48] Fabian, A.C., Rees, M.J., 1979, MNRAS 187, 13P

[49] Fendt, Ch., 1997a, A&A, 319, 1025

[50] Fendt, Ch., 1997b, A&A, 323, 999

[51] Fendt, Ch., Camenzind, M., Appl S., 1995, A&A, 300, 791

[52] Fendt, Ch., Camenzind, M., 1996, A&A, 312, 591

[53] Fendt, Ch., Elstner, D., 1999, A&A, 349, L61

[54] Fendt, Ch., Elstner, D., 2000, A&A, 363, 208

[55] Fendt, Ch., Memola, E., 2001, A&A, 365, 631

[56] Fendt, Ch., Greiner, J., 2001, A&A, 369, 308

[57] Fendt, Ch., Cemeljic, M., 2002, A&A, 395, 1043

[58] Felten, J.E., 1968, ApJ, 151, 861

[59] Felten, J.E., Arp, H.C., Lynds, C.R., 1970, ApJ, 159, 415

[60] Ferraro, V.C.A., 1937, MNRAS, 97, 458

[61] Ferreira, J., 1997, A&A, 319, 340

[62] Ferreira, J., Pelletier, G., 1993a, A&A, 276, 625

[63] Ferreira, J., Pelletier, G., 1993a, A&A, 276, 637

[64] Ferreira, J., Pelletier, G., 1995, A&A, 295, 807

[65] Ferreira, J., Pelletier, G., Appl S., 2000, MNRAS, 312, 647

[66] Ghosh, P., Pethick, C.J., Lamb, F.K., 1977, ApJ 217, 578

[67] Ghosh, P., Lamb, F.K., 1978, ApJ, 223, L83

[68] Ghosh, P., Lamb, F.K., 1979, ApJ, 232, 259

[69] Ghosh, P., Lamb, F.K., 1979, ApJ, 234, 296

[70] Gold, T., 1967, ApJ 147, 832

[71] Goldreich, P., Julian, W.H., 1969, ApJ, 157, 869

[72] Goldreich, P., Julian, W.H., 1970, ApJ, 160, 971

[73] Goodson, A.P., Winglee, R.M., Böhm, K.-H., 1997, ApJ, 489, 199

[74] Goodson, A.P., Böhm, K.-H., Winglee, R.M., 1999, ApJ, 524, 159

[75] Goodson, A.P., Winglee, R.M., 1999, ApJ, 524, 142

[76] Greiner, J., Cuby, J.G., McCaughrean, M.J., 2001, Nature, 414, 522

[77] Gubbay, J., Legg, A.J., Robertson, D.S., Moffet, A.T., Ekers, R.D., Seidel, B., 1969, Nature, 224, 1045

[78] Günther, E., Lehmann, H., Emerson, J.P., Staude, J., 1999, A&A, 341, 768

[79] Hartmann, L., MacGregor, K.B., 1982, ApJ 259, 180

[80] Hayashi, M.R., Shibata, K., Matsumoto, R., 1996, ApJ, 468, L37

[81] Henriksen, R.N., Rayburn, D.R., 1971, MNRAS, 153, 323

[82] Herrnstein, J.R., Moran, J.M., Greenhill, L.J., Blackman, E.G., Diamond, P.J., 1998, ApJ, 505, 243

[83] Heyvaerts, J. Norman, C.A., 1989, ApJ, 347, 1055

[84] Hiltner, W.A., 1959, ApJ, 130, 340

[85] Hogg, D.E., MacDonald, G.H., Conway, R.G., Wade, C.M., 1969, AJ, 74, 1206

[86] Horiuchi, S., Mestel, L., Okamoto, I., 1995, MNRAS, 275, 1160

[87] Johnstone, R.M., Penston, M.V., 1986, MNRAS, 219, 927

[88] Johnstone, R.M., Penston, M.V., 1987, MNRAS, 227, 797

[89] Junor, W., Biretta, J.A., Livio, M., 1999, Nature, 401, 891

[90] King, A.R., Lasota, J.P., Kundt, W., 1975, Phys. Rev. D 12, 3037

[91] Knight, C.A., Robertson, D.S., Rogers, A.E.E., Shapiro, I.I., Whithney, A.R., Clark, T.A., Goldstein, R.M., Marandino, G.E., Vandenberg, N.R., 1971, Science, 173, 52

[92] Königl, A., 1991, ApJ, 370, L39

[93] Kössl, D., Müller, E., 1988, A&A, 206, 204

[94] Kössl, D., Müller, E., Hillebrandt, W., 1990a, A&A, 229, 397

[95] Kössl, D., Müller, E., Hillebrandt, W., 1990b, A&A, 229, 401

[96] Koide, S., Shibata, K., Kudoh, T., 1998, ApJ, 495, L63

[97] Koide, S., Shibata, K., Kudoh, T., 1999, ApJ, 522, 727

[98] Koide, S., Meier, D.L., Shibata, K., Kudoh, T., 2000, ApJ 536, 668

[99] Krasnopolsky, R., Li, Z.-Y., Blandford, R.D., 1999, ApJ, 526, 631

[100] Krichbaum, T.P., Alef, W., Witzel, A., Zensus, J.A., Booth, R.S., Greve, A., Rogers, A.E.E., 1998, A&A, 329, 873

[101] Kudoh, T., Shibata, K., 1997a, ApJ 474, 362

[102] Kudoh, T., Shibata, K., 1997b, ApJ 476, 632

[103] Kudoh, T., Matsumoto, R., Shibata, K., 1998, ApJ 508, 186

[104] Lery, T., Heyvaerts, J., Appl, S., Norman, C.A., 1998, A&A 337, 603

[105] Lery, T., Heyvaerts, J., Appl, S., Norman, C.A., 1999a, A&A 347, 1055

[106] Lery, T., Henriksen, R.N., Fiege, J.D., 1999b, A&A 350, 254

[107] Li, Z.-Y., 1993, ApJ, 415, 118

[108] Li, Z.-Y., Chiueh, T., Begelman, M.C., 1992, ApJ 394, 459

[109] Liebert, J., Angel, J.R.P., Hege, E.K., Martin, P.G., Blair, W., 1979 Nature 279, 384

[110] Lind, K.R., Payne, D.G., Meier, D.L., Blandford, R.D., 1989, ApJ, 344, 89

[111] López, R., Raga, A., Riera, A., Anglada, G., Estalella. R., 1995, MNRAS, 274, 19L

[112] Lovelace, R.V.E., Wang, J.C.L., Sulkanen, M.E., 1987, ApJ, 315, 504

[113] Lovelace, R.V.E., Berk, H.L., Contopoulos, J., 1991, ApJ, 379, 696

[114] Lovelace, R.V.E., Romanova, M.M., Contopoulos, J., 1993, ApJ, 403, 158

[115] Lovelace, R.V.E., Romanova, M.M., Bisnovatyi-Kogan, G.S., 1995, MNRAS, 275, 244

[116] Lovelace, R.V.E., Romanova, M.M., Bisnovatyi-Kogan, G.S., 1999, ApJ, 514, 368

[117] Lüst, R., Schlüter, A., 1954, Zs. f. Ap., 34, 263

[118] Macdonald, D., Thorne, K.,S., 1982, 198, 345

[119] Macdonald, D., 1984, 211, 313

[120] Margon, B.A., Ford, H.C., Katz, J.I., Kwitter, K.B., Ulrich, R.K., Stone, R.P.S., Klemolam A., 1979a, ApJ 230, L41

[121] Margon, B.A., Ford, H.C., Grandi, S.A., Stone, R.P.S., 1979b, ApJ 233, L63

[122] Margon, B.A., 1984, Ann. Rev. Astr. Astrophys., 22, 507

[123] Martin, P., Rees, M.J., 1979, MNRAS 189, 19

[124] Mestel, L., 1968, MNRAS 138, 359

[125] Michel, F.C., 1969, ApJ, 158, 727

[126] Michel, F.C., 1973a, ApJ, 180, L133

[127] Michel, F.C., 1973b, ApJ, 180, 207

[128] Milgrom, M., 1979, A&A 76, L3

[129] Miyoshi, M., Moran, J., Herrnstein, J., Greenhill, L., Nakai, N., Diamond, P., Inoue, M., 1995, Nature, 373, 127

[130] Mirabel, I.F., Rodriguez, L.F., 1994, Nature, 371, L46

[131] Mirabel, I.F., Rodriguez, L.F., 1999, Ann. Rev. Astr. Astrophys., 37

[132] Miller, K.A., Stone, J.M., 1997, ApJ, 489, 890

[133] Mirabel, I.F., Rodriguez, L.F., 1994, Nature, 371, L46

[134] Mitton, S., Ryle, M., 1969, MNRAS, 146, 221

[135] Moffet, A.T., Gubbay, J., Robertson, D.S., Legg, A.J., 1971, High Resolution Observations of Variable Radio Sources, in: D.S. Evans et al. (eds) External Galaxies and Quasi-Stellar Objects, IAU 44, Dordrecht, Reidel, p.228

[136] Mundt, R., Fried, J.W., 1983, ApJ, 274, L83

[137] Mundt, R., Ray, T.P., Bührke, T., Raga, A.C., Solf, J., 1990, A&A, 232, 37

[138] Najita, J., Shu, F,H., 1994, ApJ 429, 808

[139] Nitta, S.,Takahashi, M., Tomimatsu, A., 1991, Phys. Review D, 44, 2295

[140] Okamoto, I., 1974a, MNRAS 166, 683

[141] Okamoto, I., 1974b, MNRAS 167, 457

[142] Okamoto, I., 1975a, MNRAS 170, 81

[143] Okamoto, I., 1975b, MNRAS 173, 357

[144] Okamoto, I., 1978, MNRAS 185, 690

[145] Okamoto, I., 1992, MNRAS 254, 192

[146] Okamoto, I., 1997, A&A 326, 1277

[147] Okamoto, I., 1999, MNRAS 307, 253

[148] Okamoto, I., 2000, MNRAS 318, 250

[149] Okamoto, I., 2001, MNRAS 327, 55

[150] Okoye, S.E., 1973, MNRAS, 165, 393

[151] Ostriker, E.C., 1997, ApJ 486, 291

[152] Ostriker, E.C., Shu, F.H., 1995, ApJ 447, 813

[153] Ouyed, R., Pudritz, R.E., 1997a, ApJ, 482, 712

[154] Ouyed, R., Pudritz, R.E., 1997b, ApJ, 484, 794

[155] Ouyed, R., Pudritz, R.E., 1999, MNRAS, 309, 233

[156] Paatz, G., Camenzind, M., 1996, A&A, 308, 77

[157] Parker, E.N., 1958, ApJ 128, 664

[158] Pelletier, G., Pudritz,, R., 1992, ApJ, 394, 117

[159] Petterson, J.A., 1975, Phys. Rev. D. 12, 2218

[160] Piddington, J.H., 1964, MNRAS, 128, 345

[161] Piddington, J.H., 1970, MNRAS, 148, 131

[162] Pneuman, G.W., Kopp, R.A., 1971, SoPh 18, 258

[163] Pudritz, R.E., Norman, C.A., 1983, ApJ 274, 677

[164] Pudritz, R.E., Norman, C.A., 1986, ApJ 301, 571

[165] Ray, T.P., Mundt, R., Dyson, J.E., Falle, S.A.E.G., Raga, A., 1996, ApJ, 468, L103

[166] Ray, T.P., Muxlow, T.W.B., Axon, D.J. et al., 1997, Nature, 385, 415

[167] Rees, M.J., 1966, Nature, 211, 468

[168] Rees, M.J., 1967, MNRAS, 135, 345

[169] Romanova, M.M., Ustyugova, G.V., Koldobas, A.V., Chechetkin, V.M., Lovelace, R.V.E., 1997, ApJ, 482, 708

[170] Ryle, M., Elsmore, B., Neville, A.C., 1965a, Nature 205, 1259

[171] Ryle, M., Elsmore, B., Neville, A.C., 1965b, Nature 207, 1024

[172] Safier, P.N., 1998, ApJ, 494, 336

[173] Safier, P.N., 1999, ApJ, 510, L127

[174] Sanders, D.B., Phinney, E.S., Neugebauer, G., Soifer, B.T., Matthews, K., 1989, ApJ, 347, 29

[175] Sakurai, N.I., 1985, A&A, 152, 121

[176] Sakurai, N.I., 1987, PASJ, 39, 821

[177] Sauty, C., Tsinganos, K., 1994, A&A, 287, 893

[178] Sauty, C., Tsinganos, K., Trussoni, E., 1999, A&A, 348, 327

[179] Shaffer, D.B., Cohen, M.H., Jauncey, D.L., Kellermann, K.I., 1972, ApJ 173, L147

[180] Shalybkov, D. Rüdiger, G., 2000, MNRAS, 315, 762

[181] Shibata, K., Uchida, Y., 1985, PASJ 37, 31

[182] Shibata, K., Uchida, Y., 1986, PASJ 38, 631

[183] Shklovskii, I.S., 1953a, Astron. J. USSR 30, 15

[184] Shklovskii, I.S., 1953b, Dokl. Akad. Nauk SSSR 90, 983

[185] Shu, F.H., Najita, J., Ostriker, E., Wilkin, F., Ruden, S.P., Lizano, S., 1994a, ApJ, 429, 781

[186] Shu, F.H., Najita, J., Ruden, S.P., Lizano, S., 1994b, ApJ, 429, 797

[187] Shu, F.H., Najita, J., Ostriker, E., Shang, H., 1995, ApJ, 455, L155

[188] Sulkanen, M.E., Lovelace, V.E., 1990, ApJ, 350, 732

[189] Takahashi, M., Nitta, S., Tatematsu, Y., Tomimatsu, A., 1990, ApJ, 363, 206

[190] Thorne, K.S., Macdonald, D., 1982, MNRAS, 198, 339

[191] Thorne, K.S., Price, R.H., Macdonald, D. (Eds), 1986, Black Holes: The membrane paradigm, Yale University Press, New Haven and London

[192] Tingay, S.J., Jauncey, D.L., Preston, R.A., et al., 1995, Nature, 374, 141

[193] Trussoni, E., Tsinganos, K., Sauty, C., 1997, A&A, 325, 1099

[194] Tsinganos, K., Sauty, C., 1992a, A&A, 255, 405

[195] Tsinganos, K., Sauty, C., 1992b, A&A, 257, 790

[196] Turland, B.D., 1975, MNRAS, 170, 281

[197] Uchida, Y., Shibata, K., 1985, PASJ, 37, 515

[198] Ustyugova, G.V., Koldoba, A.V., Romanova, M.M., Chechetkin, V.M., Lovelace, R.V.E., 1995, ApJ, 439, L39

[199] Ustyugova, G.V., Koldoba, A.V., Romanova, M.M., Chechetkin, V.M., Lovelace, R.V.E., 1999, ApJ, 516, 221

[200] v. Rekowksi, M., Rüdiger, G., Elstner, D., 2000, A&A, 353, 813

[201] Wang, J.C.L., Sulkanen, M.E., Lovelace, R.V.E., 1990, ApJ, 355, 38

[202] Weber, E.J., Davis, L., 1967, ApJ, 148, 217

[203] Whitney, A.R., Shapiro, I.I., Rogers, A.E.E., Robertson, D.S., Knight, C.A., Clark, T.A., Goldstein, R.M., Marandino, G.E., Vandenberg, N.R., 1971, Science 173, 325

[204] Wiita, P.J., Rosen, A., Norman, M., 1990, ApJ, 350, 545

[205] Zensus, J.A., Cohen, M.H., Unwin, S.C., 1995, ApJ, 443, 35

[206] Zinnecker, H., McCaughrean, M.J., Rayner, J.T., 1998, Nature, 394, 862

[207] Znajek, R.L., 1977, MNRAS, 179, 457

[208] Znajek, R.L., 1978, MNRAS, 182, 639

[209] Znajek, R.L., 1978, MNRAS, 185, 833

Appendix A
Publications attached

Stationary magnetohydrodynamic relativistic jets

1. *Collimated jet magnetospheres around rotating black holes.*
   General relativistic force-free 2D equilibrium.
   Fendt Ch., 1997, A&A, 319, 1025 I
2. *Differentially rotating relativistic magnetic jets.*
   Asymptotic trans-field force-balance including differential rotation.
   Fendt Ch., 1997, A&A, 323, 999 XIII
3. *Collimating, relativistic, magnetic jets from rotating disks.*
   The axisymmetric field structure of relativistic jets and the example of the M87 jet
   Fendt Ch., Memola E., 2001, A&A, 365, 631 XXV
4. *Magnetically driven superluminal motion from rotating black holes.*
   Solution of the magnetic wind equation in Kerr metric.
   Fendt Ch., Greiner J., 2001, A&A, 369, 308 XXXVII

Numerical magnetohydrodynamic simulations

5. *Long-term evolution of a dipolar-type magnetosphere interacting with an accretion disk*
   Fendt Ch., Elstner D., 1999, A&A, 349, L61 LIII
6. *Long-term evolution of a dipolar-type magnetosphere interacting with an accretion disk.*
   II. Transition into a quasi-stationary spherically radial outflow
   Fendt Ch., Elstner D., 2000, A&A, 363, 208 LVII
7. *Formation of protostellar jets - effects of magnetic diffusion*
   Fendt Ch., Cemeljic M., 2002, A&A, 395, 1043 LXXIII

A link to the observations

8. *Possible bending mechanisms of protostellar jets*
   Fendt Ch., Zinnecker H., 1998, A&A, 334, 750 LXXXVII
9. *Theoretical thermal X-ray spectra from relativistic MHD jets*
   Memola E., Fendt Ch., Brinkmann W., 2002, A&A, 385, 1089 XCIII

Astron. Astrophys. 319, 1025–1035 (1997)

ASTRONOMY
AND
ASTROPHYSICS

Collimated jet magnetospheres around rotating black holes

General relativistic force-free 2D equilibrium

Christian Fendt⋆

Lund Observatory, Box 43, S-22100 Lund, Sweden (chris@astro.lu.se)

Received 30 April 1996 / Accepted 27 August 1996

Abstract. There is common belief that superluminal jet motion from active galactic nuclei and from galactic high energy sources originates in the magnetized environment of a rotating black hole surrounded by an accretion disk.

The structure of these jet magnetospheres follows from solutions of the so called stream equation for the force-balance between axisymmetric magnetic surfaces. In this paper, two-dimensional force-free solutions of the stream equation are numerically obtained in a general relativistic context (3+1 formalism on Kerr geometry).

We apply the numerical method of finite elements. In this approach, the regularity conditions along the light surfaces are automatically satisfied. After an iterative adjustment of the poloidal current distribution and the shape of the jet boundary, we find magnetic field configurations without kinks at the outer light surface.

The solutions extend from the inner light surface of the Kerr black hole to the asymptotic regime of a cylindrically collimated jet with a finite radius. Different magnetic flux distributions along the disk surface were investigated. There is strong evidence for a hollow jet structure.

Key words: MHD – ISM: jets and outflows – galaxies: jets – black hole physics

1. Jet formation around black holes

Jet motion originating in the close environment of a rotating black hole is observationally indicated for two classes of sources concerning mass and energy output.

The first class are the active galactic nuclei (hereafter AGN). Following the standard model, AGN jet formation develops in the magnetized environment around rotating, super massive black holes with a mass of the order of $10^8 - 10^{10}\,M_\odot$ (Sanders et al. 1989, Blandford & Payne 1982, cf. Blandford et al. 1990, Kollgaard 1994). From evolutionary arguments (accretion of angular momentum) these black holes are believed to be very rapid rotators.

In some quasars and BL Lacertae objects, the jet knots are observed to follow helical trajectories on parsec-scale with a de-projected highly relativistic speed. The high jet velocity together with a small angle between the line of sight and the propagation vector involves a time shift from knot time to observer time, and thus the projected jet motion appears as *superluminal motion*. Examples are 3C 273 (Schilizzi 1992, Abrahan et al. 1994) and 3C 345 (Zensus et al. 1995).

Radio observations have also detected superluminal motion in the Galaxy. Examples are the high energy source 1915+105 (Mirabel & Rodriguez 1994) and the X-ray source GRO J1655-40 (Tingay et al. 1995). The de-projected jet speed of both sources is surprisingly similar ($0.92\,c$). This velocity may correspond to the escape velocity from a point near the black hole (Mirabel & Rodriguez 1995). However, there are not many details known about the intrinsic sources.

In both cases, the jets are detected in non-thermal radio emission, clearly indicating a magnetic character of the jet formation and propagation.

From the introductionary remarks above, it is clear that a quantitative analysis of the jet structure in these sources must take into account both magnetohydrodynamic (hereafter MHD) effects and general relativity.

In this paper we will numerically investigate the structure of a jet magnetosphere in Kerr geometry. The calculated field distributions represent *global* solutions to the *local* cross-field force-balance equation.

The first theoretical formulation of the electromagnetic force-equilibrium in Kerr space-time around fast rotating black holes was given by Blandford & Znajek (1977) and Znajek (1977). They presented the first solutions of the problem and discovered the possibility of extracting rotational energy and angular momentum from the black hole electromagnetically (the so called Blandford-Znajek process). Okamoto (1992) investigated the black hole magnetic field structure and the black hole evolution under influence of the Blandford-Znajek process. Ex-

⋆ Present address: Landessternwarte, Königstuhl, D-69117 Heidelberg, Germany (cfendt@lsw.uni-heidelberg.de)

amining the fast magnetosonic points of the wind and the accretion, he found analytical expressions for the poloidal current and the field rotation law.

With the development of the 3+1 split of Kerr space-time (Thorne & Macdonald 1982, Macdonald & Thorne 1982, Thorne et al. 1986) the understanding of the electrodynamics of rotating black holes became more transparent. For a chosen global time, the tensor description splits up in the usual fields $\boldsymbol{B}$, $\boldsymbol{E}$, current density $\boldsymbol{j}$, and charge density ρ. The formulation of the MHD equations becomes very similar to that of flat Minkowski space, which are used in pulsar electrodynamics.

Using this powerful tool, Macdonald (1984) calculated first the numerical solutions for the magnetic field force-balance around rotating black holes. Three models (magnetic field distribution roughly radial, uniform, or paraboidal) of differentially rotating magnetospheres were investigated, however, the integration region was limited to $\lesssim 10$ horizon radii.

Camenzind (1986, 1987) formulated a fully relativistic description of hydromagnetic flows, basically applicable to any field topology. The so-called wind equation considers the stationary force-balance of the plasma motion along the magnetic field. The (flat space) transfield equation was solved by using the method of finite elements.

Haehnelt (1990) extended this procedure for Kerr space-time in the 3+1 description. The solutions explicitly show the interrelation between the poloidal current strength and the collimation of the flux surfaces. They were calculated on separate integration domains inside and outside the light cylinder (see Camenzind 1990). However, there was a mismatch between the inner and outer solution at the light cylinder, which is a singular surface of the relativistic transfield equation. This matching problem is well known from in the literature of pulsar magnetospheres (Michel 1991).

So far, no global magnetic field solutions could yet be found originating in the accretion disk close to the rotating black hole and, passing through the outer light surface, eventually reaching the asymptotic regime of a collimated jet.

The matching problem of relativistic force-free magnetospheres was investigated in the context of stellar jets (Fendt 1994, Fendt et al. 1995). It then became clear that a mismatch at the light cylinder could be removed by a proper adjustment of the current distribution and the outer boundary condition, which could be interpreted as an adjustment of the "magnetic pressure equilibrium" between the regions inside and outside the light cylinder.

In this paper, we like to extend the results from Fendt et al. (1995) to the general relativistic context. The solutions presented here are *global* solutions for the stationary black hole force-free electrodynamics in the sense that they smoothly pass the singular surface of the outer light surface. The field lines originate near the inner light surface close to a rotating black hole and collimate to an asymptotic jet of finite radius of several (asymptotic) light cylinder radii.

The structure of this paper is as follows. In Sect. 2, basic equations of the theory of relativistic magnetospheres in the context of Kerr metric are reviewed. In Sect. 3, the model underlying the numerical calculations is discussed. We present our numerical results in Sect. 4 and discuss solutions with different topologies and jet parameters.

2. MHD description of black hole magnetospheres

The basic equations describing a magnetohydrodynamic (MHD) configuration under the assumptions of axisymmetric, stationary and ideal MHD in the context of Kerr metric were first derived by Blandford & Znajek (1977) and Znajek (1977). In this paper, we apply the MHD formulation in the 3+1 formalism introduced by Thorne & Macdonald (1982), Macdonald & Thorne (1982), or Thorne et al. (1986) (hereafter TPM). In the notation, we follow TPM and Okamoto (1992).

2.1. Space-time around rotating black holes

In the 3+1 split the space-time around rotating black holes with a mass M and angular momentum per unit mass, $a = J/Mc$ is described using Boyer-Lindquist coordinates with the line element

$$ds^2 = \alpha^2 c^2 dt^2 - \tilde{\omega}^2 \, (d\phi - \omega dt)^2 - (\rho^2/\Delta) \, dr^2 - \rho^2 \, d\theta^2 \, . \quad (1)$$

t denotes a global time in which the system is stationary, ϕ is the angle around the axis of symmetry, and r, θ are similar to their flat space counterpart spherical coordinates. The parameters of the metric tensor are defined as usual,

$$\begin{aligned} \rho^2 &\equiv r^2 + a^2 \cos^2\theta & \Delta &\equiv r^2 - 2\,G\,M\,r/c^2 + a^2 \\ \Sigma^2 &\equiv (r^2 + a^2)^2 - a^2 \Delta \sin^2\theta & \tilde{\omega} &\equiv (\Sigma/\rho) \sin\theta \\ \omega &\equiv 2\,a\,G\,M\,r/c\,\Sigma^2 & \alpha &\equiv \rho\sqrt{\Delta}/\Sigma \end{aligned}$$

ω is the angular velocity of the differentially rotating space, or the angular velocity of an observer moving with zero angular momentum (ZAMO), $\omega = (d\phi/dt)_{\rm ZAMO}$, respectively. α is the red shift function, or lapse function, describing the lapse of the proper time τ in the ZAMO system to the global time t, $\alpha = (d\tau/dt)_{\rm ZAMO}$.

The electromagnetic field $\boldsymbol{B}, \boldsymbol{E}$, the current density $\boldsymbol{j}$, and the electric charge density $\rho_{\rm c}$ are measured by the ZAMOs according to the local flat Minkowski space. These local experiments then have to be put together by a global observer for a certain global time using the lapse and shift function for the transformation from the local to the global frame. In spite of this transformation, Maxwell's equations in the 3+1 split look very similar to those in Minkowski space. There is just an additional source term from the differential rotation of space (see below).

2.2. The cross–field force–balance

The magnetospheric structure follows from the force-balance across the flux surfaces. The projection of the equation of motion perpendicular to the field lines provides the stream equation. Here, in the force-free case, only Lorentz forces (perpendicular to the flux surfaces) are considered.

Under the assumption of axisymmetry a magnetic flux function (or stream function) can be defined measuring the magnetic flux through a loop of the Killing vector $\boldsymbol{m} = \tilde{\omega}^2 \nabla\phi$,

$$\Psi(r,\theta) = \frac{1}{2\pi}\int \boldsymbol{B}_{\rm P}\cdot d\boldsymbol{A}\,, \qquad \boldsymbol{B}_{\rm P} = \frac{1}{\tilde{\omega}^2}\nabla\Psi\wedge\boldsymbol{m}. \tag{2}$$

Equivalently, the poloidal current is defined by integration of the poloidal current density through the same loop

$$I = -\int \alpha \boldsymbol{j}_{\rm P}\cdot d\boldsymbol{A} = -\frac{c}{2}\alpha\tilde{\omega}B_{\rm T}\,. \tag{3}$$

The indices P and T denote the poloidal and toroidal components of a vector. The force-free assumption,

$$\rho_{\rm c}\boldsymbol{E} + \frac{1}{c}\boldsymbol{j}\wedge\boldsymbol{B} = 0\,, \tag{4}$$

implies that the poloidal current flows parallel to the poloidal magnetic field $\boldsymbol{B}_{\rm P} \parallel \boldsymbol{j}_{\rm P}$. Thus, $I = I(\Psi)$.

With the assumption of a degenerated magnetosphere, i.e.

$$|B^2 - E^2| >> |\boldsymbol{E}\cdot\boldsymbol{B}| \simeq 0 \tag{5}$$

an angular velocity of field lines can be derived from the derivative of the time component of the vector potential

$$\Omega_{\rm F} = \Omega_{\rm F}(\Psi) = -c(dA_0/d\Psi) \tag{6}$$

With the additional assumption of stationarity, Ampère's law can be expressed as

$$\nabla\wedge\alpha\boldsymbol{B} = \frac{4\pi}{c}\alpha\boldsymbol{j} - \frac{1}{c}(\boldsymbol{E}\cdot\nabla\omega)\boldsymbol{m}\,, \tag{7}$$

(TPM). The differential rotation of space provides an additional source term with the dimension of a current density. The toroidal current density follows from a projection of Eq. (4), the equation of motion in the force-free limit, perpendicular to Ψ,

$$\begin{aligned}\frac{4\pi}{c}\alpha\, j_{\rm T} = &-\frac{\alpha\,(\Omega_{\rm F}-\omega)}{c\,\tilde{\omega}}\nabla\Psi\cdot\nabla\left(\frac{\tilde{\omega}^2(\Omega_{\rm F}-\omega)}{\alpha^2\,c}\right)\\ &-\left(\frac{\tilde{\omega}}{\tilde{\omega}_{\rm L}}\right)^2\tilde{\omega}\nabla\cdot\left(\frac{\alpha}{\tilde{\omega}^2}\nabla\Psi\right)\\ &+\frac{1}{\alpha\tilde{\omega}}\frac{4}{c^2}\,I\,I'\,.\end{aligned} \tag{8}$$

The toroidal component of Ampère's law (7) eventually leads to the stream equation, a non linear partial differential equation of second order for the flux function Ψ,

$$\tilde{\omega}\nabla\cdot\left(\alpha\,\frac{D}{\tilde{\omega}^2}\nabla\Psi\right) = \tilde{\omega}\,\frac{\omega-\Omega_{\rm F}}{\alpha c^2}\Omega_{\rm F}'\,|\nabla\Psi|^2 - \frac{1}{\alpha\tilde{\omega}}\frac{4}{c^2}\,I\,I'\,. \tag{9}$$

Here,

$$D = 1 - \left(\frac{\tilde{\omega}}{\tilde{\omega}_{\rm L}}\right)^2\,, \tag{10}$$

and $\tilde{\omega}_{\rm L}$ denotes the positions of the two light surfaces,

$$\tilde{\omega}_{\rm L}^2 = \left(\pm\frac{\alpha\,c}{\Omega_{\rm F}-\omega}\right)^2\,. \tag{11}$$

The $'$ indicates the derivative $d/d\Psi$. The + sign holds for the outer light surface with $\Omega_{\rm F} > \omega$, while the $-$ sign stands for the inner light surface, where $\Omega_{\rm F} < \omega$. Throughout this paper we will assume a constant angular velocity of the field lines, $\Omega_{\rm F}(\Psi)$ =const. This assumption will be discussed below (Sect. 3.5).

The stream equation was first derived by Blandford & Znajek (1977) and further evaluated in the 3+1 formalism by TPM. A general version of the stream equation including inertial terms and entropy was obtained by Beskin & Pariev (1993).

In the special relativistic limit, $\alpha \to 1$, $\omega \to 0$, and the stream eq. (9) becomes identical to the pulsar equation (Scharlemann & Wagoner 1973).

2.3. Normalization

For large r, $\omega \to 0$ and the metric reduces to Minkowski. We define an asymptotic light cylinder, $R_{\rm L} \equiv c/\Omega_{\rm F}$ (here and in the following (R, Z) denote the cylindrical coordinates). Using the normalization

$$\begin{aligned} r &\Leftrightarrow R_{\rm L}\,r,\\ \tilde{\omega} &\Leftrightarrow R_{\rm L}\,\tilde{\omega},\\ \nabla &\Leftrightarrow (1/R_{\rm L})\,\nabla\,,\\ \Psi &\Leftrightarrow \Psi_{\rm max}\,\Psi\,,\text{ and}\\ I &\Leftrightarrow I_{\rm max}\,I\,,\end{aligned}$$

the stream equation can be written dimensionless

$$\tilde{\omega}\nabla\cdot\left(\alpha\,\frac{D}{\tilde{\omega}^2}\nabla\Psi\right) = -g_{\rm I}\frac{1}{\alpha\tilde{\omega}}\;I\,I'\,. \tag{12}$$

The coupling constant $g_{\rm I}$ measures the strength of the (poloidal current) source term,

$$g_{\rm I} = \frac{4I_{\rm max}^2R_{\rm L}^2}{c^2\Psi_{\rm max}^2} = 4\,(\frac{I_{\rm max}}{10^{18}{\rm A}})^2(\frac{R_{\rm L}}{10^{16}{\rm cm}})^2(\frac{\Psi_{\rm max}}{10^{33}{\rm Gcm}^2})^{-2} \tag{13}$$

(A similar normalization for the $\Omega_{\rm F}$ term in Eq. (9) would reveal a coupling constant $g_\Omega = 1$.)

Two typical length scales enter the problem. (1) The scale of the horizon radius $r_{\rm H}$ determines the influence of gravitation on the metric. (2) The asymptotic light cylinder $R_{\rm L}$ describes the influence of rotational effects on the electrodynamics. The interrelation between these two scaling parameters follows from the definition of the rotation law for the field, $\Omega_{\rm F}(\Psi)$, in terms of the rotation of the black hole, $\Omega_{\rm H}$.

2.4. The regularity condition

At the light surfaces, the stream equation becomes singular and reduces to a non-linear, partial differential equation of first order,

$$\nabla D\cdot\nabla\Psi = -g_{\rm I}\frac{1}{\alpha^2}I\,I'\,. \tag{14}$$

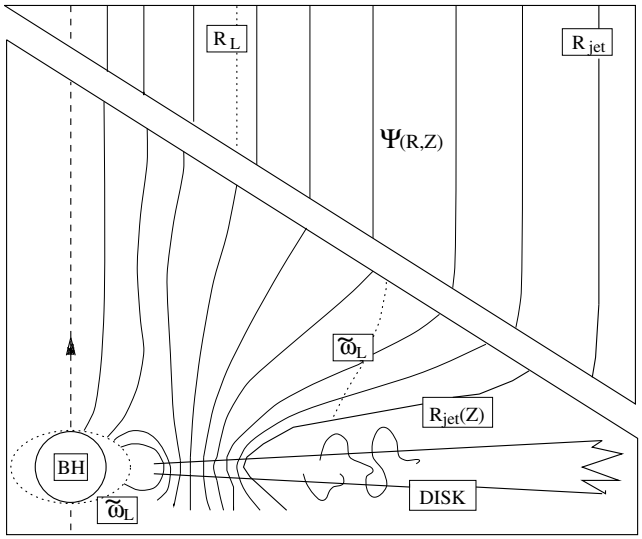

Fig. 1. Applied model topology for the jet formation around rotating black holes. The sketch shows the asymptotic region in the upper part and the inner region around the black hole (BH) in the lower part. The two regions are drawn in different scales.

This regularity condition for Ψ is equivalent to an inhomogeneous Neumann-type boundary condition on the poloidal magnetic field component parallel to the surface $D = 0$ (the light surface),

$$\frac{\partial \Psi}{\partial n} = g_{\rm I}\,\frac{1}{|\nabla D|}\,\frac{1}{\alpha^2}\,I\,I'\,, \quad \boldsymbol{n} = -\frac{\nabla D}{|\nabla D|}\,, \tag{15}$$

where $\boldsymbol{n}$ denotes the unit vector normal to the light surface.

Note that the regularity condition depends on the *strength* of the poloidal current as well as the current *distribution*. This has far reaching consequences for the global field topology. For the special relativistic case, we have shown that the shape of the jet boundary is determined by the regularity requirement (Fendt 1994, Fendt et al. 1995). As it will discussed below, the same applies in the general relativistic case.

3. The model assumptions

We now describe the model assumptions underlying the numerical calculations. The model topology basically follows the standard model for AGN (cf. Blandford 1990).

There is not very much known about the central sources of galactic superluminal jets. Since observationally the jet phenomenon of AGN and of young stellar objects as well is always connected to the signatures of an accretion disk, we assume a similar disk-jet scenario for the jet formation in *galactic* superluminal jet sources.

In the following, we discuss the three main components of the applied model - a central black hole, a surrounding accretion disk, and the asymptotic jet. A schematic overview of the model is shown in Fig. 1.

3.1. The central black hole

In the standard model for AGN the driving engine responsible for the activity is a rotating super massive black hole with a mass of about $10^8 - 10^{10}\mathrm{M}_\odot$ (Sanders et al 1989).

In the case of galactic superluminal sources, there is evidence that the central object is a black hole as well (Mirabel & Rodriguez 1995).

For the calculation of the field structure from the force-free stream equation, gravitational effects of the collapsed object play a non-obvious role. They appear in the stream equation in the description of the gravitogeometric background and in the two light surfaces.

The differential rotation of the space around Kerr black holes leads to the formation of two light surfaces (hereafter LS). Here, the rotational velocity of the field lines relative to the ZAMO equals the speed of light (see Blandford & Znajek 1977). This could be understood from the following. The concept of field lines implies the rigid rotation of each field line. Far from the hole, where ω is small, the outer LS describes the point where the field line velocity equals the speed of light seen from a static observer in the non-rotating space. Close to the hole, the space and the co-moving ZAMO is forced to (differentially) rotate. Since the field line is rigidly rotating, at a certain position (the inner LS) it will reach the speed of light in opposite direction seen from a ZAMO. Here, $\omega > \Omega_{\rm F}$, and the 'field velocity' equals $-c$.

In terms of the global jet solution, the inner LS is very close to the horizon. With the numerical method applied, there is no fundamental hindrance for a solution between the inner LS and the horizon. However, since our main interest is the jet solution, we take the inner LS as inner boundary for the integration region. The black hole horizon itself remains hidden behind the inner LS.

The Schwarzschild radius $R_{\rm S} = 2M$ defines the typical length scale for general relativistic effects,

$$R_{\rm S} = \begin{cases} 1.5\,10^6\ \left(M/5\,\mathrm{M}_\odot\right)\,\mathrm{cm} \\ 3.0\,10^{15}\ \left(M/10^{10}\,\mathrm{M}_\odot\right)\,\mathrm{cm}\,. \end{cases}$$

For rotating black holes the event horizon is changed to $r_{\rm H} = M + (M^2 - a^2)^{1/2}$. The angular velocity of the hole in terms of the Kerr parameter a and mass M is

$$\Omega_{\rm H} = \lim_{r \to r_{\rm H}} \omega = \frac{a}{2\,M}\,\frac{1}{r_{\rm H}}\,. \tag{16}$$

Here, we choose $a = 0.8$.

Mirabel & Rodriguez (1995) mentioned that the deprojected jet speed of $0.9\,c$ for the galactic superluminal jets could be related to the escape velocity from a region close to a black hole. Further, in contrast to other mildly relativistic jets ($\sim 0.3\,c$) this is indicating both a black hole as central source and, also, that the jet origin is very close to the hole at a distance of several horizon radii (Mirabel & Rodriguez 1995).

3.2. The accretion disk

An accretion disk surrounding the central black hole seems to be the essential component concerning magnetic jet formation. It is considered to be responsible for the following necessary ingredients for jet formation, propagation, and collimation.

- *Generation of magnetic field*. In contrast to pulsar or protostellar jets the magnetic field of jets from black holes, the magnetic field cannot be supplied by the central object but has to be supplied by the surrounding accretion disk.
  Khanna & Camenzind (1994, 1996a) were first to formulate the axisymmetric dynamo equations in Kerr space time. They indicated the possibility of an $\omega\Omega$ dynamo, since differential rotation of space ω provides a new source term for the dynamo action. This general relativistic dynamo effect might work very close to the black hole, at distances of about several horizon radii (Khanna & Camenzind 1996a,1996b; Brandenburg 1996).
  In our model we assume that the jet is formed by a *finite* flux distribution of the disk. The maximum flux originates from the disk at radii less than the LS radius, and $\Psi_{\rm max} \simeq 10^{33}\,{\rm G\,cm^2}$.
- *Mass injection into the jet*. The accretion disk supplies the mass for injection into the jet, since there is no mass outflow possible from the black hole itself.
  Certain disk parameters like accretion rate, magnetization and others determine the mass accretion process together with the mass ejection rate (Ferreira & Pelletier 1995). In this paper, we assume that the mass flow is not charge separated and that the plasma is highly conductive in order to justify the assumption of degeneracy (5). Further, the mass flow has to be weak enough (or highly magnetized) in order to assume a force-free source term of the stream equation.
- *The current system*. Differential rotation of the disk is responsible for the poloidal current system in the jet magnetosphere. These currents extract angular momentum from the disk and eventually allow for mass accretion into the central object.
  The poloidal current correspond to toroidal magnetic fields and its hoop stress may be responsible for a collimation of the jet.

The accretion disk physics would further determine the rotation law of the jet magnetic field, $\Omega_{\rm F}(\Psi)$ (see Sect. 3.5).

The disk evolution is definitely influenced by the evolution of the jet and vice versa (cf. Ferreira & Pelletier 1995). However, since this global problem is literally unresolved, in this paper we take into account the accretion disk only as source for the magnetic flux, i.e. as a boundary condition for the flux function Ψ.

3.3. The asymptotic jet

We assume that the asymptotic jet is collimated to a cylindrical shape. This is in agreement with VLBI observations of the knot motion in e.g. 3C 345 (Zensus et al. 1995), and also with kinematic models explaining the short period optical variations by a geometrical lighthouse effect (Camenzind & Krockenberger 1992).

In the case of the parsec-scale jet in the quasar 3C 345, the best model fits give a very small intrinsic opening angle of $\simeq 0.5^\circ$ (Zensus et al. 1995). The innermost region of the jet is not resolved observationally. In the radio VLBI measurements mentioned above, the angular beam resolution is $\sim$ 0.3 mas corresponding to $\sim$ 1 pc. This is comparable to $1000\,R_{\rm S}\,(M/10^{10}\,{\rm M}_\odot)$.

The lighthouse model of Camenzind & Krockenberger (1992) reveals a jet radius of $10\,R_{\rm L}$ for both 3C 273 and BL Lacertae objects under the assumption that the field rotates with the angular speed of the marginally stable orbit. Further, the black hole parameters were assumed to be $a = 0.9$ ($a = 0.8$) and $M = 7\,10^9\,{\rm M}_\odot$ ($M = 5\,10^7\,{\rm M}_\odot$) for 3C 273 (BL Lacertae objects). The degree of jet collimation is very high and initial opening angles of 0.1° (0.05°) are found.

In the asymptotic regime, the metric simplifies to that of flat Minkowski space. Here, the special relativistic, one-dimensional jet equilibrium of Appl & Camenzind (1993) can be applied. They were first to find a non-linear analytical solution for a cylindrically collimated, asymptotic flux distribution,

$$\Psi(x) = \frac{1}{b} \ln\left(1 + \left(\frac{x}{d}\right)^2\right) , \tag{17}$$

where $x = R/R_{\rm L}$ is defined as the cylindrical radius normalized by the asymptotic light cylinder radius. The flux distribution (17) corresponds to a core-envelope structure with core radius d. The poloidal current is concentrated within the jet core (see below). With Eq. (17) the asymptotic jet radius is defined by $\Psi(x_{\rm jet}) = 1$.

Using the method of finite elements for a numerical solution implies that we solve the *boundary* value problem. It is hence suitable to prescribe the *asymptotic* jet boundary $x_{\rm jet}$ and adjust later for the current profile parameter b (see Fendt et al. 1995 for details). This adjustment is the essential procedure in order to satisfy the regularity condition at the light surface.

In conclusion, the poloidal current distribution and the strength of the current are determined by the asymptotic jet. We choose the asymptotic jet radius in terms of asymptotic LC radii $R_{\rm jet} \simeq 3R_{\rm L}$ and $R_{\rm L} = 10\,M$.

3.4. The current distribution

The poloidal current distribution may be considered as a free function for the force-free stream function (although it is constrained by the regularity condition). In particular, since $I = I(\Psi)$ in the 3+1 description too, it is possible to apply the same current distribution for the region near the black hole as for the asymptotic, special relativistic region.

Here, we choose the analytical, non-linear solution for special relativistic (asymptotically cylindrical) pinches given by Appl & Camenzind (1993),

$$I(\Psi) = \frac{1 - e^{-b\Psi}}{1 - e^{-b}} . \tag{18}$$

The parameter b describes the shape of the current profile. Together with the flux distribution (17) this current distribution simultaneously satisfies the asymptotic transfield equation (Appl & Camenzind 1993). The current flow is concentrated within the core radius d (see Eq. (17)). The strength of the current, $g_{\rm I}$, and the shape of the profile ($b \ll 1$ diffuse pinch, $b \gg 1$ sharp pinch) control the magnetic structure and the kinematics of the jet. In particular, they determine the asymptotic jet radius and velocities.

As discussed above, in our approach we choose the jet radius as parameter and adjust the parameters $g_{\rm I}$ and b in such a way that we obtain smooth solutions across the LS with an asymptotic jet radius of a few LC radii.

Eq. (18) represents a monotonous current distribution with no return current within the jet. A closure of the poloidal current flow would be achieved via the jet hot spots terminating the jet and the interstellar/intergalactic medium. In this picture the current is generated in the disk, flows along the jet to the hot spots, and returns back to the accretion disk in the surrounding medium outside of the jet. A return current within the jet might be a more realistic concept. However, serious difficulties for a two dimensional solution are involved with such a current distribution. These are e.g. a proper satisfaction of the regularity condition, as well as the need for a proper boundary condition for the asymptotic jet. We will address this topic to our future work. The solutions presented in this paper may be interpreted as the inner part of such a return current jet.

3.5. The rotation law

As was the case with the current distribution, the rotation law for the flux surfaces is a free function of the force-free stream equation.

In general, this rotation law follows from a detailed examination of the accretion process and the dynamo action in the disk. This is far beyond the scope of this paper and the complex physics of magnetized accretion disks is not yet fully understood. Although there are several models available for the different physical processes involved, such as (magnetic) viscosity, convection, advection, diffusion, kinematics, dynamo action, or relativistic effects, for a combined treatment of all the effects the problem is far from being resolved (not to mention that the jet itself provides an important boundary condition for the disk dynamo).

Having such a solution available, the calculated rotation law, $\Omega(r)$, and flux generation, $\Psi(r)$, would determine the rotation of the magnetic field $\Omega_{\rm F}(\Psi) = \Omega(r(\Psi))$.

As an example we discuss an approximate steady state solution for the flux distribution of a thin accretion disk around a black hole, $\Psi(r) \sim \exp(-k^2 \int_r^{r_{\rm out}} D(\tilde{r}) d\tilde{r})$, where $D(r)$ is the diffusion parameter of the diffusion equation (Khanna & Camenzind 1992). For radii larger than the marginally stable orbit, $D(r) \sim r^{-2}$, and the integration gives $\Psi(r) \sim \exp(-A\sqrt{r_{\rm H}/r})$. Here, $r_{\rm out}$ is the outer disk radius and the constant A is of the order of unity. Assuming a Kepler law for the disk rotation and additionally that the foot points of the flux surfaces rotate with Kepler speed, a possible rotation law for the field lines can be derived. Inverting the above disk flux distribution then leads to the rotation law $\Omega_{\rm F}(\Psi) \sim |\ln(\Psi)|^3$.

As a consequence of differential rotation, the shape and position of the light surface would become *a priori* unknown quantities. Since these are singular surfaces and have to be considered numerically like boundaries, this would involve serious numerical complications. For this reason, for the time being, we consider $\Omega_{\rm F}(\Psi)$ = const. For the rotational velocity of the field, a fraction of the black hole rotation is assumed,

$$\Omega_{\rm F}(\Psi) = \Omega_{\rm F} = \epsilon\, \Omega_{\rm H}\,, \qquad \epsilon < 1 \tag{19}$$

For $a = 0.8, \epsilon = 0.4$, the position of the asymptotic light cylinder is at $R_{\rm L} = 10\, M$.

There is strong indication that the superluminal jets originate very close to a central black hole at distances of a few horizon radii. For galactic sources, the argument is that the jet speed is close to the escape velocity near the horizon (see Mirabel & Rodriguez 1995). Standard models for BL Lacertae objects also put the jet formation close to the central source (see Kollgaard (1994) and references therein).

Thus, for these highly relativistic jet sources, the assumption of a constant rotation of the flux surfaces may well be applied. A problem might exist for only mildly relativistic jet motion.

4. Results and discussion

We now present numerical solutions for the jet magnetosphere. The field distribution is calculated under the assumption of a small plasma loading, or in other words, in the force-free limit. Although the calculations are not entirely self-consistent, these are the first calculations of a collimated global jet magnetosphere in the context of Kerr metric.

Similar to the special relativistic, or even the Newtonian case, in a general relativistic treatment, the singularity of the stream equation at the Alfvén radius (or light surface) leads to a "kinky" structure of the magnetic field at this position, unless the regularity condition is properly satisfied.

In our previous work (Fendt 1994, Fendt et al. 1995) we investigated this problem for fast rotating, stellar magnetospheres. We found that a field matching could be achieved by adjusting both the shape of the jet boundary ($r_{\rm jet}, \theta_{\rm jet}$) and the poloidal current distribution (via the parameter b). This procedure may be interpreted as an adjustment of "magnetic pressure equilibrium" between the regions inside and outside the light cylinder.

In order to obtain smooth solutions at the outer light surface for the Kerr metric jet solutions presented here, we applied the same technique derived earlier (Fendt 1994, Fendt et al. 1995). Again, we emphasize that in the presented solutions the regularity condition at the outer LS determines the shape and the location of the jet boundary in the collimation region.

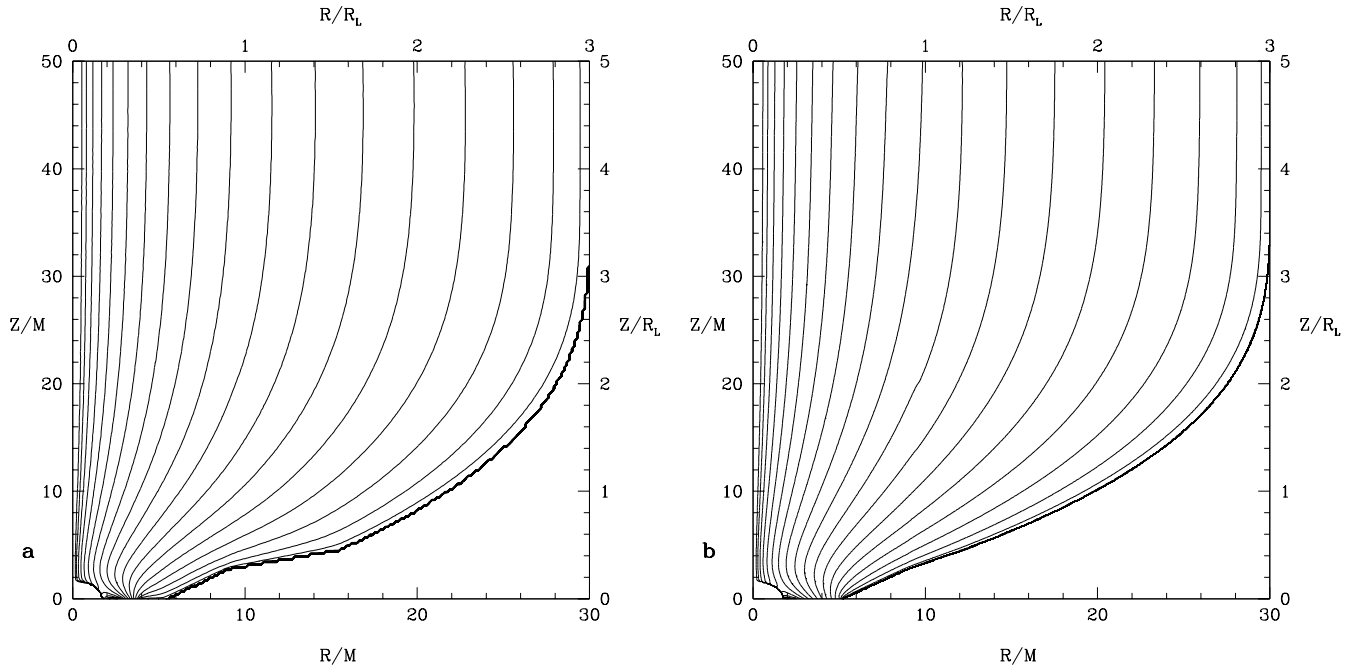

Fig. 2a and b. Magnetic flux surfaces Ψ of global Kerr jet solutions (a = 0.8, $(\Omega_{\rm F}/\Omega_{\rm H})$ = 0.4). The asymptotic jet radius is 3 asymptotic LC radii $R_{\rm L}$. Current distribution parameter **a** b = 1.0, g_I = 1.90, d = 2.29; **b** b = 0.8, g_I = 2.14, d = 2.71. Units: Ψ in $\Psi_{\rm max}$, contour levels 10^{-n^2}, n = 0, 1.8, 0.1; (R, Z) in $R_{\rm L}$ (upper and right axis), or in M (lower and left axis)

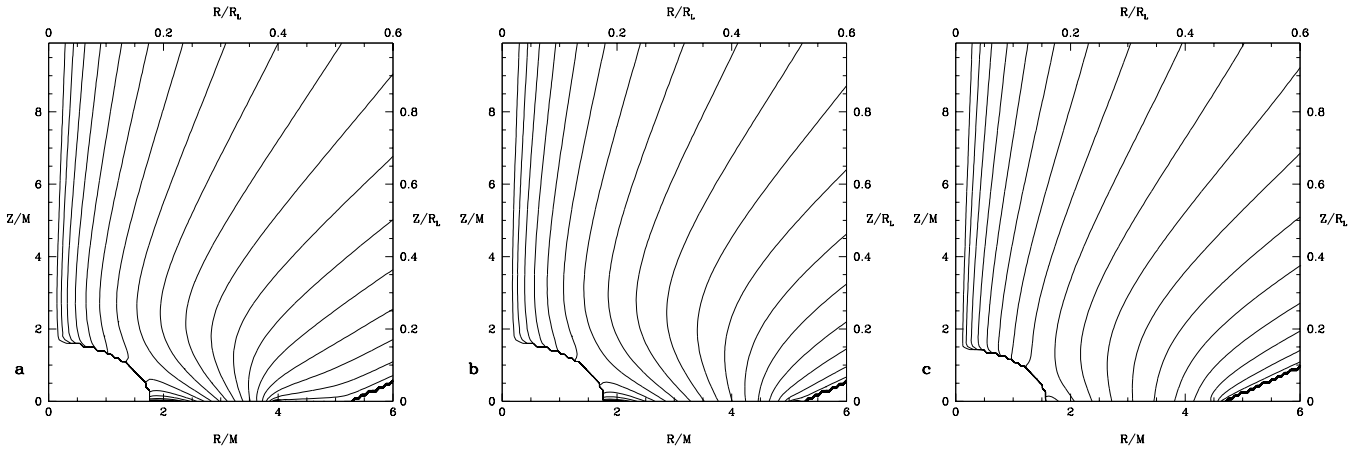

Fig. 3a–c. Magnetic flux surfaces of Kerr jet solutions. Subsets of the inner most regions with different choices of disk distribution. Disk flux distribution parameters **a** n = 4, r_o = 1.76, E = 0.05; **b** n = 3, r_o = 1.76, E = 0.03: **c** n = 2, r_o = 1.16, E = 0.05. The disk flux distribution is $\Psi_{\rm disk}(r, \pi/2) = E\,\Psi_{\rm max}(r - r_o)^n$ (see Appendix A.2). Units as in Fig. 2

4.1. The global jet solution

Fig. 2 shows two examples of global jet solutions extending from the inner LS to an asymptotic jet collimated to a cylindrical shape. The flux surfaces pass the outer LS smoothly.

The asymptotic jet radius is 3 $R_{\rm L}$ corresponding to 30 M for the parameters a = 0.8 and $(\Omega_{\rm F}/\Omega_{\rm H})$ = 0.4, or

$$R_{\rm jet} = \begin{cases} 1.5\,10^7 \ \left(M/5\,{\rm M}_\odot\right)\ {\rm cm} \\ 3.0\,10^{16}\ \left(M/10^{10}\,{\rm M}_\odot\right)\ {\rm cm}\,. \end{cases}$$

The asymptotic jet radius is basically parameterized in terms of the outer LS, i.e. in terms of the rotational velocity of the field. We chose $\Omega_{\rm F} = 0.4\Omega_{\rm H}$ under the assumption that the jet is launched within a distance of some $r_{\rm H}$ from the black hole.

If the field was rotating slower, when the flux surfaces originate further out in the disk, the asymptotic jet radius would be larger. With e.g. a = 0.8 and $(\Omega_{\rm F}/\Omega_{\rm H})$ = 0.1, we obtain an asymptotic jet radius 4 times larger. Note that the linear scaling in terms of $R_{\rm L}$ remains the same. It changes, however, in terms of $r_{\rm H}$.

We report that we were not able to obtain jet solutions with $R_{\rm jet} > 4R_{\rm L}$. The numerical procedure converges in the asymptotic region for asymptotic 1D solutions with any jet radius. However, it does not for a lower boundary condition, which is even slightly different from the asymptotic solution, and thus implying a field curvature. This negative result is not caused by numerical problems. It does not depend on numerical parameters like element size.

Instead, we take this as an indication for an upper limit for the jet radius,

$$R_{\rm jet} < 4\,R_{\rm L}\,, \tag{20}$$

of a cylindrically collimated, rigidly rotating, force-free magnetic jet.

On the other hand, differential rotation or plasma inertia may open up the jet structure. Both effects lead to an increase of poloidal current. The question is whether the corresponding de-collimating toroidal field pressure will supersede the effect by collimating tension. We suppose that the differential rotation plays a minor role as long as all the flux originates within a small region in the disk.

The jet solutions presented here are not 'self-collimated'. The prescription of an *asymptotic* jet boundary may be interpreted as an external pressure from the surrounding material. However, the shape of the collimating jet radius $R_{\rm jet}(Z)$ is determined by the regularity condition and/or the current distribution in the jet, and hence, is determined by the *internal* force-balance.

How the internal force-equilibrium affects the shape of the collimating jet can be seen in Fig. 2. In both solutions, the adjustment procedure (shape of jet boundary $\leftrightarrow$ distribution parameter b) was performed until the regularity condition is properly fulfilled. The two solutions have different poloidal current distributions, $I(\Psi)$. In comparison to the flux distribution with the broader current distribution (b = 0.8), the solution with the more concentrated current distribution (b = 1.0) involves an enhanced expansion (a slight de-collimation) beyond the outer light surface in order to obtain matching between the outer and inner solution.

4.2. The central domain and possible mass flow distribution

Fig. 3 shows subsets of the innermost part around the black hole from global solutions for different disk boundary conditions. These near-disk solutions might be interpreted as a disk corona. The overall picture could be summarized as follows.

- There is magnetic flux outgoing towards the jet.
- There is magnetic flux ingoing towards the black hole (which is hidden behind the inner LS).
- The flux surfaces near the jet axis are not directly connected with the accretion disk.
- Depending on the disk magnetic flux distribution, the curvature of the field lines close to the disk is rather different.

If for the following we imagine a possible mass flow associated with the flux surfaces, we find three different flow regimes within the field distribution – an accretion region, an outflow region, and a region empty of a plasma flow.

The ingoing flux tubes would allow for magnetic accretion from outer parts directly into the black hole. It is however questionable, whether the field strength will be so strong that plasma is accreted along field lines or whether, on the contrary, accretion will be dominated by gravitation and will thereby determine the field topology. This question cannot be answered with the present, force-free approach and depends on parameters like field strength, mass flux, or magnetization.

Under the assumption of a finite flux distribution originating very close to the black hole, the inward-outward bending flux surfaces provide evidence for a hollow jet structure. Although we have to investigate the wind equation along the flux surfaces in order to gain detailed knowledge about the plasma flow behaviour, we believe that the following thoughts and considerations might be reasonable.

First, the slope of the flux surfaces is too small to allow for a 'centrifugal' acceleration of the plasma. Blandford & Payne (1982) obtained a minimum angle enclosed by the disk and flux surface of 60° for the onset of plasma acceleration. Although this result was specifically calculated for a self-similar differentially rotating field structure and a cold wind, we believe that we can use it as an estimate for our case. It seems to be obvious that along a flux surface perpendicular to the disk, a wind driven by centrifugal instability is not possible.

If we therefore consider a hot plasma, the thermal pressure in a hot disk corona has to accelerate the plasma from the disk to heights of about 4 horizon radii above the disk. Here, the slope of the flux surfaces becomes eventually less than the critical value, allowing for 'centrifugal' acceleration. Such strong thermal pressures would require a very hot corona. However, our own experience as well as results published in the literature, show that the slow magnetosonic point of a wind flow is always located very close to the injection point. Thus, thermal pressure is unlikely to be a driving force up to high altitudes above the disk.

Secondly, from our work on the cold relativistic wind equation (Fendt & Camenzind 1996), we know that the stationary character of the flow is very sensitive on the curvature of the poloidal field in the case of a high plasma magnetization. In regions where the slope of the field line changes, it is very likely that no stationary solutions of the wind equation are possible, indicating that here shocks and instabilities may arise. These shock waves could eventually be observed in the asymptotic AGN jet as the helically moving knots seen with the VLBI radio observations (e.g. Zensus et al 1995).

Thirdly, the flux surfaces near the axis are not connected with the disk boundary but with the inner LS. Blandford & Znajek (1977) argued that all particles moving along field lines passing the inner LS must travel inwards. Along these field lines no mass outflow from the disk is possible. We found no solutions with flux surfaces extending from the disk boundary towards the jet axis.

Being aware of the crudeness of the the preceding considerations, we conclude that in the solutions presented here the

plasma will only flow within a thin layer of about $0.1\,R_{\rm jet}$ near the jet boundary, basically forming a hollow jet structure. The inner 90% of the jet cross-section will be empty of plasma flow from the disk. This picture is in good agreement with radio observations of AGN jets revealing moving knots along helical trajectories (Steffen et al. 1995, Zensus et al. 1995). It also fits within recent kinematic radiation models explaining the parsec scale motion of the jet knots by the lighthouse effect (Camenzind & Krockenberger 1992).

4.3. Angular momentum loss and Poynting flux from the black hole

The magnetosphere - poloidal current system is associated with an angular momentum flow and Poynting flux (or luminosity). The total Poynting flux in the jet $P \sim \int \Omega_{\rm F}(\Psi) I(\Psi) d\Psi$ can be calculated, using the known current distribution,

$$P = \frac{I_{\rm max}\Psi_{\rm max}}{R_{\rm L}} \left(\frac{1}{1-e^{-b}} - \frac{1}{b} \right) \tag{21}$$

(see Appl & Camenzind 1993), revealing a similar value for both field distributions in Fig. 2, $P = 0.6\,\left(I_{\rm max}\Psi_{\rm max}/R_{\rm L}\right)$.

The angular momentum loss (dJ_h/dt) from the black hole into the jet follows from the integration of the current distribution for all flux surfaces leaving the horizon to the asymptotic jet,

$$\frac{dJ_h}{dt} = -I_{\rm max}\Psi_{\rm max}\frac{1}{c}\oint I(\Psi)d\Psi\,, \tag{22}$$

and similarly for the Poynting flux (see Okamoto 1992). The outermost flux surface Ψ_h leaving the black hole (or the inner light surface) to the asymptotic jet could be estimated from Fig. 2 and Eq. (18). The integration gives

$$\frac{dJ_h}{dt} = -\frac{1}{c}\,I_{\rm max}\Psi_{\rm max}\left(\frac{\Psi_h + \frac{1}{b}\left(e^{-b\Psi_h}-1\right)}{1-e^{-b}} \right) \tag{23}$$

For the parameters of the solutions in Fig. 2, this gives an angular momentum loss from the black hole $(dJ_h/dt) \simeq 5.6\,10^{-14} I_{\rm max}\Psi_{\rm max}$ for the solution with a concentrated current distribution (Fig. 2a), and $(dJ_h/dt) \simeq 1.8\,10^{-14} I_{\rm max}\Psi_{\rm max}$ for the other one (Fig. 2b). Since the coupling g is similar for both solutions, their (dJ_h/dt) differ by a factor of 3.

What might be surprising with this result is that for two jet solutions with the same asymptotic jet radius, the same total magnetic flux and current flow, and also the same disk flux distribution, the angular momentum extraction from the black hole differs by a non-negligible value, which is determined by the *internal* structure of the jet magnetosphere. A similar calculation for the Poynting flux leads to $P_h \simeq 1.7\,10^{-3}(I_{\rm max}\Psi_{\rm max}/R_{\rm L})$ for the solution in Fig. 2a, and by the same factor 3 less for the other field distribution. The total angular momentum loss and Poynting flux in the jet differ only very few for both solutions.

We conclude this section with mentioning that the above estimates do not necessarely allow for an interpretation in terms of the dynamical evolution of the black hole. In our approach the flux surfaces emanating from the black hole/inner LS to the asymptotic jet also connect from the accretion disk to the black hole (with the same $I(\Psi)$). Thus, the same energy/angular momentum flow leaving the black hole also goes into the hole. What is important for the black hole evolution, are the total energy and angular momentum losses from the disk and the hole by the jet. However, the locally different structure of the current-magnetosphere system might affect the evolution of the accretion process and also radiative processes involved with the accretion.

5. Conclusion

In this work, we presented numerical solutions of the 2D force balance equation for strongly magnetized jets originating from the inner part of an accretion disk surrounding a black hole. The calculations were performed on the background of Kerr geometry.

The model topology underlying the calculations basically follows the standard model for AGN. The jet magnetosphere originates very close to the black hole from an accretion disk. In the solutions presented here, the field rotates rigidly with a fraction of the rotational velocity of the hole. The solutions are global solutions extending from the black hole's inner light surface to an asymptotic jet at a distance of 50 horizon radii.

The asymptotic jet is collimated to a cylindrical shape in agreement with the high degree of collimation observed for extragalactic jets. With the chosen parameters for the rotation, the asymptotic jet radius is 3 light cylinder radii or 30 horizon radii. For a black hole mass of $10^{10}\,{\rm M}_\odot$, this corresponds to a jet radius of $3.0\,10^{16}$cm. We found indications for an upper limit for the asymptotic jet radius for a force-free, cylindrical jet of about 4 light cylinder radii.

The solutions satisfy the regularity condition at the light surfaces and cross the outer light surface smoothly, i.e. without unphysical kinks in the field lines. The matching across this critical surface is achieved by a proper iterative adjustment of the current distribution and the shape of the jet boundary. It therefore determines the shape of the jet in the collimation region.

The field distribution near the disk (the 'corona') is directly influenced by the disk flux boundary condition. In general, the field solutions allow for mass in-fall towards the black hole as well as for mass outflow towards the asymptotic jet. There is strong evidence for a hollow jet structure, i.e. for a mass flow only in the outermost layers of the jet. In the asymptotic regime only the outermost 10% of the jet (in terms of radius) are likely to contain a mass flow.

The angular momentum flow and Poynting flux from the black hole into the jet could be estimated since the current distribution is known. For the field distributions investigated the solution with a concentrated jet current distribution gives angular momentum and energy losses from the hole a factor 3 higher than the other one. However, the total losses by the jet differ only slightly.

Acknowledgements. This work was supported by Swedish Natural Science Research Foundation (NFR). I thank M. Camenzind and M. Haehnelt for ideas the numerical calculations in this paper took advantage from and R. Khanna for helpful discussions. F. Quist is acknowledged for reading the manuscript. I am grateful to the referee, I. Okamoto, for clarifying comments, and especially for suggesting an estimate of the energy and angular momentum losses of the black hole from the current distribution.

Appendix A: numerical details

A.1. Finite element solver

The GSS equation is solved by means of the method of finite elements. The original code was introduced by Camenzind (1987) for relativistic astrophysical MHD applications. Haehnelt (1990) extended the procedure for Kerr metrics. The further evolution (however in special relativity) by Fendt (1994) and Fendt et al. (1995), now enables the code for an integration throughout the singular surface of the light cylinder and the calculation of smooth, global solutions. For the present investigation the latest version of the code (Fendt 1994) was re-arranged for the application in Kerr geometry.

In the finite element approach the integration region G is discretized in a set of isoparametric curvilinear 8-node elements of the serendipity class (Schwarz 1984). Within each element the flux function Ψ is expanded as

$$\Psi(r,\theta) = \sum_{i=1}^{8} \Psi_i^{(e)}\, N_i(\zeta,\eta). \tag{A1}$$

$\Psi_i^{(e)}$ denote the magnetic flux at the nodal point i of the element (e) and (ζ,η) are rectilinear coordinates on the normalized element.

For a solution, the stream equation is multiplied by a test function N (Galerkin ansatz) and integrated over the 2D plasma domain G applying Green's identity. We end up with the *weak form* of the GSS equation,

$$\int_G \frac{\alpha\, D}{\tilde{\omega}}\, \nabla N \cdot \nabla\Psi\, dA = \int_G J\, N\, dA + \int_{\partial G} \frac{\alpha\, D}{\tilde{\omega}}\, N \frac{\partial\Psi}{\partial n}\, ds, \tag{A2}$$

where n now denotes the unit vector perpendicular to the boundary ∂G, dA and ds the area and boundary elements, and J the source term of the R.H.S. of Eq. (12). With Eq. (A1) the integral equation corresponds to a matrix equation

$$\mathsf{A}(\Psi)\ \Psi = \boldsymbol{b}(\Psi), \tag{A3}$$

with the integrals on each grid element

$$A_{ij}^{(e)} = \int_{G_e} \frac{\alpha\, D}{\tilde{\omega}} \left(\Delta\partial_r N_i\ \partial_r N_j + \partial_\theta N_i\ \partial_\theta N_j \right) \frac{dr\, d\theta}{\sqrt{\Delta}}, \tag{A4}$$

and

$$b_i^{(e)} = \int_{G_e} N_i\, J^{(e)}\, \frac{\rho^2}{\sqrt{\Delta}}\, dr\, d\theta + \int_{\partial D} \frac{D}{\tilde{\omega}}\, N_i\, \partial_n\Psi\, ds \tag{A5}$$

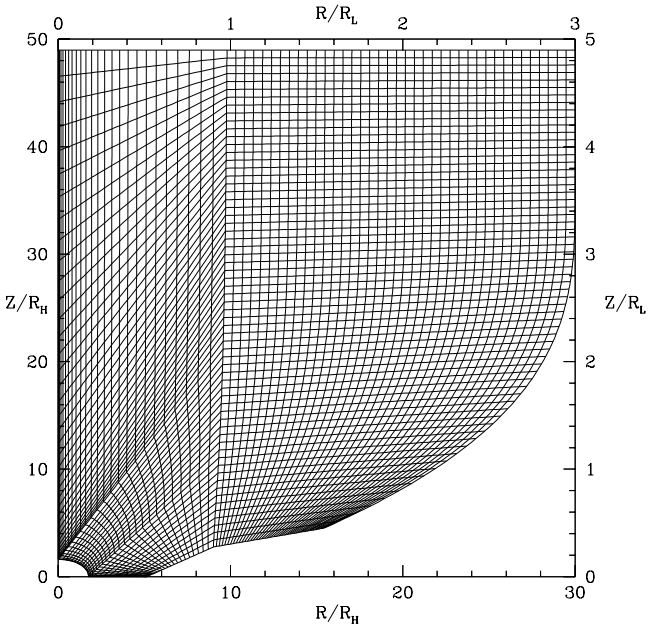

Fig. 4. Example of a numerical grid applied for the finite element code. The element boundaries must follow the shape of the two light surfaces

(Haehnelt 1990). Each component of Eq. (A3) corresponds to the force equilibrium between neighbouring nodal points of each element. Inversion of matrix equation (A3) eventually gives the solution $\Psi_i^{(e)}$ for each nodal point. The expansion (A1) provides the solution in any point $\Psi(r,\theta)$.

A.2. Boundary conditions

With the model assumptions discussed above, the computations have to satisfy the following boundary conditions.

- *Rotational axis*: $\Psi(r,0) = 0$.
- *Light surfaces*: Here, the regularity condition, Eq. (15), has to be satisfied. In the finite element approach this regularity condition is *automatically* satisfied. Like the homogeneous Neumann condition the regularity condition is a natural boundary condition on $D = 0$ in the sense that the surface integral (s. Eq. (A5)) does not contribute (see Fendt et al. 1995).
- *Disk surface*: Here, Ψ satisfies a Dirichlet condition, corresponding to a finite flux distribution,

  $$\Psi_{\rm disk}(r,\pi/2) = E\,\Psi_{\rm max}(r - r_o)^n\,. \tag{A6}$$

  For $r > (1/E)^{1/n} + r_o$, $\Psi_{\rm disk}(r,\pi/2) = 1$. The parameters r_o, E, n are chosen such that the foot points of the flux surfaces are concentrated to the innermost region. This is required by the assumption of a rigid rotation of the magnetosphere.
- *Jet boundary*: Along the jet boundary asymptotically collimating to a cylindrical shape we fix

  $$\Psi_{\rm max} = \Psi(r_{\rm jet},\theta_{\rm jet}) = 1 \tag{A7}$$

  by definition. As mentioned before, the shape of the jet boundary $(r_{\rm jet},\theta_{\rm jet})$ has to be well adjusted (and has to be

found in an iterative way) in order to satisfy the regularity requirement.

– *Asymptotic boundary* $(x, z_{\rm out})$: We assume that the jet has been collimated into a cylindrical shape. In this region with a distance of about $z \gtrsim 50\,{\rm M}$ from the black hole, the geometry is very close to Minkowski space. We use either homogeneous Neumann conditions or the non-linear analytic solution of the special relativistic, asymptotic jet equilibrium Eq. (17) as Dirichlet condition. When the outer and inner domain are calculated separately, then Dirichlet conditions are required at the upper boundary. Otherwise it would not be possible to fix the flux in this domain.

References

Abrahan, Z., et al., 1994, in J.A. Zensus, K.I. Kellermann (Eds), Compact Extragalactic Radio Sources, N.R.A.O., Socorro, p.87

Appl, S., Camenzind, M., 1993, A&A, 274, 699

Beskin, V.S., Pariev, V.I., 1993, Physics Uspekhi, 36, 529

Blandford, R.D., Znajek, R.L., 1977, MNRAS, 179, 433

Blandford, R.D., Payne, D.G., 1982, MNRAS, 199, 883

Blandford, R.D., 1990, in R.D. Blandford, H. Netzer, L. Woltjer, Active Galactic Nuclei, T.J-L. Courvoisier, M. Mayor (Eds), Lecture Notes, Saas-Fee Advanced Course 20, Springer, Heidelberg, p.242

Brandenburg, A., 1996, ApJ, 465, L115

Camenzind, M., 1986, A&A, 162, 32

Camenzind, M., 1987, A&A, 184, 341

Camenzind, M., 1990, Magnetized disk-winds and the origin of bipolar outflows, in: Klare, G. (Ed) Rev. Mod. Astron., 3, Springer, Heidelberg, p. 234

Camenzind, M., Krockenberger, M., 1992, A&A, 225, 59

Fendt, C., 1994, PhD thesis, University of Heidelberg

Fendt, C., Camenzind, M., Appl, S., 1995, A&A, 300, 791

Fendt, C., Camenzind, M., 1996, A&A, 313, 591

Ferreira, J., Pelletier, G., 1995, A&A, 295, 807

Haehnelt, M., 1990, Diploma thesis, University of Heidelberg

Khanna, R., Camenzind, M., 1992, A&A, 263, 401

Khanna, R., Camenzind, M., 1994, ApJ, 435, L129

Khanna, R., Camenzind, M., 1996a, A&A, 307, 665

Khanna, R., Camenzind, M., 1996b, in press

Kollgaard, R.I., 1994, Relativistic jets and the nature of BL Lacertae objects, in: Vistas in Astronomy, 38, 29

Macdonald, D., Thorne, K.,S., 1982, MNRAS, 198, 345

Macdonald, D., 1984, MNRAS, 211, 313

Michel, F.C., 1991, Theory of neutron star magnetospheres, The University of Chicago Press, Chicago

Mirabel, I.F., Rodriguez, L.F., 1994, Nature, 371, L46

Mirabel, I.F., Rodriguez, L.F., 1995, Superluminal motion in our Galaxy, in: H. Böhringer, G.E. Morfill, J.E. Trümper (Eds) 17th Texas Symposium on Relativistic Astrophysics and Cosmology, The New York Academy of Sciences, New York, p. 21

Okamoto, I., 1992, MNRAS, 254, 192

Sanders, D.B., Phinney, E.S., Neugebauer, G., Soifer, B.T., Matthews, K., 1989, ApJ, 347, 29

Scharlemann, E.T., Wagoner, R.V., 1973, ApJ, 182, 951

Schwarz, H.R., 1984, Methode der finiten Elemente, Teubner Studienbücher, Stuttgart

Steffen, W., Zensus, J.A., Krichbaum, T.P., Witzel, A., Qian, S.J., 1995, A&A, 302, 335

Thorne, K.S., Macdonald, D., 1982, MNRAS, 198, 339

Thorne, K.S., Price, R.H., Macdonald, D. (Eds), 1986, Black Holes: The membrane paradigm, Yale University Press, New Haven and London (TPM)

Tingay, S.J. et al., 1995, Nature, 374, 141

Takahashi, M., Nitta, S., Tatematsu, Y., Tomimatsu, A., 1990, ApJ, 363, 206

Thorne, K.S., Macdonald, D., 1982, MNRAS, 198, 339

Zensus, J.A., Cohen, M.H., Unwin, S.C., 1995, ApJ, 443, 35

Znajek, R.L., 1977, MNRAS, 179, 457

This article was processed by the author using Springer-Verlag LaTeX A&A style file *L-AA* version 3.

Astron. Astrophys. 323, 999–1010 (1997)

ASTRONOMY
AND
ASTROPHYSICS

Differentially rotating relativistic magnetic jets

Asymptotic trans- eld force-balance including differential rotation

Christian Fendt

[1] Lund Observatory, Box 43, S-22100 Lund, Sweden (chris@astro.lu.se)
[2] Landessternwarte, Königstuhl, D-69117 Heidelberg, Germany (cfendt@lsw.uni-heidelberg.de)

Received 15 October 1996 / Accepted 30 January 1997

Abstract. Highly collimated jets are observed in various astronomical objects, as active galactic nuclei, galactic high energy sources, and also young stellar objects. There is observational indication that these jets originate in accretion disks, and that magnetic fields play an important role for the jet collimation and plasma acceleration. The rapid disk rotation close to the central object leads to relativistic rotational velocities of the magnetic field lines.

The structure of these axisymmetric magnetic flux surfaces follows from the trans-field force-balance described by the Grad-Schlüter-Shafranov equation. In this paper, we investigate the asymptotic field structure of differentially rotating magnetic jets, widening the study by Appl & Camenzind (1993a,b).

In general, our results show that, with the same current distribution, differentially rotating jets are collimated to smaller jet radii as compared with jets with rigidly rotating field. Differentially rotating jets need a stronger net poloidal current in order to collimate to the same asymptotic radius. Current-free solutions are not possible for differentially rotating *disk*-jet magnetospheres with cylindrical asymptotics.

We present a simple analytical relation between the poloidal current distribution and magnetic field rotation law. A general relation is derived for the current strength for jets with maximum differential rotation and minimum differential rotation. Analytical solutions are also given in the case of a field rotation leading to a degeneration of the light cylinder.

By linking the asymptotic solution to a Keplerian accretion disk, 'total expansion rates' for the jets, and also the flux distribution at the foot points of the flux surfaces are derived. Large poloidal currents imply a strong opening of flux surfaces, a stronger gradient of field rotation leads to smaller expansion rates. There is indication that AGN jet expansion rates are less than in the case of protostellar jets. High mass AGN seem to have larger jet expansion rates than low mass AGN.

Send offprint re uests to: German address

Key words: MHD – ISM: jets and outflows – galaxies: jets – stars: magnetic field – stars: mass loss – stars: pre-main sequence

1. Jet formation from disk magnetic elds

Observations of different kinds of jet sources give convincing evidence that jet formation is always connected to the presence of an accretion disk. This holds for various scales of energy output, jet velocity and nature of the jet emitting objects as there are active galactic nuclei (AGN), galactic superluminal jet sources, mildly relativistic jets from neutron stars (e.g. SS 433), and the numerous class of protostellar jets (e.g. Zensus et al. 1995; Mirabel & Rodriguez 1995; Mundt et al. 1990, Ray et al. 1996).

It is now generally accepted that magnetic fields play an important role in jet formation and propagation for all different kinds of jet sources. These jets are believed to originate very close to the central objects in the interaction region with the accretion disk or in the disk itself.

If the central object is a black hole as it is likely for AGN and galactic superluminal jet sources, the disk is the only possible location for a field generation (by dynamo action or/and advection of magnetic flux).

In the case of protostars and neutron stars the central object also carries a relatively strong magnetic field, and it is not yet clear, whether the jet magnetic field originates in the disk or in the star. However, there must clearly be a strong interaction between the stellar field and the accretion flow in a region, where the stellar field couples to the disk.

Plasma is ejected from the disk into the magnetosphere and becomes magnetically accelerated (see Ferreira & Pelletier 1995). Electric currents and inertia associated with the plasma flow collimate the jet. The observed degree of collimation is very high. The extragalactic jets, the galactic superluminal jets as well as protostellar jets are collimated almost to a cylindrical

shape (Camenzind & Krockenberger 1992, Zensus et al. 1995; Ray et al. 1996).

While for extragalactic and galactic superluminal jets a fully relativistic description is obviously necessary, the case of protostellar jets is more complicated. The protostellar jet velocities of about $\simeq$ 400 km s^{-1} (Mundt et al. 1990) are clearly non-relativistic. However, if the field is anchored in the accretion disk, the rapid rotation of the inner disk may lead to field rotational velocities of the order of the speed of light (Camenzind 1990; see also Fendt et al 1995). In this case a relativistic treatment of the MHD would be required. We emphasise that there are no relativistic effects in the dynamics of the jet motion itself (since the Alfvén surface would be well inside the light surface, where the field rotational velocity equals the speed of light).

Appl & Camenzind (1993a,b; hereafter ACa, ACb) investigated the asymptotic trans-field equation in the case of constant field rotation. They were first to find a non-linear analytical solution for a cylindrically collimated asymptotic field distribution (ACb). They also derived relations between the interesting jet parameters jet radius, current strength, and the field and current distribution.

In previous papers these results where used as a boundary condition for the calculation of global *two*-dimensional jet magnetospheres (Fendt et al. 1995; Fendt 1996). As it was shown, the critical solution of the wind equation along the calculated field structure asymptotically approaches the analytical force-free result (Fendt & Camenzind 1996).

However, since jet motion is connected to an accretion disk, and since the accretion disk rotates differentially, the jet magnetosphere, if it is anchored in the disk, essentially obeys differential rotation. This feature should therefore be a natural ingredient for any magnetic jet structure. How differential rotation effects the asymptotic jet equilibrium, is not obvious, since it involves collimating and de-collimating terms in the force-balance equation. Ferreira (1997) showed that differential rotation plays a major role in recollimation of jets and their asymptotic behaviour.

As a principal problem for differentially rotating relativistic jet magnetospheres, the position and shape of the singular light surface is not known *a priori*, but have to be calculated iteratively in a non-trivial way together with the flux distribution.

A differentially rotating field distribution is further interesting near the jet boundary. Here, models with a rigid field rotation imply a sharp cut off of the field rotation in the jet and in the surrounding interstellar medium, while with a differentially rotating field a smoother transition is possible.

The structure of the paper is as follows. In Sect. 2 we recall some basic equations of the theory of relativistic magnetospheres and discuss several difficulties with the solution of the Grad-Schlüter-Shafranov (hereafter GSS) equation. We evaluate the GSS equation for asymptotic cylindrical jets, including differential rotation. In Sect. 3 we discuss our results. We investigate, whether current free cylindrical jets are possible. We solve the asymptotic GSS equation for different assumptions for the field rotation and finally present a general analytic relation between the current distribution and the rotation law.

2. tructure of magnetic jets

Throughout the paper we apply the following basic assumptions: *axisymmetry*, *stationarity*, and *ideal M D*. We use cylindrical coordinates (R, ϕ, Z) or, if normalised, (x, ϕ, z). The notation is similar to that of Fendt et al (1995) and ACa,b.

We emphasise that the term *asymptotic* always denotes the limit $R << Z$ and that jets with *finite* radius, $Z \rightarrow \quad , R <$ are considered.

2.1. The force-free cross–field force–balance

With the assumption of axisymmetry, a magnetic flux function Ψ can be defined,

$$\Psi = \frac{1}{2\pi} \int \boldsymbol{B}_{\rm P} \cdot d\boldsymbol{A}, \qquad R\boldsymbol{B}_{\rm P} = \nabla\Psi \wedge \quad , \tag{1}$$

measuring the magnetic flux through a surface element with radius R, threaded by the poloidal component (index 'P') of the magnetic field $\boldsymbol{B}$. With Eq. (1) the toroidal component of Ampère's law leads to the GSS equation

$$R\nabla \cdot \left(\frac{1}{R^2} \nabla\Psi \right) = -\frac{4\pi}{c} j \quad , \tag{2}$$

with the toroidal component (index ϕ) of the current density $\boldsymbol{j}$. The poloidal current, defined similarly to the magnetic flux function,

$$I = \int \boldsymbol{j}_{\rm P} \cdot d\boldsymbol{A} = -\frac{c}{2} RB \quad , \tag{3}$$

flows within the flux surfaces, $I = I(\Psi)$. The projection of the force-free, relativistic equation of motion (where inertial effects of the plasma are neglected),

$$0 = \rho_{\rm e} \boldsymbol{E} + \frac{1}{c} \boldsymbol{j} \wedge \boldsymbol{B} \,, \tag{4}$$

(with the electric field $\boldsymbol{E}$ and the charge density $\rho_{\rm e}$) perpendicular to the magnetic flux surface provides the toroidal current density,

$$\begin{aligned} \frac{1}{c} j \quad 1 - \left(\frac{R\Omega_{\rm F}}{c} \right)^2 \Bigg) \;&=\; \frac{1}{4\pi R} \frac{4}{c^2} \frac{1}{2} \frac{dI^2}{d\Psi} \\ &-\; \frac{\Omega_{\rm F}}{4\pi c^2 R} (\nabla\Psi \cdot \nabla)(R^2 \Omega_{\rm F}) \,. \end{aligned} \tag{5}$$

$\Omega_{\rm F}$ is the angular velocity of the field lines and is conserved along the flux surfaces, $\Omega_{\rm F} = \Omega_{\rm F}(\Psi)$. Both the current distribution $I(\Psi)$ and the rotation law of the field, $\Omega_{\rm F}(\Psi)$, determine the source term for the GSS equation and govern the structure of the magnetosphere. Combining Eqs. (5) and (2) the cross-field force-balance can eventually be written as

$$\begin{aligned} R\nabla \cdot \left(\frac{1 - (R\Omega_{\rm F}(\Psi)/c)^2}{R^2} \nabla\Psi \right) \;&=\; -\; \frac{4}{c^2} \frac{1}{R} \frac{1}{2} \frac{d}{d\Psi} I^2(\Psi) \\ &-\; R\,|\nabla\Psi|^2 \frac{1}{2} \frac{d}{d\Psi} \Omega_{\rm F}^2(\Psi), \end{aligned} \tag{6}$$

which is called the modified relativistic GSS equation.

At the light surface with $R = R_{\rm L} \equiv (c/\Omega_{\rm F}(\Psi))$ the rotational velocity of the field lines equals the speed of light. Here, the GSS equation becomes singular. For differentially rotating magnetospheres the shape of this surface is not known a priori and has to be calculated in an iterative way together with the 2D solution of the GSS equation. For constant field rotation the light surface is of cylindrical shape. We choose the following normalisation,

$$\begin{aligned} R, Z &\Leftrightarrow x\,R_0, z\,R_0, \\ \Omega_{\rm F} &\Leftrightarrow \Omega_{\rm F}\,(c/R_0)\,, \\ \Psi &\Leftrightarrow \Psi\,\Psi_{\rm max}\,, \\ I &\Leftrightarrow I\,I_{\rm max}\,, \\ B_{\rm P}^2 &\Leftrightarrow \quad (8\pi\Psi_{\rm max}^2/R_0^4)\,. \end{aligned}$$

For the length scale R_0 the radius of the *asymptotic* light cylinder (see below) is selected. In order to allow for an immediate comparison to rigidly rotating magnetospheres, the normalisation is chosen such that $\Omega_{\rm F} = 1$ at $x = 1$.

With the normalisation applied, Eq. (6) can be written dimensionless,

$$\begin{aligned} x\nabla\cdot\left(\frac{1-x^2\Omega_{\rm F}^2(\Psi)}{x^2}\nabla\Psi\right) = &- g\frac{1}{x}\frac{1}{2}\frac{d}{d\Psi}I^2(\Psi) \\ &- x|\nabla\Psi|^2\frac{1}{2}\frac{d}{d\Psi}\Omega_{\rm F}^2(\Psi). \end{aligned} \qquad (7)$$

g is a coupling constant describing the strength of the current term in the GSS equation,

$$g = \frac{4I_{\rm max}^2R_0^2}{c^2\Psi_{\rm max}^2} = 4\left(\frac{I_{\rm max}}{10^{18}{\rm A}}\right)^2\left(\frac{R_0}{10^{16}{\rm cm}}\right)^2\left(\frac{\Psi_{\rm max}}{10^{33}\,{\rm Gcm}^2}\right)^{-2}$$

in the case of AGN, and

$$g = 4\left(\frac{I_{\rm max}}{10^{12}{\rm A}}\right)^2\left(\frac{R_0}{10^{14}{\rm cm}}\right)^2\left(\frac{\Psi_{\rm max}}{10^{25}\,{\rm Gcm}^2}\right)^{-2}$$

for protostellar parameters. Note that g in this paper is in accordance with the definitions in Fendt et al. (1995) and differs from the definition in ACa,b by a factor of two, $g_{\rm Fendt} = 2\,g_{\rm AC}$. A coupling constant, defined in a similar way for the differential rotation term, would be equal to unity, indicating on the important role of this effect.

2.2. *here is the asymptotic light cylinder located*

We define the *asymptotic* light cylinder, R_0, as the asymptotic branch of the light surface $R_{\rm L}(\Psi)$. Asymptotically, this quantity plays the same role for the GSS equation as the light cylinder does in the case of a rigid rotation of the magnetosphere.

All asymptotic flux surfaces within R_0 rotate slower than the speed of light and $R(\Psi) < R_{\rm L}(\Psi)$. Flux surfaces outside R_0 may rotate faster than the speed of light, here $R(\Psi) > R_{\rm L}(\Psi)$. Despite a possible degeneration of the GSS equation for a special rotation law (see below), there is only a single physical asymptotic light cylinder possible. Therefore, $R_0 \equiv R(\Psi_o) \equiv R_{\rm L}(\Psi_o)$.

It should be noted that the introduction of a light cylinder $R_{\rm L}(\Psi) = c/\Omega_{\rm F}(\Psi)$ also relies on the Ideal MHD assumption. For a non-infinite plasma conductivity a *conserved angular velocity of the field lines* $\Omega_{\rm F}(\Psi)$ cannot be defined. However, even in this case, the field may move with relativistic speed. The mathematical formalism, of course, becomes more complicated and its solution is beyond the scope of this paper. An estimate of diffusion and dynamical times scales for protostellar jets, respectively, leads to the conclusion that the Ideal MHD assumption may be appropriate (Fendt 1994). For AGN this assumption would be even more valid.

2.2.1. Stellar magnetosphere

In the case of a constant field rotation the light cylinder radius just follows from the rotational velocity of the field (and does *not* depend on the flux *distribution* $\Psi(R, Z)$). Under the assumption that the field is anchored in the stellar surface, the field rotation follows from the stellar rotational period $P_\star$. The rotational period of many protostellar jet sources is not known, but in the case of T Tauri stars it is of the order of days. Thus, we estimate the light cylinder radius

$$R_{\rm L} = 2\,10^{15}{\rm cm}\left(\frac{P_\star}{5}\right) = 1.4\,10^4R_\star\left(\frac{R_\star}{2{\rm R}_\odot}\right)^{-1}\left(\frac{P_\star}{5}\right)\,.$$

This radius is of the order of the observationally resolved asymptotic jet radius of about 10^{15} cm (Mundt et al. 1990; Ray et al. 1996). HST observations indicate on slightly smaller jet radii of 20 AU (Kepner et al 1993).

For neutron stars the light cylinder is at

$$R_{\rm L} = 5\,10^9{\rm cm}\left(\frac{P_\star}{1}\right) = 4630R_\star\left(\frac{R_\star}{10^6{\rm cm}}\right)^{-1}\left(\frac{P_\star}{1}\right)\,.$$

2.2.2. Disk magnetosphere

For disk magnetospheres the rotation law is determined by the flux distribution along the disk surface together with the disk rotation. If the foot point of a flux surface on the disk (here the term *foot point* denotes the position along the field line, where ideal MHD sets in) at a radius $R_{\rm D}(\Psi)$ rotates with Keplerian speed, the flux surfaces intersect the light surface at the radius

$$R_{\rm L}(\Psi) = 570R_\star\left(\frac{R_{\rm D}(\Psi)}{R_\star}\right)^{\frac{3}{2}}\left(\frac{M}{3\,{\rm M}_\odot}\right)^{-\frac{1}{2}}\left(\frac{R_\star}{2{\rm R}_\odot}\right)^{\frac{5}{2}}$$

(here for protostellar parameters) with the mass of the central object M. The ratio between the position radius of the light surface and the light cylinder for rigid rotation is then

$$\frac{R_{\rm L}(\Psi)}{R_{\rm L}} = 0.05\left(\frac{R_{\rm D}(\Psi)}{R_\star}\right)^{\frac{3}{2}}\left(\frac{R_\star}{2{\rm R}_\odot}\right)^{\frac{3}{2}}\left(\frac{M}{3\,{\rm M}_\odot}\right)^{-\frac{1}{2}}\left(\frac{P_\star}{5}\right)^{-1}$$

(again for a protostellar disk magnetosphere). Is the central object a neutron star, this ratio decreases by a factor of about 100. For AGN we can estimate

$$R_{\rm L}(\Psi) = 4\,10^{15}{\rm cm}\left(\frac{R_{\rm D}(\Psi)}{R_{\rm S}}\right)^{\frac{3}{2}}\left(\frac{M}{10^{10}\,{\rm M}_\odot}\right),$$

and in general

$$\frac{R_{\rm L}(\Psi)}{R_{\rm S}} = \sqrt{2}\left(\frac{R_{\rm D}(\Psi)}{R_{\rm S}}\right)^{\frac{3}{2}}, \tag{8}$$

where $R_{\rm S}$ is the Schwarzschild radius of the black hole.

The question, whether or not a relativistic description is required for the jet magnetosphere, depends on the *asymptotic* radius of the flux surface, R . If for any flux surface $R_{\rm L}(\Psi) \lesssim R\ (\Psi)$, a relativistic description of the magnetosphere is required. In the contrary, if for all flux surfaces $R_{\rm L}(\Psi) > R\ (\Psi)$, the Newtonian description is appropriate. Note that even then, for two arbitrary flux surfaces Ψ_1 and Ψ_2 with $R\ (\Psi_1) < R\ (\Psi_2)$, $R_{\rm L}(\Psi_1) < R\ (\Psi_2)$ is possible.

In principal, the asymptotic field distribution is a result of the two-dimensional force-balance of the jet, and therefore should follow from the solution of the two-dimensional GSS equation. We hypothesise that the asymptotic force-free solution will uniquely be determined by the disk flux and current distribution (and vice versa).

Our results for differentially rotating jets can hardly deliver a statement about the *absolute* value of the asymptotic jet radius, but only in terms of the asymptotic light cylinder jet radius R_0.

2.3. The asymptotic force-balance

In the asymptotic regime of a highly collimated jet structure we reduce Eq. (7) to a one-dimensional equation, equivalent to the assumption $\partial\ >> \partial$.

Then, $\Psi(x,z) \rightarrow \Psi(x)$, and the conserved quantities $I(\Psi)$ and $\Omega_{\rm F}(\Psi)$ can be expressed as functions of x. If we further assume a monotonous flux distribution $\Psi(x)$, the derivatives $(\partial/\partial\Psi) \rightarrow (d\Psi/dx)^{-1}(d/dx)$. Note that this excludes hypothetical solutions with a return current from our treatment (see also Sect. 3.4.1).

With the assumptions made above, the GSS Eq. (7) reduces to an ordinary differential equation of *first order* in the derivative $(d\Psi/dx)^2$,

$$\left(1-x^2\Omega_{\rm F}^2\right)\frac{d}{dx}(\frac{d\Psi}{dx})^2 + \left(\frac{4}{x} - 2x\Omega_{\rm F}^2 - x^2\frac{d\Omega_{\rm F}^2}{dx}\right)(\frac{d\Psi}{dx})^2 + g\frac{dI^2}{dx} = 0 \tag{9}$$

Since $(x^{-2}d\Psi/dx)^2$ is related to the magnetic pressure of the poloidal field, Eq. (9) can be rewritten as

$$\left(1-x^2\Omega_{\rm F}^2\right)\frac{d}{dx} - 4x\ \left(\Omega_{\rm F}^2 + \frac{x}{4}\frac{d\Omega_{\rm F}^2}{dx}\right) = -\frac{g}{8\pi x^2}\frac{dI^2}{dx}. \tag{10}$$

The magnetic flux function then follows from integration of

$$\frac{d\Psi(x)}{dx} = x\sqrt{8\pi\ (x)} \tag{11}$$

with $\Psi(x=0)=0$. At the singular point $x=1$ the solution (x) must satisfy the regularity condition

$$(1) = \frac{g}{8\pi}\frac{dI^2(1)}{dx}\left(4+\frac{d\Omega_{\rm F}^2(1)}{dx}\right)^{-1}. \tag{12}$$

We mention that Eq. (10) can also be derived from the equation for the asymptotic force-equilibrium perpendicular to the flux surfaces,

$$\left(1-\frac{R^2}{R_{\rm L}^2}\right)\nabla\ \frac{B_{\rm P}^2}{8\pi} - \frac{RB_{\rm P}^2}{2\pi R_{\rm L}^2}\nabla\ R\ - \frac{B_{\rm P}^2\Omega_{\rm F}}{4\pi c^2}\nabla\ (R^2\Omega_{\rm F}) + \frac{1}{8\pi R^2}\nabla\ (RB\ )^2 = 0\,, \tag{13}$$

where ∇ indicates the gradient perpendicular to the flux surfaces, and where poloidal field curvature and the centrifugal force are neglected (Chiueh, Li & Begelman, 1991; ACa).

2.4. Discussion of the force-free assumption

One may question the assumption of a force-free asymptotic jet. Indeed, in a self-consistent picture of jet formation, the asymptotic jet is located beyond the collimating, non force-free wind region and beyond the fast magnetosonic surface. The asymptotic jet parameters are determined by the critical wind motion and thus, the poloidal current and the angular velocity of the field are *not* functions free of choice.

The essential point here is the assumption of a *cylindrical* shape of the asymptotic jet, an assumption, however, which is clearly indicated by the observations. The general, *non force-free* expression for the poloidal current is

$$RB\ = -4\pi\frac{\eta(\Psi)E(\Psi)}{\Omega_{\rm F}(\Psi)}\frac{x^2\ -x^2}{1-M^2-x^2},$$

where $\eta(\Psi)$ is the particle flow rate per flux surface, $E(\Psi)$ is the conserved total energy, M the Alfvén Mach number, and $x\ (\Psi)$ the Alfvén radius of the flux surface. For cylindrical flux surfaces, *all* quantities on the r.h.s. are functions of Ψ, and thus, also RB is a function of Ψ. Although RB is not equal to the force-free current, it enters Eqs. (10) and (13) in a similar way.

The centrifugal term, which was neglected in Eq. (13), is $-\ ^2\rho R\Omega^2$, with the plasma density ρ and plasma angular velocity Ω (see ACa). This term may be important for small plasma densities ρ, where $R\Omega$ might be large, as well as for high densities, where the toroidal plasma velocity is supposed to be small. We can estimate the importance of this term by normalising and introducing a coupling constant

$$g\ = \frac{\dot{M}_{\rm jet}cR_0^2}{\pi\Psi_{\rm max}^2},$$

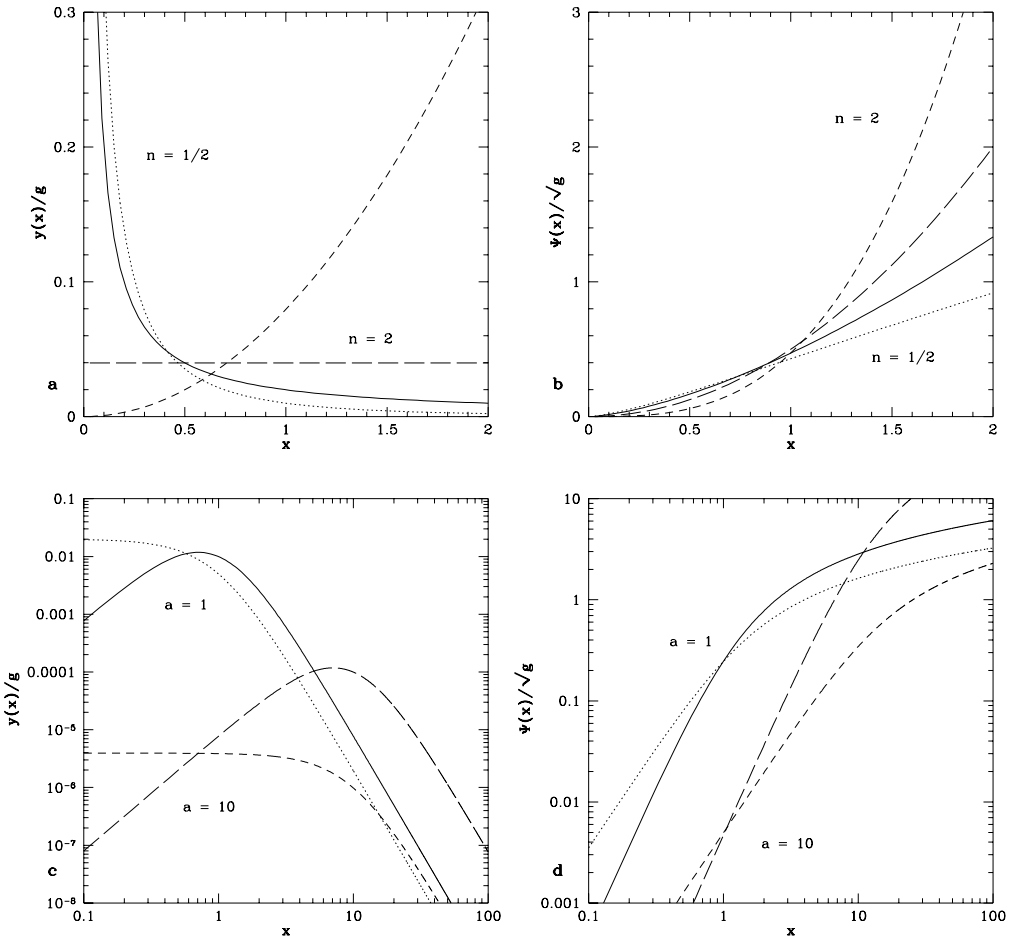

Fig. 1. a c Magnetic pressure distribution ( ) and **b d** flux distribution $\Psi(\ )$ for a field rotation law $\Omega_{\rm F}(\ ) = (1/\ )$ (solid, long-dashed) and $\Omega_{\rm F}(\ ) \equiv 1$ (dotted, short-dashed). **a b** Current distribution $(\ ) = \ ^{n}$, $n = 0.5, 2$, **c d** current distribution (22), $a = 1, 10$, $n = 2$.

which is of the order of one tenth for a jet mass loss rate $\dot{M}_{\rm jet} \simeq 10^{-2}{\rm M}_\odot{\rm yr}^{-1}$ and other parameters typical for AGN.

For protostellar jet parameters and a mass loss rate $\dot{M}_{\rm jet} \simeq 10^{-10}{\rm M}_\odot{\rm yr}^{-1}$, g increases by a factor of 1000. However, in this case we may expect that the Alfvén surface of the plasma motion is located well inside the light cylinder. Thus, the plasma, rotating with constant angular momentum beyond the Alfvén surface, has a decreasing and low angular velocity Ω (which is normalised to the $\Omega_{\rm F}$). The centrifugal term $\sim \Omega^2$ may become comparatively small. We emphasise that the latter arguments are rather (simplifying) assumptions than keen conclusions, as long as the true non force-free jet equilibrium is not investigated.

Contopoulos & Lovelace (1994) and Ferreira (1997) constructed *self-similar* solutions including centrifugal forces showing that the magnetic terms indeed may dominate the centrifugal term for large radii leading to a recollimation of the outflow.

2.5. Solution of the asymptotic GSS e uation

Eq. (10) can be solved by the method of the variation of constants. The integrating factor of the differential equation is

$$M(x) = \exp\left(\int -4x \frac{\Omega_{\rm F}^2(x) - \frac{}{4} - \Omega_{\rm F}^2(x)}{1 - x^2\Omega_{\rm F}^2(x)} dx \right) , \qquad (14)$$

with the formal solution

$$(x) = \frac{1}{M(x)} \left(- \int \frac{M(x)}{1 - x^2\Omega_{\rm F}^2(x)} \frac{g - I^2(x)}{8\pi x^2} dx \right) \qquad (15)$$

Using Eq. (12), the general solution can be evaluated,

$$(x) = \frac{1}{M(x)} \frac{g}{8\pi} \int^1 \frac{1}{\tilde{x}^2} \frac{M(\tilde{x})}{1 - \tilde{x}^2\Omega_{\rm F}^2(\tilde{x})} \frac{d}{d\tilde{x}} I^2(\tilde{x}) d\tilde{x} \, . \qquad (16)$$

As already mentioned by ACa, the solution (x) is determined by the regularity condition (12). The magnetic flux function is

$$\Psi(x) = \int_0 \ \tilde{x} \sqrt{8\pi \ (\tilde{x})} d\tilde{x} \, . \qquad (17)$$

In the case of a constant field rotation, ACb found an analytical, non-linear solution to the asymptotic GSS equation, the flux distribution

$$\Psi(x) = \frac{1}{b} \ln \left(1 + \left(\frac{x}{a} \right)^2 \right) , \qquad (18)$$

together with the current distribution

$$I(\Psi) = \frac{1 - e^{-b\Psi}}{1 - e^{-b}} , \qquad (19)$$

leading to a certain relationship between the current distribution parameter b, the core radius a, the coupling constant g, and the asymptotic jet radius $x_{\rm jet} \equiv x(\Psi = 1)$.

3. Results and discussion

We now discuss different solutions of the asymptotic GSS equation including differential rotation. We first consider the case of vanishing poloidal current. We give an analytical solution for a special rotation law leading to a 'degeneration' of the asymptotic light cylinder. Then, Eq. (10) is solved numerically for different assumptions for the asymptotic field rotation $\Omega_{\rm F}(x)$. Finally, using a general ansatz for the asymptotic field distribution we derive a relation between $I(\Psi)$ and $\Omega_{\rm F}(\Psi)$.

In general, the differential equation for the field pressure (10) can be rewritten as a differential equation for the angular velocity of the field lines,

$$\frac{d\Omega_{\rm F}^2}{dx} + \left(\frac{4}{x} + \frac{d(\ln\ )}{dx} \right) \Omega_{\rm F}^2 = \frac{g}{8\pi} \frac{1}{x^4} \frac{dI^2}{dx} + \frac{1}{x^2} \frac{d(\ln\ )}{dx}, \quad (20)$$

with the formal solution

$$\Omega_{\rm F}^2(x) = \frac{1}{x^4} \left(\quad + \frac{g}{8\pi} I^2(x) + \int x^2 \frac{d}{dx} \right) . \quad (21)$$

For *physical* reasons, $\Omega_{\rm F}^2(x)$ should be monotonous (since coupled to the disk rotation), and positive for all x. In order to be consistent with the chosen normalisation, we further require $\Omega_{\rm F}^2(1) = 1$, and $x^2\Omega_{\rm F}^2 < 1$ for $x < 1$. From the latter condition, it follows that the integration constant must vanish, $\quad = 0$. Otherwise the rotational velocity $x\Omega_{\rm F}$ of the field would diverge for $x \to 0$. Note that, although the angular velocity may diverge with $\Omega_{\rm F} \sim 1/x \quad , 0 <$ $\quad$ 1, the rotational velocity remains finite for $x \to 0$.

We can further see that for particular choice, a bounded current distribution with the core radius a,

$$I(x) = \frac{(x/a)^n}{1 + (x/a)^n} , \quad (22)$$

and for $n \quad 2$ the current term in Eq. (21) does not diverge in the limit $x \to 0$, leading to finite angular field rotation (since $\quad$ (0) must be finite), while for $n \gtrsim 1/2$ the angular velocity diverges but not the rotational velocity, $x\Omega_{\rm F} \to$ finite value.

3.1. The case of constant or vanishing current

Now we take a look at the case of a vanishing poloidal current. A constant current, $I(x) = \text{const}$, would imply a divergence in the field rotation.

If $I(x) = 0$, from the regularity condition (12) it follows that $\quad$ (1) = 0. From Eq. (21) we conclude that a physical rotation law (which does not diverge at $x = 1$) requires that the numerator $\int x^2(d\ /dx)dx$ vanishes together with the denominator x^4 . This, however, is in contradiction with the requirement of a decreasing, *monotonous* rotation law, as it can be derived from the following. A vanishing integral $\int x^2(d\ /dx)dx$ requires that the integrand changes sign at a certain position. Thus, $\quad(x)$ has to have a maximum (a minimum is ruled out, since $\quad$ (1) = 0), and also the term x^4 . On the other hand, the integral has a maximum too, but not necessarily at the same position. This implies that the ratio of numerator and denominator passes a point of inflection, where both terms equal, and therefore $\Omega_{\rm F}^2 = 1$. Since also $\Omega_{\rm F}(x = 1) = 1$ by definition, this is in contradiction with a monotonous rotation law.

We conclude only from asymptotic considerations that cylindrically collimated differentially rotating jets always carry a non-constant, net poloidal current. This is in agreement with previous results (Heyvaerts & Norman 1989, Chiueh et al. 1991).

3.2. A solution with degenerate light cylinder

The next case we will investigate is for a rotation law

$$\Omega_{\rm F}(x) = \frac{1}{x} . \quad (23)$$

Now all asymptotic field lines rotate with the speed of light, and the light cylinder degenerates. Note that this does not contradict with our choice of normalisation. The length scale is measured in units of R_0, which is the light cylinder of a rigidly rotating magnetosphere. Here, $\Omega_{\rm F}(1) \equiv (\Omega_{\rm F})_{\rm rigid} = 1$.

The rotation law (23) and the corresponding field distribution may be considered as a somehow 'limiting case' for a physical field rotation. For a rotation law with a steeper slope (e.g. for $\Omega_{\rm F}^2 \sim x^{-3}$) the rotational velocity will diverge if $x \to 0$. Also, the surface $x = 1$ then plays the role of a somehow 'inverted' light cylinder since all field lines within (outside) the light cylinder rotate faster (slower) than the speed of light. Whether this behaviour could be considered as appropriate for astrophysical application also depends on the 2D field distribution.

Since for assumption (23) the derivative term of $\quad$ disappears in Eq. (10), we can immediately write down the solution

$$(x) = \frac{g}{16\pi x} \frac{d}{dx} I^2(x) , \quad \Psi(x) = \int_0 \left(\frac{g\tilde{x}}{2} \frac{d}{d\tilde{x}} I^2(\tilde{x}) \right)^{\frac{1}{2}} d\tilde{x}. \quad (24)$$

With a current distribution $I(x) = x^n$ the field distribution is

$$(x) = \frac{g}{16\pi} 2nx^{2n-2} , \quad \Psi(x) = \frac{\sqrt{ng}}{n+1} x^{n+1} . \quad (25)$$

This gives a rotation law for the flux surfaces

$$\Omega_{\rm F}(\Psi) = \left(\frac{\sqrt{ng}}{n+1} \frac{1}{\Psi} \right)^{1/(n+1)} \quad (26)$$

We show the solution with bounded current distribution (22) and $n = 2$ in the Appendix. Fig. 1 displays both results in comparison with a field distribution resulting from a rigid rotation law, $\Omega_{\rm F} \equiv 1$.

We note that Contopoulos (1994) applied a similar rotation law for self-similar solutions of the 2D GSS equation, which take self-consistently into account also plasma inertia effects. With a current distribution $I(x) \sim x^{n-1}$, Eq. (24) reveals

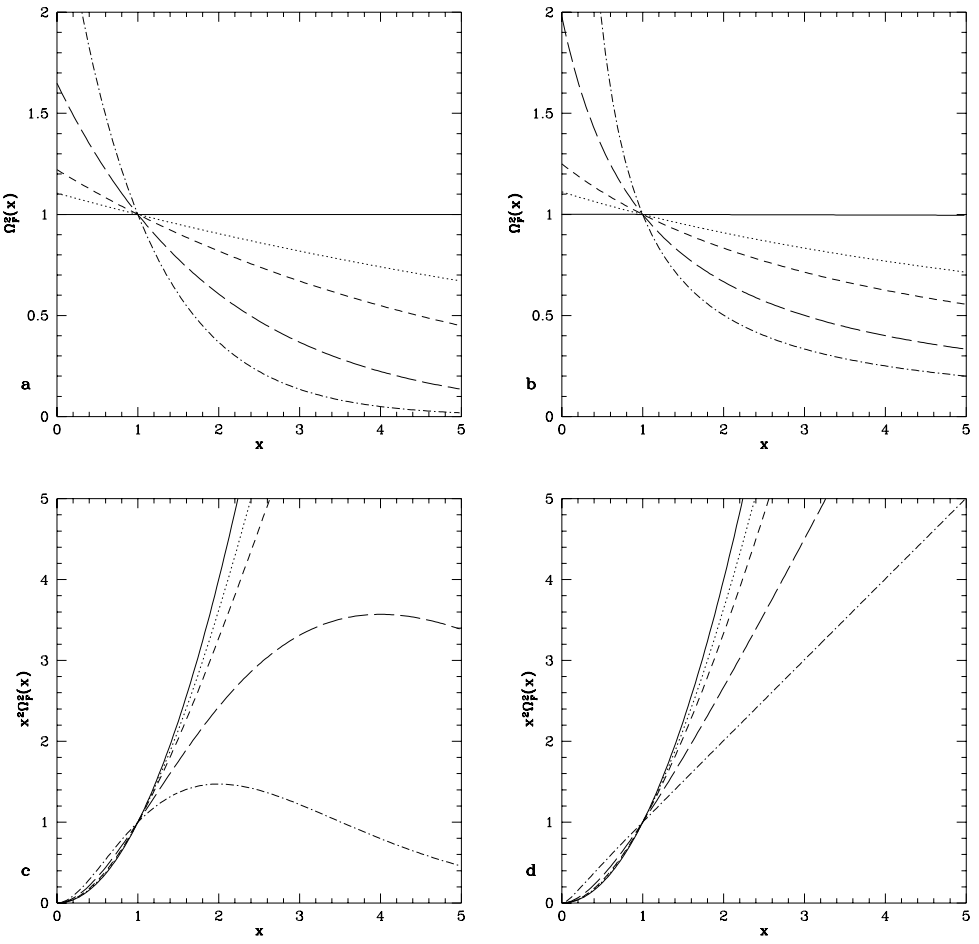

Fig. 2a–d. The rotation laws applied for the asymptotic jet magnetosphere (29) (**a**), (**c**), and (30) (**b**), (**d**). Square of the **a**, **b** angular velocity Ω_F^2, and **c**, **d** the rotational velocity $^2\Omega_F^2$. Parameters: = 0 (solid), = 0.1 (dotted), = 0.2 (short-dashed), = 0.5 (long-dashed), = 1.0 (dotted-dashed).

$\Psi(x) \sim x^n$, which is identical to the results of Contopoulos (1994). In the force free limit, his function (Ψ) is identical to our poloidal current $(2/c)I(\Psi)$.

As a simple application of this differentially rotating field distribution, the asymptotic solutions (25) and (26) are connected to an accretion disk with Keplerian rotation, $\Omega_K(x) = \sqrt{GM/c^2R_0}\,x^{-3/2}$ (we assume here that the flux surfaces originating in the disk rotate with this velocity).

Since the field rotation near the disk $\Omega_F((\Psi(x))_{\rm disk}) \equiv \Omega_K(x)$ must be the same as in the asymptotic regime, $\Omega_F(\Psi)$, the flux distribution near the disk can be calculated,

$$(\Psi(x))_{\rm disk} = \frac{\sqrt{ng}}{n+1} \left(\frac{c^2R_0}{GM}\right)^{n+1} x^{3(n+1)/2}\,. \qquad (27)$$

From the comparison of the disk flux distribution with the asymptotic flux distribution, it follows that for a certain flux surface the ratio between it's asymptotic radius, x Ψ and the radius near the disk $x_{D\ \Psi}$ is

$$\frac{x\quad\Psi}{x_{D\ \Psi}} = \sqrt{\frac{c^2R_0}{GM}}\,x_{D\ \Psi}\,. \qquad (28)$$

We can further calculate the foot point of the outermost flux surface, Ψ = 1, from Eq. (27), and with that and Eq. (28) the 'total expansion rate' of the jet

$$\frac{x_{\rm jet}}{x_{D\ \Psi=1}} = \left(\frac{(n+1)}{\sqrt{ng}}\right)^{1/3(n+1)} \left(\frac{c^2R_0}{GM}\right)^{1/3}\,.$$

The first term in this equation varies rather weakly with g, and is of the order of unity (unless g is not much larger or much less than unity). For the second term we calculate for AGN ($M = 10^{10}\,M_\odot$, $R_0 = 10^{16}$ cm) a number value of about 2, which is surprisingly small, and for protostars ($M = 3\,M_\odot$, $R_0 = 10^{15}$ cm) a value of $\sim$ 1200, respectively. This result may indicate on an intrinsic difference between the two jet sources. However, we should keep in mind that inertial forces may change the protostellar jet expansion rate and that the assumed current distribution might not be appropriate.

Comparing the field distribution near the disk (27) and in the asymptotic region (25) at small radii $x < 1$,

$$\frac{\Psi(x)_{\rm disk}}{\Psi(x)} = \left(\frac{c^2R_0}{GM}x\right)^{(n+1)}\,,$$

we may principally expect a recollimation of certain flux surfaces, depending on the source parameters M, R_0 and the ra-

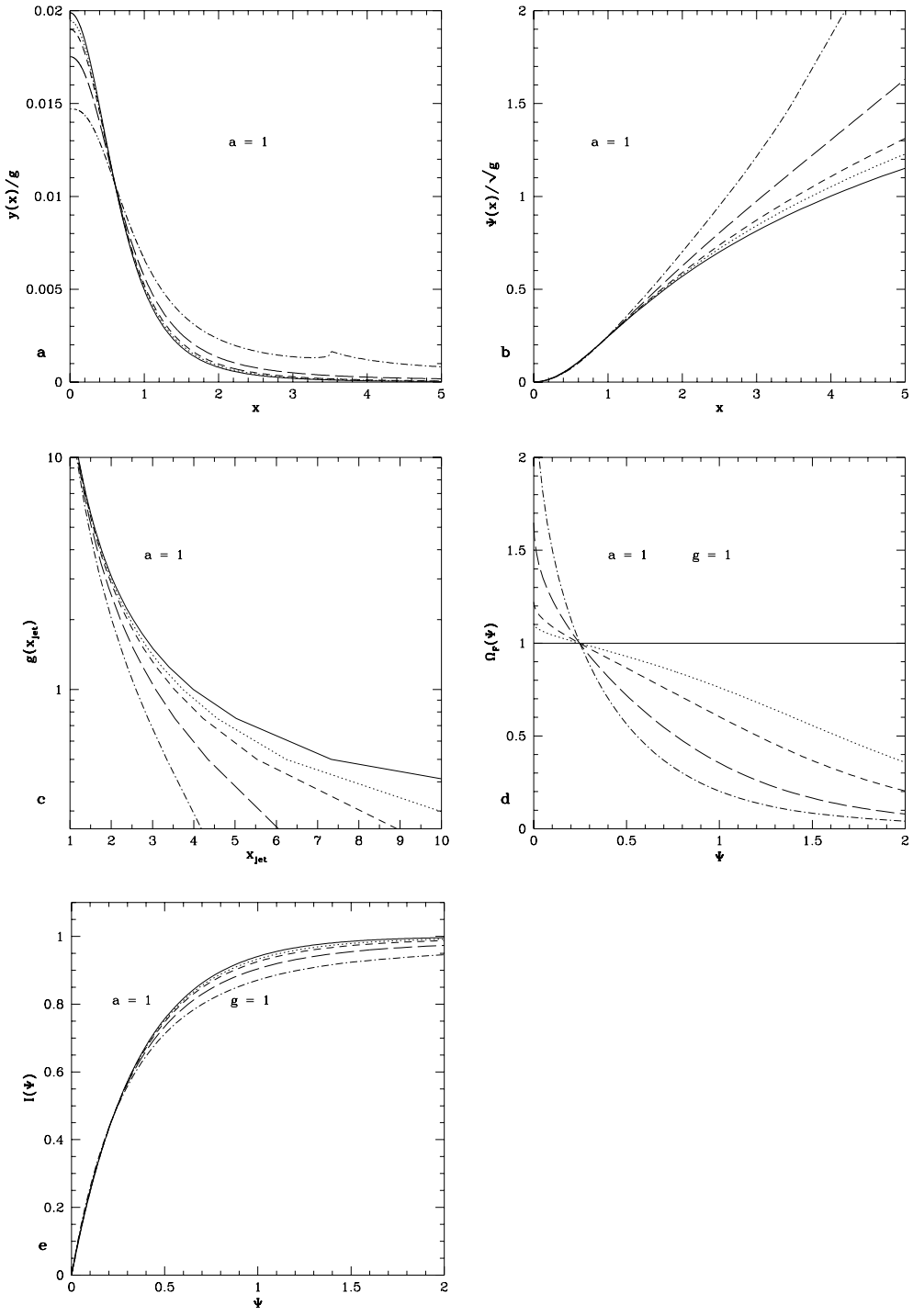

Fig. 3a–e. a Magnetic pressure distribution ( ) and **b** flux distribution $\Psi(\ )$. **c** Coupling constant as a function of the jet radius. The field rotation law is (29) with different steepness parameters, = 0 (solid), = 0.1 (dotted), = 0.2 (short-dashed), = 0.5 (long-dashed), = 1.0 (dotted-dashed). The solid curves coincide with the analytical result from ACb. Note that the solid curves correspond to the dotted curves in Fig. 1c and 1d.

dius x. However, we believe that such kind of conclusions (e.g. 'recollimation predominantly for low mass AGN') might be exaggerated, since not very much is known about the disk field distribution and rotation, especially for small radii near the star, black hole, or disk boundary layer.

3.3. Numerical solutions of the asymptotic GSS including differential rotation

In this section *numerical* solutions to the asymptotic GSS equation with differential rotation are presented. Here, the current distribution is prescribed, and Eq. (10) is solved for different assumptions for the rotation law, $\Omega_{\rm F}(x) = \Omega_{\rm F}(\Psi(x))$.

In order to allow a comparison with rigid rotation solutions we chose a bounded current distribution (22) (with $n = 2$) in parallel to the work of ACa,b. For the rotation law we require that

(i) it is finite at $x = 0$, (ii) $\Omega_{\rm F}(x = 1) = 1$, in accordance with the normalisation, and (iii) $\Omega_{\rm F}^2 > 0 \quad \Psi < 1$. These requirements are satisfied by e.g. the following functions,

$$\Omega_{\rm F}^2(x) \;=\; e^{h-h} \tag{29}$$

$$\Omega_{\rm F}^2(x) \;=\; \frac{\exp\left(\frac{1}{+}\right)}{x+1}, \quad \equiv \frac{1}{\ln(\quad +1)} - 1\,, \tag{30}$$

where plays the role of a steepness parameters (see Fig. 2).

There is a further condition (iv) for a rotation law. Rotation laws remaining valid for $x \rightarrow$, have to be flatter than $\Omega_{\rm F} \sim 1/x$. Otherwise the rotational *velocity* of the field lines will pass a maximum and finally decreases to values $x^2\Omega_{\rm F}^2$ 1 (Fig. 2c). Note that ansatz (29) cannot be applied for arbitrarily large radii in the case of a high steepness parameter . Since rotation law (29) is applied for a finite flux distribution, there is no serious problem as long as the turn-over of the rotational velocity is located beyond the jet radius. Ansatz (30) is more general, however, the analytical expressions look more complicated.

In Fig. 3 we display the numerical solutions of the asymptotic force balance for ansatz (29). A solution with ansatz (30) looks very similar, we therefore omitted the plot. The solid curves show the field distribution with constant field rotation coinciding with the result of ACb, the other curves the result with increasing steepness of the rotation law, respectively.

The small peak in the field pressure (Fig. 3a) along the solution with the very steep rotation law results from numerical difficulties with the above mentioned decrease of rotational velocity for large radii and does not appear for the other ansatz.

From the solutions $\Psi(x)$ and $I(x)$ or $\Omega_{\rm F}(x)$, we can derive the distribution of the conserved quantities $I(\Psi)$ and $\Omega_{\rm F}(\Psi)$ (Fig. 3d, 3e), which could be applied for force-free 2D calculations.

Fig. 3c shows the relation between the coupling constant (measuring the strength of the poloidal current) and the jet radius. In order to obtain jets with the same radius, the current strength has to be increased with increasing steepness of $\Omega_{\rm F}$. The same behaviour is mirrored in Fig. 3e, if we compare the poloidal current at the jet boundary, $I(\Psi = 1)$, for different .

The force-equilibrium is affected by differential rotation predominantly in the outer part of the jet. The field distribution within the core radius a of the asymptotic jet is not concerned very much by differential rotation, although a slight decollimating effect can be observed. The behaviour changes beyond of $x = a$, where the collimating effect is stronger than the de-collimation effect in the inner part.

Our results clearly show that differential rotation has a *collimating* influence. Depending on the steepness parameter, the asymptotic jet radius (defined by $\Psi = 1$) varies by a factor up to 2, which could be even larger for a lower coupling g. Note that the spatial scaling is in terms of the asymptotic jet radius R_0. This parameter, however, and thus the absolute scaling can only be inferred from a 2D solution. In Sect. 2.2 we gave arguments that, due to the rapid rotation of the accretion disk, R_0 could be closer to the jet axis compared to solutions with constant rotation $\Omega_{\rm F} = \Omega_\star$.

3.4. A non-linear analytical solution

In this section we derive a general analytical solution for the rotation law $\Omega_{\rm F}(\Psi)$. We assume a form of flux distribution parameterised as in Eq. (18). However, in contrary to the case of rigid rotation, the parameter $b = \ln(1 + (x_{\rm jet}/a)^2)$ is not *a priori* coupled to the current distribution (e.g. Eq. 19). Then, the asymptotic GSS can be transformed into an ordinary differential equation for $\Omega_{\rm F}^2$,

$$\frac{d}{d\Psi}\Omega_{\rm F}^2(\Psi) + \frac{2b}{e^{b\Psi}-1}\Omega_{\rm F}^2(\Psi) \;=\; \frac{g\,b^2}{4}\frac{(e^{b\Psi})^2}{(e^{b\Psi}-1)^2}\frac{d}{d\Psi}I^2(\Psi) - \frac{1}{a^2}\frac{2\,b}{e^{b\Psi}-1} \tag{31}$$

Now we investigate, whether a combination of current distribution and rotation law can be found, which is consistent with the chosen flux distribution. The general solution of Eq. (31) is

$$\Omega_{\rm F}^2(\Psi) = \frac{+\frac{1}{4}g\,b^2 I^2(\Psi) - a^{-2}e^{-b\Psi}(e^{-b\Psi}-2)}{(1-e^{-b\Psi})^2}\,, \tag{32}$$

with the integration constant . This solution diverges for $\Psi \rightarrow 0$ unless $= -1/a^2$. Thus, we obtain

$$\Omega_{\rm F}^2(\Psi) = \frac{1}{4}g\,b^2\frac{I^2(\Psi)}{(1-e^{-b\Psi})^2} - \frac{1}{a^2}\,, \tag{33}$$

and vice versa a relation for the current distribution in terms of $\Omega_{\rm F}(\Psi)$. In the limit $\Psi \rightarrow 0$ the solution approaches

$$\lim_{\Psi\rightarrow 0}\Omega_{\rm F}^2(\Psi) = \frac{1}{a^2} + \frac{g}{8}\lim_{\Psi\rightarrow 0}\frac{d^2}{d\Psi^2}I^2(\Psi)\,. \tag{34}$$

For a current distribution (19) we end up with the result of ACb with constant angular velocity of the field, $\Omega_{\rm F} = 1$.

Since by definition $I(\Psi = 1) = 1$, $x_{\rm jet} = a\sqrt{e^b - 1}$, we can derive an expression for the coupling constant

$$g = \frac{4}{b^2}(1-e^{-b})^2 \quad \Omega_{\rm F}^2(1) + \frac{e^b-1}{x_{\rm jet}^2}\right)\,. \tag{35}$$

Eq. (35) is visualised in Fig. 4. We see that differential rotation plays a dominant role only for low-g / low-b jets, i.e. jets with low poloidal current and a broad field distribution (i.e. large core radius). Note that although a is shifted to lower values for steeper differential rotation, the magnetic flux $\Psi(x = a)$ remains unchanged. In the limiting case of rigid rotation the parameter b describes steepness of the poloidal current distribution. We can rewrite Eq.(35) in terms of the core radius a of the field distribution

$$g = 4\frac{\Omega_{\rm F}^2(1) + \left(1/a\right)^2}{\ln(1+(x_{\rm jet}/a)^2)} \quad \frac{\left(x_{\rm jet}/a\right)^2}{1+\left(x_{\rm jet}/a\right)^2}\right)^2 \tag{36}$$

This shows that in order to obtain the same asymptotic magnetic jet structure (with the same parameters a, b, or $x_{\rm jet}$ in Eq. (18)), the current has to be larger (parameterised by the coupling constant g) in the case of larger gradients of the rotation

law. Similarly, for a fixed ratio ($x_{\rm jet}/a$) and g, but decreasing $\Omega_{\rm F}(1)$, also the core radius a (and thus $x_{\rm jet}$) is decreasing.

The thick line in Fig. 4 is the limiting value for the coupling constant g for rigid rotation, where the core radius a diverges (ACb). It corresponds to a minimum current required for rigid rotating magnetic jets, $g = 4\,(1-e^{-b})^2/b^2$. In the case of differential rotation, this value is decreased by a factor $\Omega_{\rm F}(1)^2$.

Eqs. (35) and (36) are a general result resting only on the assumption of the field distribution (18). No assumption was yet made about the *function* $\Omega_{\rm F}(\Psi)$. Any solution $I(\Psi)$, $\Omega_{\rm F}(\Psi)$ has to lie within the limiting curves of $\Omega_{\rm F}(1) = 1$ and $\Omega_{\rm F}(1) = 0$ in Fig. 4. The ratio of the coupling constants for constant rotation ($\Omega_{\rm F}(1) = 1$) and for maximum differential rotation ($\Omega_{\rm F}(1) = 0$) is

$$\frac{g_{\rm max}}{g_{\rm min}} = 1 + \frac{x_{\rm jet}^2}{e^b - 1}\,. \tag{37}$$

Again we derive the 'total expansion rate' similar to Sect. 3.2 by comparison of the asymptotic solution with Keplerian disk rotation,

$$\frac{x_{\rm jet}^3}{x_{D\ \Psi=1}^3}\left(\frac{GM}{c^2 R_0}\right) = \frac{1}{4} g b^2 \frac{x_{\rm jet}^3}{\left(1-e^{-b}\right)^2} - (e^b - 1)\, x_{\rm jet}, \tag{38}$$

where no assumption was made about a specific field rotation. Strong currents and large asymptotic jet radii imply a strong opening of the flux surfaces. If we rewrite Eq. (38) in terms of the field rotation,

$$\frac{x_{\rm jet}}{x_{D\ \Psi=1}} = \left(\frac{c^2 R_0}{GM}\right)^{\frac{1}{3}} x_{\rm jet}\, \Omega_{\rm F}^{\frac{2}{3}}(1) = \left(2\frac{R_0}{R_{\rm S}}\right)^{\frac{1}{3}} x_{\rm jet}\, \Omega_{\rm F}^{\frac{2}{3}}(1)\,, \tag{39}$$

we see that a stronger gradient in the field rotation (a lower value of $\Omega_{\rm F}(\Psi = 1)$) leads to a lower expansion rate. A vanishing field rotation of the outermost flux surface leads to a vanishing, unphysical, expansion rate.

With reasonable numerical parameters the different central objects (see Sect. 2.2), the numerical values for the expansion rate are

$$\frac{x_{\rm jet}}{x_{D\ \Psi=1}} = 2\, x_{\rm jet}\, \Omega_{\rm F}^{\frac{2}{3}}(1) \left(\frac{M}{10^{10}\,{\rm M}_\odot}\right)\left(\frac{R_0}{10^{16}{\rm cm}}\right)^{-1}$$

in the case of AGN, and

$$\frac{x_{\rm jet}}{x_{D\ \Psi=1}} = 600\, x_{\rm jet}\, \Omega_{\rm F}^{\frac{2}{3}}(1) \left(\frac{M}{3\,{\rm M}_\odot}\right)\left(\frac{R_0}{10^{15}{\rm cm}}\right)^{-1}$$

for protostellar objects.

We may assume that AGN jets are highly relativistic with $1 << x_{\rm jet} \sim 100$, and therefore are strong *differential* rotators, $1 >> \Omega_{\rm F}(1) \sim 0.1$. Their expansion rate would then be of the order of 50. In the case of protostars $x_{\rm jet} \sim 1$, and thus $\Omega_{\rm F}(1) \sim 1$. The expansion rate would then be of the order of 600. The applied number values for $x_{\rm jet}$ and $\Omega_{\rm F}(1)$ are only raw estimates, indicating 'steep' or 'flat' rotation laws and 'highly' or 'weakly' relativistic field rotation, respectively.

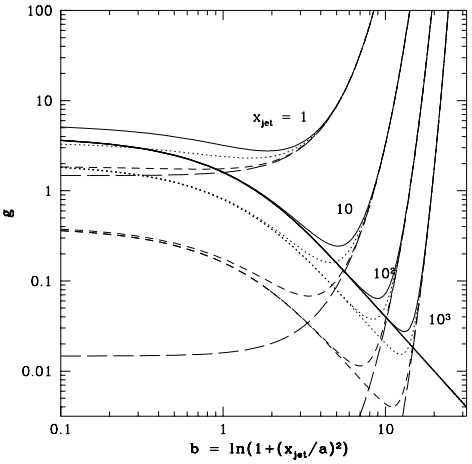

Fig. 4. Interrelation between the jet parameters g, $b = \ln(1+(\ _{\rm jet}/a)^2)$, $_{\rm jet}$ and the angular field velocity at the jet boundary, $\Omega_{\rm F}^2(\Psi = 1)$. $\Omega_{\rm F}^2(1) = 1$ (solid), $\Omega_{\rm F}^2(1) = 0.5$ (dotted), $\Omega_{\rm F}^2(1) = 0.1$ (short-dashed), $\Omega_{\rm F}^2(1) = 0$ (long-dashed). The thick solid curve is the boundary of the forbidden regime, where no rigid rotating jet solutions are possible. The solid curves coincide with the result from ACb.

Keeping all the uncertainties in mind, we may generally expect lower expansion rates for the AGN. Especially the expansion rates for protostars have to be taken with care (see also discussion end of Sect.3.2). However, a rather general conclusion might be that high mass, fast rotating AGN have higher jet expansion rates than their low mass slower rotating counterparts.

If we rewrite Eq. (35) we find an expression for the ratio of the jet radii in terms of the field rotation of the outermost flux surface.

3.4.1. The question of non-monotonous flux distribution

We note a general difficulty with non-monotonous flux distributions. In this case the jet magnetosphere would consist of flux surfaces with different foot points, but with the same absolute flux, e.g. $\Psi_1 = \Psi_2$. These flux surfaces are not directly connected within the integration domain.

There is no physical reason, why they should not carry a different poloidal current, as long it is conserved along Ψ_1 and Ψ_2, respectively. However, in this case the description of the poloidal current as a function $I(\Psi)$, seems to fail. Instead it is supposed, that always $I(\Psi_1) = I(\Psi_2)$, and one *has* to assume such kind of current distribution.

The problem is more serious for the other 'free' function, the field rotation $\Omega_{\rm F}(\Psi)$. Here, if we suppose an accretion disk as source for the magnetic flux, all foot points of the flux surfaces *must* rotate with monotonously decreasing angular velocity. Again, the description does not support a different field rotation for Ψ_1 and Ψ_2. This statement is also valid for a non force-free description.

We conclude that the monotonous disk rotation could only support monotonous flux distributions. Therefore, assumption (18) for the analytical solution seems to be rather general.

3.4.2. A special analytical rotation law

As an example for a current distribution appropriate for differential rotation we may chose

$$I(\Psi) = B\left(1 - e^{-b\Psi}\right) e^{-\Psi}; \qquad B \equiv \left(1 - e^{-b}\right)^{-1} e \ . \quad (40)$$

The steepness parameter d describes the variation from constant rotation. This leads to a field rotation

$$\Omega_{\rm F}^2(\Psi) = \frac{1}{4} g\, b^2 B^2 e^{-2\Psi} - \frac{1}{a^2}\,, \quad (41)$$

The jet radius is by definition at $\Psi = 1$, and from Eq. (18) it follows $x_{\rm jet} = a\sqrt{e^b - 1}$. Since $\Omega_{\rm F}(\Psi(x = 1)) = 1$, we calculate for the flux distribution parameter

$$a^2 = \left(\frac{1}{4} g b^2 B^2\right)^{1/(1+2d/b)} - 1\Bigg)^{-1} . \quad (42)$$

Again, $d = 0$ gives the result derived by ACb. Otherwise, a and also $x_{\rm jet}$ is decreased for fixed g and b.

The expression for the coupling constant is

$$g = \frac{4}{b^2}(1 - e^{-b})^2 e^{-2} \quad 1 + \frac{e^b - 1}{x_{\rm jet}^2}\right)^{1+(2d/b)} . \quad (43)$$

The angular velocity of the outermost flux surface is

$$\Omega_{\rm F}^2(\Psi = 1) = 1 + \frac{1}{4} g b^2 B^2 e^{-2} - \left(\frac{1}{4} g b^2 B^2\right)^{1/(1+2d/b)} . \quad (44)$$

The interrelation of the parameters g, b, d and $x_{\rm jet}$ is similar to Fig. 4. However, the parameter d has to be chosen such that $\Omega_{\rm F}^2(x_{\rm jet}) \gtrsim 0$, and $g(b; d, x_{\rm jet})$ lies within the limiting curves of $\Omega_{\rm F}(1) = 1$ and $\Omega_{\rm F}(1) = 0$ in Fig. 4.

4. Conclusions

In this paper the asymptotic force-balance across collimated magnetic flux surfaces was investigated. Relativistic effects due to rapid rotation of the field as well as differential rotation was included in the treatment.

The related astrophysical scenario is that of a highly collimated magnetic jet originating in an accretion disk, as observed in active galactic nuclei, galactic high energy sources with superluminal jets, and also protostellar jets with non-relativistic jet motion.

We presented numerical solutions of the asymptotic jet equilibrium for different assumptions of the field rotation. For a general assumption for the asymptotic field distribution we also derived an analytical solution.

The main results are the following

- *Differential rotation* always leads to a *decrease of the jet radius* in terms of the asymptotic light cylinder radius.
- This effect can be balanced by an increase of the poloidal current.
- The inner structure of the jets remains more or less unchanged, the outer part becomes 'compressed' by differential rotation.
- Jet expansion rates could be estimated under the assumption of a certain rotation law for the foot points of the field (e.g. Keplerian).
- A general analytical solution was derived for the asymptotic flux distribution together with the rotation law of the field lines and the current distribution.

Depending on the steepness of the rotation law, the ratio in the jet radius between jets with and without differential rotation can be of the order of two. We also showed that differential rotation plays a role only for jets with low poloidal current and a broad field distribution.

In order to maintain jets with the same jet radius, but with a different gradient of field rotation, the strength of the poloidal current must be increased. In this sense, differential rotation may be considered as collimating effect and poloidal currents as decollimating effect. However, compared to the rigid rotating field distribution, the minimum poloidal current required is decreased by a factor, which depends on the rotation rate of the outermost flux surface.

While within the asymptotic one-dimensional limit jets with arbitrary radius could be obtained, there are indications that 2D solutions of the relativistic GSS equation (but without differential rotation) only exist for asymptotic jet radii of the order of several light cylinder radii (Fendt et al 1995, Fendt 1996). It was impossible to obtain numerical solutions with jet radii larger than ~ 5 light cylinder radii. This result was not caused by numerical effects. The results of the present paper indicate that the jet radii are even smaller.

A central question is therefore the scaling of light cylinder radius in terms of stellar (or black hole) radii. This, however, could only be inferred from a two-dimensional solution of the trans-field equation. We believe that inclusion of inertial effects would possibly widen the jet. However, one should keep in mind that in the case of self-similar jets Contopoulos & Lovelace (1994) and Ferreira (1997) have shown that centrifugal forces could be balanced by magnetic tension leading to a recollimation of the jet.

A critical point of the present investigation is that the interaction between the jet boundary and the ambient medium is not included in the force-balance. Hence, the question whether the jet is self-collimated or pressure collimated by the ambient medium cannot be answered. However, if we take a certain jet radius as given (by e.g. observational arguments), the results of this paper give examples of the local force-free force-balance of a jet with such a radius. In this picture the field pressure at the jet boundary must be balanced by the external pressure. Smaller or larger jet radii would change the jet parameters accordingly.

By comparing the field rotation near the foot points of the field lines (near a 'disk') and in the asymptotic regime, we were

able to give some estimates on the expansion rate of the jets. Protostellar jets seem to have high expansion rates of the order of 1000, but these values are biased by the force-free assumption for the force-balance. Expansion rates of AGN jets are lower, a typical value might be 10. It can be said that high-mass fast-rotating AGN jet expansion rates are expected to be higher than those from low-mass slow rotating ones.

Acknowledgements. This work was supported by Swedish Natural Science Research Foundation (NFR) and partly by the Sonderforschungsbereich (SFB) 328 of the University of Heidelberg. I thank Max Camenzind and Stefan Appl for discussions. Lennart Lindegren is acknowledged for putting the mathematical software packet *Mathcad* at my disposal. The paper also benefited from the conversation with the referee Jonathan Ferreira.

Appendix A: another analytical solution with degenerate light cylinder

Here we give the analytical expression for the field pressure and flux distribution for a solution with $\Omega_{\rm F}(x) = (1/x)$ and a bounded current distribution (22) with $n = 2$,

$$(x) = \frac{g}{16\pi}\frac{4}{a^2}\frac{(x/a)^2}{\left(1+(x/a)^2\right)^3},$$

$$\Psi(x) = \sqrt{2ga^2}\quad \ln\left(\frac{x}{a}+\sqrt{1+(x/a)^2}\right) - \quad \overline{\frac{(x/a)^2}{1+(x/a)^2}}\Bigg).$$

The field rotation law can be expressed by an implicit equation

$$\frac{\Psi(\Omega_{\rm F})}{\sqrt{2ga^2}} = \quad \ln\quad \frac{1+\sqrt{1+(a\Omega_{\rm F})^2}}{a\Omega_{\rm F}}\Bigg) - \quad \overline{\frac{1}{1+(a\Omega_{\rm F})^2}}\Bigg)$$

Suppose that we have Keplerian rotation of the foot points along the disk, $\Omega_{\rm F} = \Omega_{\rm K} = \sqrt{GM/c^2R_0}x^{-3/2}$, it follows for the disk flux distribution

$$(\Psi(x))_{\rm disk} = \sqrt{2ga^2}\quad \ln\quad \frac{x^{3/2}}{a\sqrt{\tilde{a}}}\quad 1+\quad \overline{1+\frac{a^2\tilde{a}}{x^3}}\Bigg)\Bigg) - \quad \overline{\frac{x^3}{x^3+a^2\tilde{a}}}\Bigg), \tag{A1}$$

where $\tilde{a} \equiv (R_{\rm S}/2R_0)$. For the 'total expansion rate' $(x_{\ \Psi=1}/x_{D\ \Psi=1})$ of the jet we derive an implicit equation

$$\ln\quad \frac{\sqrt{\tilde{a}}x_{\ \Psi=1}}{x^{3/2}_{D\ \Psi=1}}\frac{1+\quad \overline{1+a^2/x^2_{\ \Psi=1}}}{1+\quad \overline{1+a^2\tilde{a}/x^3_{D\ \Psi=1}}} =$$

$$= \quad 1+\frac{a^2}{x^2_{\ \Psi=1}}\Bigg)^{-\frac{1}{2}} - \quad 1+\frac{a^2\tilde{a}}{x^2_{D\ \Psi=1}}\Bigg)^{-\frac{1}{2}}$$

References

Appl, S., Camenzind, M., 1993a, A&A, 270, 71 (ACa)
Appl, S., Camenzind, M., 1993b, A&A, 274, 699 (ACb)
Camenzind, M., 1990, Rev. Mod. Ast
Camenzind, M., Krockenberger, 1992, A&A, 225, 59
Chiueh, T., Li., Z., Begelman, M.C., 1991, ApJ, 377, 462
Contopoulos, J., Lovelace, R.V.E., 1994, 429, 139
Contopoulos, J., 1994, ApJ, 432, 508
Fendt, C., 1994, PhD thesis, University of Heidelberg
Fendt, C., Camenzind, M., Appl, S., 1995, A&A 300, 791
Fendt, C., Camenzind, M., 1996, A&A, 312, 591
Fendt, C., 1996, A&A, accepted
Ferreira, J., Pelletier, G., 1995, A&A, 295, 807
Ferreira, J., 1997, A&A, in press
Heyvaerts, J., Norman, C.A., 1989, ApJ, 347, 1055
Kepner, J., Hartigan, P., Yang, C., Strom, S., 1993, ApJ, 415, L121
Heyvaerts, J., Norman, C.A., 1989, ApJ, 347, 1055
Mirabel, I.F., Rodriguez, L.F., 1995, Superluminal motion in our Galaxy, in: H. Böhringer, G.E. Morfill, J.E. Trümper (Eds) 17th Texas Symposium on Relativistic Astrophysics and Cosmology, The New York Academy of Sciences, New York, p.21
Mundt, R., Ray, T.P., Bührke, T., Raga, A.C., Solf, J., 1990, A&A, 232, 37
Ray, T.P., Mundt, R., Dyson, J.E., Falle, S.A.E.G., Raga, A., 1996, ApJ, 468, L103
Zensus, J.A., Cohen, M.H., Unwin, S.C., 1995, ApJ, 443, 35

This article was processed by the author using Springer-Verlag LaTeX A&A style file *L-AA* version 3.

A&A 365, 631–641 (2001)
DOI: 10.1051/0004-6361:20000057

Astronomy & Astrophysics

Collimating, relativistic, magnetic jets from rotating disks

The axisymmetric field structure of relativistic jets and the example of the M 87 jet

C. Fendt and E. Memola

Astrophysikalisches Institut Potsdam, An der Sternwarte 16, 14482 Potsdam, Germany
e-mail: cfendt@aip.de; ememola@aip.de

Received 25 April 2000 / Accepted 19 October 2000

Abstract. We investigate the axisymmetric structure of collimating, relativistic, strongly magnetized (force-free) jets. In particular, we include the differential rotation of the foot points of the field lines in our treatment. The magnetic flux distribution is determined by the solution of the Grad-Shafranov equation and the regularity condition along the light surface. With differential rotation, i.e. the variation of the iso-rotation parameter $\Omega_{\rm F}$, the shape of the light surface is not known a priori and must be calculated in an iterative way. For the first time, we have calculated the force-free magnetic structure of truly two-dimensional, relativistic jets, anchored in a differentially rotating disk. Such an approach allows for a direct connection between parameters of the central source (mass, rotation) and the extension of the radio jet. In particular, this can provide a direct scaling of the location of the asymptotic jet light cylinder in terms of the central mass and the accretion disk magnetic flux distribution. We demonstrate that differentially rotating jets must be collimated to a smaller radius in terms of the light cylinder if compared to jets with rigid rotation. Also, the opening angle is smaller. Further we present an analytical estimate for the jet opening angle along the asymptotic branches of the light surface. In general, differential rotation of the iso-rotation parameter leads to an increase of the jet opening angle. Our results are applicable for highly magnetized, highly collimated, relativistic jets from active galactic nuclei and Galactic superluminal jet sources. Comparison to the M 87 jet shows agreement in the collimation distance. We derive a light cylinder radius of the M 87 jet of 50 Schwarzschild radii.

Key words. accretion, accretion disks – MHD – methods: numerical – ISM: jets and outflows – galaxies: individual: M 87 – galaxies: jets

1. Formation of magnetic jets

Observations of astrophysical jet sources have now established the idea that jet formation is always connected to the presence of an accretion disk and strong magnetic fields. This holds for various scales of energy output, jet velocity and nature of the jet emitting objects. Examples are jets from active galactic nuclei (AGN), Galactic superluminal jet sources, the example of a mildly relativistic jet from a neutron star (SS 433) and the numerous class of protostellar jets (see Zensus et al. 1995; Mirabel & Rodriguez 1995; Mundt et al. 1990; Ray et al. 1996). Magnetic jets are believed to originate very close to the central object in the interaction region with the accretion disk. Beside observational arguments also theoretical considerations have shown that magnetic fields play an important role in jet formation and propagation (Blandford & Payne 1982; Pudritz & Norman 1983; Shibata & Uchida 1985; Sakurai 1985; Camenzind 1987; Lovelace et al. 1991).

If the central object is a black hole as it is the case for AGN and Galactic superluminal jet sources, the surrounding accretion disk is the only possible location for a field generation (by dynamo action or/and advection of flux). In the case of stellar objects (protostars, white dwarfs or neutron stars), the central star also carries a relatively strong magnetic field and it is not yet clear, whether the jet magnetosphere originates in the disk or in the star. However, a strong interaction between stellar field and accretion flow is evident. The jet formation process itself is not yet fully understood theoretically. In particular, for the mass transfer from the disk into the jet and the process of magnetic field generation a complete physical model is missing.

However, over the last decades the basic ideas of Blandford & Payne (1982) have been extended by various authors. The general picture is the following. Matter

Send offprint requests to: C. Fendt

is lifted from the disk into the magnetosphere and becomes magnetically accelerated (Ferreira 1997). Toroidal magnetic fields, generated by inertial back-reaction of the plasma on the poloidal field, may collimate the disk magnetosphere into a highly collimated jet flow (Camenzind 1987; Chiueh et al. 1991; Lovelace et al. 1991). In general, due to the complexity of the MHD equations, stationary relativistic models of magnetic jets has to rely on simplifying assumptions such as self-similarity (Contopoulos 1994, 1995), some other prescription of the field structure (Li 1993; Beskin 1997) or the restriction to asymptotic regimes (Chiueh et al. 1991; Appl & Camenzind 1993; Nitta 1994, 1995). For highly magnetized jets the force-free limit applies. This allows for a truly two-dimensional calculation of the magnetic field structure (Fendt et al. 1995; Fendt 1997a). Relativistic magnetohydrodynamics implies that poloidal electric fields, which are not present in Newtonian MHD, cannot be neglected anymore.

From the observations we know that extragalactic jets as well as Galactic superluminal jets and protostellar jets are collimated almost to a cylindrical shape (Zensus et al. 1995; Ray et al. 1996; Mirabel & Rodriguez 1995). Theoretically, it has been shown that current carrying relativistic jets must collimate to a cylinder (Chiueh et al. 1991). For the asymptotic limit of a cylindrically collimated magnetic relativistic jet, Appl & Camenzind (1993) found a non-linear analytical solution for the trans-field force-balance in the case of a constant iso-rotation parameter. These results were further generalized for jets with differential rotation (Fendt 1997b). Such an asymptotic field distribution is especially interesting for jets emerging from (differentially rotating) accretion disks.

In previous papers, we applied the asymptotic jet model of Appl & Camenzind (1993) as a boundary condition for the calculation of *global, two-dimensional,* force-free jet magnetospheres for rapidly rotating stars (Fendt et al. 1995) or rapidly rotating black holes (Fendt 1997a). In this paper, we continue our work on 2D force-free jet magnetospheres applying an asymptotic jet with *differential rotation* of the iso-rotation parameter $\Omega_{\rm F}$ as boundary condition for the global jet structure. Such an approach allows for a connection between the differentially rotating jet source – the accretion disk – and the asymptotic collimated jet. Since jet motion seems intrinsically connected to the accretion disk, differential rotation of the field lines should be a natural ingredient for any magnetic jet structure. As a principal problem for differentially rotating relativistic jet magnetospheres, position and shape of the singular light surface are not known a priori, but have to be calculated in an iterative way together with the magnetic flux distribution.

In Sect. 2 we recall some basic equations of the theory of relativistic magnetospheres and discuss several difficulties with the solution of the Grad–Shafranov (hereafter GS) equation. After some comments on the numerical approach in Sect. 3, we discuss our results in Sect. 4. A summary is given in Sect. 5.

2. Structure of magnetic jets

Throughout the paper we apply the following basic assumptions: *axisymmetry*, *stationarity* and *ideal MHD*. We use cylindrical coordinates (R, ϕ, Z) or (x, ϕ, z) if normalized. The term *"asymptotic"* always denotes the limit of $Z \gg R$ unless explicitly stated otherwise. We consider jets with a *finite* radius, $R < \infty$ for $Z \to \infty$.

2.1. The force–free, cross–field force–balance

With the assumption of axisymmetry, a magnetic flux function can be defined

$$\Psi = \frac{1}{2\pi} \int \boldsymbol{B}_{\rm P} \cdot {\rm d}\boldsymbol{A}, \qquad R\boldsymbol{B}_{\rm P} = \nabla\Psi \wedge \boldsymbol{e}_\phi, \tag{1}$$

measuring the magnetic flux through a surface element with radius R and, in a similar way, the poloidal current through the same area

$$I = \int \boldsymbol{j}_{\rm P} \cdot {\rm d}\boldsymbol{A} = -\frac{c}{2} R B_\phi, \tag{2}$$

which, in the force-free case, flows parallel to the flux surfaces, $I = I(\Psi)$.

The structure of the magnetic flux surfaces is determined by the toroidal component of Ampère's law, $\nabla \times \boldsymbol{B}_{\rm P} = 4\pi \boldsymbol{j}_\phi / c$, where the toroidal electric current density has to be calculated from the equation of motion projected perpendicular to the flux surfaces (Camenzind 1987; Fendt et al. 1995). For strong magnetic fields, inertial forces of the matter can be neglected. This is the *force-free* limit and the equation of motion reduces to $0 = c\rho_{\rm c}\boldsymbol{E} + \boldsymbol{j} \times \boldsymbol{B}$ with the charge density $\rho_{\rm c}$.

Combining Ampère's law and the force-free equation of motion the cross-field force-balance can be written as the modified relativistic GS equation,

$$\begin{aligned} R\nabla \cdot \left(\frac{1 - (R\Omega_{\rm F}(\Psi)/c)^2}{R^2} \nabla\Psi \right) = & - \frac{4}{c^2} \frac{1}{R} \frac{1}{2} \left(I^2(\Psi) \right)' \\ & - R\,|\nabla\Psi|^2 \frac{1}{2} \left(\Omega_{\rm F}^2(\Psi) \right)', \end{aligned} \tag{3}$$

where the primes denote the derivative $\frac{\rm d}{{\rm d}\Psi}$ (see Camenzind 1987; Okamoto 1992).

$\Omega_{\rm F}$ is conserved along the flux surfaces, $\Omega_{\rm F} = \Omega_{\rm F}(\Psi)$. We will call it the *iso-rotation* parameter, defined by Ferraro's law of iso-rotation. It can be understood as the angular velocity of the plasma, reduced by the slide along the field lines. Sometimes, it is called the angular velocity of the field lines. Both, the current distribution $I(\Psi)$ and the rotation law $\Omega_{\rm F}(\Psi)$ determine the source term for the GS equation and govern the structure of the magnetosphere. We apply the following normalization,

$$\begin{aligned} R, Z &\Leftrightarrow x\,R_0, z\,R_0, \\ \Omega_{\rm F} &\Leftrightarrow \Omega_{\rm F}\,(c/R_0)\,, \\ \Psi &\Leftrightarrow \Psi\,\Psi_{\rm max}\,, \\ I &\Leftrightarrow I\,I_{\rm max}\,. \end{aligned}$$

As the length scale for the GS Eq. (3) the asymptotic radius R_0 of the light surface is selected (see below). In order to allow for a direct comparison to rigidly rotating magnetospheres, the normalization was chosen such that $\Omega_{\rm F} = 1$ at $x = 1$. With the chosen normalization, Eq. (3) can be written dimensionless,

$$x\nabla\cdot\left(\frac{1-x^2\Omega_{\rm F}^2(\Psi)}{x^2}\nabla\Psi\right) = -\frac{1}{x}\frac{g}{2}\left(I^2(\Psi)\right)' - x|\nabla\Psi|^2\frac{1}{2}\left(\Omega_{\rm F}^2(\Psi)\right)'. \quad (4)$$

g is a coupling constant describing the strength of the current term in the GS equation,

$$g = \frac{4I_{\rm max}^2R_0^2}{c^2\Psi_{\rm max}^2} = 4\left(\frac{I_{\rm max}}{10^{18}{\rm A}}\right)^2\left(\frac{R_0}{10^{16}{\rm cm}}\right)^2\left(\frac{\Psi_{\rm max}}{10^{33}\,{\rm Gcm}^2}\right)^{-2}$$

where the parameters are chosen for extragalactic jets. In this paper, g is in accordance with the definition in Fendt et al. (1995) and differs from the definition in Appl & Camenzind (1993) by a factor of two, $g_{\rm Fendt} = 2\,g_{\rm AC}$[1]. Interestingly, a coupling constant, defined in a similar way also for the differential rotation term, would be equal to unity. The GS equation is numerically solved applying the method of finite elements (see Appendix).

Along the light surface, where $D \equiv 1 - x^2\Omega_{\rm F}^2(\Psi) = 0$, the GS equation reduces to the regularity condition,

$$\nabla\Psi\cdot\nabla D = -g\frac{1}{2}\left(I(\Psi)^2\right)' - \frac{1}{2}|\nabla\Psi|^2\left(\ln\left(\Omega_{\rm F}(\Psi)^2\right)\right)', \quad (5)$$

which is equivalent to a Neumann boundary condition. However, for differentially rotating magnetospheres with $\Omega_{\rm F} = \Omega_{\rm F}(\Psi)$ the shape of this surface is not known a priori and has to be calculated in an iterative way together with the two-dimensional solution of the GS equation. For constant $\Omega_{\rm F}$ the light surface is of cylindrical shape. As we have shown in a previous publication (Fendt et al. 1995), our finite element code satisfies the regularity condition *automatically*, since the surface integral along the light surface vanishes.

2.2. Discussion of the force-free assumption

It is clear that relativistic jets must be highly magnetized. Only a high plasma magnetization gives jet velocities close to the speed of light (Fendt & Camenzind 1996). Therefore, for the calculation of *field structure* the force-free limit seems to be reasonable. However, one may question the assumption of a force-free *asymptotic* jet. In a fully self-consistent picture of magnetic jet formation, the asymptotic jet is located beyond the collimating, non force-free wind region and beyond the fast magnetosonic surface. The asymptotic jet parameters are determined by the wind motion. Thus, poloidal current and iso-rotation parameter of the field are *not* functions free of choice. The force-free region of a jet is located close to its origin, where the speed is low. Beyond the Alfvén surface plasma kinetic energy dominates the magnetic energy, which is just the contrary to force-freeness.

For small plasma density, the Alfvén surface of the wind flow approaches the light surface. In this case the fast magnetosonic surface moves to infinity for a conical flow. Okamoto (1999) argues that a force-free field distribution extending to infinity in both x and z direction will asymptotically be of conical shape, i.e. un-collimated. However, his approach differs from ours in the sense that he *assumes* that all field lines will cross the light cylinder. Such an assumption *per se* prohibits any collimation. On the other hand, perfect jet collimation is an observational fact. Astrophysical jets (of very different energy scales) appear collimated to cylinders of finite radius.

In general, the non force-free relativistic GS equation shows three inertial contributions,

$$0 = -\tilde{\kappa}\left(1-M^2-x^2\Omega_{\rm F}^2\right) + \left(1-x^2\Omega_{\rm F}^2\right)\frac{\nabla_\perp B_{\rm P}^2}{8\pi} + \frac{\nabla_\perp B_\phi^2}{8\pi} + \nabla_\perp P + \left(\frac{B_\phi^2}{4\pi} - \rho u_\phi^2\right)\frac{\nabla_\perp x}{x} - \frac{B_{\rm P}^2\Omega_{\rm F}}{4\pi}\nabla_\perp(x^2\Omega_{\rm F}),$$

where $\nabla_\perp$ indicates the gradient perpendicular to Ψ, $\tilde{\kappa} \equiv \kappa B_{\rm P}^2/4\pi = \boldsymbol{n}\cdot(\boldsymbol{B}_{\rm P}\cdot\nabla)\boldsymbol{B}_{\rm P}/4\pi$ the poloidal field curvature, ρ the mass density, u_ϕ the toroidal velocity, P the gas pressure and M the Alfvén Mach number (Chiueh et al. 1991). One can show that in the asymptotic, cylindrical jet the contribution of inertial terms in the force-balance across the field is weak. The contribution of gas pressure is usually negligible in astrophysical jets. Also, the centrifugal force does not play a role for radii larger than the Alfvén radius, since outside the Alfvén surface (where $M^2 = 1 - x^2\Omega_{\rm F}^2$) the plasma moves with constant angular momentum. The curvature term vanishes in cylindrical geometry. Therefore, since for cylindrical jets the contribution from inertial terms is weak, the configuration is comparable to the force-free case. The source term of the GS equation may be reduced to a form similar to the common force-free limit. We suggest the phrase "quasi force-free" for such a configuration because the GS equation looks force-free even if the physical system is not magnetically dominated.

In the force-free limit of a highly magnetized plasma the previous arguments also apply. However, in difference to the asymptotic regime considered above, the low plasma density implies that inertial terms are weak over the *whole* two-dimensional jet region. The centrifugal term ρu_ϕ is weak even if the Alfvén surface now comes close to the light surface. Numerical calculations of the plasma motion along the field have shown that, for a high magnetization, the Alfvén Mach number M grows almost linearly with radius but remains relatively low (Fendt & Camenzind 1996). Thus, the inertial curvature term should not play a

[1] Due to the fact that the jet radius (where $\Psi = 1$) is not known before the asymptotic GS equation has been solved (Fendt 1997b), the normalization with g leads to a current distribution $I(\Psi)$ which is *not* normalized to unity. This difference in normalization is "hidden" in the coupling constant g, which could, in principal, be re-scaled appropriately.

dominant role. Contopoulos & Lovelace (1994) find from self-similar solutions that centrifugal forces are dominated by magnetic forces leading to a re-collimation of the outflow.

In summary, our discussion of the inertial terms in the force-balance equation has shown that these terms are generally weak in the case of a high magnetization. We therefore think that for the calculation of the magnetic field structure in relativistic jets the force-free assumption is acceptable. The main motivation of the force-free assumption is clearly the reason of simplification. There is yet no other way to calculate a truly two-dimensional field distribution for relativistic jets. Naturally, with a force-free solution, nothing can be said about the flow acceleration itself.

2.3. Location of the asymptotic light cylinder

The radius of the asymptotic light cylinder R_0 is the natural length-scale for the GS solution. A scaling of the GS solution in terms of the properties of the central object (e.g. its mass) relies on the proper connection between the asymptotic jet and the accretion disk. This is feasible only if differential rotation $\Omega_{\rm F}(\Psi)$ is included in the treatment (see Sect. 3).

In the following we consider the location of the light surface and its relation to the relativistic character of the magnetosphere from a general point of view. The light cylinder of a flux surface Ψ is defined as a cylinder with radius $R = R_{\rm L}(\Psi) \equiv c/\Omega_{\rm F}(\Psi)$. At this position the GS equation becomes singular. However, this light cylinder is only important for the field line *if* the field line actually intersects it as for $\Psi_{\rm out}$ in Fig. 1. Only then, relativistic effects become dominant. For example, the poloidal electric field scales with the radius in units of the light cylinder radius, $E_{\rm P} = (R/R_{\rm L})B_{\rm P}$. On the other hand, in the case of $\Psi_{\rm in}$ in Fig. 1, the asymptotic radius of the flux surface is smaller than its light cylinder radius $R_{\rm L}(\Psi_{\rm in})$ (located between $\Psi_{\rm in}$ and Ψ_0), therefore relativistic effects are small. For jet solutions with rigid rotation $\Omega_{\rm F}$ all flux surfaces have the same light cylinder radius. Thus, the singular light surface of the magnetosphere is a cylinder. For jet solutions with differential rotation $\Omega_{\rm F}$ the flux surfaces have different light cylinder radii. The singular surface of the magnetosphere is not a cylinder anymore.

It is now interesting to note that the case of differential rotation $\Omega_{\rm F}(\Psi)$ allows for a hypothetical field distribution where (i) the light radius of most of the flux surfaces is located within the jet radius, but where also (ii) the asymptotic radius of the flux surfaces is always smaller than their light radius. Such a field distribution would not have a singular light surface and could be considered as "non relativistic", even if the hypothetical light radii of many field lines are inside the jet radius. Such a situation is not possible if the magnetosphere is constrained by a constant rotation $\Omega_{\rm F}$. This underlines the importance of the treatment of differential rotation for jets from accretion disks.

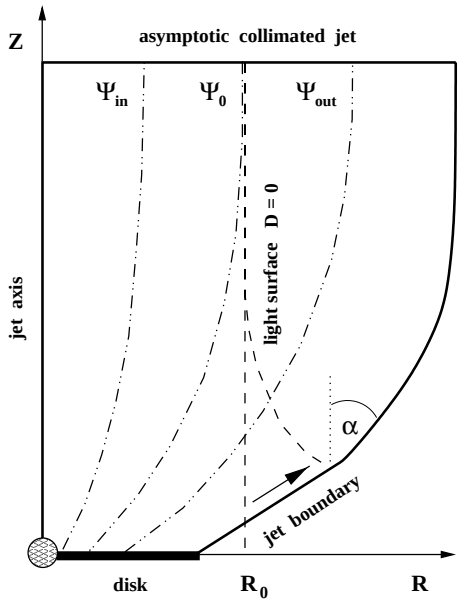

Fig. 1. Sketch of the jet model. Axisymmetric jet magnetic flux surfaces Ψ projected into the meridional plane. The central object, located within the inner boundary (solid disk), is surrounded by an accretion disk. Helical magnetic field lines (laying on the flux surfaces) are anchored in the differentially rotating disk at the foot points $R_{\rm D}(\Psi)$. The jet boundary is defined by the flux surface $\Psi = 1$. The upper boundary condition is a cylindrically collimated jet solution (Fendt 1997b). The arrow indicates the numerical deformation of the initially vertical boundary of the inner solution (at $x = 1$) into the curved light surface. The flux surfaces $\Psi_{\rm in}$ ($\Psi_{\rm out}$) have an asymptotic radius smaller (larger) than the asymptotic light cylinder R_0, which is the asymptotic branch of the light surface $R_{\rm L}(\Psi)$ for large z. The flux surface Ψ_0 coincides with the light surface asymptotically. The jet half opening angle is α (see Sect. 2.4, Fig. 2)

A relativistic description for the jet magnetosphere is always required if the jet contains a flux surface for which the light radius is smaller than the asymptotic radius.

2.4. The regularity condition and the jet opening angle

The regularity condition (5) is the natural boundary condition along the light surface. Although it is impossible to solve Eq. (5) explicitly, a general relation concerning the jet opening angle can be derived. First, we rewrite Eq. (5) as

$$B_z = \frac{1}{4} g (I^2)' - \frac{1}{4} B_{\rm P}^2 \left(\frac{1}{\Omega_{\rm F}^2} \right)' , \tag{6}$$

where $\Omega_{\rm F}(\Psi) = 1/x_{\rm L}(\Psi) \equiv R_0/R_{\rm L}(\Psi)$ has been applied. From Eq. (6) it follows for the radial field component $B_x^2 = -g(I^2(\Psi))'/(1/\Omega_{\rm F}^2(\Psi))'$, if Ψ intersects the light surface with vanishing B_z. On the other hand, considering a field line perpendicular to the light surface, $\nabla\Psi \perp \nabla D$, this provides a condition for the axial field component,

$$B_z = \frac{g}{2} (I^2)' = \frac{B_{\rm P}^2}{2} \left(\frac{1}{\Omega_{\rm F}^2} \right)' . \tag{7}$$

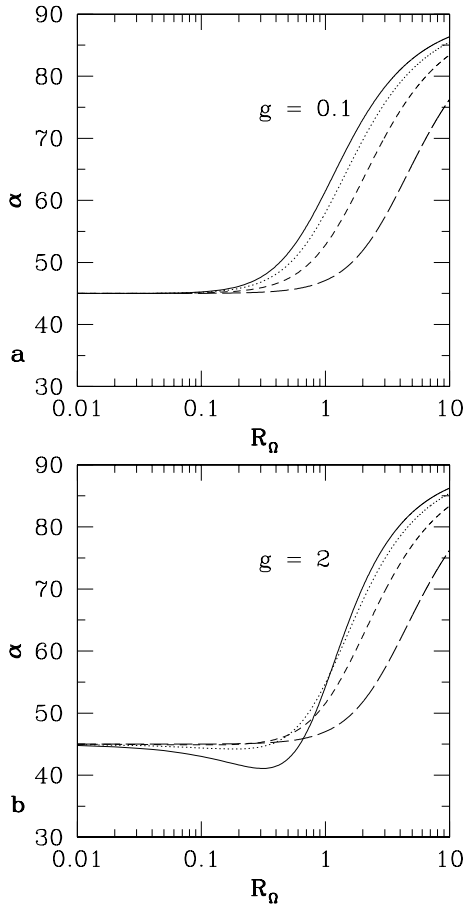

Fig. 2. Jet half opening angle $\alpha(\Psi = 1)$ for the analytical asymptotic jet solution and along the asymptotic branch of the light surface in x-direction (see Eq. (8)). Coupling constant $g = 0.1$ **a)** and $g = 2$ **b)**. Asymptotic magnetic flux distribution parameter (Eq. (9)) $b = 0.5$ (solid), $b = 1$ (dotted), $b = 2$ (short-dashed), $b = 5$ (long-dashed)

Interestingly, this is *either* only a function of the current distribution $I(\Psi)$ *or* depends only from the specification of the rotation law $\Omega_{\rm F}(\Psi)$. Further, in this case it is always $B_z > 0$, since $(1/\Omega_{\rm F}^2)' = (x_{\rm L}^2)' > 0$. In particular, for the asymptotic ($z \to \infty$) part of the magnetosphere, this implies that *only collimating field lines can cross the light surface*.

Now we consider the asymptotic branches of the light surface. For the asymptotic branch in z-direction it holds $(\nabla D)_x \gg (\nabla D)_z \simeq 0$. Further, it is $B_x(\ln \Omega_{\rm F}^2)' = 0$, implying either a collimated field structure, $B_x \equiv 0$ or rigid rotation, $(\Omega_{\rm F}(\Psi))' \equiv 0$. From this we conclude that in the asymptotic regime of a cylindrical light surface, also the flux surfaces along this light cylinder must be of cylindrical shape. Collimation must occur in the non-asymptotic region of the jet.

If we now assume that there exists an asymptotic part of the light surface in x-direction (where $x \gg z$) and that $(\nabla D)_z \gg (\nabla D)_x \simeq 0$, we derive an equation for the half jet *opening angle*,

$$\alpha(\Psi) = \tan^{-1}\left(\sqrt{1 + \frac{1}{4} g \frac{(I^2(\Psi))'(\Omega_{\rm F}^2(\Psi))'}{\Omega_{\rm F}^4(\Psi)}}\right), \qquad (8)$$

for the flux surfaces in this region. As a general example we apply the analytical solution obtained for the asymptotic jet (Fendt 1997b),

$$\Psi(x) \equiv \frac{1}{b}\ln\left(1 + \left(\frac{x}{a}\right)^2\right), \quad b \equiv \ln\left(1 + \left(\frac{x_{\rm jet}}{a}\right)^2\right),$$
$$\Omega_{\rm F}^2(\Psi) = \frac{g\,b^2}{4}\left(\frac{I^2(\Psi)}{(1-{\rm e}^{-b\Psi})^2} - \frac{1}{(1-{\rm e}^{-b})^2}\right) + \Omega_{\rm F}^2(1) \quad (9)$$

for Eq. (9). Here, b is a measure for the ratio of jet radius to jet core radius a. Finally, we obtain the half opening angle for the outermost flux surface $\Psi = 1$,

$$\alpha = \tan^{-1}\left(\sqrt{1 + R_\Omega\left(4R_\Omega\left(\frac{{\rm e}^b - 1}{b{\rm e}^b}\right)^2 + \frac{g/2}{{\rm e}^b - 1}\right)}\right), \quad (10)$$

where R_Ω is defined as $(\Omega_{\rm F}(1))'/\Omega_{\rm F}(1)$. Note, that Eq. (10) is only valid in the limit of $(\nabla D)_x \simeq 0$. Figure 2 shows the variation of the opening angle α with the parameters a and b for two choices of the strength of the poloidal electric current. In general, jets with a strong differential rotation $\Omega_{\rm F}(\Psi)$ (i.e. large R_Ω) have a larger opening angle. Also, jets with a large ratio of jet to core radius have a smaller opening angle. Therefore, jets originating in a small part of the accretion disk, equivalent to small value of R_Ω, will be collimated to a smaller opening angle. It is interesting to note that, in the case of a rigid rotation, the limiting half opening angle is 45°, *independently* of g and b.

3. The jet-disk connection, providing the true length scale of the GS solution

The natural length scale of the relativistic GS Eq. (3) is the asymptotic light cylinder R_0 (see Sect. 2.3). Its size is related to the iso-rotation parameter $\Omega_{\rm F}(\Psi)$, which itself is connected to the angular rotation of the foot points of the field lines. Concerning the GS equation, the size of R_0 follows purely from electro-magnetic quantities, if the coupling constant g is chosen. The GS solution can be scaled to any central object from stars to galactic nuclei as long as the interrelation of the parameters $\Psi_{\rm max}$, $I_{\rm max}$ and R_0 provides the same g. So far, no connection has been made to the type of central object. Here, we treat the question where the asymptotic light cylinder is located in physical units.

In the case of rigid rotation, the light cylinder radius is usually estimated by choosing a distinct radial distance from the central object and defining $\Omega_{\rm F}$ under the assumption that the jet magnetosphere is anchored in that point. If the central object is a black hole, the marginally stable orbit implies an upper limit for $\Omega_{\rm F}$. For jets in AGN this estimate leads to the common conclusion that the light cylinder radius is at about $10\,R_{\rm S}$ and the typical jet radius at about $100\,R_{\rm L}$. Clearly, such arguments relies on the *assumption* that the field line emerging at this very special radius defining $\Omega_{\rm F}$ also extends to the light cylinder radius $R_{\rm L}$ (see Sect. 2.3).

This picture changes, if differential rotation $\Omega_{\rm F}(\Psi)$ is considered. Different flux surfaces anchor at different foot point radii and have different light radii (Sect. 2.3). Assuming a Keplerian rotation, the light surface radius $R_{\rm L}(\Psi)$ is located at

$$R_{\rm L}(\Psi) = 4\ 10^{15}\ {\rm cm} \left(\frac{R_{\rm D}(\Psi)}{R_{\rm S}}\right)^{3/2} \left(\frac{M}{10^{10}\,M_\odot}\right)\ , \qquad (11)$$

where $R_{\rm S}$ is the Schwarzschild radius of a point mass and $R_{\rm D}(\Psi)$ the foot point of the flux surface Ψ on a Keplerian disk. A more general equation is

$$\frac{R_{\rm L}(\Psi)}{R_{\rm S}} = \sqrt{2}\left(\frac{R_{\rm D}(\Psi)}{R_{\rm S}}\right)^{3/2}. \qquad (12)$$

$R_{\rm D}(\Psi)$ is determined from the magnetic flux distribution along the disk and is defined by a certain disk model. Figure 3 shows the location of the light radius $R_{\rm L}$ for a field line anchored at a foot point radius $R_{\rm D}$ in a Keplerian disk around a central object of mass M (see Eq. (11)). Note that the unit of the field line footpoint radius in Eq. (12) and Fig. 3 is the Schwarzschild radius. Therefore, Fig. 3 is appropriate only for relativistic jets. The footpoint radii for protostellar jets are several *stellar* radii, corresponding to about 10^6 Schwarzschild radii (which would be located far above the box in Fig. 3).

So far, nothing can be said about the location of the asymptotic radius of the field lines in general. The essential question is where the asymptotic radius of a flux surface is located in respect to its light cylinder. This question can only be answered by a detailed model considering the two-dimensional field distribution *including differential rotation* $\Omega_{\rm F}(\Psi)$. Only in such a model, the flux distribution of the asymptotic jet can be connected to the flux distribution of the "star"-disk system. Certainly, both boundary conditions – asymptotic jet and accretion disk – rely on model assumptions. However, in a self-consistent model these boundary conditions have to follow certain constraints (see Sects. 4.1, 4.3).

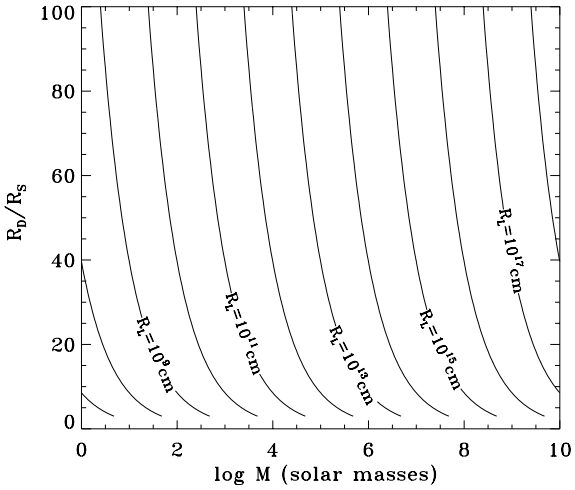

Fig. 3. Location of the light cylinder radius of a flux surface $R_{\rm L}(\Psi)$, anchored at a certain foot point radius $R_{\rm D}(\Psi)$ in units of the Schwarzschild radius $R_{\rm S}$ in a Keplerian disk around a point mass M. Note that for non collapsed stellar objects the footpoint radii of the jet field lines are located at about $10^6 R_{\rm S}$

4. The two-dimensional jet solution

4.1. Disk and jet boundary condition

Three important boundary conditions determine the two-dimensional flux distribution. The first boundary condition is in the asymptotic region. Here we assume a cylindrically collimated jet. We apply the magnetic flux distribution derived by Fendt (1997b), where the rigidly rotating jet model of Appl & Camenzind (1993) is extended for differential rotation $\Omega_{\rm F}(\Psi)$. In particular, our asymptotic jet shows the typical jet core-envelope structure of magnetic flux and electric current, i.e. a configuration where most of the magnetic flux and poloidal electric current is concentrated within a "core" radius. The asymptotic model provides not only the asymptotic magnetic flux boundary condition but also the $\Omega_{\rm F}(\Psi)$ and $I(\Psi)$ distribution for the whole two-dimensional jet magnetosphere. In the model of Fendt (1997b) these functions follow from the solution of the one-dimensional (asymptotic) GS equation across the cylindrical jet and the prescription of $I(x) = (x/a)^2/(1+(x/a)^2)$ together with $\Omega_{\rm F}^2(x) = {\rm e}^{h-hx}$, where a is the core radius of the electric current distribution and h governs the steepness of the $\Omega_{\rm F}$-profile[2].

The second boundary condition is the magnetic flux distribution along the disk. This distribution is in general *not known* as a solution of the full MHD disk equations. Typical models rely on various simplifying assumptions, as e.g. stationarity, the distribution of magnetic resistivity or the disk turbulence governing a dynamo process. We apply an analytic flux distribution similar to the model of Khanna & Camenzind (1992), who calculated the stationary accretion disk magnetic field structure around a super massive black hole. The typical behavior of the magnetic flux distribution is (i) a slight increase of magnetic flux along the innermost disk, (ii) a small or vanishing flux at the inner disk radius, (iii) a strong increase of magnetic flux at intermediate radius (the core radius) and (iv) a saturating behavior for large radii. Using the normalization introduced above, we choose the following disk boundary magnetic flux distribution,

$$\Psi_{\rm disk}(x) = \frac{1}{\tilde{b}} \ln\left(1+\left(\frac{x-x_{\rm in}}{\tilde{a}}\right)^2\right) \qquad (13)$$

with $\tilde{b} = \ln(1+(x_{\rm disk}-x_{\rm in})^2/\tilde{a}^2))$ (see Fig. 4). The parameters are: the core radius $\tilde{a}$, the disk outer radius, $x_{\rm disk}$ and the disk inner radius, $x_{\rm in}$. For simplicity, we choose $x_{\rm in} \simeq 0$ without loss of generality. Such a choice will definitely not influence the global jet solution which is normalized to the asymptotic light cylinder radius.

[2] For figures of these functions and the related $\Psi(x)$, $\Omega_{\rm F}(\Psi)$ and $I(\Psi)$ distribution, we refer to Fendt (1997).

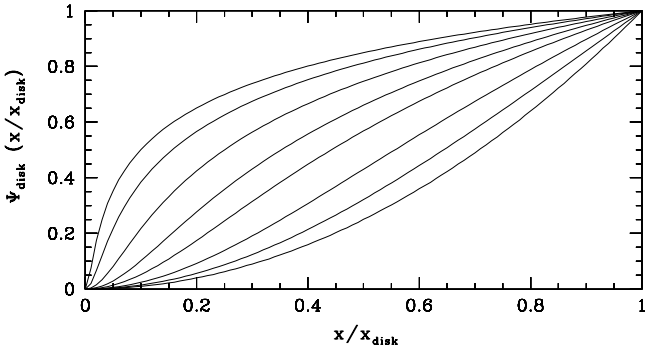

Fig. 4. Magnetic flux distribution along the disk $\Psi_{\rm disk}(x)$ as defined in Eq. (13). Parameters: $x_{\rm in} = 0$, $x_{\rm disk}/\tilde{a} = 100$, 40, 15, 7, 4, 2, 1, 0.01

The third boundary condition is the jet boundary $x_{\rm jet}(z)$. Along this boundary the flux distribution is $\Psi = 1$ by definition. However, the shape of this boundary is not known a priori. It must be determined by the regularity of the solution across the light surface (see also Fendt et al. 1995). A slightly different shape may give the same solution. However, the main features of the solution as opening angle or locus of the collimation are fixed by the internal equilibrium. Therefore, the regularity condition governs the shape of the jet boundary. For a given $I(\Psi)$, $\Omega_{\rm F}(\Psi)$, disk and jet boundary condition, the jet radius $x_{\rm jet}(z)$ is uniquely determined.

The inner spherical grid boundary with radius $x_\star$ close to the origin, indicates the regime of the central source, possibly enclosing a collapsed object. Neutron stars or magnetic white dwarfs may carry their own magnetic field, a black hole can only be threaded by the disk magnetic field. In any case, the magnetic flux distribution is a combination of "central" magnetic flux and disk magnetic flux $\Psi = \Psi_\star + \Psi_{\rm disk}$. For simplicity we assume that the magnetic flux increases monotonically from the axis to the disk edge and $\Psi(x_\star) = \Psi_\star(x_\star)$ and $\Psi_{\rm disk}(x_\star) = 0$.

4.2. The two-dimensional collimating magnetic field structure

Results of numerical solutions of the GS equation are presented in Fig. 5. Shown is the two-dimensional structure of the magnetic flux surfaces as projection of the helical field lines onto the meridional plane. In general, for a choice of the "free functions" $I(\Psi)$ and $\Omega_{\rm F}(\Psi)$, here taken from the asymptotic cylindrical jet solution, the field structure is determined by the boundary conditions and the regularity condition along the light surface.

We calculated two solutions with a different choice for the steepness parameter in the iso-rotation $\Omega_{\rm F}$. The first solution is for $h = 0.2$ (Fig. 5, *left*). This is more close to the case of rigid rotation. Indeed the solution look rather similar to the solutions presented in Fendt et al. (1995). The second solution is for $h = 0.5$ (Fig. 5, *right*). The steeper profile for the rotation law implies a smaller asymptotic jet radius (Fendt 1997b). This can be seen in comparison with the rigid rotation solutions (Fendt et al. 1995). However, a larger poloidal electric current can balance the effect of differential rotation. Therefore, the $h = 0.2$ solution (with $g = 2.5$) collimates to a smaller asymptotic jet radius than the $h = 0.5$ solution (with $g = 2.0$). A $h = 0.2$ solution with $g = 2.0$ would have a jet radius of 2.4. The second solution with the steeper profile of the rotation law $\Omega_{\rm F}(\Psi)$ would better fit to a Keplerian disk rotation. A perfect match would require an even steeper $\Omega_{\rm F}(\Psi)$-profile (see below).

The mean half opening angle of the jet magnetospheres is about 60°. As discussed above, the shape of the outermost flux surface ($\Psi = 1$) is *not* prescribed but is a result of our calculation eventually determined by the regularity condition. After crossing the light surface the jets collimate to their asymptotic radius within a distance from the source of about 1–2 R_0 along the jet axis. The opening angle of the second solution is smaller, however, the jet collimation is achieved only at a larger distance from the central source. In our examples, the "jet expansion rate", which we define as the ratio of the asymptotic jet radius to the foot point jet radius (the "disk radius"), is about 10. The true scaling of the jet magnetosphere in terms of the size of the central object can be determined by connecting the jet iso-rotation parameter $\Omega_{\rm F}(\Psi)$ to the disk rotation (see next section).

We note that, although in our computations the jet boundary $x_{\rm jet}(z)$ is determined by the force-balance within the jet, and therefore subject to the regularity condition, with our results we do not prove the magnetohydrodynamic *self-collimation process* of the jet flow. Clearly, the calculated jet magnetosphere is self-collimated in the sense that its structure has been determined only by the internal properties. However, the actual collimation process of the jet flow from an un-collimated conical outflow into a cylinder could only be investigated by time-dependent simulations taking into account the interaction with the ambient medium.

On the other hand, we can assume that our jet solution is embedded in an ambient medium. If we further assume an equilibrium between the internal pressure (magnetically dominated) and external (gas) pressure along the jet boundary, we may derive the gas pressure distribution in the ambient medium, since we know the magnetic pressure distribution along the collimating jet radius. In this case, the jet solution may be considered as collimated by ambient pressure.

To our understanding one may claim a self-collimation only, if the jet flow collimates *independently* from external forces. Since in our treatment we do not consider the interrelation with the medium outside the jet, we cannot decide whether the flow is self-collimated or pressure collimated.

The field structure is governed by the choice of the functions $I(\Psi)$ and $\Omega_{\rm F}(\Psi)$, here taken from an asymptotic jet solution. In combination with the disk magnetic flux distribution (13) we can determine two parameters interesting for the jet-disk interaction. These are (i) the

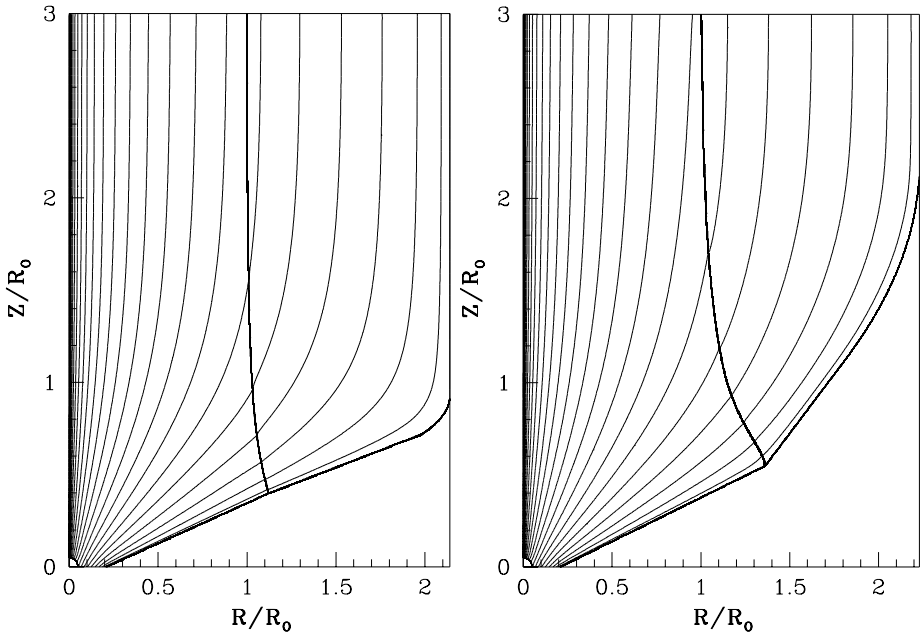

Fig. 5. Two-dimensional magnetic flux distribution $\Psi(x,z)$ for two different *asymptotic* rotation laws. *Left*: $h = 0.2$, $g = 2.5$ *Right*: $h = 0.5$, $g = 2.0$. Shown are iso-contours of the magnetic flux (equivalent to poloidal magnetic field lines) with contour levels $\Psi_n = 10^{-(0.1\,n)^2}$, $n = 0, ..., 25$. Note that due to the choice of contour levels the iso-contour density does not mirror the field strength

magnetic angular momentum loss per unit time and unit radius from disk into the jet and (ii) the toroidal magnetic field distribution along the disk. With $I(\Psi)$ as the angular momentum flux per unit time per unit flux tube, the (normalized) angular momentum flux per unit time per unit radius is $\mathrm{d}\dot{J}/\mathrm{d}x = -xB_z I(x)$ along the disk. Figure 6 shows the behavior of both quantities for our jet model with the steeper profile of the rotation law, $h = 0.5$. As we see, most of the magnetic angular momentum is lost in the outer parts of the disk. This may have interesting applications for accretion disk models taking into account a magnetized wind as a boundary condition. The total magnetic angular momentum loss is determined by the normalization, $\dot{J} = -(I_{\max}\Psi_{\max}/c)\int I(\Psi)\mathrm{d}\Psi$ or $\dot{J} = -(\sqrt{g}\Psi_{\max}/2R_0)\int I(\Psi)\mathrm{d}\Psi$. The magnetic toroidal field distribution along the disk has a maximum at about half the disk radius.

Clearly, these parameters are biased by the magnetic flux disk boundary condition (13) of our model. However, we believe that the main features are rather general and valid for any poloidal current and magnetic flux distribution with the typical core-envelope structure.

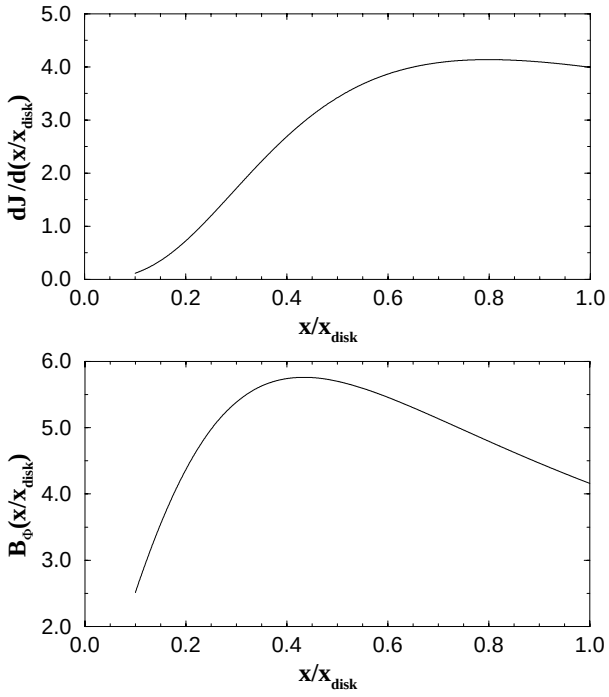

Fig. 6. Magnetic angular momentum loss per time unit per unit radius $\mathrm{d}\dot{J}/\mathrm{d}x$ at radius x (*above*) and disk toroidal field distribution $B_\phi(x)$ (*below*) for the jet solution with $h = 0.5$ shown in Fig. 5

4.3. Scaling relations of disk and jet

As discussed above, the two-dimensional magnetic field distribution connecting the asymptotic jet region with the lower disk boundary allows for a direct scaling of the jet in terms of the size of the central object. This is simply based on the assumption that the foot points of the field lines are rotating with Keplerian speed, $\Omega_\mathrm{F} = \Omega_\mathrm{K}$ and to the fact that in ideal MHD the iso-rotation parameter Ω_F is conserved along the field lines. It is therefore possible to construct a self-consistent model of the whole "star"-disk-jet system with only a small set of free parameters. In the following we will motivate such a model.

The first example demonstrates how the connection between the asymptotic jet and the disk, applied for our very special model assumption, provides a specific estimate for the asymptotic light cylinder R_0. Normalizing the Keplerian velocity $\Omega_{\rm K}$ in the same way as $\Omega_{\rm F}$ (Sect. 2.1), we obtain the expression

$$R_0 = \frac{GM}{c^2\Omega_{\rm K}^2}\frac{1}{x^3} = \frac{GM/c^2}{\Omega_{\rm F}^2(\Psi=1)x_{\rm disk}^3} = \frac{0.5R_{\rm S}}{\Omega_{\rm F}^2(\Psi=1)x_{\rm disk}^3} \cdot (14)$$

Iso-rotation parameter $\Omega_{\rm F}(\Psi)$ and disk radius $x_{\rm disk}$ are fixed by our model. Therefore, the asymptotic light cylinder is proportional to the mass of the central object. For $\Omega_{\rm F}^2(1) = 0.54$ (which refers to the $h = 0.5$ model) and $x_{\rm disk} = 0.2$ the asymptotic light cylinder is $R_0 = 116\ R_{\rm S}$, which is about 2 times larger compared to the jet solution with a rigid rotation $\Omega_{\rm F} \equiv 1$ and will increase for larger values of h. With the choice of g, the value of R_0 constraints the maximum poloidal magnetic flux and electric current. Here, no assumption is made about the flux distribution along the disk.

In the second example we determine the disk magnetic flux distribution $\Psi(x)$ combining the asymptotic jet rotation law $\Omega_{\rm F}(\Psi)$ with a Keplerian disk rotation $\Omega_{\rm K}(x)$. From Eq. (14) follows that $\Omega_{\rm F}(\Psi)/\Omega_{\rm F}(1) = \Omega_{\rm K}(x)/\Omega_{\rm F}(\Psi=1) = (x/x_{\rm disk})^{-3/2}$. In combination with the numerically derived $\Omega_{\rm F}(\Psi)$ this gives the $\Psi(x)$ along the disk (Fig. 7). The figure shows that the disk flux distribution derived from the asymptotic jet is distributed only over the outer part of the disk. This can be interpreted in two ways. First it may imply a relatively large inner disk radius and, hence, an asymptotic jet radius small in terms of radii of the central object. Secondly, it just underlines the fact that in our model the distribution of the asymptotic jet iso-rotation parameter is too flat in order to be truly connected to a disk magnetic flux with an extended radial distribution. For a model taking into account the disk Keplerian rotation in a fully self-consistent way, the magnetic flux distribution which has to be used as disk boundary condition for the GS solution is the one derived in Fig. 7.

On the other hand, the assumption of a Keplerian disk rotation together with a certain disk magnetic flux distribution provides an expression for the iso-rotation parameter $\Omega_{\rm F}(\Psi) = \Omega_{\rm K}(x(\Psi)) = (GM/R_0c^2)\left(\tilde{a}^2\left(\mathrm{e}^{\tilde{b}\,\Psi}-1\right)\right)^{-3/2}$. Here, the disk magnetic flux distribution (13) has been used. Eventually, one finds

$$\frac{\Omega_{\rm K}(\Psi)}{\Omega_{\rm F}(1)} = \left(\frac{x_{\rm disk}}{\tilde{a}}\right)^{3/2}\left(\left(1+\left(\frac{x_{\rm disk}}{\tilde{a}}\right)^2\right)^{\Psi}-1\right)^{-3/4} . (15)$$

This function is definitely steeper compared to the $\Omega_{\rm F}(\Psi)$-distributions which have been derived in Fendt (1997b) and are used in the present paper. Here, we see the limitation of our ansatz. A steeper profile for rotation law is not yet possible to treat with our code due to the lack of numerical resolution. The non-linear character of the GS equation becomes more problematic due to the gradients in the $\Omega_{\rm F}$-source term.

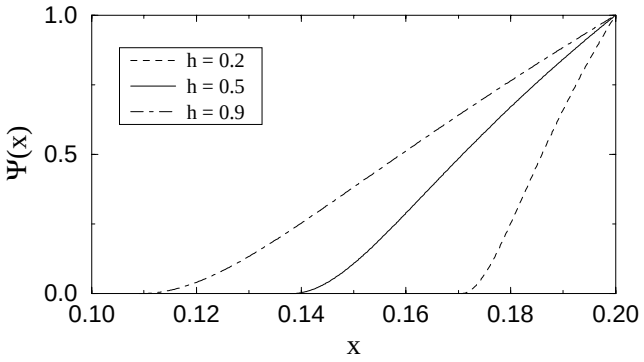

Fig. 7. Magnetic flux distribution $\Psi(x)$ along the disk surface as determined from the asymptotic jet properties and the Keplerian rotation of the disk

In summary, only a model including differential rotation $\Omega_{\rm F}(\Psi)$ may provide a connection between the asymptotic jet, the disk magnetic flux distribution and also the size of the central object. With our model we have presented a reasonable first solution for a self-consistent treatment.

4.4. Application to the M 87 jet

The jet of M 87 shows superluminal motion clearly indicating a highly relativistic jet velocity (Biretta et al. 1999). Recent radio observations have been able to resolve the innermost region of the M 87 jet formation region with 0.33×0.12 mas beam resolution (Junor et al. 1999), corresponding to $2.5-7.0\ 10^{16}$ cm. Assuming a central supermassive black hole of $3\ 10^9\ M_\odot$ (Ford et al. 1994), this is equivalent to about $30\,R_{\rm S}$! The derived jet full opening angle is 60° up to a distance of 0.04 pc from the source with a "strong collimation" occurring afterwards (Junor et al. 1999).

We now apply our two-dimensional jet model to these observations and compare the geometrical scales. Such a comparison is not possible for e.g. self-similar models. From the observed radio profile resolving the inner M 87 jet (see Fig. 1 in Junor et al. 1999), we deduce a jet radius of about 120 Schwarzschild radii. With this, the first important conclusion is that the ratio of jet radius to light cylinder radius must be definitely less than the value of 100 which is usually assumed in the literature. A number value of 3−10 seems to be much more likely. Numerical models of two-dimensional general relativistic magnetic jets fitting in this picture were calculated by Fendt (1997a). These solutions, however, do not take into account the differential rotation $\Omega_{\rm F}(\Psi)$.

Junor et al. (1999) claim that the M 87 jet radius in the region "where the jet is first formed cannot be larger than" their resolution of $30\,R_{\rm S}$. Our conclusion is that the expansion rate is limited in both directions. The new radio observations give a minimum value of 3. Theoretical arguments limit the expansion rate to the

value of about 20, since the jet mass flow must originate outside the marginally stable orbit which is located at 3−6 R_S. Clearly, if the jet radius is really as small as observed in M 87, general relativistic effects may vary the field structure in the jet formation region.

From our model solutions, we derive a light cylinder radius of the M 87 jet of about 50 R_S. The value derived from Eq. (14) differs from that by a factor of two, but is biased by the unknown size of the disk radius $x_{\rm disk}$. This parameter, however, does not affect the global solution. Considering the standard relativistic MHD theory, nothing special is happening at the light cylinder. For a highly magnetized plasma wind the light surface corresponds to the usual Alfvén surface which itself does not affect the flow of matter. Hence, the light cylinder is un-observable.

Also the opening angle in our numerical solution is larger than the observed value by a factor of two. This cannot be due to projection effects since any inclination between jet axis and the line of sight will increase the observed opening angle. We hypothesize that a numerical model with a steeper profile for the iso-rotation parameter will give a smaller jet opening angle comparable to the observed data. This is not surprising, since the jet footpoint anchored in a Keplerian disk rotates faster than in our model. Nevertheless, comparing the collimation distance observed in the M 87 jet and assuming a similar ratio of jet radius to light cylinder radius as in our model with $h = 0.5$, we find good agreement. The collimation distance is 2 R_0.

In summary, we conclude that the example of the M 87 jet gives clear indication that the light cylinder of AGN jets might not be as large as previously thought. Although our model does not fit the observed geometrical properties of the inner M 87 jet perfectly, we find in general a close compatibility.

5. Conclusions

We have investigated the two-dimensional magnetic field distribution in collimating, relativistic jets. The structure of the axisymmetric magnetic flux surfaces is calculated by solving the relativistic force-free Grad-Shafranov equation numerically. In relativistic MHD, *electric fields* become important in difference to Newtonian MHD. The simplifying assumption of the force-free limit has been applied as relativistic jets must be highly magnetized.

The central point of our paper is the consideration of differential rotation of the foot points of the field lines, i.e. a variation of the iso-rotation parameter $\Omega_F(\Psi)$. The underlying model is that of a magnetic jet anchored in an accretion disk. Two main problems had to be solved in order to calculate a two-dimensional field distribution: a) to determine the a priori unknown location of the light surface, b) the proper treatment of the regularity condition along that light surface. The light surface is the force-free equivalent of the Alfvén surface and provides a singularity in the Grad-Shafranov equation. We summarize our results as follows.

(1) We find numerical solutions for the two-dimensional magnetic flux distribution connecting the asymptotic cylindrical jet with a differentially rotating disk. In our example solutions the asymptotic jet radius is about 2.5 times the asymptotic light cylinder radii. This is the first truly two-dimensional relativistic solution for a jet magnetosphere including differential rotation of the iso-rotation parameter $\Omega_F(\Psi)$. The physical solution, being characterized by a smooth transition across the light surface, is unique for a certain parameter choice for the rotation law Ω_F.

(2) The half opening angle of the numerical jet solution is about 60 degrees. Cylindrical collimation is achieved already after a distance of 1–2 asymptotic light cylinder radii along the jet axis. Differential rotation decreases the jet opening angle, but increases the distance from the jet origin where collimation is achieved. The "jet expansion rate", defined as the ratio of the asymptotic jet radius to the jet radius at the jet origin, is about 10.

(3) From the analytical treatment of the regularity condition along the asymptotic branches of the light surface we derive a general estimate for the jet opening angle. We find that the jet half opening angle is larger than 45° and increases for a steeper profile of the differential rotation Ω_F.

(4) Our two-dimensional ansatz, in combination with the treatment of differential rotation, allows for a connection of the asymptotic jet solution with the accretion disk. Certain disk properties can be deduced from the asymptotic jet parameters. Examples are the disk toroidal magnetic field distribution, with a maximum at half of the disk radius and the angular momentum flux per unit time and unit radius. This is interesting as a boundary condition for accretion disk models. We find that most of the angular momentum is lost in the outer part of the disk.

(5) Application of our model to the M 87 jet gives good agreement qualitatively. From our numerical solution we derive an asymptotic light cylinder of the M 87 jet of about 50 Schwarzschild radii. Collimation of the jet would be achieved after a distance of two asymptotic light cylinder radii from the source. This value is comparable with the observations, however, the opening angle in our model is larger by a factor of two.

In summary, we have presented the first global two-dimensional solutions for a relativistic jet magnetosphere taking into account differential rotation of the jet footpoints. From our *jet* model we may determine certain physical quantities in the *disk* that are not possible to observe, as e.g. the angular momentum flux distribution at the disk-jet interface. Comparison with the M 87 jet shows that our model seems to be consistent with the observations, therefore allowing for a derivation of the collimation distance, the light cylinder radius and the jet expansion rate for that example. Clearly, such features as the time-dependent ejection of knots and the interaction process between disk, jet and central source cannot be answered by our approach. Time-dependent relativistic MHD

simulations of the whole "star"-disk-jet system would be necessary, however, such codes are not yet fully developed.

Acknowledgements. Part of this work was initiated when C. F. was holding a guest stipend of the Sonderforschungsbereich (SFB) 328 of the University of Heidelberg. E. M. acknowledges a grant (FE 490/1-1) from the Deutsche Forschungsgemeinschaft (DFG).

Appendix A: Numerical methods

For the solution of the two-dimensional GS equation we apply the method of finite elements as developed by Camenzind (1987) and Fendt et al. (1995). Differential rotation $\Omega_{\rm F}(\Psi)$ implies two major complications for the numerical computation. The first one is the fact that position and shape of the light surface $D = 0$ is not known a priori. Along the light surface the boundary condition is the regularity condition, which, however, itself depends on the two-dimensional solution $\Psi(x, z)$. The second problem is the GS source term for the differential rotation, containing the gradient of the magnetic flux, $|\nabla \Psi|^2$. Compared to the case of rigid rotation, this introduces another (and stronger) non-linearity in the GS equation. Therefore, a fragile numerical convergence process can be expected.

An additional complication is that our grid of finite elements of second order may be inadequate for a calculation of monotonous gradients between the elements if the numerical resolution is too low. However, for appropriate numerical parameters as grid size, element size and iteration step size, we were finally able to overcome these difficulties.

A.1. Determination of the light surface

Here we discuss the iteration procedure we use to determine the location of the light surface. Because the rotation law $\Omega_{\rm F}(\Psi)$ is prescribed, the radius where the light surface, $D = 0$, intersects the jet boundary, $\Psi = 1$, is known,

$$x_{\rm L}(\Psi = 1) = 1/\Omega_{\rm F}(\Psi = 1). \tag{A.1}$$

However, the corresponding position in z-direction is not known. Some estimates can be made about shape and inclination of the light surface in the limit of large radii (see Sect. 2.4), but a general solution is not yet known.

We start the iteration procedure calculating the inner solution (defined as the field distribution inside the light surface) with an outer grid boundary at $x = 1$ (for comparison see Fig. 1). This choice is equivalent to the light cylinder in the case of rigid rotation. For differential rotation the radius $x = 1$ is defined as asymptotic light cylinder (for large z). For low z-values the boundary $x = 1$ is located inside the light surface $x_{\rm L}(\Psi) = 1/\Omega_{\rm F}(\Psi)$. Along this outer boundary (of the *inner* solution), we apply a homogeneous Neumann boundary condition. Usually, this implies that the field lines will cross that boundary perpendicularly. However, in our case the homogeneous Neumann boundary condition transforms into the regularity condition *if* the boundary becomes equivalent to the singular light surface. As shown in Fendt et al. (1995), this transformation applies "automatically" in our finite element code. This is due to the facts that (i) finite element code solves the *integrated* GS equation and (ii) the boundary integral, which is proportional to $D = 1 - x^2\Omega_{\rm F}^2$, vanishes along the light surface.

With the GS solution of the first iteration step we estimate the deviation of the chosen outer boundary from the true light surface by calculating $D = 1 - x^2\Omega_{\rm F}^2(\Psi)$. For the lowest z-value prescribed, we know that $D = 1 - x^2\Omega_{\rm F}^2(\Psi = 1)$. Then, the outer grid boundary (x, z) is slowly moved to a larger radius with $\Delta x \sim D(x, z)^2$. As a consequence of the different numerical grid, the field distribution will change. The value of D will, however, decrease. This procedure is repeated until D is below a certain limit, $D \simeq 0$. Having obtained the solution inside the light surface, that field distribution is taken as inner boundary condition for the outer solution.

References

Appl, S., & Camenzind, M. 1993, A&A, 274, 699
Beskin, V. S. 1997, Phys. Uspekhi, 40, 659
Biretta, J. A., Sparkes, W. B., & Maccetto, F. 1999, ApJ, 520, 621
Blandford, R. D., & Payne, D. G. 1982, MNRAS, 199, 883
Camenzind, M. 1987, A&A, 184, 341
Camenzind, M. 1990, RvMA, 3, 234
Chiueh, T., Li, Z.-Y., & Begelman, M. C. 1991, ApJ, 377, 462
Contopoulos, J., & Lovelace, R. V. E. 1994, ApJ, 429, 139
Contopoulos, J. 1994, ApJ, 432, 508
Contopoulos, J. 1995, ApJ, 446, 67
Fendt, C., Camenzind, M., & Appl, S. 1995, A&A, 300, 791
Fendt, C., & Camenzind, M. 1996, A&A, 313, 591
Fendt, C. 1997a, A&A, 319, 1025
Fendt, C. 1997b, A&A, 323, 999
Ferreira, J. 1997, A&A, 319, 340
Ford, H. C., et al. 1994, ApJ, 435, L27
Junor, W., Biretta, J. A., & Livio, M. 1999, Nat, 401, 891
Khanna, R., & Camenzind, M. 1992, A&A, 263, 401
Li, Z.-Y. 1993, ApJ, 415, 118
Lovelace, R. V. E., Berk, H. L., & Contopoulos, J. 1991, ApJ, 379, 696
Mirabel, I. F., & Rodriguez, L. F. 1995, in Superluminal motions in our Galaxy, 17th Texas Symposium on Relativistic Astrophysics and Cosmology, ed. H. Böhringer, G. E. Morfill, & J. E. Trümper, Annals of the New York Academy of Sciences, New York, 21
Mundt, R., Bührke, T., Solf, J., Ray, T. P., & Raga, A. C. 1990, A&A, 232, 37
Nitta, S.-Y. 1994, PASJ, 46, 217
Nitta, S.-Y. 1995, MNRAS, 276, 825
Okamoto, I. 1992, MNRAS, 254, 192
Okamoto, I. 1999, MNRAS, 307, 253
Ray, T. P., Mundt, R., Dyson, J. E., Falle, S. A. E. G., & Raga, A. C. 1996, ApJ, 468, L103
Pudritz, R. E., & Norman, C. A. 1983, ApJ, 274, 677
Shibata, K., & Uchida, Y. 1985, PASJ, 37, 31
Sakurai, T. 1985, A&A, 152, 121
Zensus, J. A., Cohen, M. H., & Unwin, S. C. 1995, ApJ, 443, 35

A&A 369, 308–322 (2001)
DOI: 10.1051/0004-6361:20010108

Astronomy & Astrophysics

Magnetically driven superluminal motion from rotating black holes

Solution of the magnetic wind equation in Kerr metric

C. Fendt and J. Greiner

Astrophysikalisches Institut Potsdam, An der Sternwarte 16, 14482 Potsdam, Germany

Received 21 August 2000 / Accepted 19 January 2001

Abstract. We have investigated magnetically driven superluminal jets originating from rotating black holes. The stationary, general relativistic, magnetohydrodynamic wind equation along collimating magnetic flux surfaces has been solved numerically. Our jet solutions are calculated on a global scale of a spatial range from several to several 1000 gravitational radii. Different magnetic field geometries were investigated, parameterized by the shape of the magnetic flux surface and the magnetic flux distribution. For a given magnetic flux surface we obtain the complete set of physical parameters for the jet flow. In particular, we apply our results to the Galactic superluminal sources GRS 1915+105 and GRO 1655−40. Motivated by the huge size indicated for the Galactic superluminal knots of about 10^9 Schwarzschild radii, we point out the possibility that the jet collimation process in these sources may be less efficient and therefore intrinsically different to the AGN. Our results show that the observed speed of more than $0.9\,c$ can be achieved in general by magnetohydrodynamic acceleration. The velocity distribution along the magnetic field has a saturating profile. The asymptotic jet velocity depends either on the plasma magnetization (for a fixed field structure) or on the magnetic flux distribution (for fixed magnetization). The distance where the asymptotic velocity is reached, is below the observational resolution for GRS 1915+105 by several orders of magnitude. Further, we find that highly relativistic speeds can be reached also for jets *not* emerging from a region close to the black hole, if the flow magnetization is sufficiently large. The plasma temperature rapidly decreases from about 10^{10} K at the foot point of the jet to about 10^6 K at a distance of 5000 gravitational radii from the source. Temperature and the mass density follow a power law distribution with the radius. The jet magnetic field is dominated by the toroidal component, whereas the velocity field is dominated by the poloidal component.

Key words. accretion, accretion disks-Black hole physics – MHD – stars: mass loss – ISM: jets and outflows – galaxies: jets

1. Introduction

1.1. Relativistic jets and galactic superluminal motion

Apparent superluminal jet motion originating in the close environment of a rotating black hole is observationally indicated for two classes of sources concerning mass and energy output. One class is the family of radio loud active galactic nuclei (hereafter AGN). In the AGN standard model highly relativistic jet motion is explained by *magnetohydrodynamic* processes in a black hole – accretion disk environment (for a review see Blandford 1990). Jets are magnetically accelerated and possibly also collimated by magnetic forces. However, the detailed interaction process of the magnetized black hole – accretion disk system which is believed to lead to the ejection of high velocity blobs is not yet fully understood.

Send offprint requests to: C. Fendt, e-mail: cfendt@aip.de

The other class are galactic binary systems for which radio observations have also detected superluminal motion (see reviews of Fender 2000 or Greiner 2000). The two most prominent examples are the high energy sources GRS 1915+105 (Mirabel & Rodriguez 1994) and GRO 1655−40 (Hjellming & Rupen 1995; Tingay et al. 1995). The de-projected jet speed of both sources is $\gtrsim 0.9\,c$ and surprisingly similar, although for GRS 1915+105 also a higher velocity component has been observed recently (Fender et al. 1999). GRO 1655−40 is a binary consisting of a $7.02 \pm 0.22\,M_\odot$ black hole and a $2.3\,M_\odot$ F-subgiant (Orosz & Bailyn 1997) at a distance of 3 kpc. GRS 1915+105 is at 10–12 kpc distance (Fender et al. 1999), but the component masses of the presumed binary are not known. Order of magnitude estimates based on X-ray variability and QPO properties range from 10–80 $M_\odot$ (Morgan et al. 1997; Greiner et al. 1998). As for the AGN jet sources, observational evidence for a black

hole – accretion disk system is found also for the Galactic superluminal sources. Observations have also indicated that accretion disk instabilities may be related to jet ejection (Greiner et al. 1996; Belloni et al. 1997; Mirabel et al. 1998). Therefore, the jet formation process for extragalactic jets and their Galactic counterparts may be the same, although the mechanism that accelerates and collimates the GRS 1915+105 ejecta is yet unclear (Rodriguez & Mirabel 1999).

Optical polarization measurements have been obtained for the microquasar GRO J1655–40 (Scaltriti et al. 1997; Gliozzi et al. 1998). The polarization angle is approximately parallel to the accretion disk plane. The amount of polarization has been found to vary smoothly with the orbital phase, being smallest at binary phase 0.7–0.8. It has been noted that the occasionally observed X-ray dips occur at the same phase interval (Ueda et al. 1998; Kuulkers et al. 1998) suggesting that it may be related to either a thickening of the disk rim at the impact site of the accretion stream from the companion or the overflow of this stream above/below the disk. The orbital polarization modulation rules out a synchrotron origin in the jet, and implies the presence of electron scattering plasma above the accretion disk which is asymmetrically distributed or asymmetrically illuminated. The existence of such scattering plasma is consistent with the interpretation of the iron features as observed with ASCA as absorption lines and edges in a thick, cool torus of column $N_{\rm H} > 10^{23}$ cm^{-2} (Ueda et al. 1998).

The relativistic speed observed for the Galactic superluminal sources ($\sim$0.9–0.98 c de-projected) corresponds to a bulk Lorentz factor of $\gamma = 2$–5 although this number is not very accurate (e.g. Fender et al. 1999). Therefore, for any theoretical investigation of these objects at least special relativity has to be taken into account. If the superluminal motion originates close to a black hole, also general relativistic effects may become important.

The ejection of matter itself is not a stationary process. In GRS 1915+105 also repeated emission of knots is observed (Rodriguez & Mirabel 1999). X-ray and radio observations suggest that a wide range of ejected mass and ejection frequency is possible.

Though the galactic jet sources are nearby, they are not better resolved spatially because the distance ratio between AGN and microquasars is smaller than their mass ratios. Nevertheless, an important implication may also come from the observed size of the superluminal knots which are observationally resolved. In the case of GRS 1915+105 the characteristic dimension of the "jet" is 35 mas, equivalent to 7 10^{15} cm at a distance of 12.5 kpc (Rodriguez & Mirabel 1999). We emphasize that such a knot size corresponds to $\sim 10^9$ Schwarzschild radii for $R_{\rm S} = 1.5\ 10^6\,(M/5\,M_\odot)$cm! This is a huge factor and may be in distinctive difference to the AGN jets. Similarly, the VLBA data show the core as a collimated jet down to a distance of 10 AU from the central source with an opening angle of $<10^\circ$ (see Mirabel & Rodriguez 1999) corresponding to $10^7\,(M/5\ M_\odot)$ Schwarzschild radii. The length of the radio jet is about 100 AU.

However, when interpreting the observed emission region, one has to keep in mind that this region may not represent the jet flow itself, but some *part* of another, larger, structure. For example, in some extragalactic jet sources there is indication that the knots travel along helical trajectories, believed to be prescribed by a large-scale helical magnetic field of an almost cylindrically collimated jet (Zensus et al. 1995; Camenzind & Krockenberger 1992).

In GRO 1655−40 the motion of the radio knots is complicated and requires (at least) precession between different ejections (Hjellming & Rupen 1995). The knot structures in GRS 1915+105 remained fixed implying that the whole knot moves with the same speed without spatial diffusion and with an axial velocity profile more or less constant.

Based on minimum energy arguments and only relativistic electrons responsible for the synchrotron radiation in the knots of GRS 1915+105, Rodriguez & Mirabel (1999) derive a magnetic field strength of about 50 mG to 7 mG, the decrease resulting from the expansion of the knot. They also estimate the rest mass of a knot of $\geq 10^{23}$ g, and together with (steady) photon luminosity of $\simeq 3\ 10^{38}\,{\rm erg\,s^{-1}}$, exclude radiation as driving mechanism for the knots.

1.2. Theory of magnetic jets

From the introductory remarks it is clear that a quantitative analysis of superluminal motion must take into account both magnetohydrodynamics (hereafter MHD) and (general) relativity.

The first theoretical formulation of the electromagnetic force-equilibrium in Kerr space-time around rotating black holes was given by Blandford & Znajek (1977) and Znajek (1977), who discovered the possibility of extracting rotational energy and angular momentum from the black hole electromagnetically.

Camenzind (1986, 1987) formulated a fully relativistic stationary description of MHD flows, basically applicable to any field geometry. The structure of such collimating jet magnetospheres in the case of Kerr space time was presented by Fendt (1997). Solutions of the so-called wind equation in Kerr geometry (see below) considering the stationary plasma motion along the magnetic field were obtained by Takahashi et al. (1990), however, mainly discussing the accretion flow onto the black hole.

While the asymptotic structure of the propagating jets becomes more and more understood with the help of time-dependent magnetohydrodynamical, also relativistic, simulations (e.g. Nishikawa et al. 1997; Mioduszewski et al. 1997; Hardee et al. 1998), the process of jet formation itself and the collimation of the outflow region is a task still too complex for numerical simulations. The involved length scales and gradients require a high resolution in grid size and time stepping. Koide et al. (1998) were first to perform

general relativistic MHD simulations of jet formation close to the black hole. In their model, the interaction of an initially cylindrical magnetic field with a Keplerian accretion disk results first in an inflow of matter towards the black hole. This accretion stream interacts with the hydrostatic corona around the black hole giving rise to a relativistic gas pressure driven jet. At larger radii a magnetically driven wind is initiated from the accretion disk. The simulations were performed for less than two rotations of the inner disk (corresponding to less than 0.02 rotations of the disk at the outer edge of the grid). Although these results of the first fully general relativistic MHD simulations look indeed very exciting, some objections can be raised about the underlying model. The initial condition applied is that of a hydrostatic corona around a black hole, an assumption which is not compatible with the boundary of a black hole horizon. Such a configuration is not stable and will immediately collapse. Recently, the authors extended their work applying an initial coronal structure in steady infall surrounding a non-rotating black hole (Koide et al. 1999). They find a two-layered jet consisting of a magnetically driven jet around a gas-pressure driven jet. In addition, Koide et al. (2000) considered the quasi-steady infall of the corona around a Kerr black hole. They find that jet formation seems to differ for co-rotating and counter-rotating disks. The jet ejection tends to be easier in the latter case with a jet origin much closer to the hole. Also, a new feature of another magnetically driven (though sub-relativistic) jet appears within the gas-pressure driven jet. The computations were lasting over a few inner disk orbits. Therefore, the observed events of mass ejection could still be a relict of the initial condition and may not be present in the long-term evolution. Clearly, it would be interesting to perform the Koide et al. simulations for a longer time and look whether the mass ejection continues over many disk orbits, whether the simulation evolves into a final stationary state (as e.g. in Ouyed & Pudritz 1997; Fendt & Elstner 2000), or whether the jet formation retains its unsteady behavior which could explain the emission of superluminal knots observed in the relativistic jets.

1.3. Aim of the present study

In this paper, a stationary magnetic jet flow along a given magnetic flux surface is investigated in the context of general relativity. Due to the stationary approach, we cannot treat any time-dependent phenomena. Our emphasis is to trace the *large scale* behavior of the flow from it's origin close to the black hole to large distances. This is an essential point in particular for the Galactic superluminal sources because of the possible huge spatial extension of the jets compared to the central black hole. The stationary model allows for a *global* treatment of the jet flow, i.e. an investigation over a large range of magnitudes for density and magnetic field strength. This is not yet feasible with time-dependent MHD codes presently available. In particular, we address the following topics.

- For a given geometry of the magnetic field, which are the resulting jet *dynamical parameters* as velocity, density or temperature?
- How important are the effects of general relativity? Does the superluminal flow indeed originate very close to a black hole?
- From the investigation of different field geometries we expect some hints to the jet opening angle and the length scale of the collimation process.

The structure of this paper is as follows. In Sect. 2, basic equations for relativistic magnetospheres are reviewed in the context of Kerr metrics. In Sect. 3, the model underlying our numerical calculations is discussed. We present our numerical results in Sect. 4 and discuss solutions with different geometry and jet parameters. We summarize our paper in Sect. 5.

2. Description of a MHD flow in Kerr metric

Under the assumptions of axisymmetry, stationarity and infinite conductivity, the MHD equations reduce to a set of two basic equations describing the local force-balance across the field and along the field (for references, see, e.g., Blandford & Znajek 1977; Thorne et al. 1986; Camenzind 1986, 1987; Okamoto 1992; Beskin & Pariev 1993; Beskin 1997).

The trans-field or *Grad-Shafranov equation* determines the field structure, whereas the *wind equation* describes the flow dynamics along the field. Due to the stationarity assumption, certain conservation laws apply. The total energy density, the total angular momentum density, the mass flow rate per flux surface and the iso-rotation parameter are conserved quantities along the surfaces of constant magnetic flux (Camenzind 1986).

In this paper the motion of a magnetized plasma is calculated from the wind equation. The plasma moves along a prescribed axisymmetric magnetic flux surface which originates in a region close to a rotating black hole.

2.1. Space-time around rotating black holes

The space-time around a rotating black hole with a mass M and angular momentum per unit mass a is described using Boyer-Lindquist coordinates with the line element

$$\mathrm{d}s^2 = \alpha^2 \mathrm{d}t^2 - \tilde{\omega}^2 \left(\mathrm{d}\phi - \omega \mathrm{d}t\right)^2 - \left(\rho^2/\Delta\right) \mathrm{d}r^2 - \rho^2 \, \mathrm{d}\theta^2, \quad (1)$$

where t denotes the global time, ϕ the angle around the axis of symmetry, r, θ similar to there flat space counterpart spherical coordinates, and where geometrical units $c = G = 1$ have been applied (see Appendix A for further definitions). The horizon of the Kerr black hole is located at $r_{\mathrm{H}} = M + \sqrt{M^2 - a^2}$. We will normalize all radii to gravitational radii $r_{\mathrm{g}} = r_{\mathrm{H}}(a = M) = M$. The angular

velocity of an observer moving with zero angular momentum (ZAMO) is $\omega = (\mathrm{d}\phi/\mathrm{d}t)_{\mathrm{ZAMO}}$, corresponding to the angular velocity of the differentially rotating space. The lapse function is $\alpha = (\mathrm{d}\tau/\mathrm{d}t)_{\mathrm{ZAMO}}$ describing the lapse of the proper time τ in the ZAMO system to the global time t.

2.2. Description of the electromagnetic field

In the 3+1 split of Kerr space time (Thorne et al. 1986) the electromagnetic field $\boldsymbol{B}, \boldsymbol{E}$, the current density $\boldsymbol{j}$, and the electric charge density ρ_{c} can be described very similar to the usual expressions, if measured by the ZAMO's according to the locally flat Minkowski space. These local experiments then have to be put together by a global observer for a certain global time using the lapse and shift function for the transformation from the local to the global frame.

With the assumption of axisymmetry a magnetic flux surface can be defined measuring the magnetic flux through a loop of the Killing vector $\boldsymbol{m} = \tilde{\omega}^2 \nabla\phi$,

$$\Psi(r,\theta) = \frac{1}{2\pi}\int \boldsymbol{B}_{\mathrm{p}} \cdot \mathrm{d}\boldsymbol{A}\,, \qquad \boldsymbol{B}_{\mathrm{p}} = \frac{1}{\tilde{\omega}^2}\nabla\Psi \wedge \boldsymbol{m}, \tag{2}$$

corresponding to the magnetic flux through an area $\pi(r\,\sin\theta)^2$ around the symmetry axis (in the limit of Minkowski space).

With the assumption of a degenerated magnetosphere, $||\boldsymbol{B}|^2 - |\boldsymbol{E}|^2| >> |\boldsymbol{E}\cdot\boldsymbol{B}| \simeq 0$ an "angular velocity of field lines" can be derived from the derivative of the time component of the vector potential $\Omega_{\mathrm{F}} = \Omega_{\mathrm{F}}(\Psi) = -2\pi c(\mathrm{d}A_0/\mathrm{d}\Psi)$. We will denote this quantity with the term "iso-rotation parameter".

2.3. The wind equation

It has been shown that a stationary, polytropic, general relativistic MHD flow along an axisymmetric flux surface $\Psi(r,\theta)$ can be described by the following *wind equation* for the poloidal velocity $u_{\mathrm{p}} \equiv \gamma v_{\mathrm{p}}/c$,

$$u_{\mathrm{p}}^2 + 1 = -\sigma_{\mathrm{m}} \left(\frac{E}{\mu}\right)^2 \frac{k_0 k_2 + \sigma_{\mathrm{m}} 2 k_2 M^2 - k_4 M^4}{(k_0 + \sigma_{\mathrm{m}} M^2)^2}\,, \tag{3}$$

where

$$\begin{aligned} k_0 &= g_{33}\Omega_{\mathrm{F}}^2 + 2g_{03}\Omega_{\mathrm{F}} + g_{00}, \\ k_2 &= 1 - \Omega_{\mathrm{F}}\frac{L}{E}, \\ k_4 &= -\left(g_{33} + 2g_{03}\frac{L}{E} + g_{00}\frac{L^2}{E^2}\right) / \left(g_{03}^2 - g_{00}g_{33}\right) \end{aligned}$$

(Camenzind 1986; Takahashi et al. 1990). The Alfvén Mach number M is defined as $M^2 = 4\mu n u_{\mathrm{p}}^2/\tilde{B}_{\mathrm{p}}^2$, with the proper particle density n, the specific enthalpy μ, and a poloidal magnetic field $\tilde{B}_{\mathrm{p}} = B_{\mathrm{p}}/(g_{00)} + g_{03}\Omega_{\mathrm{F}})$, rescaled for mathematical convenience. The quantity σ_{m} stands for the sign of the metric (we have chosen $\sigma_{\mathrm{m}} = -1$, see Appendix A). For a polytropic gas law with the index $\Gamma \equiv n/m$, the wind Eq. (3) can be converted into a polynomial equation,

$$\sum_{i=0}^{2n+2m} A_i(x;\Psi,\Phi;\Omega_{\mathrm{F}};E,L,\sigma_\star)\, u_{\mathrm{P}}^{i/m} = 0\,, \tag{4}$$

(Camenzind 1987; Englmaier 1993; Jensen 1997), where the coefficients A_i are now defined as functions of the normalized cylindrical radius $x = R/r_{\mathrm{g}}$ (see Appendix B). The shape of the axisymmetric magnetic flux surface Ψ is prescribed as function $z(x;\Psi)$. The flux function $\Phi = \sqrt{-g}\tilde{B}_{\mathrm{p}}$ describes the opening of the flux tube. The faster Φ decreases the faster magnetic energy is converted into kinetic energy. We define the dimensionless magnetization parameter[1] at the "injection" point $x_\star$ following Takahashi et al. (1990),

$$\sigma_\star = \frac{\Phi_\star^2}{4\pi m_{\mathrm{p}} I_{\mathrm{p}\star}}, \tag{5}$$

measuring the Poynting flux in terms of particle flux $I_{\mathrm{p}} \equiv \sqrt{-g}\, n u_{\mathrm{p}}$, where m_{p} is the particle mass (here the proton mass). The magnetization determines the maximum energy available for plasma acceleration and thus determines also the asymptotic poloidal velocity. The other wind parameters are total energy density E, total angular momentum L, and the iso-rotation parameter Ω_{F}. The non relativistic limit of Eq. (4) has been solved numerically by Kudoh & Shibata (1995, 1997).

We choose the polytropic index $\Gamma = 5/3$ for a hot relativistic proton-electron plasma (a hot electron-positron plasma would imply $\Gamma = 4/3$). Then, at each radius x the polynomial Eq. (4) has $2n + 2m = 16$ solutions. Some of these mathematical solutions have no physical meaning, e.g. because u_{p}^2 is negative. The remaining physical solutions form a bunch of different curves in the $u_{\mathrm{p}}(x)$-diagram representing different solution branches (see our solution S1 in Appendix C, Fig. C.1). The unique branch of the "wind" solution starts at a small radius with small velocity continuing outwards with increasing velocity. For an other parameter choice also "accretion" branches can be found, starting from a large radius with small velocity and continuing inwards with increasing velocity (not shown in Fig. C.1).

However, not for all parameters E, L, σ there exist *physical* solutions which are continuous functions of x and therefore defined along the whole flux surface. It is well known that at the magnetosonic points the wind Eq. (3) becomes singular (see Camenzind 1986; Takahashi et al. 1990). Regularity of the solution requires a flow velocity equal to the speed of the MHD waves in order to obtain a smooth (self-consistent) transition at the magnetosonic

[1] Note that this definition for the magnetization varies from the original Michel magnetization parameter $\sigma_{\mathrm{M}} = \Phi_{\mathrm{M}}^2/4\pi f_{\mathrm{M}} c R_{\mathrm{L}}^2$, where Φ_{M} is the magnetic flux, f_{M} the mass flux and R_{L} the light cylinder. Usually, the general relativistic equations are normalized to the gravitational radius, whereas the special relativistic equations are normalized to the light cylinder.

points. In order to match astrophysical boundary conditions we fix the following parameters,

- *the "injection" radius,* $x_\star$, the location where the matter couples to the magnetic field. This radius also determines the iso-rotation parameter Ω_F;
- *the "injection" velocity* $u_{\mathrm{p}\star} = u_\mathrm{p}(x_\star)$, defining the initial kinetic energy;
- *the Alfvén radius* x_A, which fixes the total angular momentum of the flow.

The critical wind solution for a given flux surface can then be found by varying the flow parameters in Eq. (4). Due to numerical convenience, we vary

- *the sound speed* $c_{\mathrm{s}\star}$ at the injection radius, defining the initial density (or gas pressure and temperature);
- *the magnetization* parameter at the injection point $\sigma_\star(\Psi) = \Phi_\star^2/(4\pi m_\mathrm{p} I_{\mathrm{p}\star})$.

In turn, the condition of a regular flow at the magnetosonic points fixes the sound speed and magnetization and, thus, jet mass flow rate and temperature.

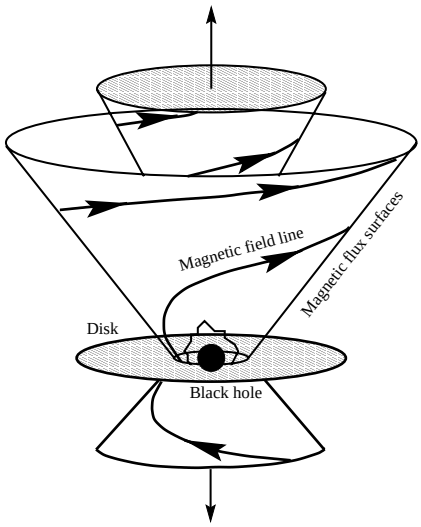

Fig. 1. Model geometry applied for our numerical calculations. The poloidal field structure is prescribed as magnetic flux surfaces with different opening angle. The flux surfaces have different foot point radii along the accretion disk (not visible). The central source is a black hole implying that general relativistic effects have to be taken into account. The toroidal field follows from the solution of the wind equation

3. The model assumptions

3.1. The model in general

Observationally the jet phenomenon of AGN, young stellar objects and microquasars is always connected to the signatures of an accretion disk. We therefore assume a similar disk-jet scenario for the jet formation in *Galactic* superluminal jet sources. In general our model geometry follows the standard model for jet formation in AGN (cf. Blandford 1990).

Two typical length scales enter the problem. (i) The gravitational radius r_g measures the influence of gravity on the metric. (ii) The asymptotic light cylinder R_L describes the influence of rotation on the electrodynamics.

3.2. The central black hole

The black hole mass and angular momentum determine the geometry of space. Since we use dimensionless equations normalized to the gravitational radius, our results scale with the mass of the black hole. For parameter estimates we assume a black hole mass of $5\,M_\odot$ which is about the value inferred for the galactic superluminal sources. The angular momentum a as the other black hole parameter is not known for any of the relativistic jet sources. Interpretation of the high effective temperatures of the accretion disk as well as the stable QPO frequency (as Thirring-Lense effect) suggests that $a \gtrsim 0.9$ for GRS 1915+105 and GRO 1655−40 (Zhang et al. 1997). Theoretically, one may expect a rapidly rotating black hole because of angular momentum conservation during the collapse and also accretion of angular momentum from the accretion disk (King & Kolb 2000). Here, we choose $a = 0.8$, a value which is not extreme, but clearly different to Schwarzschild metric. The rotation rate of the black hole is defined as $\Omega_\mathrm{H} \equiv \omega(r_\mathrm{H}) = a/(2Mr_\mathrm{H})$. The Kerr parameter a does not influence the solution of the wind equation directly. However, for rotating black holes the marginally stable orbit r_ms is closer to the horizon, $r_\mathrm{ms} = 6r_\mathrm{g}$ for $a = 0$ and $r_\mathrm{ms} \simeq r_\mathrm{g}$ for $a \simeq 1$ (This is the case for a co-rotating disk. For a retrograde disk rotation $r_\mathrm{ms} \simeq 9r_\mathrm{g}$ for $a \simeq 1$). Therefore, assuming that the jet magnetic field is anchored just at the marginally stable orbit, for a rapidly rotating black hole the maximum angular velocity of the jet foot points increases by a factor of $6^{3/2}/2 = 7.4$. Correspondingly, the light cylinder radius of the jet moves inward by the same factor.

In addition to the well-known special relativistic light cylinder, the differential rotation of the space ω leads to the formation of a second light surface. At this position the "rotational velocity" of the field lines relative to the ZAMO equals the speed of light (see Blandford & Znajek 1977). The position of the two light surfaces $\tilde{\omega}_\mathrm{L}$ is defined by $\tilde{\omega}_\mathrm{L}^2 = (\pm\alpha\, c/(\Omega_\mathrm{F} - \omega))^2$, where the + (−) sign holds for the outer (inner) light surface with $\Omega_\mathrm{F} > \omega$ ($\Omega_\mathrm{F} < \omega$). However, these light surfaces have no direct implication for the MHD flow. In the limit of a strong magnetization, the MHD Alfvén surfaces (for inflow and outflow) approach the corresponding light surfaces.

3.3. The accretion disk

X-ray observations of GRS 1915+105 detected strong intensity variations indicating major instabilities of an accretion disk (Greiner et al. 1996). Belloni et al. (1997) find that the highly variable X-ray spectra could be explained if the inner disk is alternatively removed and replenished due to a thermal-viscous instability. Simultaneous X-ray

and infrared observations of GRS 1915+105 revealed evidence for a disk–jet interrelation (Eikenberry et al. 1998; Mirabel et al. 1998). The observed flares in the X-ray and IR bands have a consistent offset delay of ∼30 min indicating an origin from the same event.

The accretion rate in GRS 1915+105 and GRO J1655−40 can be determined from the observed X-ray luminosities (e.g. Greiner et al. 1998). Depending on the chosen efficiency (5% in non-rotating versus 42% in maximally rotating black holes) the accretion rate ranges between 1–9 10^{-7} $M_\odot$ yr^{-1} (GRS 1915+105) and 0.8–7 10^{-8} $M_\odot$ yr^{-1} (GRO J1655−40), respectively.

From the theoretical point of view an accretion disk surrounding the black hole is the essential component concerning magnetic jet formation. It is considered to be responsible for the following necessary ingredients for jet formation, propagation, and collimation.

- The *generation of the magnetic field*. In contrast to stellar jets the magnetic field of jets from black holes cannot be supplied by the central object but has to be generated by the surrounding accretion disk. Dynamo action in general relativistic accretion disks were discussed by Khanna & Camenzind (1996a, 1996b) and Brandenburg (1996);
- The *mass loading of the jet*. The accreting material becomes partly diverted into the jet. Evidently, no mass outflow is possible from the black hole itself, in difference to a stellar wind. The (non-relativistic) self-similar accretion-ejection mechanism was investigated by Ferreira (1997);
- The *electric current* system. Differential rotation of the disk is also responsible for driving the poloidal electric current system in the jet magnetosphere. Such a current extracts angular momentum from the disk and eventually allows for mass accretion into the central object.

3.4. Model parameters for the wind motion

3.4.1. The magnetization parameter

The leading parameter for the wind solution along a fixed poloidal field is the magnetization parameter (5). Renormalization to astrophysical units gives

$$\sigma_\star(\Psi) = \frac{\Phi_\star^2}{4\pi m_{\rm p} I_{\rm p\star}} \rightarrow \frac{B_{\rm p\star}^2 R_\star^4}{c\dot{M}_{\rm jet}(\Psi) r_{\rm g}^2} = \frac{B_{\rm p\star}^2 r_{\rm g}^2}{c\dot{M}_{\rm jet}(\Psi)} \left(\frac{R_\star}{r_{\rm g}}\right)^4 \quad (6)$$

where $\dot{M}_{\rm jet}(\Psi) \simeq 4\pi m_{\rm p} n_\star c u_{\rm p\star} R_\star^2$ is the jet mass flux enclosed by an area of radius $R_\star$. A first order estimate of the magnetization can be derived from the disk equipartition field strength. Then, with a reasonable assumption on the jet mass flow rate related to the disk accretion rate, this gives the jet magnetization. Although the equipartition field strength is model-dependent, the different models (e.g. either advection dominated disk or standard disk, either Kramer's opacity or Thomson scattering) give rather similar results. A self-similar advection dominated disk model with the accretion rate $\dot{M}_{\rm acc}$ gives

$$B_{\rm eq} \simeq 2.5\ 10^9\ {\rm G}\ \alpha_{\rm vis}^{-\frac{1}{2}} \left(\frac{M}{5\ M_\odot}\right)^{-\frac{1}{2}} \left(\frac{\dot{M}_{\rm acc}}{\dot{M}_{\rm E}}\right)^{\frac{1}{2}} \left(\frac{R}{r_{\rm g}}\right)^{-\frac{5}{4}}, \quad (7)$$

where $\dot{M}_{\rm E} = 1.1\ 10^{-7}(M/5\ M_\odot)\, M_\odot\, {\rm yr}^{-1}$ is the Eddington luminosity and $\alpha_{\rm vis}$ is the viscosity parameter (see e.g. Narayan et al. 1998). In comparison, an optically thin standard accretion disk with Thomson opacity gives $B_{\rm eq} \simeq \sqrt{8\pi P} = \sqrt{8\pi a T^4/3} \simeq 1.8\ 10^8\ {\rm G}\, \alpha_{\rm vis}^{-1/2} (M/5\ M_\odot)^{-1/2} (R/r_{\rm g})^{-3/4}$ (see Blandford 1990). Note that these estimates are only valid within certain limits of the accretion rate and the disk radius. Using the advection dominated disk model equipartition field strength, we obtain the following estimate for the magnetization at the injection radius,

$$\sigma_\star(\Psi) = 16 \frac{1}{\alpha_{\rm vis}} \left(\frac{M}{5\ M_\odot}\right) \left(\frac{\dot{M}_{\rm jet}}{\dot{M}_{\rm acc}}\right)^{-1} \left(\frac{R_\star}{r_{\rm g}}\right)^{3/2}. \quad (8)$$

A comparison with the original Michel magnetization parameter $\sigma_{\rm M}$ must take into account a factor $(r_{\rm g}/R_{\rm L})^2$. The magnetization parameter derived from the field distribution in a standard accretion disk model (see above) will give a similar result. We emphasize that we do not "apply" a certain disk model (e.g. the ADAF model) in our computations. However, a comparison in the context of accretion disk theory just puts our wind parameters on a safer ground. Note, that neither the ADAF model nor the standard disk model takes into account the influence of magnetic fields. Moreover, the ADAF estimates as cited in Eq. (7) rely on the self-similar assumption. Compared to the standard disk, by definition, the matter in the ADAF disk would be rapidly advected possibly influencing also the wind ejection. However, such a detailed treatment is beyond the scope of this paper and may only be considered in numerical simulations investigating the disk-jet interaction itself (Koide et al. 1998, 1999, 2000)

3.4.2. The magnetic field distribution

The normalized magnetic field distribution is prescribed by

– *the shape of the field line*, $z(x)$;
– *the magnetic flux distribution*, $\Phi(x) = \tilde{\Phi}(x)\sqrt{-g/(\rho^2\Delta)}$.

We apply different functions for $z(x)$ and $\tilde{\Phi}(x)$ in order to investigate the influence of collimation, rotation and magnetic flux distribution on the acceleration of matter. One example is $z(x) = 0.1(x-x_0)^{6/5}$ describing an almost conical surface with only a slight collimation (see Fig. 2). Here, x_0 defines the intersection of the field line with the equatorial plane, with x_0 somewhat smaller than $x_\star$. The idea behind this choice is that the matter is expected to couple to the jet magnetic field *above* the accretion disk (with $z(x_\star) > 0$). An example for the magnetic flux distribution

Table 1. Comparison of leading parameters for the wind solution. Magnetic flux distribution $\tilde{\Phi}/\tilde{\Phi}_\star$, shape of the poloidal field line $z(x)$, iso-rotation parameter Ω_F, sound speed at the injection radius $c_{\mathrm{s}\star}$, magnetization at the injection radius $\sigma_\star$, cylindrical Alfvén radius x_A, cylindrical injection radius $x_\star$, total energy E, normalized to $m_\mathrm{p}c^2$ normalized total angular momentum $\tilde{L} = L/E$, asymptotic velocity $u_{\mathrm{p}\infty}$, and angular momentum parameter of the black hole a. Other Parameters are: $\Gamma = 5/3$, $u_{\mathrm{p}\star} = 0.006$ (S3–S9), $u_{\mathrm{p}\star} = 0.17$ (S3q, S3u2), $u_{\mathrm{p}\star} = 0.21$ (S3u3)

	prescribed		calculated								
	$\tilde{\Phi}/\tilde{\Phi}_\star$	$z(x)$	Ω_F	$c_{\mathrm{s}\star}$	$\sigma_\star$	x_A	$x_\star$	E	$\tilde{L}$	$u_{\mathrm{p}\infty}$	a
S3	~ 1	$0.1(x-x_0)^{6/5}$	0.035	0.05165	979.4	22.931	8.3	2.7887	20.04	2.531	0.8
S3c2	~ 1	$0.1(x-x_0)^{3/2}$	0.035	0.0529	1356	22.931	8.3	2.764	19.95	2.58	0.8
S4	$\sim x^{-1/2}$	$0.1(x-x_0)^{6/5}$	0.035	0.049	2380	22.931	8.3	2.7879	20.04	2.60	0.8
S4b	$\sim x^{-1/2}$	$0.1(x-x_0)^{6/5}$	0.014	0.0390	14 680	57.0	15.3	2.6730	47.07	2.48	0.8
S9	$\sim x^{-1/2}$	$0.1(x-x_0)^{3/2}$	0.035	0.05165	2777	22.92	8.3	2.7572	19.93	2.57	0.8
S3q	~ 1	$0.1(x-x_0)^{6/5}$	0.14	0.31	480	5.83	3.3	8.917	6.616	8.48	0.8
S3u	~ 1	$0.1(x-x_0)^{6/5}$	0.14	0.27	100	5.33	3.3	3.16	5.69	2.96	0.8
S3u2	~ 1	$0.1(x-x_0)^{6/5}$	0.14	0.27	82.5	5.33	3.3	4.66	6.35	4.55	10^{-8}
S3u3	~ 1	$0.1(x-x_0)^{6/5}$	0.14	0.27	205.7	5.33	3.3	4.65	6.35	4.48	10^{-8}

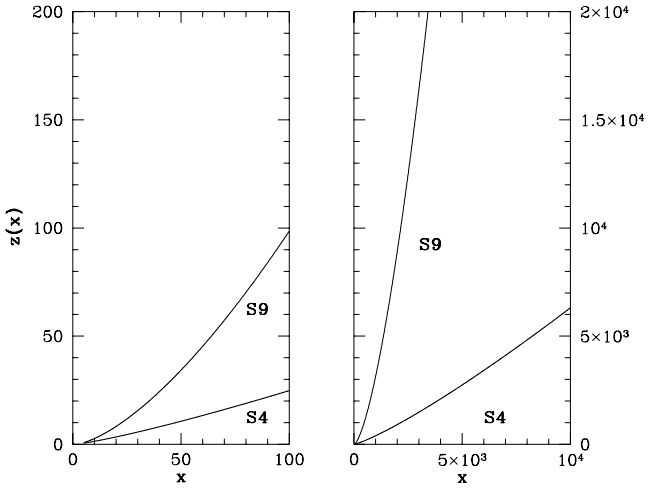

Fig. 2. Projected magnetic flux surface. Shape of the poloidal field line/flux surface as function $z(x)$ for the solutions S4 (and S4b, S3, S1) and S9 (and S3c2)

is $\tilde{\Phi}(x) = (x/x_\star)^{-1/2}$, resulting in magnetic flux function $\Phi(x)$ decreasing with radius faster than a monopole where $\Phi(x) = 1$.

Prescribing both the flux distribution and the shape of the flux surface does not over-determine the problem. The magnetic flux function Φ describes the opening of the magnetic flux tubes. With $z(x)$, the *shape* of the flux surface chosen, the choice of the flux *function* just defines the position of the "other" flux surfaces. In a fully self-consistent approach, the field structure is determined by the solution of the Grad-Shafranov equation. Such solutions are not yet available.

3.4.3. The plasma temperature

The temperature distribution along the field line follows a polytropic gas law, $T = T_\star \left(n/n_\star\right)^{\Gamma-1}$. In our approach the temperature at the injection radius $x_\star$ is determined by choosing the sound speed at this point, $c_{\mathrm{s}\star}$,

$$T_\star = \frac{\Gamma - 1}{\Gamma} \left(\frac{c_{\mathrm{s}\star}^2}{\Gamma - 1 - c_{\mathrm{s}\star}^2} \right) \frac{m_\mathrm{p} c^2}{k_\mathrm{B}}. \tag{9}$$

For typical parameters applied in our calculations, $c_{\mathrm{s}\star} = 0.05$, $\Gamma = 5/3$ this gives a gas temperature of the disk corona of about $1.5\ 10^{10}$ K at a jet injection radius $x_\star = 8.3$. This temperature is in rough agreement with the disk temperature of the advection dominated accretion disk models at small radii (Narayan et al. 1998). A smaller $x_\star$ requires a higher sound speed parameter implying a higher temperature $T_\star$.

3.4.4. The iso-rotation parameter Ω_F

The iso-rotation parameter $\Omega_\mathrm{F}(\Psi)$ of the field line is determined from the position of the injection radius $x_\star$. This choice corresponds to the interpretation often applied for Ω_F as the "angular rotation of the field lines". Here, we assume that the field lines are anchored in a Keplerian disk, $\Omega_\mathrm{F} \simeq \Omega_\mathrm{Disk} \simeq \Omega_\mathrm{K}(x_\star)$. The angular velocity of the last stable circular orbit around a Kerr black hole is $\Omega_\mathrm{F}(x_\star) \sim \pm(x_\star^{3/2} \pm a)^{-1}$ (the $\pm$ stands for co-rotation or retrograde rotation, respectively). For a radial position not too close to the black hole, the angular velocity in the accretion disk follows its Newtonian value. Close to a black hole Ω_F is limited due to the "rotation of space" ω. An injection radius $x_\star = 8.3$ gives $\Omega_\mathrm{F} = 0.04$ which is about $0.1\,\Omega_\mathrm{H}$ for $a = 0.8$.

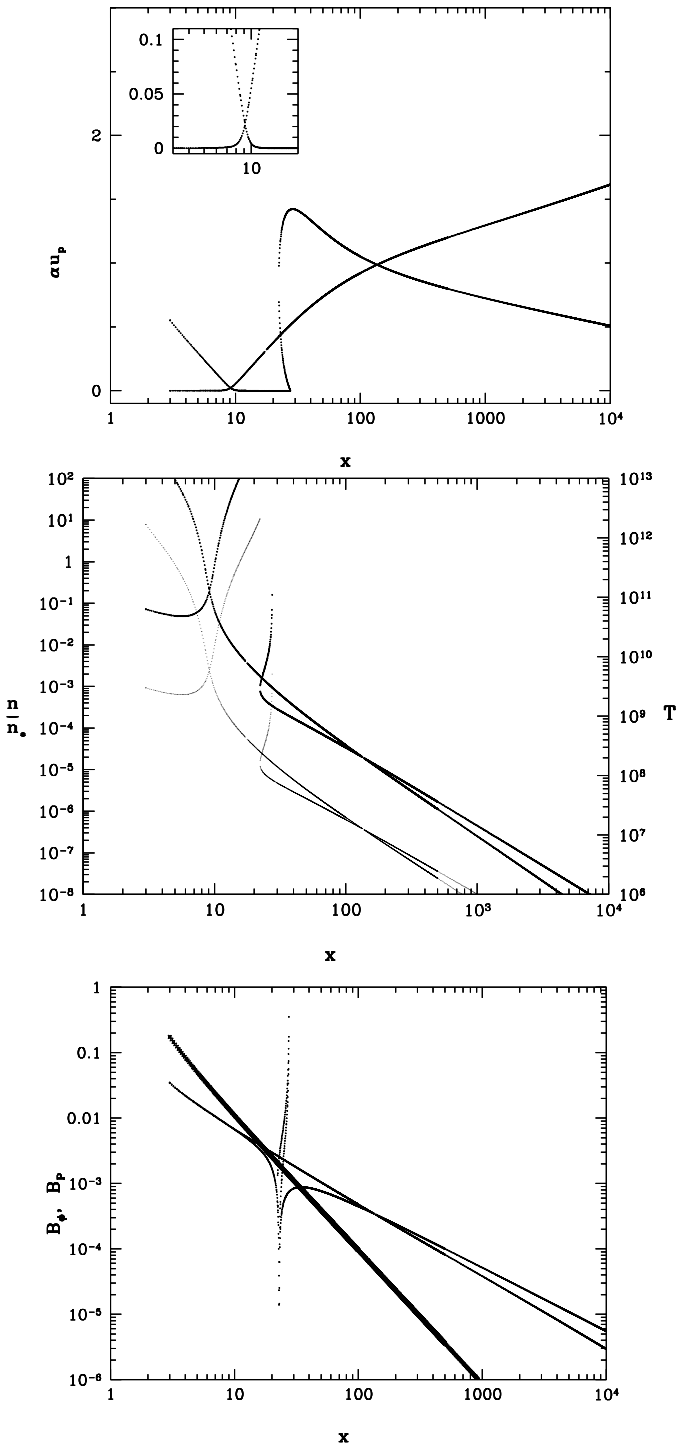

Fig. 3. Solution S3. Properties of the critical wind solution along a given flux surface (see parameters in Table 1). The small window shows the solution branches around the slow magnetosonic point enlarged. The wind branch is the one with increasing velocity. The critical (magnetosonic) points are located at the intersections of the two solution branches (see Appendix C for details). *Top*: poloidal velocity $\alpha u_{\rm p}$ (in c). The asymptotic jet velocity of $u_{\rm p} = 2.5$ is reached after about $x = 10^8$. *Middle*: normalized proper particle density n (*thick line*) and temperature T in K (*thin line*). *Below*: normalized poloidal (*thick line*) and toroidal (*thin lines*) field strength, $B_{\rm p}, B_\phi$. Note that the injection radius is $x_\star = 8.3$

4. Results and discussion

We now discuss our numerical solutions of the general relativistic magnetic wind equation for different field geometries and input parameters. With the prescribed poloidal field our solution is uniquely defined by the conditions along the jet foot point and the condition of regularity across the magnetosonic points. Due to the stationarity assumption and the prescription of the field distribution, the spatial range of the computation is in principle not limited in radius. This is essential if one considers the huge size of Galactic superluminal jets in terms of the size of the central object.

In general, we show that the acceleration of plasma from regions close to a black hole to the speed of $0.92\,c$ observed for Galactic superluminal motion is possible to achieve. Depending on the poloidal magnetic field distribution, the asymptotic speed of the jet is reached at a radius of about 100 gravitational radii.

For comparison the leading parameters for our astrophysical solutions are summarized in Table 1. For illustration, we show the example solution S1 demonstrating the typical features of the wind solution branches in the case of super- or sub-critical parameters (Fig. C.1, Appendix C). The meaning of our figures is explained in detail in Appendix C.

4.1. The wind solution – a collimating relativistic jet

The time scale for the superluminal GRS 1915+105 jet is at least one month until the blobs become invisible in radio light. Mirabel & Rodriguez (1994) estimated that the ejection event for a blob lasts about 3 days. This time period would correspond to a value of $\Omega_{\rm F} = 0.016$ (for $M = 5\ M_\odot$) and an injection radius of about $x_\star \simeq 15$. The orbital period of the foot points rotating at the marginally stable orbit (for $a = 0.8$) is an order of magnitude less. The time scale derived for the intervals between the emission of jet knots is much larger as the period of the marginally stable orbit. The true location of the jet origin not yet known. Therefore, we suggest that the jet foot point should be located outside the marginally stable orbit in order to maintain a jet flow for some time. For the first set of solutions we chose a foot point radius of $x_\star = 8.3$ or $x_\star = 15.3$.

The fact that the kinematic time scale of the blobs is at least 10 times larger than the time scale for the generation of the blobs supports the assumption of stationarity in our calculations. Clearly, on the long-term time evolution the presence of the blobs them self tells us that the jet flow is time-dependent.

Compared to the other solutions in this sample with $x_\star = 8.3$, solution S3 is weakly magnetized (Fig. 3). The initial opening angle of the magnetic flux surface is large (Fig. 2). The magnetic flux function $\tilde{\Phi}(x)$ is constant along the field line. The asymptotic poloidal velocity of $u_{\rm p} = 2.5$ is reached beyond a radius $x \simeq 10^8$ (corresponding to a distance from the black hole of $z(x) \simeq 4\ 10^8$).

Figure 3 also shows the distribution of other dynamical variables. The poloidal field strength $B_{\rm p}$ decreases with the opening of the magnetic flux surfaces. While the poloidal field distribution is prescribed in our approach, the toroidal magnetic field profile is a result of computation and therefore determined by the critical wind solution. At the injection point the toroidal field strength is about two times smaller than the poloidal component. Outside the Alfvén radius the toroidal field becomes much larger than the poloidal component. For large radii the magnetic field helix is dominated by the toroidal component. In this region we find the toroidal field component following a power law distribution $\mathrm{d}(\log B_\phi) \simeq \mathrm{d}(\log x)$. Therefore, in the asymptotic part the poloidal electric current is almost constant $I \sim xB_\phi \sim$ const. In relativistic MHD electric –fields cannot be neglected. The electric field orientation is perpendicular to the magnetic flux surfaces and the field strength is $|\boldsymbol{E}_\perp| = (R/R_{\rm L})B_{\rm P}$. Therefore, the electric field is dominating the poloidal magnetic field outside the light cylinder.

Density and temperature are interrelated by the polytropic gas law. At the injection point the gas temperature $T \simeq 10^{10}$ K (Fig. 3). The proper particle density at the injection point $n_\star$ depends from the choice of the mass flux (in units of the magnetic flux). Therefore, the calculated density profile $n(x)$ may be applied to different mass flow rates (as long as the magnetization $\sigma_\star$ is the same). Density and temperature decrease rapidly along the field line following the polytropic expansion. For $x \gtrsim 30$ the proper particle density follows a power law $n/n_\star = 4\ 10^{-5} x^{-1.8}$. At $x \simeq 1000$ the gas temperature is about 10^6 K. Therefore we can estimate the size of a X-ray emitting region of about several $1000\, r_{\rm g}$ in diameter. For the example of GRS 1915+105 this corresponds to $3.5\ 10^{-9}$ arcsec. It would be interesting to calculate the X-ray spectra of such an relativistically expanding high temperature gas distribution.

Solution S3c2 has the same distribution of the magnetic flux function Φ as solution S3. The magnetic flux surfaces, however, are collimating more rapidly. The derived critical wind solution has a higher magnetization, although the terminal speed and the total energy density $E(\Psi)$ of the S3c2 solution is similar to S3. Because of the higher magnetization type S3c2 jet solutions have a correspondingly lower mass flow rate. The asymptotic speed is reached already at about $x = 1000$ equivalent to a distance from the central black hole of about $z = 3200$.

Solution S9 relies on the same magnetic flux surface as S3c2. As a difference to S3c2, the magnetic flux function decreases with radius implying a (spatially) faster magnetic field decay. As a consequence, the jet reaches its asymptotic velocity of $u_{\rm p} = 2.57$ even at about $x = 100$. The derived flow magnetization is higher compared to S3c2 and S3 balancing the fast decay of the magnetic field distribution and we obtain the same asymptotic speed. This is interesting because it proves that not only the magnetization, but also the distribution of the magnetic flux along the field line determines the asymptotic speed.

Note that solution S9 reaches the same asymptotic speed as S3c2 only because of its higher magnetization. Indeed, a solution similar to S9, but having the same magnetization $\sigma_\star = 1356$ as for S3c2, only reaches an asymptotic speed of $u_{\rm p} = 1.81$ (not shown). Also, such a solution would be only very weakly magnetized in the asymptotic regime as the normalized flow magnetization changes as $\sigma \sim 1/\sqrt{x}$ for the $\Phi \sim 1$ solutions or $\sigma \sim 1/x$ for the $\Phi \sim 1\sqrt{x}$ solutions[2], respectively. Similarly, in comparison, the asymptotical toroidal magnetic field is weaker by some orders of magnitude (a factor ten at $x = 1000$). In all the solutions presented in this paper the *asymptotic* jet is dominated by the kinetic energy. For the solutions with the large injection radius $x_\star = 8.3$, the magnetic energy is being converted into kinetic energy almost completely already at a radius of about several 100 gravitational radii.

Solution S4 has the same magnetic flux distribution as S9, however, the field line is only weakly collimating. The asymptotic jet speed and the magnetization parameter is about the same. Only, the initial acceleration is weaker because the magneto-centrifugal mechanism works less efficient in the field with a smaller opening angle.

Solution S4b has essentially the same field distribution as S4, but the injection radius is chosen larger. Therefore, the iso-rotation parameter $\Omega_{\rm F}$ is decreased by a factor of $(8.3/15.3)^{3/2}$. As a result, a critical wind solution with a comparable asymptotic speed could be obtained only for a very high plasma magnetization. This proves that highly relativistic jets can be expected even if the jet is not emerging from a region close to the black hole. Such a solution is feasible if the mass flow rate in the jet decreases with radius faster than the field strength (or flux distribution). The question remains whether such field strengths can be found at this position.

We summarize the results of this section. The asymptotic speed is determined by the plasma magnetization and the distribution of the magnetic flux along the field line. The shape of the magnetic flux surface determines the velocity *profile* along the field, thus, the position where the asymptotic velocity is reached. Highly relativistic outflows can be obtained even if the jet foot point is *not* very close to the black hole. However, in this case a high plasma magnetization is necessary. But this seems to be in contradiction to the accretion disk theory (see below).

4.2. The role of the magnetization

The magnetic acceleration of jets and winds can be understood either as a consequence of converting Poynting flux (magnetic energy) to kinetic energy or due to Lorentz forces along the poloidal field line. In general, the higher

[2] However, in the hot wind equation it is not possible to change only one single parameter in order to obtain a new set of critical wind solutions. In the case discussed above, with the decreased magnetization (i.e. an increased mass flow rate), the Alfvén radius is correspondingly smaller (here, $x_{\rm A} = 21.11$ compared to $x_{\rm A} = 22.93$ for S9).

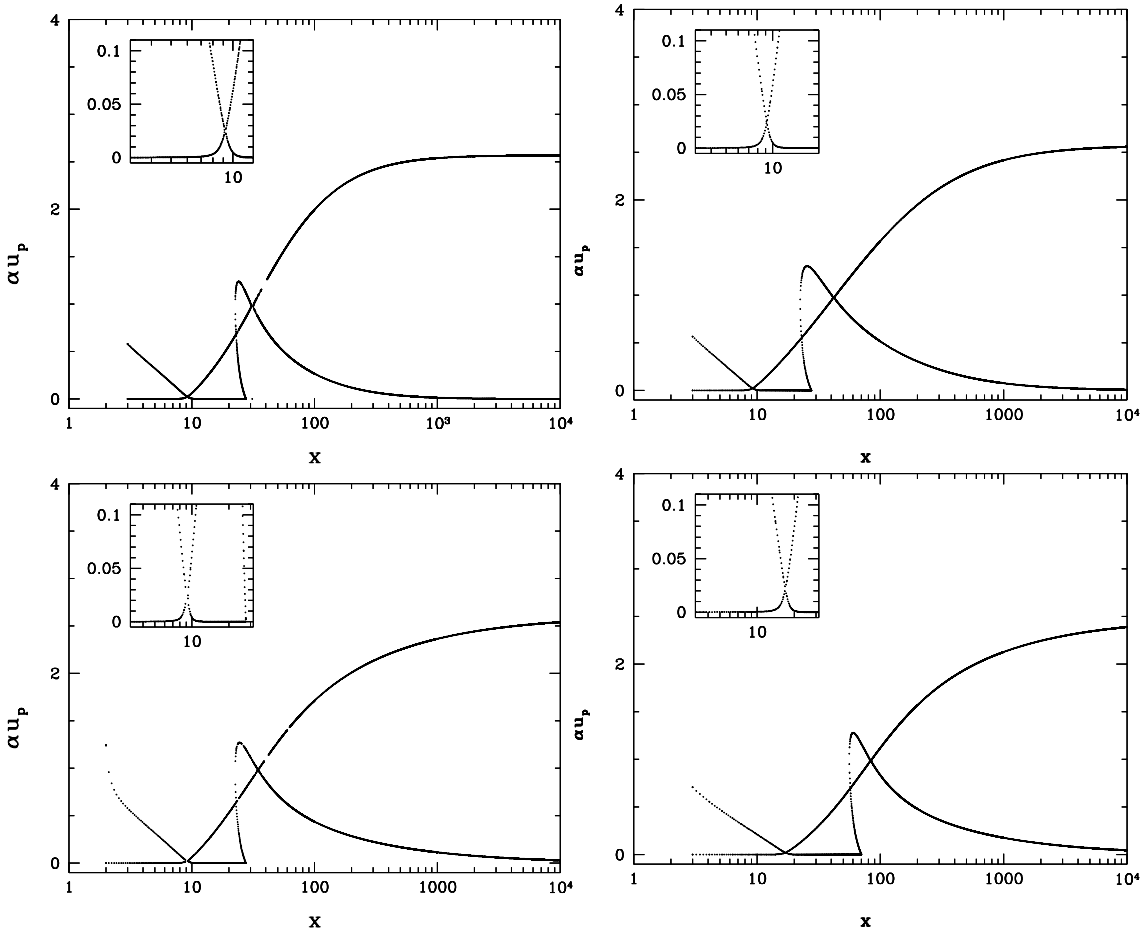

Fig. 4. Wind solutions S9 (*upper left*), S3c2 (*lower left*), S4 (*upper right*), S4b (*lower right*). Branches of poloidal velocity $\alpha u_{\rm p}$ along the field line in units of the speed of light. For the solution parameters see Table 1. See caption of Fig. 3 for further explanation

the plasma magnetization the more energy can be transformed into kinetic energy of the wind. It has been shown theoretically for a cold wind that the relation between magnetization and asymptotic velocity is that of a power law, $u_{\rm P\infty} \sim {\sigma_{\rm M}}^{1/3}$, for conical outflows (Michel 1969) and for collimating flows (Fendt & Camenzind 1996), if the flux distribution is the same, respectively. However, both papers do not consider gravity (and no general relativistic effects). The new solutions presented in this paper are in general agreement with those results in the sense that a higher magnetization leads to a higher velocity. However, we are dealing with the *hot* wind equation and cannot derive a power law distribution from Table 1, since the other wind parameters may vary between the different solutions. In difference to the cold wind solutions the magnetization is not a free parameter. Instead, it is fixed by the regularity condition at the magnetosonic points.

The wind magnetization is determined by the disk properties at the jet injection points along the disk surface. For a standard thin disk model that the ratio of the mass flow rate in the jet to the disk accretion rate is about 1% (Ferreira 1997). The observational data for various jet-disk systems are consistent with this theoretical value. The accretion disk magnetic flux can be estimated assuming equipartition between magnetic field pressure (energy) and gas pressure (thermal energy) in the disk (see Sect. 3.4.1). From Eq. (7) we find an equipartition field strength of about $B_{\rm eq} \simeq 5\ 10^8$ G, if $\alpha_{\rm vis} \simeq 0.1$ and $R_\star = 10 r_{\rm g}$. Equation (8) then defines an upper limit for the plasma magnetization at the injection radius, $\sigma_\star = 5\ 10^4$, for $\dot{M}_{\rm jet} \simeq 0.1\ \dot{M}_{\rm acc}$. Such a value is in general agreement with our solutions (Table 1). The maximum equipartition field strength estimated with the above given formulae can be much larger for Galactic black hole jet sources as for AGN (see Eq. (7)). For a low black hole mass (with a smaller horizon) the disk comes closer to the singularity and therefore becomes hotter.

Again, we note that our estimate for the magnetization comes from comparison of different disk models (Sect. 3.4.1). However, this does not mean that we *apply* a certain disk model for our computations.

Finally, we come back to the wind solutions S4 and S4b. As already mentioned, these solutions demonstrate that the jet origin must not be necessarily close to the black hole. One may think that a strong magnetization at larger disk radii would do the job. On the other hand, the equipartition field strength in the disk decreases with radius implying that the highest magnetization and, thus,

jet velocities must be expected from the inner part of the disk. Only, if the mass transfer rate from the disk into the jet decreases more rapidly with radius than the field strength, the *magnetization* increases.

4.3. The influence of the rotating black hole

As the main issue of our paper is the search for MHD wind solutions in Kerr metric, it is necessary to clarify the role of general relativity for the jet acceleration itself. Clearly, at an injection radius of $R_\star = 8.3$ general relativistic effects are not very dominant.

For comparison we have calculated wind solutions for a smaller injection radius $x_\star = 3.3$ (solution S3q, S3u, Figs. D.1, D.2). The main effect is a much higher asymptotic velocity resulting from the rapid rotation, Ω_F, at the smaller radius $x_\star$. With our choice $\Omega_\mathrm{F} = 0.14$ the asymptotic velocity drastically increases from $u_\mathrm{p} = 2.503$ (S3) to $u_\mathrm{p} = 8.4792$ (S3q). In order to obtain the critical solution for the higher rotation rate, the wind parameters have to be changed accordingly. $\sigma_\star$ is decreased by a factor of two, while $c_{\mathrm{s}\star}$ and $u_{\mathrm{p}\star}$ must be increased substantially. The large sound speed is in agreement with the smaller injection radius, since a higher disk temperature and pressure is expected close to the hole. The Alfvén radius is decreased by a factor of four, however, its location relative to the outer light cylinder remains the same.

The limiting case of Minkowski metric can be achieved by setting $M = 0$ and $a = 0$ in the Boyer-Lindquist parameters (see Appendix A). For such a wind solution (S3u2) the magnetization is lower, although the asymptotic wind speed is the same as in the Schwarzschild case (see Fig. D.2). This becomes clear if we take into account that for S3u2 the wind flow does not have to overcome the gravitational potential. Thus, less magnetic energy is needed to obtain the same asymptotic speed by magnetic acceleration. Further, we find from solutions for different angular momentum parameters a that in general the wind flow originating from a black hole with a smaller a is faster. As an extreme example we show the solution S3u3 calculated with $a \simeq 0$ but otherwise the same parameter set (see Fig. D.2). This solution is magnetized stronger compared to the case of $a = 0.8$, thus, resulting in a higher asymptotic wind velocity. We believe that the reason for such a behavior is the fact that the effective potential of a black hole weakens (at this location) for increasing values of a. Therefore, less magnetic energy is necessary to overcome the effective potential.

In the end, the results of this section are not surprising. They demonstrate that the wind/jet is basically *magnetically driven*. As a consequence, the acceleration takes place predominantly across the Alfvén point as expected from MHD theory. Therefore, the scenario is similar to the case of classical pulsar theory in Minkowski metric. For relativistic jets with a high magnetization the Alfvén point is always very close to the light surface, which is defined by the angular velocity of the field line foot point. Usually, the Alfvén point is located at a radius large compared to the gravitational radius. Thus, the influence of the general relativistic metric is marginal. Only, if the Alfvén radius comes close to the hole, the choice of the metric will determine the jet acceleration.

4.4. The question of collimation

The huge size observed for the knots of the Galactic superluminal sources leaves the possibility that the jet is basically *un-collimated*.

Our numerical solutions have shown that the asymptotic speed of the jet does not depend very much on the degree of collimation in the flow. That speed is reached within a distance of about $10^8 r_\mathrm{g}$. However, the observed upper limit for the knot size is still a factor 10 larger. Therefore, from our solutions, the observed knots are consistent with both a collimated and an un-collimated jet flow. In particular, solution S9 which is more collimated, has the same asymptotic speed as solution S4.

In the case of extragalactic jets a high degree of collimation is indicated. The "lighthouse model" by Camenzind & Krockenberger (1992) gives opening angles of only $0\overset{\circ}{.}1$ for the quasar 2C 273 or $0\overset{\circ}{.}05$ for typical BL Lac objects. The question arises whether there could be an intrinsic difference between the jets of AGN and Galactic high energy sources. Why should Galactic superluminal jets be un-collimated? A difference in the jet magnetization seems to be unlikely since the jet velocities are comparable. We hypothesize that if the jets of these sources are systematically different, this should rather be caused by the conditions in the jet environment. If the jets are collimated by external pressure, a different external/internal pressure ratio will affect the degree of jet collimation. Extragalactic jets are believed to be confined by an external medium (see Fabian & Rees 1995; Ferrari et al. 1996). It is likely that Galactic superluminal sources provide an example where the jet pressure exceeds the pressure of the ambient medium. While AGN jets bore a funnel through the galactic bulge, Galactic superluminal jets freely expand into the empty space. Such a picture seems to be supported by the fact that the Galactic superluminal jet knots move with constant velocity over a long distance.

5. Summary

We have investigated magnetically driven superluminal jets originating from a region close to a rotating black hole. The stationary, general relativistic, magnetohydrodynamic wind equation along collimating magnetic flux surfaces was solved numerically. The wind solutions were normalized to parameters typical for Galactic superluminal sources.

The assumption of stationarity allows us to calculate the jet velocity on a *global* scale over a huge radial range in terms of radius of the central source. The wind is launched close to the rotating black hole at several gravitational

radii. The calculation was performed up to a radius of 10^4 gravitational radii, but is in general not limited in radius. In some cases the asymptotic speed may be reached only at a distance of several 10^8 gravitational radii. Different magnetic field geometries were investigated. The model allows for a choice of the *shape* of the magnetic flux surface *and* the *flux distribution* of that field.

The physical wind solution is defined by the regularity condition at the magnetosonic points. As the poloidal field is prescribed, the choice of the following input parameters determines the wind solution completely, (i) the injection radius of the matter into the jet, (ii) the injection velocity and (iii) the plasma magnetization (the ratio of magnetic flux to mass flux). The results of our numerical computation are the following.

- In general, the observed speed for Galactic superluminal sources of more than $0.9\,c$ can be achieved;
- The flow acceleration is magnetohydrodynamic and takes place predominantly around the Alfvén point. General relativistic effects are important only if the wind originates very close to the black hole. In order to overcome the gravitational potential, the critical wind solution must be higher magnetized in order to reach a similar asymptotic speed. This has been proven by calculating the Schwarzschild and Minkowski limit of the wind equation;
- For a fixed magnetic field distribution the asymptotic jet velocity depends mainly on the plasma magnetization, in agreement with earlier papers (Michel 1969; Fendt & Camenzind 1996). The higher the plasma magnetization, the higher the final speed. The velocity distribution along the magnetic field shows a saturating profile depending on the distribution of the magnetic flux;
- The magnetic flux distribution along the field line also influences the plasma acceleration. Since the real field distribution is not known, we have considered two cases which show the typical behavior and which are probably close to the reality. We find that the jet velocity in a (spatially) faster decaying field can be the same as long as the magnetization at the injection point is high enough in order to balance the effect of the decrease in field strength;
- For jet solutions *not* emerging from a region close to the black hole, a highly relativistic velocity can be obtained if the flow magnetization is sufficiently large. However, one we hypothesize that the field strength required for such a magnetization can be generated only close to the black hole;
- Investigation of flux surfaces with a different degree of collimation has shown that both field distributions allow for a relativistic velocity. The asymptotic jet velocity is reached considerably earlier in the case of the faster collimating flux surface. The jet reaches its asymptotic speed at a distance from the injection point of $3000 r_{\rm g}$ or $10^5 r_{\rm g}$, depending on the degree of collimation. The latter we measure with the opening angle of the collimating flux surface at this point and is about 15° or 45°, respectively. This distance is below the observational resolution by several orders of magnitude. Therefore, the question of the degree of collimation for the superluminal jets of GRS 1915+105 and GRO 1655−40 could not be answered;
- Motivated by the huge size of the observed knots in the Galactic superluminal jets, we point out the possibility that the jet collimation process in these sources may be intrinsically different in comparison to the AGN. For example, the upper limit for the knot diameter in GRS 1915+105 is about 10^9 Schwarzschild radii, which is distinct from typical estimates for AGN jets with diameters of about 100–1000 Schwarzschild radii;
- The gas temperature at the injection point is about 10^{10} K which is one order larger than the disk temperature at this point. With the polytropic expansion the temperature decreases rapidly to about 10^6 K at a distance of 5000 Schwarzschild radii from the source. Both the temperature and the mass density follow a power law distribution with the radius;
- The calculations show that the jet magnetic field is dominated by the toroidal component. Similarly, the velocity field is dominated by the poloidal component.

In summary, our numerical calculations have shown that the highly relativistic speed observed for galactic superluminal sources can be achieved by magnetic acceleration. For a given magnetic flux surface we obtain the complete set of physical parameters for the jet flow. The calculated temperature, density and velocity profile along the jet would provide a interesting set of input parameters for computing the spectral energy distribution.

Acknowledgements. C. F. thanks Mikael Jensen at Lund Observatory for discussions and the analytical proof of the equations in Appendix B. We acknowledge fruitful comments by the referee Dr. Koide helping to improve the presentation of this paper, especially Sect. 4.3.

Appendix A: Parameters of Kerr metric

For the reason of completeness, here we list the parameters applied in the equations of Kerr geometry. In Boyer-Lindquist coordinates with the parameters

$$\begin{aligned} \rho^2 &\equiv r^2 + a^2\,\cos^2\theta, & \Delta &\equiv r^2 + a^2 - 2M\,r, \\ \Sigma^2 &\equiv (r^2+a^2)^2 - a^2\Delta\sin^2\theta, & \tilde{\omega} &\equiv (\Sigma/\rho)\,\sin\theta, \\ \omega &\equiv 2\,a\,M\,r/c\,\Sigma^2, & \alpha &\equiv \rho\sqrt{\Delta}/\Sigma, \end{aligned}$$

the components of the metric tensor are defined as

$$\begin{aligned} g_{00} &= \sigma_{\rm m}(2r/\rho(r,\theta)^2 - 1) \\ g_{03} &= -\sigma_{\rm m} 2ra\sin(\theta)^2/\rho(r,\theta)^2 \\ g_{11} &= \sigma_{\rm m}\rho(r,\theta)^2/\Delta(r,\theta) \\ g_{22} &= \sigma_{\rm m}\rho(r,\theta)^2 \\ g_{33} &= \sigma_{\rm m}\Sigma(r,\theta)^2\sin(\theta)^2/\rho(r,\theta)^2 \\ g &\equiv {\rm Det}({\rm g}_{\mu\nu}) = -g_{11}g_{22}(g_{30}^2 - g_{00}g_{33}). \end{aligned}$$

In our paper we have chosen a negative sign of the metric, $\sigma_{\rm m} = -1$.

Appendix B: Wind polynomial

Here we provide the polynomial coefficients of the general relativistic magnetohydrodynamic wind Eq. (4). For a derivation, see Camenzind (1986), Takahashi et al. (1990), or Jensen (1997). The specific angular momentum, properly normalized, is

$$\tilde{L} = -(g_{03} + \Omega_{\rm F} g_{33})/(g_{00} + \Omega_{\rm F} g_{03}). \quad \text{(B.1)}$$

For convenience we define the following parameters,

$$\begin{aligned} C_1 &= \frac{c_{\rm s\star}^2}{\Gamma - 1 - c_{\rm s\star}^2} \left(u_{\rm p\star} \sqrt{\frac{g_\star}{g}} \frac{\Phi}{\Phi_\star} \right)^{\Gamma - 1}, \quad C_2 = \sqrt{-g} \frac{\Phi_\star}{\Phi \sigma_\star} \\ D_1 &= g_{00} + 2\Omega_{\rm F} g_{03} + \Omega_{\rm F}^2 g_{33}, \quad D_2 = (1 - \Omega_{\rm F} \tilde{L})^2 \\ D_3 &= -(g_{33} + 2\tilde{L} g_{03} + \tilde{L}^2 g_{00})/(g_{03}^2 - g_{00} g_{33}). \end{aligned}$$

With the corresponding values at the injection radius $x_\star$ the total specific energy density of the flow E is defined as

$$E^2 = \frac{-\sigma_{\rm m} \mu_\star^2 (u_{\rm p\star}^2 + 1)(D_{1\star} + \sigma_{\rm m} M_\star^2)^2}{(D_{1\star} + 2\sigma_{\rm m} M_\star^2) D_{2\star} + D_{3\star} M_\star^4}, \quad \text{(B.2)}$$

where $M_\star$ denotes the Alfvén Mach number at the injection radius. The polynomial coefficients of the wind Eq. (4) are

$$\begin{aligned} \tilde{a}_{1,2n+2m} &= C_2^2 \\ \tilde{a}_{2,2n+m} &= 2\sigma_{\rm m} C_2 D_1 \\ \tilde{a}_{3,2n} &= D_1^2 + C_2^2 + \sigma_{\rm m} E^2 C_2^2 D_3 \\ \tilde{a}_{4,2n-m} &= 2\sigma_{\rm m} C_2 D_1 + 2E^2 C_2 D_2 \\ \tilde{a}_{5,2n-2m} &= D_1^2 + \sigma_{\rm m} E^2 D_1 D_2 \\ \tilde{a}_{6,n+3m} &= 4 C_1 C_2^2 \\ \tilde{a}_{7,n+2m} &= 6\sigma_{\rm m} C_1 C_2 D_1 \\ \tilde{a}_{8,n+m} &= 2C_1 D_1^2 + 4C_1 C_2^2 + \sigma_{\rm m} 2E^2 C_1 C_2^2 D_3 \\ \tilde{a}_{9,n} &= \sigma_{\rm m} 6 C_1 C_2 D_1 + 2E^2 C_1 C_2 D_2 \\ \tilde{a}_{10,n-m} &= 2C_1 D_1^2 \\ \tilde{a}_{11,4m} &= 6 C_1^2 C_2^2 \\ \tilde{a}_{12,3m} &= 6\sigma_{\rm m} C_1^2 C_2 D_1 \\ \tilde{a}_{13,2m} &= C_1^2 D_1^2 + 6C_1^2 C_2^2 + \sigma_{\rm m} E^2 C_1^2 C_2^2 D_3 \\ \tilde{a}_{14,m} &= 6\sigma_{\rm m} C_1^2 C_2 D_1 \\ \tilde{a}_{15,0} &= C_1^2 D_1^2 \\ \tilde{a}_{16,5m-n} &= 4 C_1^3 C_2^2 \\ \tilde{a}_{17,4m-n} &= 2\sigma_{\rm m} C_1^3 C_2 D_1 \\ \tilde{a}_{18,3m-n} &= 4 C_1^3 C_2^2 \\ \tilde{a}_{19,2m-n} &= 2\sigma_{\rm m} C_1^3 C_2 D_1 \\ \tilde{a}_{20,6m-2n} &= C_1^4 C_2^2 \\ \tilde{a}_{21,4m-2n} &= C_1^4 C_2^2. \end{aligned}$$

All coefficients with the same second index have to be summed up, $A_i = \sum_j \tilde{a}_{j,i}$. The polytropic indices $n = 5$, $m = 3$ give a polynomial of 16th order.

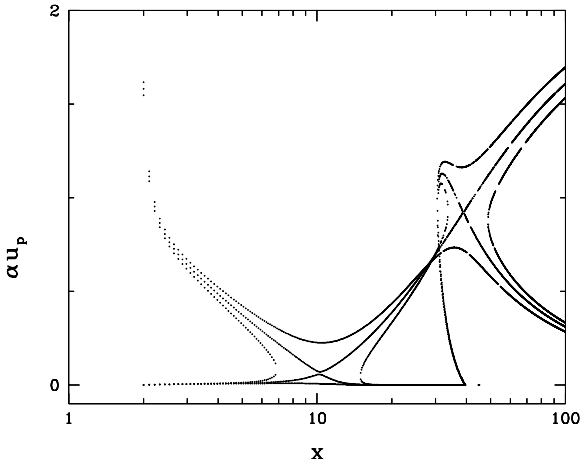

Fig. C.1. Example solution S1. Overlay of solutions $u_{\rm p}(x)$ for three different parameter sets. $\sigma_\star = 49830$, $c_{\rm s\star} = 0.4585$ gives the critical solution which is regular across the magnetosonic points. The critical *wind* solution is the continuous branch starting with low velocity and accelerating to high speed. The magnetization $\sigma_\star$ is the critical parameter for the FM point, whereas $c_{\rm s\star}$ is the critical parameter for the SM point. Sub- or super-critical solutions are obtained by variation of the parameters $\sigma_\star$, $c_{\rm s\star}$. The choice of $\sigma_\star = 51\,830$, $c_{\rm s\star} = 0.4485$ results in gaps in $x(u_{\rm p})$, the choice of $\sigma_\star = 48\,830$, $c_{\rm s\star} = 0.4685$ in gaps in $u_{\rm p}(x)$. The other parameters are $x_{\rm A} = 31.2$, $u_{\rm p\star} = 0.01$, $x_\star = 3.0$, $\Omega_{\rm F} = 0.1$ $\Omega_{\rm H} = 0.025$, $a = 0.8$

Appendix C: Example wind solution in Kerr metric

Here we show an example solution of the wind Eq. (4). The parameters are chosen such that a variation of $\sigma_\star$ and $c_{\rm s\star}$ clearly demonstrates the criticality of the wind solution. They do not necessarily match astrophysical constraints. However, the asymptotic poloidal velocity is comparable to the speed of the Galactic superluminal sources. The solution (solution S1) considers a highly magnetized plasma flow with $\sigma_\star \simeq 5\,10^4$. The flux geometry is that of a slightly collimating cone with an opening angle decreasing with distance from the source.

Figure C.1 shows the solution branches with a positive $u_{\rm p}^2$. An overlay of solutions for three parameter sets is displayed in order to show the typical behavior of wind solution. There is only one unique solution, the critical solution, with one branch continuing from small to large radii without any gaps in $u_{\rm p}$ or x. The magnetosonic points are located at the intersections of the solution branches of the critical solution. The *critical* wind solution is regular at all three magnetosonic points. It is defined by a *unique* set of the parameters E, L and σ (for $\Omega_{\rm F}$ prescribed). In the critical solution the slow magnetosonic point is passed close to the foot point of the jet. The Alfvén point is located at $x = 31$ and the fast magnetosonic point not far beyond. The asymptotic speed of the flow is $u_{\rm p} = 2.28$, equivalent to $v_{\rm p} \simeq = 0.9\,c$ (not shown in the figure).

Sub- or super-critical wind parameters lead to solution branches which are not defined for all radii or all velocities. Even for a slight variation of these parameters the solution will be not continuous anymore, implying "jumps"

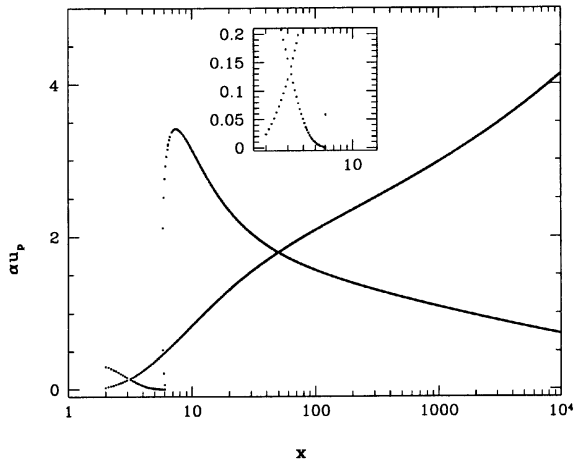

Fig. D.1. Example solutions with a small injection radius $x_\star = 3.3$. Rotation rate $\Omega_\mathrm{F} = 0.14$. Solution S3q with $a = 0.8$, $x_\mathrm{A} = 5.83$, $\sigma_\star = 480$ has a high asymptotic velocity $u_\mathrm{p} = 8.48$

or "shocks" across the gaps in the solution branches. At these locations the stationary character of the solution most probably breaks down. Such solution branches are inconsistent with the assumptions and are therefore referred to as *unphysical*.

Appendix D: The wind solution for a small injection radius

For comparison, we show solutions of the wind equation with a small injection radius $x_\star = 3.3$ as well as solutions in the limit of Minkowski and Schwarzschild metric (for a discussion see Sect. 4.3). Solution S3q corresponds to solution S3, however, with a magnetization smaller by a factor of two. The asymptotic speed is $u_\mathrm{p} = 8.48$ and much larger than for S3. Also solutions S3u, S3u2, S3u3 correspond to S3 and S3q. However, in this case the Alfvén radius and the derived magnetization parameter are lower resulting in a lower asymptotic speed. Solution S3u is the Kerr solution for $a = 0.8$, S3u3 the Schwarzschild solution ($a = 10^{-8}$), and S3u2 the Minkowski solution where we set $a = 10^{-8}$ and $M = 0$ in the Boyer-Lindquist parameters (see Appendix A). For a comparison of all solutions see Table 1.

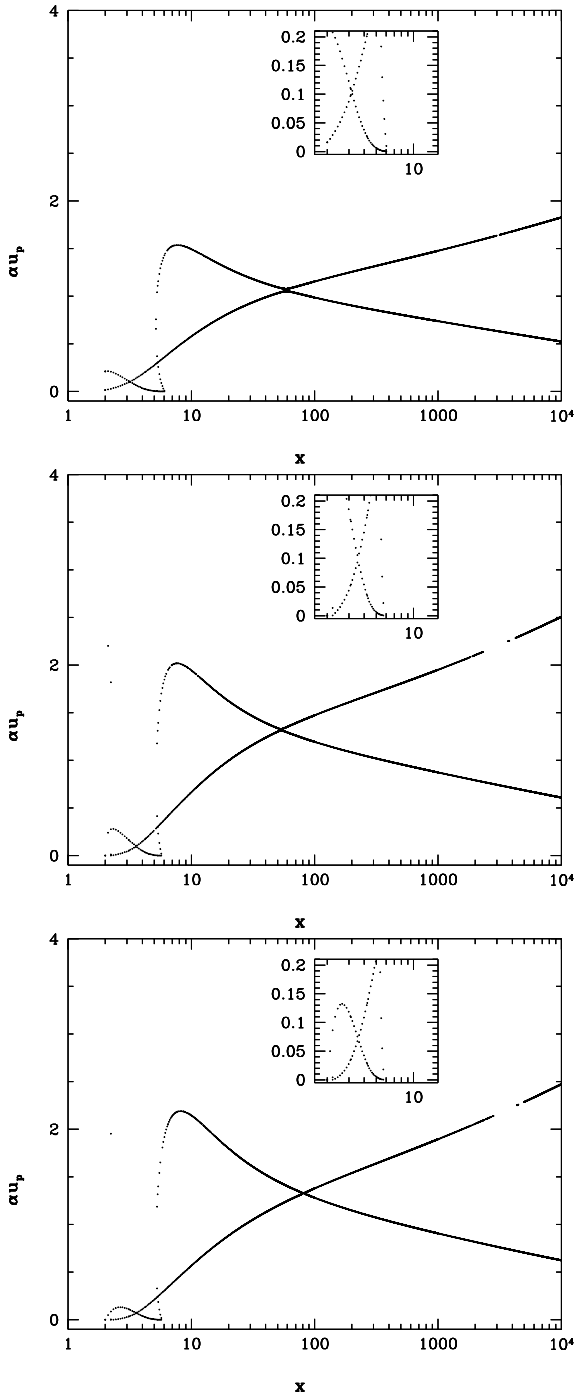

Fig. D.2. Example solutions with a small injection radius $x_\star = 3.3$. Rotation rate $\Omega_\mathrm{F} = 0.14$. *Top*: solution S3u with $a = 0.8$, $x_\mathrm{A} = 5.33$, and a smaller $\sigma_\star = 100$ and a lower asymptotic velocity $u_\mathrm{p} = 2.96$. *Middle*: solution S3u3 in Schwarzschild metric, $a = 10^{-8}$, $x_\mathrm{A} = 5.33$. The asymptotic speed is $u_\mathrm{p} = 4.48$ with $\sigma_\star = 205.7$. *Bottom*: solution S3u2 in Minkowski metric, $a = 10^{-8}$, $M = 0$. The asymptotic speed is $u_\mathrm{p} = 4.55$ while $\sigma_\star = 82.5$

References

Belloni, T., Mendez, M., King, A. R., van der Klis, M., & van Paradijs, J. 1997, ApJ, 479, L145
Beskin, V. S., & Pariev, V. I. 1993, Physics Uspekhi, 36, 529
Beskin, V. S. 1997, Physics Uspekhi, 40, 659
Blandford, R. D., & Znajek, R. L. 1977, MNRAS, 179, 433
Blandford, R. D., & Payne, D. G. 1982, MNRAS, 199, 883
Blandford, R. D. 1990, in Lecture Notes, Saas-Fee Advanced Course 20, ed. R. D. Blandford, H. Netzer, & L. Woltjer, Active Galactic Nuclei, ed. T. J.-L. Courvoisier, & M. Mayor (Springer, Heidelberg), 242
Brandenburg, A. 1996, ApJ, 465, L115
Camenzind, M. 1986, A&A, 162, 32
Camenzind, M. 1987, A&A, 184, 341
Camenzind, M., & Krockenberger, M. 1992, A&A, 225, 59
Eikenberry, S. S., Matthews, K., Morgan, E. H., Remillard, R. A., & Nelson, R. W. 1998, ApJ, L61
Englmaier, P. 1993, Diploma Thesis, University of Heidelberg

Fabian, A. C., & Rees, M. J. 1996, MNRAS, 277, L55
Fender, R., Garrington, S. T., McKay, D. J., et al. 1999, MN, 304, 865
Fender, R. 2000 Astrophysics and Cosmology: A collection of critical thoughts, Lecture Notes in Physics (Springer), in press [astro-ph/9907050]
Fendt, C., & Camenzind, M. 1996, A&A, 313, 591
Fendt, C. 1997, A&A, 319, 1025
Fendt, C., Elstner, D. 2000, A&A, 363, 208
Ferrari, A., Massaglia, S., Bodo, G., & Rossi, P. 1996, Phenomenology and modelling of large-scale jets, in ed. Tsinganos, Solar and astrophysical magnetohydrodynamic flows (Kluwer, Dordrecht), 607
Ferreira, J. 1997, A&A, 319, 340
Gliozzi, M., Bodo, G., Ghisellini, G., Scaltriti, F., & Trussoni, E. 1998, A&A, 337, L39
Greiner, J., Morgan, E. H., & Remillard, R. A. 1996, ApJ, 473, L107
Greiner, J., Morgan, E. H., & Remillard, R. A. 1998, New Astr. Rev., 42, 597
Greiner, J. 2000, in Cosmic Explosions, Proc. 10th Ann. Maryland Astrophys. Conf., ed. S. Holt, & W. W. Zhang, AIP, in press [astro-ph/9912326]
Hjellming, R. M., & Rupen, M. P. 1995, Nature, 375, 464
Hardee, P. E., Rosen, A., Hughes, P. A., & Duncan, G. C. 1998, ApJ, 500, 599
Jensen, M. 1997, General relativistic MHD winds from supermassive black holes, Master Thesis, Lund Observatory
Khanna, R., & Camenzind, M. 1996a, 307, 665
Khanna, R., & Camenzind, M. 1996b, 313, 1028
King, A. R., & Kolb, U. 1999, MNRAS, 305, 654
Koide, S., Shibata, K., & Kudoh, T. 1998, ApJ, 495, L63
Koide, S., Shibata, K., & Kudoh, T. 1999, ApJ, 522, 727
Koide, S., Meier, D. L., Shibata, K., & Kudoh, T. 2000, ApJ, 536, 668
Kudoh, T., & Shibata, K. 1995, ApJ, 452, L41
Kudoh, T., & Shibata, K. 1997, ApJ, 474, 362
Kuulkers, E., Wijnands, R., Belloni, T., et al. 1998, ApJ, 494, 753
Michel, F. C. 1969, ApJ, 158, 727
Mirabel, I. F., & Rodriguez, L. F. 1994, Nature, 371, L46
Mirabel, I. F., & Rodriguez, L. F. 1995, Superluminal motion in our Galaxy, in Proceedings of the 17th Texas Symposium on Relativistic Astrophysics, in press
Mirabel, I. F., Dhawan, V., Chaty, S., et al. 1998, A&A, 330, L9
Mioduszewski, A. J., Hughes, P. H., & Duncan, G. C. 1997, ApJ, 476, 649
Morgan, E. H., Remillard, R. A., & Greiner, J. 1997, ApJ, 482, 993
Narayan, R., Mahadevan, R., & Quataert, E. 1998, Advection-dominated accretion around black holes, in Theory of Black Hole Accretion Disks, ed. M. A. Abramowicz, G. Bjornsson, & J. E. Pringle (Cambridge University Press), 148
Nishikawa, K.-I., Koide, S., Dakai, J.-I., et al. 1997, ApJ, 483, L45
Okamoto, I. 1992, MNRAS, 254, 192
Orosz, J. A., & Bailyn, C. D. 1997, ApJ, 477, 876
Ouyed, R., Pudritz, R. E. 1997, ApJ, 482, 712
Rodriguez, L. F., & Mirabel, I. F. 1999, ApJ, 511, 398
Scaltriti, F., Bodo, G., Ghisellini, G., Gliozzi, M., & Trussoni, E. 1997, A&A, 325, L29
Thorne, K. S., Price, R. H., & Macdonald, D. 1986, Black Holes: The membrane paradigm (Yale University Press, New Haven and London) (TPM)
Tingay, S. J., Jauncey, D. L., & Preston, R. A. 1995, Nature, 374, 141
Takahashi, M., Nitta, S., Tatematsu, Y., & Tomimatsu, A. 1990, ApJ, 363, 206
Ueda, Y., Inoue, H., Tanaka, Y., et al. 1998, ApJ, 492, 782
Zensus, J. A., Cohen, M. H., & Unwin, S. C. 1995, ApJ, 443, 35
Zhang, N. S., Cui, W., & Chen, W. 1997, ApJ, 482, L155
Znajek, R. L. 1977, MNRAS, 179, 457

Astron. Astrophys. 349, L61–L64 (1999)

ASTRONOMY AND ASTROPHYSICS

LETTER

Letter to the Editor

Long-term evolution of a dipolar-type magnetosphere interacting with an accretion disk

Christian Fendt and Detlef Elstner

Astrophysikalisches Institut Potsdam, An der Sternwarte 16, D-14482 Potsdam, Germany (cfendt,delstner@aip.de

Received 5 July 1999 / Accepted 24 August 1999

Abstract. The evolution of a stellar dipolar-type magnetosphere interacting with a Keplerian disk is investigated numerically using the ideal MHD ZEUS-3D code in the axisymmetry option. We compute the innermost region around the stellar object using a non-smoothed gravitational potential. The disk is taken as a boundary condition prescribing the mass inflow into the corona. Depending mainly on the magnetic field strength, our simulations last several hundred Keplerian periods of the inner disk. The main result is that the dipolar structure of the magnetic field almost completely disappears. An expanding bubble of hot gas of low density forms disrupting the initial dipolar field structure. A disk wind accelerates within the time limit of the simulation to velocities of about 0.5 the Keplerian speed and potentially may develop into a stationary collimated jet. We argue that non-stationary jet phenomena should probably caused by a time-dependent disk. Simulations with a rotating and a non-rotating star show significant differences. In the case of a rotating star during the very first time steps a high speed outflow along the axis is initiated which does not exist in the case of a non-rotating star.

Key words: Magnetohydrodynamics (MHD) – accretion, accretion disks – ISM: jets and outflows – stars: magnetic fields – stars: mass-loss – stars: pre-main sequence

1. Introduction

A stellar dipolar-type magnetic field surrounded by an accretion disk is a common model scenario for various astrophysical objects. Examples are the classical T Tauri stars, magnetic white dwarfs (cataclysmic variables) and neutron stars (high mass X-ray binaries). Some of these sources show Doppler shifted emission lines and highly collimated jets are observed in young stellar objects. Magnetic fields are thought to play the leading role for the jet acceleration and collimation (Blandford & Payne 1982; Pudritz & Norman 1983; Camenzind 1990; Shu et al. 1994a,b; Fendt et al. 1995; Fendt & Camenzind 1996).

In general, two classes of papers concerning magnetohydrodynamic simulations of jet formation from accretion disks have been published recently. In one class, the evolution of dipolar-type magnetic fields in interaction with a disk is investigated including also a treatment of the disk (Hayashi et al. 1996; Goodson et al. 1997 (GWB97); Miller & Stone 1997; Kudoh et al. 1999). In these papers a collapse of the inner disk is indicated giving rise to episodic ejections of plasmoids. A two-component structure of the flow develops – a collimated axial jet and a disk wind flow. Using an adaptive grid GWB97 were able to combine a huge spatial scale (2 AU) with a high spatial resolution near the star ($0.1\mathrm{R}_{\odot}$)!

However, all these simulations could be performed only for a few Keplerian periods of the inner disk! Further, the applied disk initial condition is not compatible with a magnetized disk. It is not surprising that the disk immediately becomes unstable giving rise to ejections. Clearly, it is not yet numerically feasible to include the disk structure self-consistently. The second class of papers deals with the evolution of a magnetized disk wind taking the disk only as a boundary condition for the inflow, an idea first proposed by Ustyugova et al. (1995) (see also Ouyed & Pudritz 1997 (OP97); Romanova et al. 1997, Ustyugova et al. 1999 (U99)). A monotonous flux distribution across the field is assumed. For a certain initial magnetic field a final stationary collimating jet flow could be found (OP97; U99).

We are essentially interested in the evolution of the ideal MHD magnetosphere and the formation of winds and jets and not in the evolution of the disk itself. Therefore, we do not include magnetic diffusivity into our simulations. The disk acts only as a boundary condition for the corona/jet region. In this sense we will follow the ideas developed by OP97. The winding-up process of magnetic field due to differential rotation between the star and the disk would be present even if diffusivity in a disk is taken into account. A treatment of the long-term evolution of such systems is essential for their interpretation, since it is then when they are being observed.

Here, we present first results of our simulations. We give a more detailed discussion in a forthcoming publication. A movie will be provided under *http://kosmos.aip.de/∼cfendt*.

2. Basic equations

Using the ZEUS-3D MHD code (Stone & Norman 1992a,b; Hawley & Stone 1995) in the axisymmetry option we solve the system of time-dependent ideal MHD equations,

$$\frac{\partial \rho}{\partial t} + \nabla \cdot (\rho \boldsymbol{v}) = 0, \; \frac{\partial \boldsymbol{B}}{\partial t} - \nabla \times (\boldsymbol{v} \times \boldsymbol{B}) = 0, \; \nabla \cdot \boldsymbol{B} = 0, \quad (1)$$

$$\rho \left[\frac{\partial \boldsymbol{v}}{\partial t} + (\boldsymbol{v} \cdot \nabla)\, \boldsymbol{v} \right] + \nabla (P + P_{\rm A}) + \rho \nabla \Phi - \boldsymbol{j} \times \boldsymbol{B} = 0, \quad (2)$$

$$\rho \left[\frac{e}{\partial t} + (\boldsymbol{v} \cdot \nabla)\, e \right] + P (\nabla \cdot \boldsymbol{v}) = 0, \quad (3)$$

with the magnetic field $\boldsymbol{B}$, velocity $\boldsymbol{v}$, gas density ρ, gas pressure P, internal energy e, electric current density $\boldsymbol{j} = \nabla \times \boldsymbol{B}/4\pi$, and gravitational potential Φ. We assume a polytropic gas, $P = K\rho^{5/3}$ and do not solve the energy equation (3). Additionally, we have introduced a turbulent magnetic pressure due to Alfvén waves, $P_{\rm A} \equiv P/\beta_T$, with a constant β_T (OP97)

Using dimensionless variables, $r' \equiv r/r_i$, $z' \equiv z/z_i$, $v' \equiv v/v_{K,i}$, $t' \equiv t r_i/v_{K,i}$, $\rho' \equiv \rho/\rho_i$, $P' \equiv P/P_i$, $B' \equiv B/B_i$, $\Phi' = -1/\sqrt{(r'^2 + z'^2}$', where the index i refers to parameter values at the inner disk radius r_i, the normalized equation of motion eventually being solved with the code is

$$\frac{\partial \boldsymbol{v}'}{\partial t'} + (\boldsymbol{v}' \cdot \nabla')\, \boldsymbol{v}' = \frac{2\, \boldsymbol{j}' \times \boldsymbol{B}'}{\delta_i\, \beta_i\, \rho'} - \frac{\nabla' (P' + P'_{\rm A})}{\delta_i\, \rho'} - \nabla' \Phi' \,. \quad (4)$$

Here is $\beta_i \equiv 8\pi P_i/B_i^2$ and $\delta_i \equiv \rho_i v_{K,i}^2/P_i$ with the Keplerian speed $v_{K,i}^2 \equiv \sqrt{GM/r_i}$. For a 'cold' corona ($P'_{\rm A} > 0$) it follows $\beta_T = 1/(\delta_i(\gamma - 1)/\gamma - 1)$. In the following we will omit the primes and will discuss only normalized variables.

3. The model, initial and boundary conditions

We apply the same boundary and initial conditions as developed by OP97 with the exception of a initial *dipolar-type* magnetic field from a stellar surface. Due to our choice of cylindrical coordinates we cannot treat the star as a sphere. The field distribution along our *straight* lower boundary, $z = 0$, corresponds to that along a surface with $z = z_{\rm D}$ across a dipolar-type field with a point-like star. This boundary is divided into a 'star', $r = 0, ...r_\star$, a gap from $r_\star$ to $r_i = 1.0$, and the disk from r_i to $r_{\rm out}$. Hydrodynamic inflow boundary conditions (b.c.) are set along this axis. Matter is injected from the disk into the corona with $\boldsymbol{v}_{\rm P} = v_{\rm inj} v_{\rm K} \boldsymbol{B}_{\rm P}/B_{\rm P}$, and $\rho_{\rm inj}(r) = \eta_i\, \rho(r, 0)$. The stellar rotational period can be chosen arbitrarily.

The initial density distribution is in hydrostatic equilibrium, $\rho = (r^2 + z^2)^{-3/4}$. The initial magnetic field structure is that of a force-free deformed dipole calculated with a finite element code described elsewhere (Fendt et al. 1995). There, the vector potential A_ϕ is computed using the double grid resolution. Then, the initial field distribution for the ZEUS code is derived with respect to the staggered mesh. In the undisturbed regions the initial field remains force-free on a level of $0.01\,\%$. A *force-free* initial field is essential in order to apply a hydro*static* corona as initial condition. The maximum $|\nabla \cdot \boldsymbol{B}|$ is 10^{-15}.

We have chosen an initial field distribution of a current-free magnetic dipole, artificially deformed by 'dragging' of an accretion disk, and an 'opening' of the field close to the outflow boundaries. This implies a poloidal field inclined to the disk surface supporting the launching of a disk wind. The amount of 'dragging' can be chosen by the b.c. in the finite element code. The stability of our initial condition is demonstrated in Fig. 1: density and field in the yet undisturbed regions perfectly match during the first decades of evolution ($t < 75$).

The b.c. for the poloidal magnetic field is set by the initial field distribution and the divergence-free condition (2). The b.c. for the toroidal component of the magnetic field is $B_\phi = \mu_i/r$ for $r \geq r_{\rm i}$, consistent with a Keplerian disk without any magnetic force. The emf b.c. along the r-axis is calculated directly from the velocity and field distribution prescribed, $\boldsymbol{\mathcal{E}}(\boldsymbol{r}) = \boldsymbol{v}(r) \times \boldsymbol{B}(r)$. For a rotating star $\boldsymbol{\mathcal{E}} \neq 0$.

We have carefully tested the application of the ZEUS-3D code to our model assumptions by recalculating the results of OP97 (obtained with the ZEUS-2D code) and found very good agreement (Fendt & Elstner 1999, in preparation). Another signature of the quality of our simulations is the stability of the hydrostatic initial condition and force-freeness over several decades of the computation.

4. Results and discussion

We have investigated numerically the evolution of a stellar dipolar-type magnetosphere in interaction with a Keplerian accretion disk using the ideal MHD ZEUS-3D code in the axisymmetry option. We are able to follow the evolution over more than 200 Keplerian periods of the inner disk (or 2.2 periods at the outer disk at $20\, r_i$)! The stellar radius is $r_\star = 0.5\, r_i$ The other parameters applied are $\delta_i = 100$, $\beta_i = 0.2$, $\mu_i = -1.0$, $\eta_i = 100$, $v_{\rm inj} = 0.001$, similar to OP97. For a typical protostar this corresponds to a disk density at r_i of

$$\rho_D = 10^{-11} \eta_i \beta_i \delta_i \left(\frac{B_i}{10\,{\rm G}} \right)^2 \left(\frac{r_i}{10\,{\rm R}_\odot} \right) \left(\frac{M}{{\rm M}_\odot} \right)^{-1} {\rm g\,cm^{-3}}. \quad (5)$$

Our main result is that the initial dipolar-type field structure disappears on spatial scales larger than the inner disk radius and a slowly collimating disk wind evolves (Fig. 1). An expanding low density 'bubble' forms disrupting the field and moving with an axial speed of $v_z \simeq 0.4 v_{K,i}$ (at $t = 100$). A weak back-flow of material exists close to the axis.

The general behavior of the system is independent from a variation of the field strength. For strong fields, the bubble is moving faster, however, the numerical life time of the simulation is accordingly shorter. This is a major difference to OP97, resulting from the inner 'stellar' b.c. and differential rotation between star and disk. After $t = 75$, torsional Alfvén waves reach the outer region and the whole initial field distribution is distorted. A flow along the field develops close to the disk. Its inclination angle *slowly* increases with time. We interpret this as indication for a possible stationary final state. We hypothesize that such a solution will look similar to the jet solutions of OP97, since the disk inflow condition is the same. OP97 have shown that for a certain initial magnetic field distribution the evolving jet flow becomes stationary after about 400 Keplerian periods. Also, Romanova et al. (1997) find a stationary collimating disk wind, however, applying a monopole-type initial field structure. Further extending this approach, U99 have generally proven the

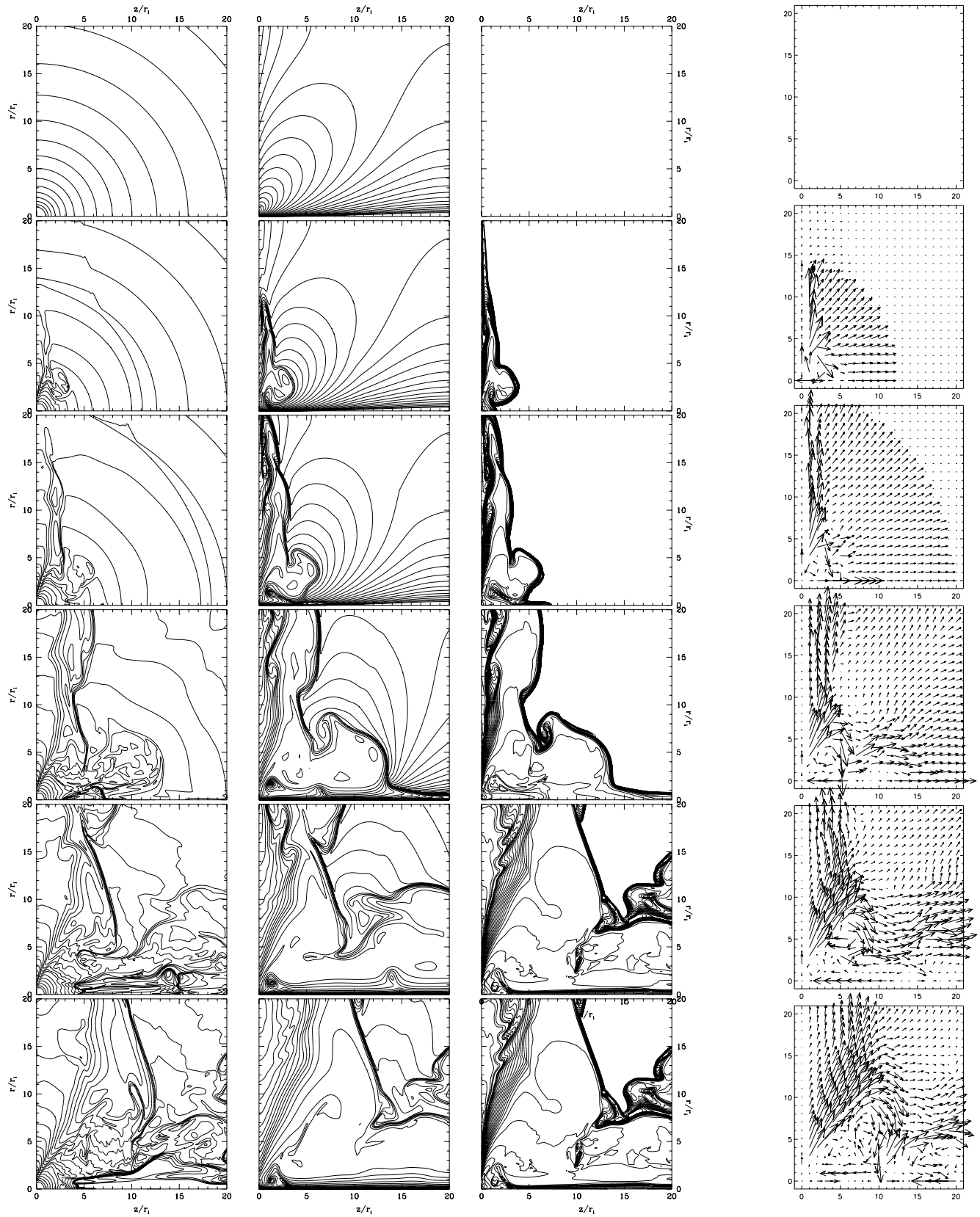

Fig. 1. Evolution of a dipolar-type magnetosphere in interaction with a Keplerian disk. Shown is (from *left* to *right*) the density ρ, magnetic field distribution ($B_{\rm P}$-lines and B_ϕ contours) and velocity vectors (on scale only within each frame) for $t = 0, 25, 50, 100, 150, 200$ (from *top* to *bottom*). The inflow from the disk along the r-axis is parallel to the initial poloidal field. The innermost density contour ($\rho = 1.0$) indicates the inner disk radius $r_{\rm i} = 1.0$. The stellar radius along the r-axis is $r_\star = 0.5\, r_{\rm i}$. The numerical resolution is 250×250 grid elements.

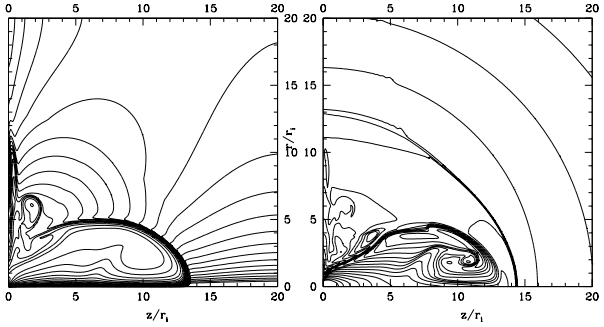

Fig. 2. Example solution of the magnetosphere for stellar rotation for the time step $t = 25$, corresponding also to 25 stellar rotational periods. Density distribution (*left*) and poloidal magnetic field lines (*right*). Same contour levels as in Fig. 1.

existence of stationary disk jets in agreement with predictions of the stationary MHD theory. In our simulations the disk wind accelerates to poloidal velocities of $v_{\rm p} > 0.5 v_{K,i}$. The wind is launched predominantly from the inner disk, due to the fact that the poloidal field strength drops very fast! In difference to OP97 the magnetic field (with the initial dipole) does not evolve into a *monotonous* flux distribution across the field, but into a *reversed* field structure with a neutral line of vanishing field strength! The dipole survives close to the star with a density distribution similar to the initial one.

Simulations with a rotating and a non-rotating star show significant differences (Fig. 2), although differential rotation between star and disk is present in both scenarios. For a rotating star a collimated high-speed outflow is generated close to the axis during the first periods, in agreement with the GWB97 results. However, this axial jet does not survive very long, if not an additional inflow of a *stellar wind* is prescribed.

Hayashi et al. (1996) and GWB97 already demonstrated that a stellar magnetic dipole connected to a disk is deformed within some Keplerian periods. However, the fate of such a field geometry over many rotational periods has not been investigated. One may suppose that the X-ray flares found by Hayashi et al. might be a phenomenon occurring only during the very first decades of rotation until the star-field-disk system has substantially developed from its initial state. Although we find the same general structure of the flow evolution – jet and disk wind – our study gives strong indication that episodic outbursts do not appear on longer time-scales. However, as GWB97 discuss, outbursts are initiated from the time-dependent behavior of the accretion disk, the structure of which we do *not* treat. Our conclusion is that a *stationary* disk most probably will produce a stationary outflow on large scales!

We now compare our results with stationary jet models in the literature. (Note that protostellar jet formation observed on dimensions of $\lesssim 1000\, r_i$ cannot yet be studied on a *global* spatial scale with the numerical codes presently available due to the lack of numerical resolution). Camenzind (1990) developed a basic model of jet formation from a magnetized young star - accretion disk system. Stationary model calculations based on such a scenario did not find jet solutions if a large-scale dipolar stellar field is applied as b.c., whereas a dipole concentrated only to the star permitted an asymptotic jet with monotonous field distribution across the jet (Fendt et al. 1995, Fendt & Camenzind 1996). Our simulations shows that this innermost dipole is not destroyed. In the Shu et al. (1994a,b) model the jet flow emerges centrifugally accelerated from a so-called X-point at the inner disk radius. A critical field line divides the closed dipolar loops from the open wind/jet field. At a quick look our simulations seem to favor the hypothesis of Shu et al., their critical surface corresponding to our dominant flow channel emanating from the inner disk radius. However, in our simulation, the strong acceleration at this location is due to the strong differential rotation at this point and the subsequent induction of toroidal magnetic fields, while in Shu et al.'s theory centrifugal forces play the dominant role.

In summary, our long-term simulations show that (1) short-term simulations should be interpreted with care, being probably biased by the initial condition. Further, (2) the long-term evolution indicates on a possible final *stationary* state of a collimating high speed disk wind, in difference to papers on this topic published previously. Direct comparison of the simulations with a rotating and a non-rotating star shows that (3) the first steps of the evolution differ greatly. In the long-term evolution, however, both systems may evolve quite similar. This would imply that (4) jet formation depends mainly on the disk and not on the stellar rotation. Such a 'prediction' may be tested by observing jet sources with different rotational periods.

Further studies are needed to understand the complex behavior of the flow and field evolution. We will present a more detailed analysis of our results in a subsequent paper.

Acknowledgements. We thank the LCA team and M. Norman for the possibility to use the ZEUS code. We further thank R. Ouyed for encouraging help and valuable discussions.

References

Blandford R.D., Payne D.G., MNRAS, 1982, 199, 883
Camenzind M., 1990, Magnetized disk-winds and the origin of bipolar outflows, in: G. Klare (ed.) Rev. Mod. Astron. 3, Springer, Heidelberg, p.234
Fendt C., Camenzind M., Appl S., 1995, A&A, 300, 791
Fendt C., Camenzind M., 1996, A&A, 313, 591
Goodson A.P., Winglee R.M., Böhm K.-H., 1997, 489, 199 (GWB97)
Hawley J.F., Stone J.M., 1996, Comp. Physics Comm., 89, 127
Hayashi M.R., Shibata K., Matsumoto R., 1996, ApJ, 468, L37
Kudoh T., Matsumoto R., Shibata K., 1999, ApJ, 508, 186
Miller K.A., Stone J.M., 1997, ApJ, 489, 890
Ouyed R., Pudritz R.E., 1997, ApJ, 482, 712 (OP97)
Pudritz R.E., Norman C.A., 1983, ApJ, 274, 677
Romanova M.M., Ustyugova G.V., Koldoba A.V., Chechetkin V.M., Lovelace R.V.E., 1997, ApJ, 482, 708
Shu F.H., Najita J., Wilkin F., Ruden S.P., Lizano S., 1994a, ApJ, 429, 781
Shu F.H., Najita J., F., Ruden, S., Lizano, S., 1994b, ApJ, 429, 797
Stone J.M., Norman M.L., 1992a, ApJSS, 80, 753
Stone J.M., Norman M.L., 1992b, ApJSS, 80, 791
Ustyugova G.V., Koldoba A.V., Romanova M.M., Chechetkin V.M., Lovelace R.V.E., 1995, ApJ, 439, L39
Ustyugova G.V., Koldoba A.V., Romanova M.M., Chechetkin V.M., Lovelace R.V.E., 1999, ApJ, 516, 221 (U99)

Astron. Astrophys. 363, 208–222 (2000)

ASTRONOMY AND ASTROPHYSICS

Long-term evolution of a dipole type magnetosphere interacting with an accretion disk

II. Transition into a quasi-stationary spherically radial outflow

C. Fendt and D. Elstner

Astrophysikalisches Institut Potsdam, An der Sternwarte 16, 4482 Potsdam, Germany (cfendt, delstner@aip.de)

Received 10 April 2000 / Accepted 25 July 2000

Abstract. The evolution of an initially stellar dipole type magnetosphere interacting with an accretion disk is investigated numerically using the ideal MHD ZEUS-3D code in the 2D-axisymmetry option. Depending mainly on the magnetic field strength, our simulations may last several thousands of Keplerian periods of the inner disk. A Keplerian disk is assumed as a boundary condition prescribing a mass inflow into the corona. Additionally, a stellar wind from a rotating central star is prescribed. We compute the innermost region around the stellar object applying a non-smoothed gravitational potential.

Our major result is that the initially dipole type field develops into a spherically radial outflow pattern with two main components, a disk wind and a stellar wind component. These components evolve into a quasi-stationary final state. The poloidal field lines follow a conical distribution. As a consequence of the initial dipole, the field direction in the stellar wind is opposite to that in the disk wind. The half opening angle of the stellar wind cone varies from 30° to 55° depending on the ratio of the mass flow rates of disk wind and stellar wind. The maximum speed of the outflow is about the Keplerian speed at the inner disk radius.

An expanding bubble of hot, low density gas together with the winding-up process due to differential rotation between star and disk disrupts the initial dipole type field structure. An axial jet forms during the first tens of disk/star rotations, however, this feature does not survive on the very long time scale. A neutral field line divides the stellar wind from the disk wind. Depending on the numerical resolution, small plasmoids are ejected in irregular time intervals along this field line. Within a cone of 15° along the axis the formation of small knots can be observed if only a weak stellar wind is present.

With the chosen mass flow rates and field strength we see almost no indication for a flow self-collimation. This is due to the small net poloidal electric current in the (reversed field) magnetosphere which is in difference to typical jet models.

Key words: Magnetohydrodynamics (MHD) – accretion, accretion disks – ISM: jets and outflows – stars: magnetic fields – stars: mass-loss – stars: pre-main sequence

Send offprint requests to: C. Fendt

1. Introduction

A stellar dipole type magnetic field surrounded by an accretion disk is the common model scenario for a variety of astrophysical objects. Examples are the classical T Tauri stars, magnetic white dwarfs (in cataclysmic variables) and neutron stars (in high mass X-ray binaries). Part of these sources exhibit Doppler shifted emission lines indicating wind motion. Highly collimated jets have been observed from young stellar objects and X-ray binaries, where also quasi-periodic oscillations (QPO) are observed. In general, magnetic fields are thought to play the leading role for the jet acceleration and collimation (Blandford & Payne 1982; Pudritz & Norman 1983; Camenzind 1990; Shu et al. 1994; Fendt et al. 1995).

Recently, several papers were considering the evolution of a stellar magnetic dipole in interaction with a diffusive accretion disk. Hayashi et al. (1996) observed magnetic reconnection and the evolution of X-ray flares during the first rotational periods. Miller & Stone (1997) Goodson et al. (1997) included the evolution of the (diffusive) disk structure in their calculation. In these papers a collapse of the inner disk is indicated depending on the magnetic field strength and distribution. The inward accretion flow develops a shock near the star. The stream becomes deflected resulting in a high-speed flow in axial direction.

The results of Goodson et al. (1997, 1999) and Goodson & Winglee (1999) are especially interesting since combining a huge spatial scale (2 AU) with a high spatial resolution near the star ($0.1\mathrm{R}_\odot$). However, to our understanding it is not clear, how the initial condition (a standard α-viscosity disk) is really developing in their code without any physical viscosity. Secondly, not very much is said about the amount of magnetic diffusivity. The assumption of constant diffusivity cannot really reflect the two component model of disk and coronal out flow.

Time-dependent simulations lasting only a short time scale depend strongly on the initial condition and the calculation of the evolution of such a magnetosphere over *many* rotational periods is an essential step. In particular, this is an important point if the initial condition is not in equilibrium. In summary, we note that all calculations including the treatment of the disk structure could be performed only for a few Keplerian periods of the inner disk (and a fraction of that for the outer disk).

At this point, we emphasize that the observed kinematic time scale of protostellar jets can be as large as 10^3–10^4 yrs, corresponding to 5×10^4–5×10^5 stellar rotational periods (and inner disk rotations)! For example, proper motion measurements for the HH30 jet (Burrows et al. 1996) give a knot velocity of about 100–300 $\mathrm{km\,s^{-1}}$ and a knot production rate of about 0.4 knot per year. Assuming a similar jet velocity along the whole jet extending along 0.25 pc (Lopez et al. 1995), the kinematic age is about 1000 yrs.

A different approach for the simulation of magnetized winds from accretion disks considers the accretion disk 'only' as a *boundary condition* for the mass inflow into the corona. Since the disk structure itself is not treated, such simulations may last over hundreds of Keplerian periods. This idea was first applied by Ustyugova et al. (1995). Extending this work, Romanova et al. (1997) found a stationary final state of a slowly collimating disk wind in the case of a split-monopole initial field structure after 100 Keplerian periods. Ouyed & Pudritz (1997, hereafter OP97) presented time-dependent simulations of the jet formation from a Keplerian disk. For a certain (already collimating) initial magnetic field distribution, a stationary state of the jet flow was obtained after about 400 Keplerian periods of the inner disk with an increased degree of collimation. In a recent extension of their work both groups were considering the influence of the grid's shape on the degree of collimation (Ustyugova et al. 1999) and the effect of the mass flow rate (Ouyed & Pudritz 1999). Ouyed & Pudritz (2000) investigate the problem of jet stability and magnetic collimation extending the axisymmetric simulations to 3D.

In this paper, we are essentially interested in the evolution of the ideal MHD magnetosphere and the formation of winds and jets and not in the evolution of the disk structure itself. Therefore, we do not include magnetic diffusivity into our simulations. The disk acts only as a boundary condition for the corona/jet region. The winding-up process of poloidal magnetic field due to strong differential rotation between the star and the disk would always be present even if a disk diffusivity would have been taken into account. The disk diffusivity will never be so large that a rigid rotation of the magnetosphere in connection with the disk can be maintained.

In that sense our simulations represent an extension of the OP97 model, taking additionally into account the central star as a boundary condition and a stellar dipole type field as initial condition. First results of our simulations were presented in Fendt & Elstner (1999, hereafter FE99). Here we give a more detailed discussion together with new results. Movies of our simulations will be provided under *http://www.aip.de/∼cfendt*.

2. Basic equations

Using the ZEUS-3D MHD code (Stone & Norman 1992a,b; Hawley & Stone 1995) in the 2D-axisymmetry option we solve the system of time-dependent ideal magnetohydrodynamic equations,

$$\frac{\partial\rho}{\partial t}+\nabla\cdot(\rho\boldsymbol{v})=0\,, \tag{1}$$

$$\frac{\partial\boldsymbol{B}}{\partial t}-\nabla\times(\boldsymbol{v}\times\boldsymbol{B})=0\,, \tag{2}$$

$$\nabla\cdot\boldsymbol{B}=0\,, \tag{3}$$

$$\rho\left[\frac{\partial\boldsymbol{v}}{\partial t}+(\boldsymbol{v}\cdot\nabla)\,\boldsymbol{v}\right]+\nabla(P+P_{\rm A})+\rho\nabla\Phi-\boldsymbol{j}\times\boldsymbol{B}=0\,, \tag{4}$$

where $\boldsymbol{B}$ is the magnetic field, $\boldsymbol{v}$ the velocity, ρ the gas density, P the gas pressure, $\boldsymbol{j}=\nabla\times\boldsymbol{B}/4\pi$ the electric current density. and Φ the gravitational potential. We assume a polytropic ideal gas, $P=K\rho^\gamma$ with a polytropic index $\gamma=5/3$. Similar to OP97, we have introduced a turbulent magnetic pressure due to Alfvén waves, $P_{\rm A}\equiv P/\beta_T$, where β_T is assumed to be constant. OP97 considered the turbulent magnetic pressure in order to support the cold corona of e.g. young stellar accretion disks for a given gas pressure. Clearly, the assumption of a *constant* β_T is motivated by the reason of simplification. Using dimensionless variables, $r'\equiv r/r_i$, $z'\equiv z/z_i$, $v'\equiv v/v_{K,i}$, $t'\equiv tr_i/v_{K,i}$, $\rho'\equiv\rho/\rho_i$, $P'\equiv P/P_i$, $B'\equiv B/B_i$, $\Phi'=-1/\sqrt{r'^2+z'^2}$', where the index i refers to parameter values at the inner disk radius r_i, the normalized equation of motion eventually being solved with the code is

$$\frac{\partial\boldsymbol{v}'}{\partial t'}+(\boldsymbol{v}'\cdot\nabla')\,\boldsymbol{v}'=\frac{2\,\boldsymbol{j}'\times\boldsymbol{B}'}{\delta_i\,\beta_i\,\rho'}-\frac{\nabla'(P'+P'_{\rm A})}{\delta_i\,\rho'}-\nabla'\Phi'\,. \tag{5}$$

The coefficients $\beta_i\equiv8\pi P_i/B_i^2$ and $\delta_i\equiv\rho_i v_{K,i}^2/P_i$ with the Keplerian speed $v_{K,i}\equiv\sqrt{GM/r_i}$, correspond to the plasma beta and the Mach number of the rotating gas. For a 'cold' corona with $P'_{\rm A}>0$, it follows $\beta_T=1/(\delta_i(\gamma-1)/\gamma-1)$. In the following we will omit the primes and will discuss only normalized variables if not explicitly declared otherwise.

Note that in our figures the horizontal axis is always the z-axis and the vertical axis is the r-axis.

3. The model – numerical realization

In general, our model represents a system consisting of a central star and an accretion disk separated by a gap. Star and disk are initially connected by an dipole type magnetosphere. Axisymmetry is assumed. The stellar rotational period can be chosen arbitrarily. The disk is in Keplerian rotation. Disk and star are taken into account as an inflow boundary condition. It has the advantage that the behavior of the wind flow can be studied independently from the evolution of the accretion disk.

This is an essential point, since the numerical simulation of the magnetized disk structure represents itself one of the most complicated and yet unresolved problems of astrophysics. It is therefore unlikely to find a proper disk initial condition which is in equilibrium. Yet, all MHD disk simulations could be performed only for a few Keplerian periods (e.g. Hayashi et al. 1996, Miller & Stone 1997; Kudoh et al. 1998). A global solution of the disk-jet evolution does not yet seem to be numerically feasible.

The general disadvantage involved with such a fixed disk (plus star) boundary condition is that the fundamental question of the wind/jet formation evolving out of the accretion disk cannot be investigated.

3.1. Numerical grid and initial condition

Prescribing a stable force-equilibrium as initial condition is essential for any numerical simulation. Otherwise the simulation will just reflect the relaxation process of such an unstable (and therefore arbitrary) initial condition to a state of stability. In particular this would be important if only few time steps are computed.

In our model, we assume an initially force-free (and also current-free) magnetic field together with a density stratification in hydrostatic equilibrium. Such a configuration will remain in its initial state if not disturbed by a boundary condition. The initial density distribution is $\rho(r,z) = (r^2+z^2)^{-3/4}$. The gravitational point mass is located half a grid element below the origin. Due to our choice of cylindrical coordinates we cannot treat the stellar surface as a sphere. Along the *straight* lower r-boundary we define the 'stellar surface' from $r = 0$ to $r = r_\star$, a gap from $r = r_\star$ to $r = r_i = 1.0$, and the disk from $r = 1.0$ to $r = r_{\rm out}$ (see Fig. 1).

We have chosen an initial field distribution of a force-free, current-free magnetic dipole, artificially deformed by (i) the effect of 'dragging' of an accretion disk, and (ii) an 'opening' of the field lines close to the outflow boundaries. The initial field distribution is calculated using a stationary finite element code described in Fendt et al. (1995). In this approach, the axisymmetric ϕ-component of the vector potential A_ϕ is computed (as solution of the well-known Grad-Shafranov equation) using a numerical grid with twice the resolution of the grid applied in the ZEUS code. Our finite element code allows for a solution of the stationary boundary value problem for *any* boundary condition. Thus, we are able to define any force-free solution as initial condition for the simulation.

With that, from the vector potential the initial field distribution for the time-dependent simulation is derived with respect to the ZEUS-3D staggered mesh,

$$B_z(i,j) \;=\; 2\,(A_{\phi;i,j+1} - A_{\phi;i,j})/(r^2_{i,j+1} - r^2_{i,j})\,,$$
$$B_r(i,j) \;=\; -\,(A_{\phi;i+1,j} - A_{\phi;i,j})\,/\,(r_{i,j}\,(r_{i+1,j} - r_{i,j}))\,. \quad (6)$$

Here, the first and second index i and j denote the z- and r-direction, respectively. A suitable normalization factor is multiplied in order to match the field strength defined by the coefficients β_i and δ_i. With this approach the maximum normalized $|\nabla \cdot \boldsymbol{B}|$ is 10^{-15} and $|\boldsymbol{j} \times \boldsymbol{B}| = 0.01|\boldsymbol{B}|$.

The boundary conditions for the initial magnetic field distribution calculated with the finite element code are the following. (i) A dipolar field along the stellar surface $r < r_\star$ given as Dirichlet condition; (ii) a homogeneous Neumann condition along the gap between star and disk; (iii) a detached dipolar field along the disk (as Dirichlet condition),

$$A_\phi(r) = \left(\frac{1}{r}\frac{r^2}{(r^2+z_{\rm D}^2)^{3/2}}\right)\tilde{A}(r); \quad \text{with}\,\tilde{A}(r) = r^{-3/2}, \quad (7)$$

and (iv) a homogeneous Neumann condition along the outer boundaries. This implies a poloidal field inclined to the disk surface which would support magneto-centrifugal launching of a disk wind. The amount of 'dragging' can be defined by choosing a different function $\tilde{A}(r)$. The initial field is calculated with a z-offset, $z_{\rm D}^2 \gtrsim r_\star/\sqrt{2}$. This offset avoids un-physically strong field strengths close to the stellar surface, but leaves the field in a force-free configuration. Again, we emphasize that such a *force-free* initial field is essential in order to apply a hydro*static* corona as initial condition.

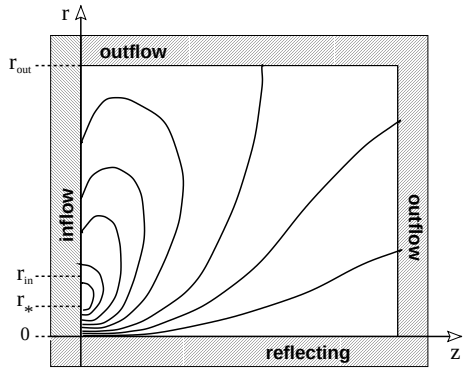

Fig. 1. Numerical model. Active region (white) and boundary region (pattern). Star, gap and Keplerian disk are prescribed along the r-inflow boundary with the stellar radius $r_\star$, inner disk radius $r_{\rm i} \equiv 1.0$, and maximum radius $r_{\rm out}$. The numerical grid size is 250×250. For clarification, the poloidal field lines of the initial dipole type magnetic field are shown as a sketch. The field smoothly continues into the ghost zones.

3.2. The boundary conditions

The boundary condition for the poloidal magnetic field along the inflow boundary is fixed to the initial field. The magnetic flux from the star and disk is conserved. The field along the lower boundary $z = 0$ corresponds to that given by Eq. (7). The boundary condition for the toroidal magnetic field component is $B_\phi = \mu_i/r$ for $r \geq r_{\rm i}$ with the parameter $\mu_i = B_{\phi,{\rm i}}/B_{\rm i}$. No toroidal field is prescribed at the stellar surface.

Hydrodynamic boundary conditions are 'inflow' along the r-axis, 'reflecting' along the symmetry axis and 'outflow' along the outer boundaries. The inflow parameters into the corona are defined with respect to the three different boundary regions – star, gap and disk. The matter is 'injected' into the corona parallel to the poloidal field lines, $\boldsymbol{v}_{\rm inj}(r,0) = \kappa_i v_{\rm K}(r)\boldsymbol{B}_{\rm P}/B_{\rm P}$ with a density $\rho_{\rm inj}(r,0) = \eta_i\,\rho(r,0)$. This defines the normalized mass flow rate in the disk wind,

$$\dot{M}_{\rm D} = 2\pi \int_{r_{\rm i}}^{r_{\rm out}} \rho_{\rm inj,D}\, v_{\rm inj,D}\, dr = 2\pi\eta_{\rm i,D}\kappa_{\rm i,D}\left(\frac{1}{r_{\rm i}} - \frac{1}{r_{\rm out}}\right). \quad (8)$$

Additionally to the disk wind boundary condition, we assume a wind component also from the stellar surface $r < r_\star$. The density profile of the stellar wind injection is the same as for the disk $\rho_{{\rm inj},\star}(r,0) = \eta_{i\star}\,\rho(r,0)$. In the examples discussed in this paper, the injection velocity is chosen as constant $\boldsymbol{v}_{{\rm inj},\star}(r,0) = \kappa_{{\rm i},\star} v_{\rm K,i}\boldsymbol{B}_{\rm P}/B_{\rm P}$. This gives a mass loss rate of the stellar wind component of

$$\dot{M}_\star = 2\pi \int_{r_0}^{r_\star} \rho_{{\rm inj},\star}\, v_{{\rm inj},\star}\, dr = 2\pi\eta_{{\rm i},\star}\kappa_{{\rm i},\star}\left(\frac{1}{\sqrt{r_0}} - \frac{1}{\sqrt{r_\star}}\right). \quad (9)$$

In this case, r_0 is the radius of the center of the innermost grid element (the `x2b(3)` value in the ZEUS code staggered mesh) and is therefore biased by the numerical resolution.

This is motivated partly by numerical reasons and partly by the fact that *stellar winds* are indeed observed. Concerning the first point, the initial setup of a force-free magnetosphere will be distorted within the very first evolutionary steps giving rise to Lorentz forces. These forces disturb the initial *hydrostatic* equilibrium resulting in a mass outflow from the regions above the star. As a consequence, this part of the magnetosphere will be depleted of matter, if no additional mass inflow from the star is present. The small density implies a strong decrease in the numerical time step discontinuing the simulation.

On the other hand, an additional mass flow from the stellar surface is not unlikely. Stellar winds are common among active stars, most probably being present also in the systems investigated in this paper. Yet, it is not known whether stellar jets originate as disk winds (Pudritz & Norman 1983) or as a stellar wind (Fendt et al. 1995). Variations of the 'standard' protostellar MHD jet model usually deal with a two-component outflow (Camenzind 1990; Shu et al. 1994). Model calculations of the observed emission line regions also indicate a two-component structure (Kwan & Tademaru 1995). Therefore, the stellar wind boundary condition seems to be reasonable.

The ratio of the mass flow rates in the two outflow components will definitely influence the jet structure. Therefore, we have chosen different values for that ratio in our simulations (Table 1). Long-term evolution runs over several hundreds of rotational periods we have only obtained considering a rather strong stellar wind flow which stabilizes the region close to the rotational axis. Since the velocity and density profiles decrease rather fast along the disk, the contribution to $\dot{M}_{\rm disk}$ from radii larger than $r_{\rm out}$ is negligible.

The electro-motive force boundary condition along the inflow axis is calculated directly from the prescribed velocity and magnetic field distribution, $\boldsymbol{\mathcal{E}(r)} = \boldsymbol{v}(r) \times \boldsymbol{B}(r)$. Note that magnetic field and velocity have to be taken properly from the staggered mesh points in order to give $\boldsymbol{\mathcal{E}(r)}$ as an *edge-centered* property. In the case of a stellar rotation, $\boldsymbol{\mathcal{E}} \neq 0$ for $r < r_\star$.

3.3. Numerical tests

Before applying the ZEUS-3D code to our model we performed various test simulations, in particular a recalculation the OP97 2D jet simulations (see Appendix). Our choice of initial density distribution is stable with very good accuracy. Following OP97 this was tested by a run without the inflow boundary conditions and magnetic field. Another signature of our proper initial magnetohydrostatic condition is the stability of the hydrostatic initial condition during the simulation itself.

Force-freeness of the magnetic field distribution can be tested by calculating the $\boldsymbol{j}(r,z) \sim \nabla \times \boldsymbol{B}$ current distribution which ideally should vanish as a consequence of the initial condition applied. Force-freeness can not fully be satisfied when transforming the finite element solution to the ZEUS code initial condition, however, an error of $0.01\,\%$ is acceptable in order to avoid artificial effects during the first time steps until the field distribution has evolved from its initial state.

The stability of our initial condition is demonstrated in Fig. A.1 showing an overlay of several initial time steps of an example simulation without a stellar rotation presented in FE99. The density and field distribution in the yet undisturbed regions perfectly match during the first decades of evolution ($t < 75$).

Table 1. The table shows the parameter set varying for the four simulation runs S2, S4, L3, L5. Simulation L1 is from FE99. All the other parameters remain the same ($\beta_i = 1.0$, $\beta_T = 0.03$, $\delta_i = 100$, $\mu_i = -1.0$, $r_\star = 0.5$).

	$\kappa_{\rm i,\star}$	$\kappa_{\rm i,D}$	$\eta_{\rm i,\star}$	$\eta_{\rm i,D}$	$\Omega_\star$	$\dot{M}_{\rm D}/\dot{M}_\star$
L1	–	10^{-3}	–	100	–	–
S2	10^{-6}	10^{-3}	10^3	1	1	0.5
S4	10^{-4}	10^{-3}	10^3	10^3	1	2.8
L3	10^{-4}	10^{-3}	200	200	1	1.8
L5*	10^{-4}	10^{-3}	10^3	100	1	0.2

* Disk injection velocity profile is $\sim v_{\rm K}^2(r)$

4. Results and discussion

In the following we discuss the results of four example simulations denoted by S2, S4, L3, L5 (see Table 1). All the simulations presented in this paper consider a rotating star at the center. The stellar rotational period is chosen as $\Omega_\star = (v_{K,i}/R_i) = 1$, with a magnetospheric co-rotation radius located at the inner disk radius. The evolution of a non-rotating central star is discussed in FE99, although it was not possible to perform the simulation as long as the examples presented here.

As a general behavior, the initial dipole type structure of the magnetic field disappears on spatial scales larger than the inner disk radius and a two component wind structure – a disk wind and a stellar wind – evolves. Our main result is the finding of a *quasi-stationary* final state of a spherically radial mass outflow evolving from the initial dipole type magnetic field on the very extended time evolution. For the boundary conditions applied the calculated flow structure show only few indication for collimation.

The general features in the evolution of the system are independent from a variation of the field strength. For strong fields, the evolution is faster. Thus, for simulations which are limited in time due to numerical problems, a decrease in the field strength would not help. Although the numerical life time of the simulation would be accordingly longer, the result for the final time step will be the same.

4.1. Four simulations of the long-term magnetospheric evolution – an overview

The four example simulations basically differ in the mass flow rates from disk and star and the size of the physical domain investigated (Table 1). All other parameters, $\beta_i = 1.0$, $\delta_i = 100$, $\mu = -1.0$, $r_\star = 0.5$, $\gamma = 5/3$, and the numerical mesh of

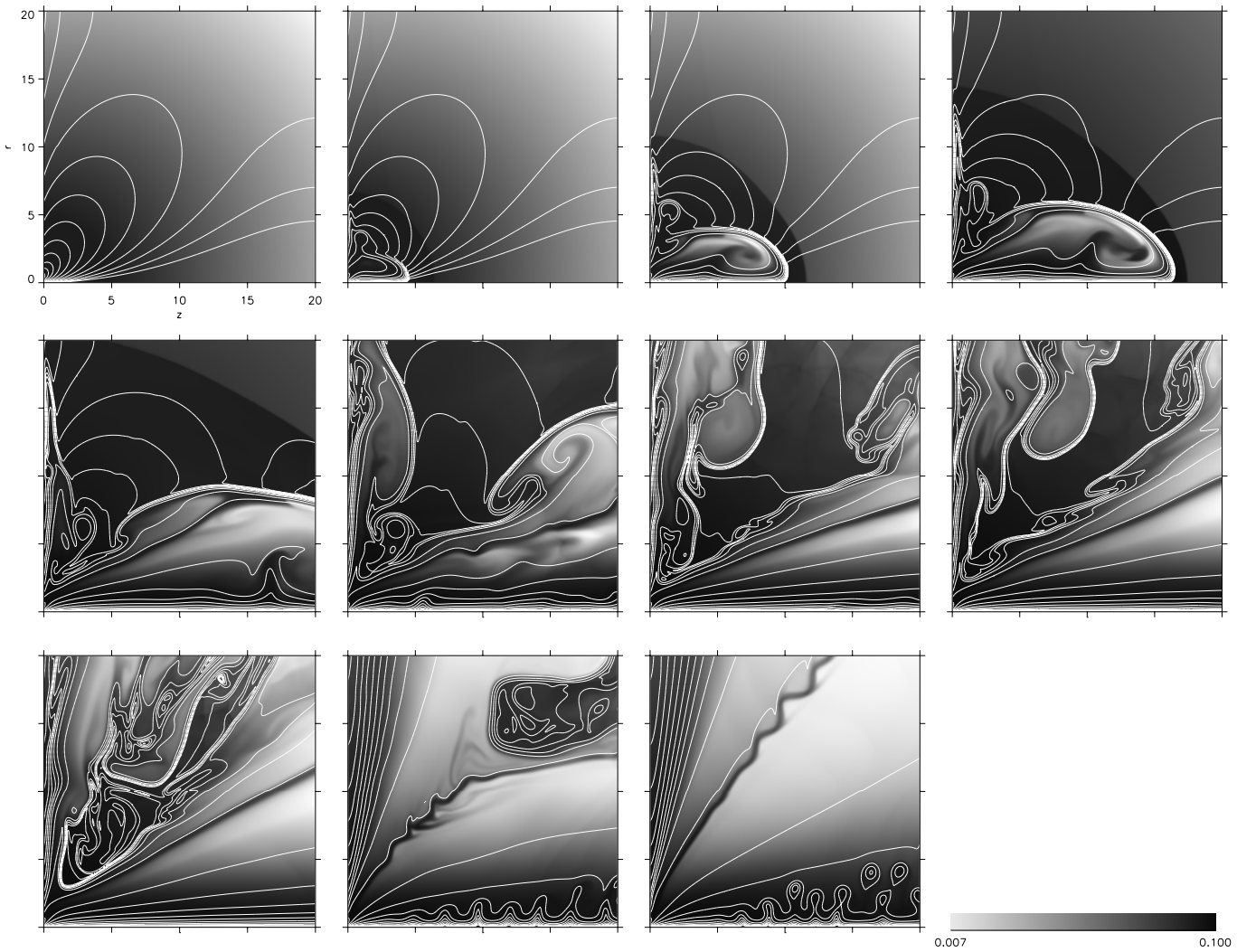

Fig. 2. Simulation S2 in a box of $20 \times 20\, r_{\rm i}$. Shown are density (grey scale) and poloidal field lines (contour lines) for $t = 0, 10, 20, 30, 50, 100, 200, 300, 500, 1000, 2500$ (from *left* to *right* and *top* to *bottom*). The density at the inner disk radius is $\rho_{\rm i} = 1.0$. The legend shows the density limits used for the color coding (which itself uses the inverse density profile). The stellar radius is $r_\star = 0.5\, r_{\rm i}$.

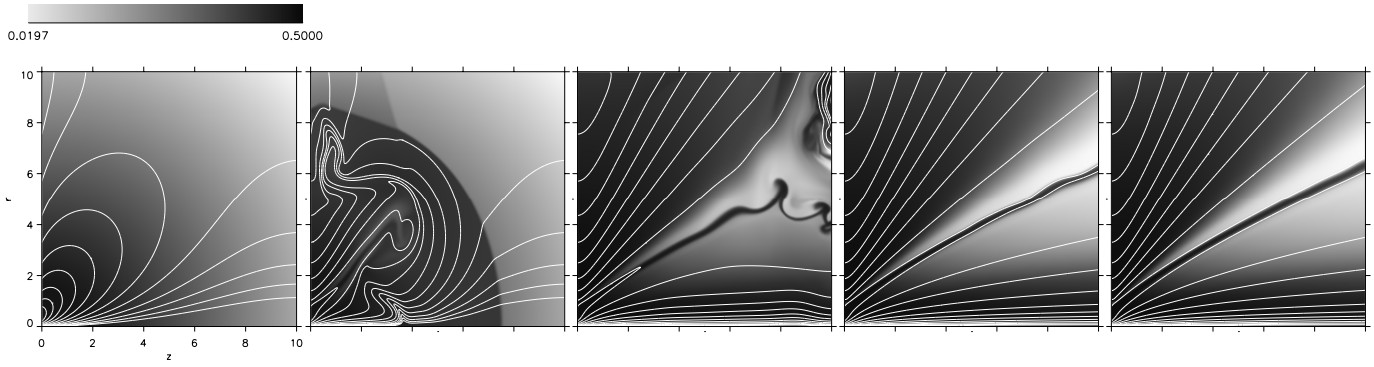

Fig. 3. Simulation S4 in a box of $10 \times 10\, r_{\rm i}$. Density and poloidal field lines. Notation equivalent to Fig. 2. Time steps $t = 0, 10, 40, 400, 600 t_i$.

250×250 grid elements remain the same. The first simulation (solution **S2**) considers a rectangular box of physical size of 20x20 inner disk radii (Fig. 2, Fig. 5, Fig. 7). The stellar wind mass flow rate is comparatively large, $\dot{M}_\star / \dot{M}_{\rm D} = 2$. The stellar wind injection velocity is very low in order to not disturb a possible weak wind solution already by the boundary condition. The disk wind boundary condition is the same as in OP97 and FE99. Due to the relatively large physical size of the computational domain the stability of the initial condition can be observed for several decades of rotational periods. The

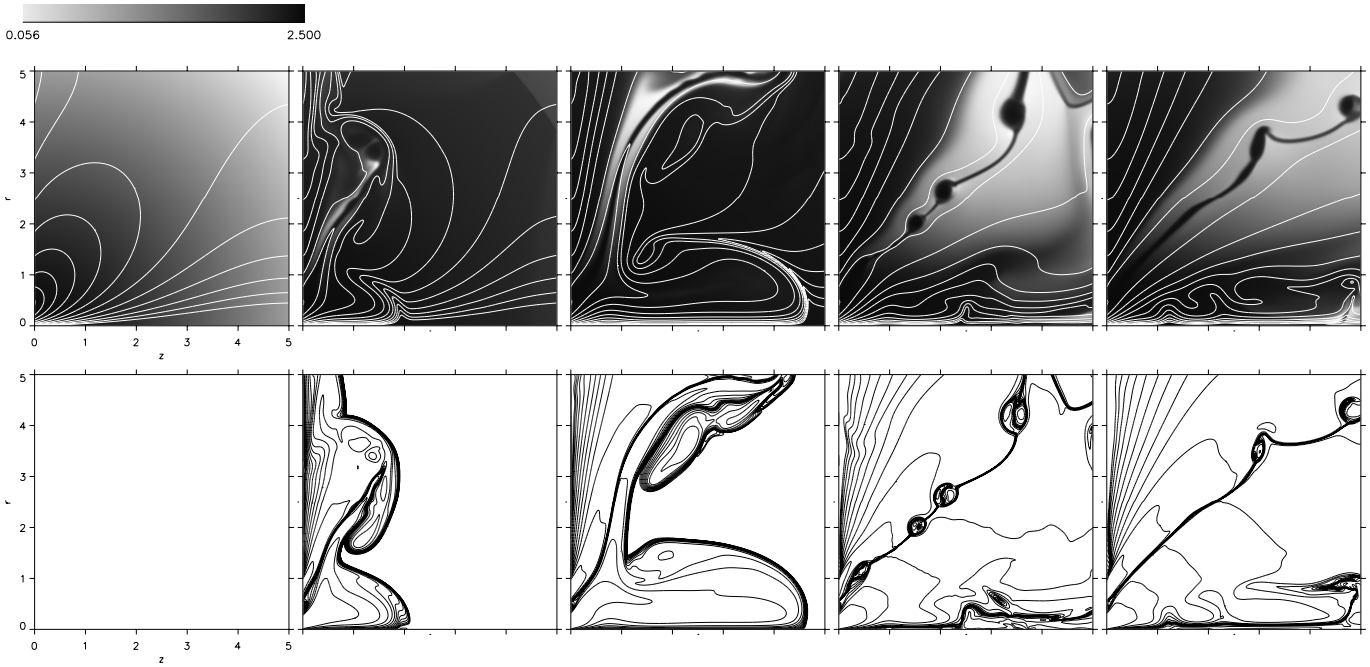

Fig. 4. High resolution simulation L3 in a box of $5 \times 5\, r_{\rm i}$. *Above* Density and poloidal field lines. Notation equivalent to Fig. 2. *Below* Contour plots of the toroidal magnetic field strength. The toroidal field is positive (negative) outside (inside) the neutral line. Time steps are $t = 0, 10, 20, 80, 160$ (from *left* to *right*).

torsional Alfvén waves leave the grid after about $t = 40$. The second simulation (solution **S4**) considers a rectangular box of physical size of 10x10 inner disk radii (Fig. 3, Fig. 5, Fig. 7). Now the total mass flow is dominated by the disk wind. This choice of parameters can be directly seen from the simulation by comparing the size of axial flow and the 'bubble' evolving from the disk flow. Clearly, the disk flow is more prominent. The third (solution **L3**) considers a rectangular box of physical size of only 5x5 inner disk radii (Fig. 4, Fig. 6). Similar to solution S4, the total mass flow is dominated by the disk wind. This high resolution simulation zooms into the innermost region around the star. In particular, the neutral line is clearly resolved. We finally discuss another example (**L5**) in which the stellar wind is dominating the disk wind. This simulation perfectly evolves into final stationary state. For L5 the velocity injection profile is chosen differently from the examples discussed above in order to increase the disk flow magnetization. All parameter runs show a similar gross behavior indicating that our run S2 with lowest resolution is sufficient in order to investigate the main features of the flow evolution. In general, a high stellar wind mass loss rate will stabilize the outflow.

4.2. The first evolutionary stages

During the first stages of the long-term evolution the magnetospheric structure is characterized by the following main features: The *winding-up* of the dipolar poloidal field, the formation of a *neutral field line*, a *transient axial jet* feature, a two component outflow consisting of a *stellar wind* and a *disk wind*.

4.2.1. Winding-up of the poloidal field

The winding-up process of poloidal magnetic field due to differential rotation between star and disk and the static initial corona induces a toroidal field (Fig. 4) with a positive sign along field lines located outside the slowly emerging neutral field line. Inside the neutral field line B_ϕ has negative sign. This is in difference to OP97 and other simulations assuming a monotoniccally distributed initial field.

Torsional Alfvén waves propagate outwards distorting the initial field structure. After about $t = 40$ these waves reach the outer boundary (Fig. 2). The region beyond the wave front remains completely undisturbed. The region between the Alfvén wave front and the flow bow shock is adjusted to a new equilibrium and also remains in equilibrium until it is reached by the generated outflow (See the density contour lines close to the disk in Fig. A2. The grey scale density plots cannot show this feature). Within this Alfvén wave front the magnetic field becomes distorted from its initial force-free state (compare the field line structure of the closed loops in Fig. 2 for $t \leq 30$). The distortion of the force-free field due to propagating Alfvén waves results in Lorentz forces initiating an axial 'jet' feature close to the axis. As we will see later, this axial jet, however, is a transient feature.

The winding-up of poloidal magnetic field seems to be similar to the effect proposed by Lovelace et al. (1995). However, in our case, this process is initiated by the differential rotation between star and hydrostatic corona. Only later, the wound-up toroidal field is maintained by both, differential rotation between star and disk and the inertia of the outflow.

4.2.2. A neutral field line dividing stellar and disk field

The wound-up magnetic field lines stretch forming a neutral field line of vanishing field strength. The matter around this field line is distributed in a layer of low density (Fig. 4). Around this layer an expanding 'bubble' is formed due to the additional magnetic pressure due to toroidal fields which disrupts the initial dipolar field structure (Fig. 3). When the bubble has left the grid, the field lines which are separated by the the neutral line remain disconnected. This is due to the differential rotation between star and disk. The actual appearance of the axial jet and the low density bubble depends mainly on the mass flow rates from disk and star. The bubble is most prominent in simulation S4 where the disk mass flow rate is largest.

4.2.3. A transient axial jet feature

In the beginning of the simulations a jet feature evolves along the rotational axis. Its pattern velocity is about $0.2\,v_{\rm K,i}$ (S2) or $0.3\,v_{\rm K,i}$ (L3). Such an axial jet is known as a characteristic result of MHD simulations performed in the recent literature (Hayashi et al. 1996; Goodson et al. 1997, 1999; Goodson & Winglee 1999; Kudoh et al. 1998). It is often claimed that this feature is connected to the real (protostellar) jets observed on the AU-scale. Apart from the fact that the spatial dimension and velocity do not fit with the observations, we will see that the formation of this feature is a result of the adjustment process of the initially hydrostatic state to a new dynamic equilibrium and will disappear on the long-term evolution.

Winding-up of the initially force-free magnetic field by differential rotation during the first time steps immediately leads to a not force-free field configuration. The resulting magnetic forces accelerate the material of the initially hydrostatic corona forming an axial jet. This process works as long as initially distributed coronal matter is present at this location. As time develops the jet feature becomes weaker and weaker. Disk wind and the stellar wind become the dominant flow pattern and the axial jet dies out after about $t > 100$ (Fig. 2). In comparison, in simulation L1 (FE99), where a stellar wind is absent, the coronal density along the axis decreases until it is below the numerically critical value and the simulation stops.

The intermittent character of the axial jet flow is best seen in the velocity structure (Fig. 5). The velocity vectors of the axial flow are largest during the first time steps. However, after sweeping-out the initial corona, a weak wind flow from the stellar surface succeeds the jet.

4.2.4. The disk wind

The disk wind accelerates within tens of grid elements from its low injection speed to fractions of the Keplerian speed. The acceleration mechanism is mainly due to the centrifugal force on the disk matter reaching the non-rotating corona, where the gravitational force is balanced by the pressure and not by a centrifugal force as in the disk. The flow is already super Alfvénic due to the weak dipolar field strength in the disk. Thus, magneto-centrifugal acceleration along the inclined dipole type field lines of the initial magnetic field is *not* the acceleration mechanism. More above the disk also the Lorentz force along the field contributes to the acceleration (see Sect. 4.4.3.). The inclination angle between field lines (equivalent to the outflow direction) and the disk depends on the mass flow rate. For the parameter range investigated we see no indication for a disk wind collimation because the Lorentz force points away from the axis (see below).

4.2.5. The stellar wind

The rotating stellar magnetosphere generates a stellar wind. Due to the strong magnetic field close to the star the flow starts sub-Alfvénic. It is initially magneto-centrifugally driven with a roughly spherical Alfvén surface located at $1.5r_{\rm i}$ (L3) or closer (S2, S4, L5) to the stellar surface. The most dominant flow pattern of the stellar wind is in the part with the widest opening angle (Fig. 5). Although the Lorentz force points radially inwards no collimation is observed because of a strong pressure gradient. Depending on the mass loss rates the stellar wind evolves faster or slower than the disk wind (Fig. 5).

4.3. The long-term evolution

The long-term evolution of the flows depends critically on the choice of inflow boundary conditions into the corona. The total mass flow rate into the corona determines how fast the flow will establish a (quasi-)stationary state. The stellar wind - disk wind mass flow ratio determines (i) the opening angle of the outflow, (ii) the opening angle of the cone of the neutral line which is the boundary layer between the stellar wind and the disk wind, and (iii) the stationarity of the axial flow (see Table 2). In general the outflow undergoes a highly time-variable and turbulent evolution. However, after relaxation of the MHD system from the initial magneto hydrostatic state into the new *dynamical* equilibrium, we observe an outflow from disk and star distributed smoothly over the whole hemisphere and moving predominantly in spherically radial direction.

In simulation S2 the flow structure is highly time-variable over many hundreds of periods. The intermediate region between the two components – stellar wind and disk wind – is characterized by turbulent motions of very low velocity. But also the disk wind seems to be unstable. During the intermediate time evolution only the flow pattern along the z-axis relaxes. Compared to the evolution of the stellar wind, the disk wind needs definitely more time to establish a stationary structure. However, after all these turbulent evolutionary steps, with few changes in the general appearance of the flow pattern over hundreds of rotational periods, *after about 2000–2500 rotations a quasi-stationary outflow has been established* over the whole grid (Fig. 2). Only the region around the neutral line dividing stellar and disk wind and the region along the z-axis is subject to small scale instabilities. Interestingly, the flow along the symmetry axis which shows a stable behavior during the intermediate time evolution, finally becomes unstable. A conical

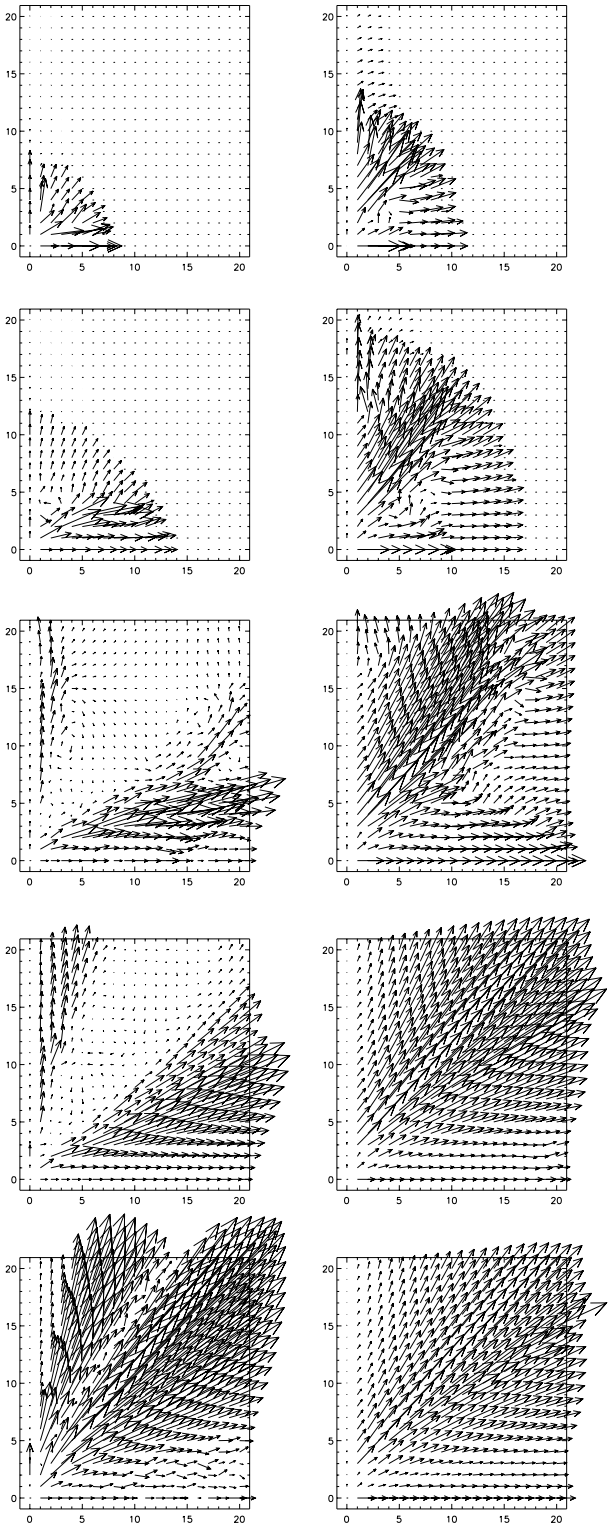

Fig. 5. Evolution of the poloidal velocity in the simulations S2 (*left*) and S4 (*right*). Time steps (from *top* to *bottom*). $t = 10, 20, 100, 500, 2500$ (S2) and $t = 5, 10, 20, 100, 600$ (S4). Vectors scale only within each frame.

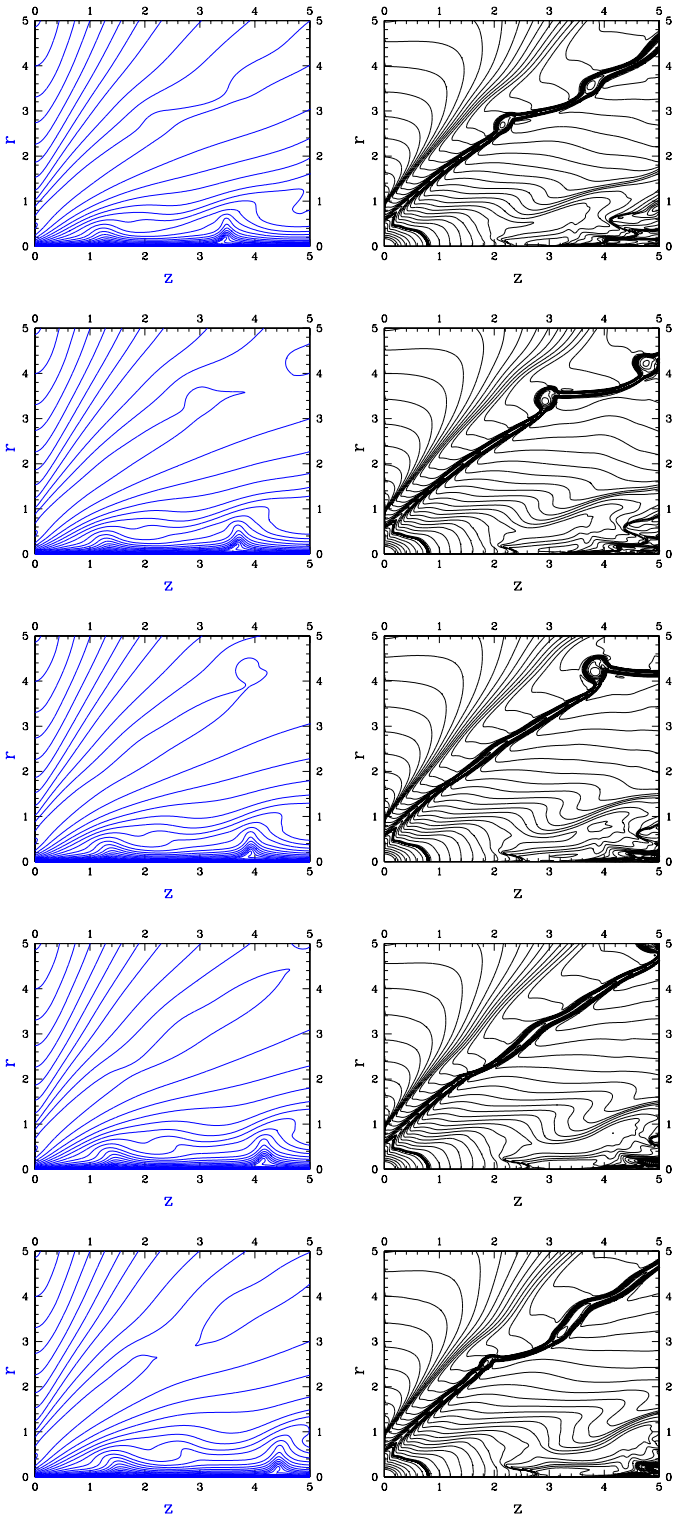

Fig. 6. Highly time-resolved evolution of simulation L3. Poloidal magnetic field lines (*left*) and density contours (*right*). Time steps $t = 200, 201, 202, 203, 204$ (from *top* to *bottom*).

flow consistent of a knotty structure evolves with a full opening angle of $30°$. At this time the opening angle of the neutral layer cone dividing stellar wind from disk wind has been increased compared to the intermediate time steps. This de-collimation of the outer flow causes a de-stabilization of the axial flow. In this

sense, the stellar wind flow is stabilized by the ambient (disk wind) pressure. The formation of knots and instabilities along the symmetry axis depends on the stellar wind mass flow rate (see below). The full opening angle of 'knot flow' is about 30°to 50°. We emphasize that due to the knot size and knot spacing, these features are not correlated to the observed knots of protostellar jets. It seems more related to QPO's observed in X-ray binaries. The knot velocity is about 10% of the Keplerian speed at the disk inner radius.

In simulation S4 the quasi-stationary state is reached earlier after about 200 inner disk rotations according to the smaller box size (Fig. 3). The region around the neutral field line is resolved better. We observe the formation of a wavy structure with an amplitude of $0.5\,r_{\rm i}$ and a wavelength of $r_{\rm i}$. These 'waves' travel outwards and leave the grid. The wave generation is somewhat arbitrary in time. Whereas the region enclosing the neutral layer first seems to have reached a steady state at about $t = 100$, at $t = 600$ the wave structure evolves again. This is related to the evolution along the symmetry axis. Here, in the contrary, at $t = 100$ the simulation still showed a wavy pattern, whereas at $t = 600$ a smooth steady state has evolved. The flow structure at $t = 400$ seems to be completely smooth and stable. The long-term evolution shows that this stability is in fact a transient feature as far as the neutral layer region is concerned (see below).

Simulation L3 shows that the neutral line has a complex structure. Two current sheaths emerge, one from the stellar radius, the other from the inner disk radius (Fig. 4). These are indicated by the density and poloidal magnetic field 'islands' emitted along this field line (Fig. 4, time step 80 and 160). Fig. 6 shows the evolution of the solution L3 with a high time resolution $\Delta t = 1$ after $t = 200$. At this time the simulation has not yet evolved into a quasi-stationary state. It can be seen how plasmoids are formed and move outwards along the neutral line. Most probably, this would be a region of on-going reconnection processes. A similar behavior was found first by Hayashi et al. (1996) including also magnetic diffusion in their treatment. However, the simulation lasted only for one inner disk rotational period (with a star at rest). Our long-term simulations show that the formation of such plasmoids will continue. We do not believe that the lack of diffusion in our treatment is a serious problem concerning this point because the time scale given by the plasmoid velocity is smaller than the time scale given by magnetic diffusion.

Fig. 5 shows the poloidal velocity vectors of the simulations S2 and S4 at selected time steps (compare to Figs. 3 and 4). The general feature is that the axial jet feature seen in the first time steps disappears. The outflow exhibits a two-component structure. Depending on the inflow density profile the 'asymptotic' (i.e. close to the grid boundaries) velocity profile changes slightly. High velocities (larger than $v_{\rm K,i}$) are only observed far from the axis. For solution S2 we obtain an asymptotic speed of $1.5\,v_{\rm K,i}$ for both components with a velocity profile decreasing across the neutral field line. The flow velocity along the axis is $0.2\,v_{\rm K,i}$. For solution S4 the asymptotic speed of $1.5\,v_{\rm K,i}$ for the stellar wind component and with a velocity profile increasing across the neutral field line $2\,v_{\rm K,i}$. The latter is due to the low density at this point. The disk wind has not yet accelerated to high velocities. This is due to the wide opening angle of the stellar wind cone and the small physical grid size. The flow velocity along the axis about $0.5\,v_{\rm K,i}$. For solution L5 the 'asymptotic' speed of the stellar wind is low and $\leq v_{\rm K,i}$. The velocity profile is in general similar to that of solution S4.

The duration of our simulation runs (L3, L5, S2, S4) is not limited by numerical reasons. They have been terminated when the flow evolution has reached a *quasi* stationary state. For simulation S2 this means that after about 2500 rotations the main pattern in the flow evolution does not change anymore. In particular, the outer part of the wind flow does not vary in time, while knots are still generated along the axis. For simulation S4, after 400 time steps most of the flow region is in a stationary state. Only the wavy structure along the neutral field line, which is also connected to the formation of knots, continuously evolves and disappears. This structure is *not* a dangerous instability for the outflow (see also Fig. 7). For solution L3, the simulation has been terminated when parts of the flow (the outer disk wind flow) had reached a stationary state. The inner solution close to the axis does not reach such a stationary state. In this case, our intention is to investigate the neutral line with better spatial resolution. Simulation L5 was terminated some time after the stationary state has been reached for the whole outflow.

4.4. A stationary final state: a radial outflow evolved from an initially dipolar magnetosphere

The main result of our simulations is that the initial dipolar magnetosphere evolves into a spherically radial outflow consisting of two components. Depending on the inflow parameters (mass flow rates, magnetic field strength) our simulations reach a quasi-stationary state. A weak non-stationarity may be present along the neutral field line, which is dividing the stellar wind from the disk wind. Also, for a weak stellar wind flow a turbulent flow pattern may evolve along the axis. Such outflows we call *quasi-stationary*, if the main flow pattern does not change in time. The disk wind and the outer cone of the stellar wind reach a kind of stationary state, where the density profile and field line structure remain almost constant in time.

For the S2 solution the half opening angle of stellar wind cone is about $55°$. This angle remarkably changes during the flow evolution. During the initial evolutionary decades the turbulent region between the stellar wind and the disk wind collimated the stellar wind to a narrower cone. Clearly, such a neutral line is a rather unstable situation. Reconnection will most probably occur which we cannot properly treat with our ideal MHD approach. Increasing the numerical resolution (simulation L3) shows the emission of plasmoids along the neutral line (see below). Fig. 7 shows an overlay of three time steps of solution S2 at $t = 2600, 2650, 2700$ clearly indicating the stationary character of disk wind and most parts of the stellar wind together with the non-stationary axial flow and the small-scale wave pattern along the neutral field line.

In the case of solution S4 the quasi-stationary state is reached earlier after about $t = 400$ (Fig. 3). The comparatively large

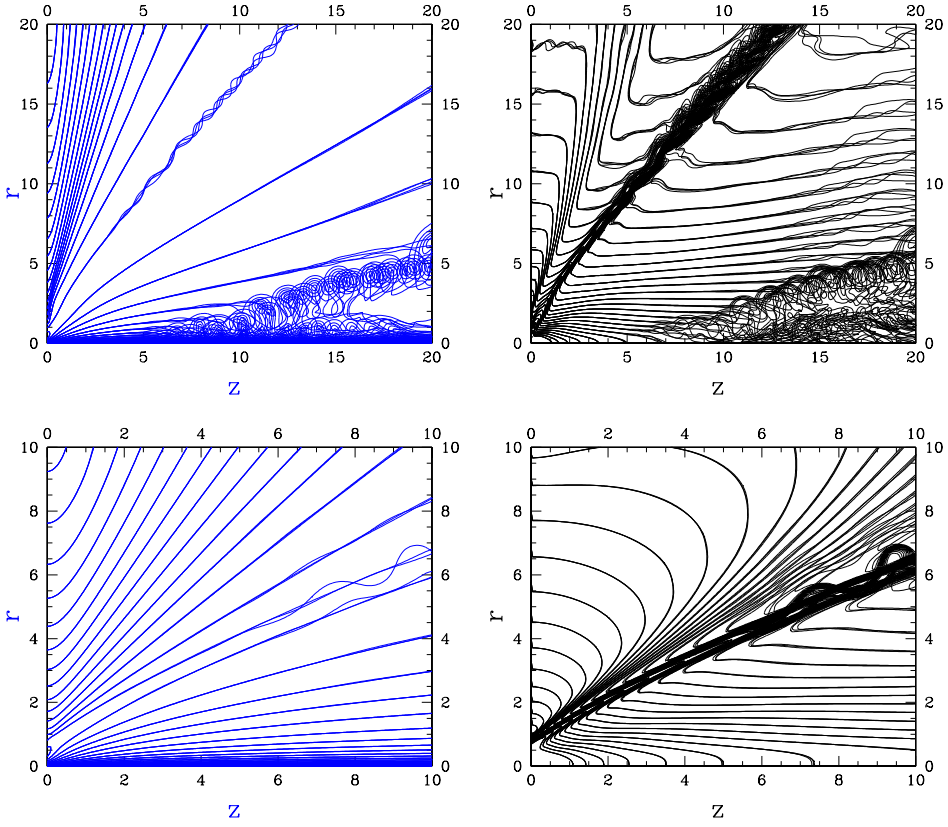

Fig. 7. Evolution of simulation S2 (upper) and S4 (lower) on the very long time scale. Shown are overlays of the poloidal field lines (*left*) and density contours (*right*). Three time steps are superposed, $\tau = 2600, 2650, 2700$ (S2) and $\tau = 575, 600, 625$ (S4).

Table 2. Terminal poloidal velocity of the wind components from the disk $v_{\rm p,disk}^{\rm max}$, from the star $v_{\rm p,star}^{\rm max}$, along the axis $v_{\rm p,axial}$, and from the gap $v_{\rm p,gap}^{\rm max}$, time when stationary state has been reached $t_{\rm s}$, and the inclination angle between disk and neutral layer α for the different simulations.

	$v_{\rm p,disk}^{\rm max}$	$v_{\rm p,star}^{\rm max}$	$v_{\rm p,axial}$	$v_{\rm p,gap}^{\rm max}$	$t_{\rm s}$	α
L1	1.0	?	?	?	?	?
S2	1.0	1.5	0.2	1.5	2500	35°
S4	1.5	2.1	0.6	1.5	400	60°
L3	1.0	1.3	0.2	1.7	?	50°
L5	0.9	1.0	0.2	3.0	150	35°

stellar wind mass flow rate stabilizes the flow along the axis and no turbulent pattern evolves. On the other hand, due to the low disk wind mass flow rate the half opening angle of the neutral line cone is smaller. It is 35° compared to 55° for solution S2. Again, Fig. 7 demonstrates the stationarity of the simulation with an overlay of three time steps $t = 575, 600, 625$. In comparison with solution S2 now the whole flow pattern is stationary. In particular the region along the axis remains stable. The only time-dependent feature is the neutral line exhibiting a slowly variable wave structure.

Increasing (i) the total mass flow rate and (ii) also the stellar wind to disk wind mass flow ratio will result in an almost perfectly stationary flow (solution L5; see below). Having a similar mass flow ratio, also the opening angle is similar to solution S2. The stationarity of solution L5 will be investigated in more detail below.

The blobs (or rather tori) generated in simulation S2 move with pattern speed of about 0.1 the Keplerian speed at r_i. Their size is about the inner disk radius but depends from the mass flow ratio and the numerical resolution. We emphasize that due to the knot size and time scale of knot formation in our simulation, their connection with the jet knots observed in protostellar jets on the large scale distance of tens of AU is questionable. This statement also holds for comparable structures observed in similar simulations presented in the literature (Ouyed & Pudritz 1997, Goodson et al. 1997, 1999; Goodson & Winglee 1999).

On the other hand, from the unstable character of the axial flow together with the lack of collimation we may conclude that the model configuration investigated in our paper is unlikely to produce collimated jets. Furthermore, we hypothesize that this behavior may be the one of the reasons why highly magnetized star-disk systems – containing magnetic white dwarfs or neutron stars – do not have jets.

In general, the maximum terminal poloidal velocity is of the order of the Keplerian speed at the disk inner radius (see Table 2). The speed is highest along the field lines from the gap due to the low flow density. The axial flow speed is low. Its mass density depends on the injection parameters and could be relatively large (S4, L5) or low (L3, S2), but is generally less than 10% of the density at the inner disk radius. The maximum stellar wind speed is reached along field lines with the largest opening angle and is above the Keplerian speed at the disk inner radius (Fig. 5). The same holds for the maximum disk wind speed.

However, in this case the maximum speed is reached along the field lines with a foot point at small radius. This is partly due to length of the acceleration distance, partly due to the rapid rotation of the disk material at small radii.

4.4.1. The question of dipolar accretion

In all our different simulation runs we never observe a signature of dipolar accretion as it is would be expected from models of young stellar jet formation (e.g. Camenzind 1990, Shu et al. 1994). Instead, a magnetically driven wind develops from the stellar surface. Note that this strong stellar outflow is *permitted* but *not prescribed* by the inflow boundary condition along the star, since the inflow velocity is very low. We emphasize that even in our simulation L1 for a non rotating star (Fendt & Elstner 1999), where no stellar wind can develop, no dipolar accretion occurred. Therefore, we believe that it is not the boundary condition which prevails the matter from falling from the disk to the star. In fact, dipolar accretion has never been observed in the literature of numerical MHD simulations considering the star-disk interaction (e.g. Hayashi et al. 1996, Goodson et al. 1997, Miller & Stone 1997), but this might also be caused by the comparatively short time evolution in those simulations.

We think that the main reason that hinders the dipolar accretion is the choice of the co-rotation radius equal to the inner disk radius. Only disk material orbiting inside the co-rotation radius could be accreted along the field lines.

It is clear that such an accretion process along converging field lines is difficult to treat numerically. Certainly, this important topic has to be investigated more deeply. We defer this to a future paper.

4.4.2. The question of collimation

The quasi-stationary two-component outflow obtained in our simulations shows almost *no indication for collimation*. This seems to be in contradiction to the literature (OP97, Romanova et al. 1997). However, the non-collimation of the flows can be explained following the analysis of Heyvaerts & Norman (1989). They have shown that only jets carrying a net poloidal current will collimate to a cylindrical shape. However, in our case we have an initially dipole type magnetosphere and the final state of a spherically radial outflow enclosing a neutral line with a poloidal magnetic field reversal. The toroidal field reversal also implies a reversal of the poloidal current density with only a weak *net* poloidal current. In such a configuration, a self-collimation of the flow as obtained by OP97 or Romanova et al. (1997) cannot be achieved. In both of these publications a net poloidal current flows along the *monotoniccally* distributed field lines.

One might expect to obtain the OP97 results of a collimating jet as a limiting case in the present simulations, just due to the fact that the inflow boundary condition along the disk is the same as in their setup. However, we think that this is not possible since the initial field structure and, thus, the flux distribution in the lower boundary is completely different. A combination of the OP97 field distribution together with a central dipole might do the job. Still, the problem would be the very different field strength of both components, since the dipolar field will decrease by a factor of 10–50 towards the inner disk radius. Thus, the stellar field is always dominating the numerical simulation. We defer the treatment of such a completely new numerical setup to a future paper.

Apart from this argument concerning a flow self-collimation we mention the hypothesis raised by Spruit et al. (1997) claiming that a "poloidal collimation" is responsible for the jet structure. Such a poloidal collimation would rely on the magnetic pressure onto the jet flow from the disk magnetic field *outside* the jet. Their condition for poloidal collimation, a disk magnetic field distribution $B_{\rm P} \sim r^{-q}$ with $q \leq 1.3$, is clearly not satisfied in our case of a dipole type field distribution along the disk (which is conserved from the initial condition because of flux conservation). For a dynamo generated field in the disk this condition is satisfied (Rüdiger et al. 1995). This holds also for the disk field distribution of OP97. In this sense, our simulations are consistent with Spruit et al. (1997), although we do not argue that our results support their hypothesis that "poloidal collimation" is the main process to produce jets.

We further note the results of Ustyugova et al. (1999) who claim that the shape of the numerical box influences the degree of collimation. A rectangular box extended along the symmetry axis would lead to an artificial flow collimation, whereas a quadratic box simulation (as used in our simulation) did not result in a collimated structure. A recent study by Okamoto (1999) also has raised strong arguments against a MHD self-collimation. In particular, he claims that *electric current-closure* will inhibit a self-collimation, a point which is not always considered in MHD jet models. Current-closure, however, is satisfied in our model due to the reversed dipole type initial field.

Nevertheless, strongly collimated astrophysical jet flows are observed. For the moment we speculate that an increase of the *disk field strength* would probably enhance the degree of collimation. So far we doubt whether an increase of the size of the computational box will be sufficient, because in our model the field distribution and mass flow rate decrease strongly with radius.

4.4.3. The final steady state - application of stationary MHD

It is well known from standard MHD theory that an axisymmetric stationary MHD flow is defined by five integrals of motion along the magnetic flux function $\Psi(r,z) \equiv 2\pi \int \boldsymbol{B}_{\rm P} \cdot d\boldsymbol{A}$. Stationarity implies the following conserved quantities along the flux surface Ψ: The mass flow rate per flux surface, $\eta(\Psi) \equiv \mathrm{sign}(\boldsymbol{v}_{\rm P} \cdot \boldsymbol{B}_{\rm P})\, \rho v_{\rm P}/B_{\rm P}$, the iso-rotation parameter $\Omega_{\rm F}(\Psi) \equiv (v_\phi - \eta B_\phi/\rho)/r$, the total angular momentum density per flux surface, $L(\Psi) \equiv r(v_\phi - B_\phi/\eta)$, and the total energy density $E(\Psi)$. Therefore, for a time-dependent axisymmetric simulation evolving into a stationary state, these functions must be constant along the field lines. Fig. 8 demonstrates such a behavior for the example solution L5 for the quantities $\eta(\Psi)$,$\Omega_{\rm F}(\Psi)$ and $L(\Psi)$. An overlay of each of these functions with the con-

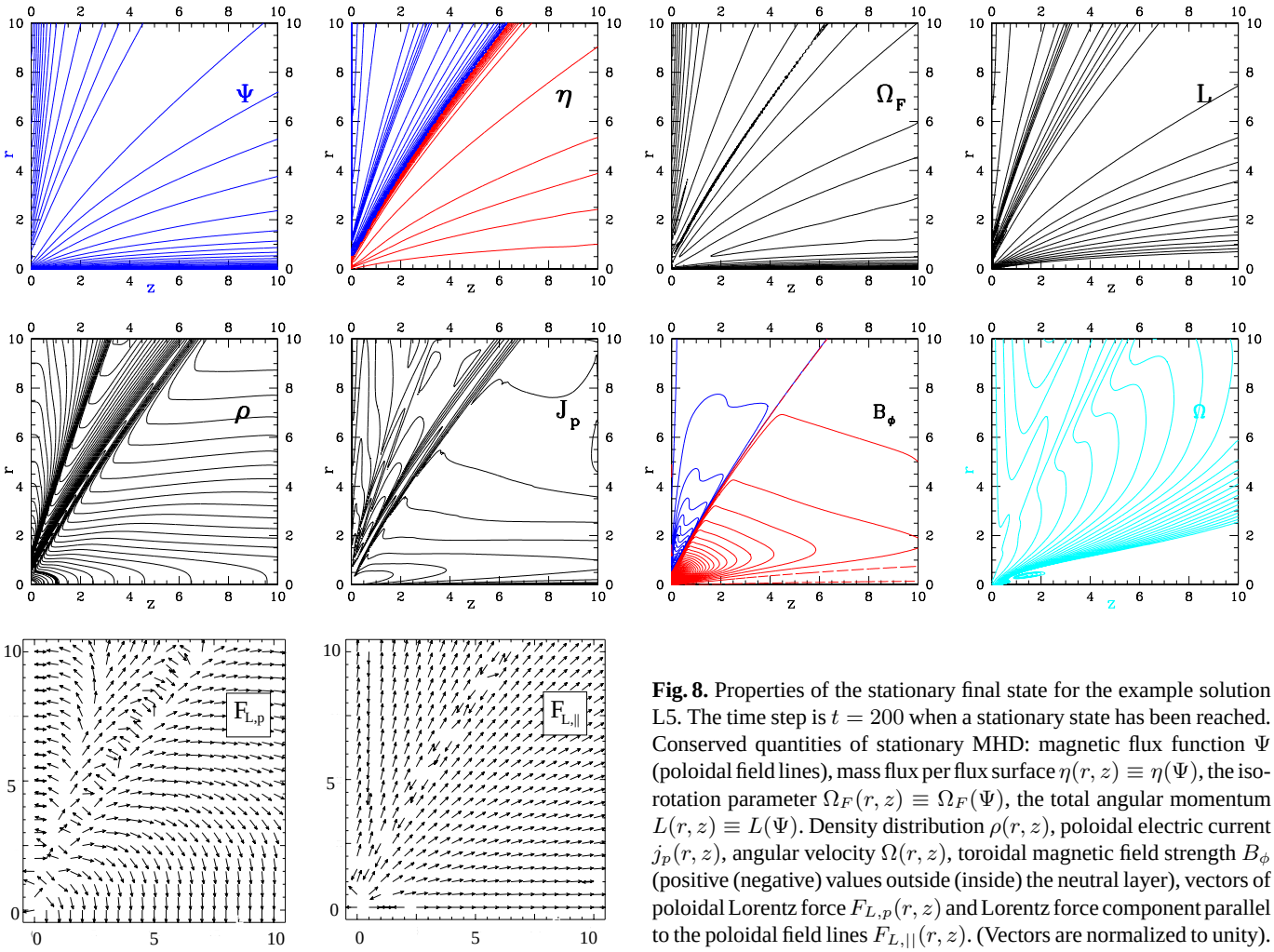

Fig. 8. Properties of the stationary final state for the example solution L5. The time step is $t = 200$ when a stationary state has been reached. Conserved quantities of stationary MHD: magnetic flux function Ψ (poloidal field lines), mass flux per flux surface $\eta(r,z) \equiv \eta(\Psi)$, the isorotation parameter $\Omega_F(r,z) \equiv \Omega_F(\Psi)$, the total angular momentum $L(r,z) \equiv L(\Psi)$. Density distribution $\rho(r,z)$, poloidal electric current $j_p(r,z)$, angular velocity $\Omega(r,z)$, toroidal magnetic field strength B_ϕ (positive (negative) values outside (inside) the neutral layer), vectors of poloidal Lorentz force $F_{L,p}(r,z)$ and Lorentz force component parallel to the poloidal field lines $F_{L,||}(r,z)$. (Vectors are normalized to unity).

tour plot of the field lines $\Psi(r,z)$ would show that the contours are perfectly 'parallel'. This clearly proves the stationary character of the final state of simulation L5. For comparison, Fig. 8 shows the distribution of the poloidal electric current density, the toroidal magnetic field, and the angular velocity of the plasma.

For a stationary solution it is interesting to investigate the Lorentz force projected parallel and perpendicular to the field lines. The poloidal Lorentz force vectors (Fig. 8) show that in the region of the highest poloidal velocities, the Lorentz force is more or less aligned with the field lines. In the region of low poloidal velocity the main component of the Lorentz force is perpendicular to the field lines. As discussed above (Sect. 4.4.2.) the perpendicular component of the Lorentz force acts collimating inside the neutral layer and de-collimating outside the neutral layer.

Another interesting feature is the *direction* of the parallel component of the Lorentz force (see Fig. 8). Close to the disk boundary there is a region where this component changes sign and the Lorentz force is therefore *decelerating* the matter[1]. This demonstrates that in the stationary final state the Lorentz force is *not* the main driving mechanism of the disk material from the disk into the corona. It is only at a larger height above the disk that the parallel component of the Lorentz force accelerates the plasma.

As a summary of this section we show in Fig. 9 the final stationary state of the example solution L5 plotted for all four hemispheres. This figure (and only this one) is *rotated by* $90°$ with the z-axis in vertical direction. This gives a comparative look how the simulation has evolved from the initial dipolar structure to the spherically radial outflow final state.

5. Summary

We have performed numerical simulations of the evolution of a stellar dipole type magnetosphere in interaction with a Keplerian accretion disk using the ideal MHD ZEUS-3D code in the axisymmetry option. The simulations are lasting over hundreds (or even thousands) of rotational periods of the inner disk. The central star is rotating with a co-rotation radius chosen as the disk inner radius. A smooth mass inflow is prescribed into the corona which is initially in hydrostatic equilibrium. The initial dipole type magnetic field distribution is force-free. The density

[1] In Fig. 8, this region is only one vector element wide. However, a better resolution shows that this region extends to about $z = 1$ along the outer disk

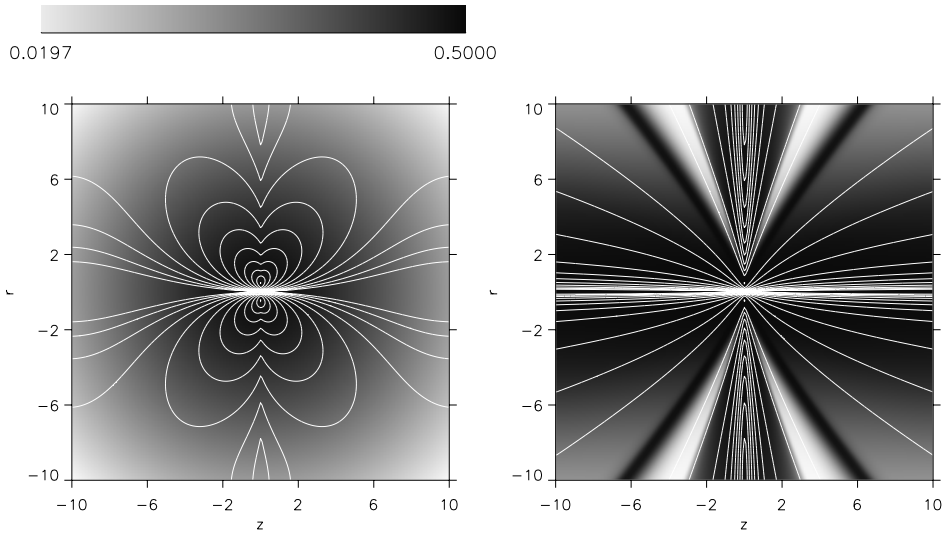

Fig. 9. Density distribution and poloidal magnetic field lines of simulation L5 for initial time step (*left*) and for the final stationary state (*right*) plotted for all four hemispheres.

and velocity profile as well as the magnetic field profile along the inflow boundary has not been changed during the computation.

Our main results are summarized as follows.

(1) The initial dipolar field breaks up by a combined action of the winding-up process due to differential rotation between the star and disk and the wind mass loss from star and disk. 'Stellar' and 'disk' field lines remain disconnected after the disrupting 'bubble' has left the computational grid.
(2) A two-component MHD wind leaves both the disk and the rotating star moving away in radial direction. The two components are divided by a neutral field line. The magnetic field direction (both, poloidal and toroidal) is positive outside the neutral line and negative inside. This field reversal is a characteristic difference from jet simulations of OP97 and Romanova et al. 1997.
(3) Mainly dependent on the wind mass flow rates a stationary or quasi-stationary state evolves after hundreds or thousands of inner disk rotations. The disk wind always evolves into a stationary state. A high stellar wind mass loss rate supports 'complete stationarity', i.e. stationarity also for the stellar wind component.
(4) The initial driving mechanism of the disk wind are centrifugal forces of the rotation matter leaving the disk in vertical direction. At larger heights above the disk, this matter becomes magnetically accelerated. The maximum flow speed is about the Keplerian velocity at the inner disk radius. The hight speed is observed in the outer layers of the stellar wind and in the upper layers of the disk wind.
(5) Depending on the stellar wind mass flow rate, knots may form along the symmetry axis. The size of these knots is about the inner disk radius, but also depends weakly on the grid resolution. The knot pattern velocity is about 10% of the Keplerian speed at the disk inner radius. The full opening angle of 'knot flow' is about 30°to 50°. Concerning the knot's size and spacing, it is unlikely that these features are correlated to the observed knots in protostellar jets, but may be connected to QPO's in X-ray binaries.
(6) There is almost no indication for a flow self-collimation. The flow structure remains more or less conical. We believe that the main reason for the lack of collimation is the field reversal between stellar and disk wind also implying a reversal in the poloidal current density. Thus, the net poloidal current will be weak. This is a major difference to OP97 and Romanova et al. 1997. However, this result could also interpreted in terms of a missing poloidal collimation mechanism proposed by Spruit et al. (1997).
(7) No signature of an accretion stream along a dipolar field channel towards stellar surface is observed. This may be due to the fact that the dipolar field has completely disappeared or due to our choice of the co-rotation radius.

Our results are in general applicable to any star-disk system which is coupled by magnetic fields. One critical aspect may be that we assume a fixed boundary condition for the magnetic field in the disk. However, if the field structure in the corona changes as drastically as we have shown, this might influence also the magnetic flux distribution in the disk. But then, for a proper time-dependent disk boundary condition, the disk structure should be treated in a more detailed manner. This however, is beyond the scope of the present paper. From our results we like to put forward the following main hypotheses.

(8) Star-disk systems are supposed to have a two component wind/jet structure.
(9) A strong stellar field (equivalent to a low stellar mass loss rate) leads to instabilities along the rotational axis. A strong and stable jet is unlikely in such objects. This may be one reason why highly magnetized stars with disks like neutron stars or magnetic white dwarfs do *not* have jets. A disk field generated by a turbulent dynamo could be a better candidate for driving the jet.
(10) The current model of magnetized accretion in young stars along dipolar field lines from disk to star have to be reconsidered. The magnetospheric structure often inferred from stationary models (Camenzind 1990; Shu et al. 1994)

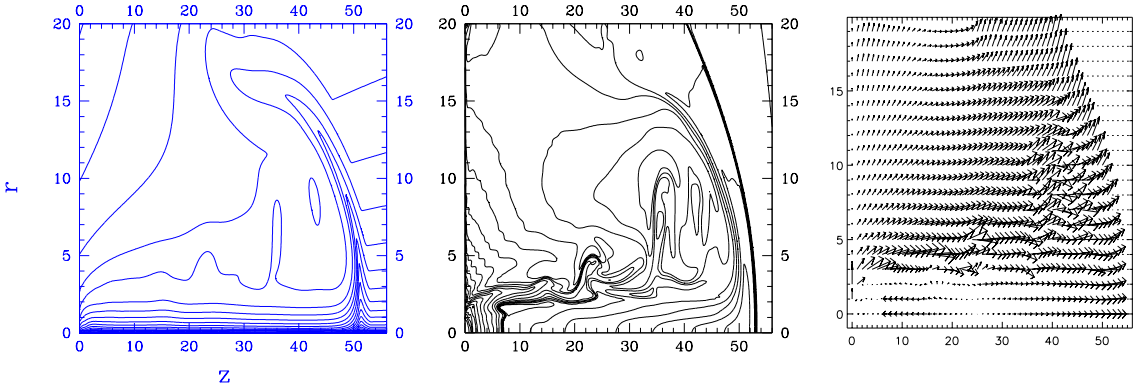

Fig. A.1.. Numerical test example. Re-calculation of the OP97 jet model. From *left* to *right*: Poloidal magnetic field lines, density contours, and poloidal velocity vectors at $t = 100$, calculated with $\beta_i = 0.28$. The location of the shock front is the same for all three plots (in difference to OP97).

may completely change if the time-dependent evolution is considered.

Acknowledgements. Encouraging discussions with R. Pudritz and R. Ouyed are acknowledged by C.F. We thank the LCA team and M. Norman for the possibility to use the ZEUS code.

Appendix A: numerical tests

Here, we will discuss numerical test solutions. The first test example is the recalculation of the OP97 solution of an axisymmetric jet propagating from a rotating Keplerian disk. Such a scenario is similar to the one treated in the present paper, however, with a parabolic-type initial potential field configuration and without a central rotating star. Fig. A.1 shows the result of our simulation at $t = 100$. At this time the jet bow shock has traveled 52 units along the z-axis. In the long-term evolution, the location of the magneto-sonic surfaces agrees with the results of OP97. However, as a (minor) difference we note that for our test simulations fitting to the OP97 results the value for the plasma-beta is smaller by about a factor of $\sqrt{4\pi}$ compared to OP97. We use the original ZEUS code normalized with $P_{\rm gas} \sim B^2/2$ (instead of the usual $P_{\rm gas} \sim B^2/8\pi$) (user manual). Therefore, in order to match the definition of the plasma beta as $\beta_i = 8\pi P_i/B_i^2$, one must define the field strength properly (this gives a factor of $\sqrt{4\pi}$ in the field strength). Thus, the difference in the β_i may be due to a different normalization applied in OP97 (Ouyed 2000, private communication). We have deduced this factor by *comparing both simulations*. Additionally, it becomes understandable with the normalization of the ZEUS code magnetic field. For $\beta_i = 1.0$ in *our* simulations the jet solution is appropriate slower, reaching only $z = 42$ after 100 time steps[2]. Concluding that our recalculation of the OP97 model was successful, we note however the tiny 'wave' pattern of our density contours (Fig. A.1). This wave pattern is present only in the hydrodynamic variables, but not in the magnetic field. These density variations are less then 10%.

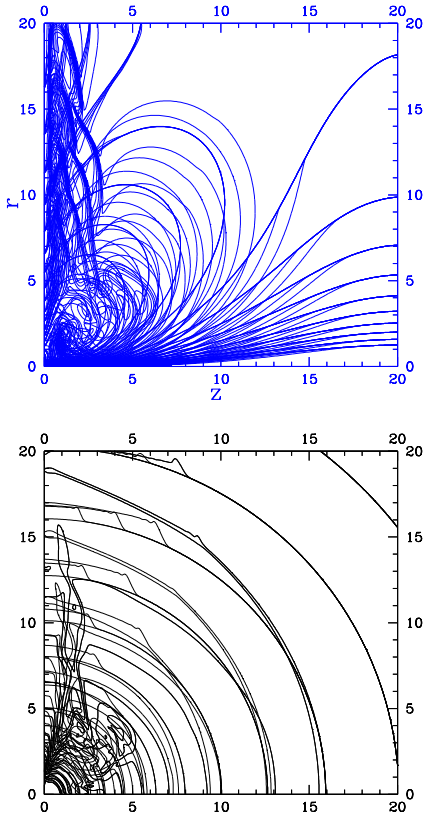

Fig. A.2. Numerical test example. Solution L1 without stellar rotation. Overlay of a couple of initial time steps (at $t = 0, 10, 20, 30, 40, 50$). Poloidal magnetic field lines (*top*) and density contours (*bottom*). Thick lines indicate the initial distributions. The solutions perfectly match in the regions not yet disturbed by the inflow boundary condition. The long term evolution of this solution is shown in FE99.

[2] This is, by the way, remarkably similar to the location of the shock front in the velocity plot (Fig. 6) in OP97, which is different from the one in their density plot (Fig. 3). However, we note that a 'wrong' plasma-beta must be visible in the location of the magneto-sonic surfaces. This is not the case. Therefore, we conclude the differences in β_i are just due to a different field normalization in the actual codes

As a second example for a numerical test, we show an overlay of the density contours and poloidal field lines of six initial time steps of the simulation L1, *before* the torsional Alfvén wave has passed the outer (upper) grid boundary. It can be seen that upstream of the bow shock front the magneto-hydrostatic initial condition remains in perfect equilibrium. Thus, force-freeness of the initial magnetic field as well as the hydrostatic equilibrium is satisfied with good accuracy. Without the inflow boundary condition at $z = 0$ the initial equilibrium will remain unchanged.

References

Blandford R.D., Payne D.G., 1982, MNRAS 199, 883

Burrows C.J., Stapelfeldt K.R., Watson A.M., et al., 1996, ApJ 473, 437

Camenzind M., 1990, In: Klare G. (ed.) Magnetized disk-winds and the origin of bipolar outflows. Rev. Mod. Astron. 3, Springer, Heidelberg, p. 234

Fendt C., Camenzind M., Appl S., 1995, A&A 300, 791

Fendt C., Elstner D., 1999, A&A 349, L61

Goodson A.P., Winglee R.M., Böhm K.-H., 1997, ApJ 489, 199

Goodson A.P., Böhm K.-H., Winglee R.M., 1999, ApJ 524, 159

Goodson A.P., Winglee R.M., 1999, ApJ 524, 142

Hawley J.F., Stone J.M., 1995, Comp. Physics Comm. 89, 127

Hayashi M.R., Shibata K., Matsumoto R., 1996, ApJ 468, L37

Heyvaerts J. Norman C.A., 1989, ApJ 347, 1055

Kudoh T., Matsumoto R., Shibata K., 1998, ApJ 508, 186

Kwan J., Tademaru E., 1995, ApJ 454, 382

Lovelace R.V.E., Romanova M.M., Bisnovatyi-Kogan G.S., 1995, MNRAS 275, 244

Lopez, R., Raga A., Riera A., Anglada G., Estalella R., 1995, MNRAS 274, L19

Miller K.A., Stone J.M., 1997, ApJ 489, 890

Okamoto I., 1999, MNRAS 307, 253

Ouyed R., Pudritz R.E., 1997, ApJ 482, 712 (OP97)

Ouyed R., Pudritz R.E., 2000, submitted

Pudritz R.E., Norman C.A., 1983, ApJ 274, 677

Romanova M.M., Ustyugova G.V., Koldoba A.V., Chechetkin V.M., Lovelace R.V.E., 1997, ApJ 482, 708

Rüdiger G., Elstner D., Stepinski T.F., 1995, A&A 298, 934

Shu F.H., Najita J., Ostriker E., et al., 1994, ApJ 429, 781

Spruit H.C., Foglizzo T., Stehle R., 1997, MNRAS 288, 333

Stone J.M., Norman M.L., 1992a, ApJS 80, 753

Stone J.M., Norman M.L., 1992b, ApJS 80, 791

Ustyugova G.V., Koldoba A.V., Romanova M.M., Chechetkin V.M., Lovelace R.V.E., 1995, ApJ 439, L39

Ustyugova G.V., Koldoba A.V., Romanova M.M., Chechetkin V.M., Lovelace R.V.E., 1999, ApJ 516, 221

A&A 395, 1045–1060 (2002)
DOI: 10.1051/0004-6361:20021442

Astronomy & Astrophysics

Formation of protostellar jets – effects of magnetic diffusion

C. Fendt[1,2] and M. Čemeljić[2]

[1] Universität Potsdam, Institut für Physik, Am Neuen Palais 10, 14469 Potsdam, Germany
[2] Astrophysikalisches Institut Potsdam, An der Sternwarte 16, 14482 Potsdam, Germany
e-mail: cfendt@aip.de;cemeljic@aip.de

Received 24 May 2002 / Accepted 24 September 2002

Abstract. Protostellar jets most probably originate in turbulent accretion disks surrounding young stellar objects. We investigate the evolution of a disk wind into a collimated jet under the influence of magnetic diffusivity, assuming that the turbulent pattern in the disk will also enter the disk corona and the jet. Using the ZEUS-3D code in the axisymmetry option we solve the time-dependent resistive MHD equations for a model setup of a central star surrounded by an accretion disk. The disk is taken as a time-independent boundary condition for the mass flow rate and the magnetic flux distribution. We derive analytical estimates for the magnitude of magnetic diffusion in a protostellar jet connecting our results to earlier work in the limit of ideal MHD. We find that the diffusive jets propagate slower into the ambient medium, most probably due to the lower mass flow rate in the axial direction. Close to the star we find that a quasi stationary state evolves after several hundred (weak diffusion) or thousand (strong diffusion) disk rotations. Magnetic diffusivity affects the protostellar jet structure as follows. The jet poloidal magnetic field becomes de-collimated. The jet velocity increases with increasing diffusivity, while the degree of collimation for the hydrodynamic flow remains more or less the same. We suggest that the mass flux is a proper tracer for the degree of jet collimation and find indications of a critical value for the magnetic diffusivity above which the jet collimation is only weak. We finally develop a self-consistent picture in which all these effects can be explained in the framework of the Lorentz force.

Key words. accretion, accretion disks – MHD – ISM: jets and outflows – stars: mass loss – stars: pre-main sequence – galaxies: jets

1. Introduction

Observations of young stellar objects (YSOs) have revealed two main features during the phase of star formation – the presence of accretion disks and energetic outflows, often observed as bipolar jets (Mundt et al. 1984; Lada 1985; Ray et al. 1996). Images and spectra show that these flows are of high-velocity ($\simeq$300 km s^{-1}) and well collimated (opening angle $<10^\circ$ on scales of 1000 AU). The data also suggest that the jet collimation must be achieved already close to the central source, at distances $\leq$100 AU. The jet mass outflow rates are $\sim 10^{-10}$–10^{-8} $M_\odot$/yr and typically a factor 10–100 smaller than the disk accretion rates.

Besides the special case of protostellar jets, all astrophysical jets detected so far seem to be attached to objects where an accretion disk is indicated to be present. In particular, this holds for jets observed in radio loud active galactic nuclei and quasars (Bridle & Perley 1982), highly energetic galactic objects as Sco X–1 (Padman et al. 1991), and microquasars (Mirabel et al. 1992).

Send offprint requests to: C. Fendt,
e-mail: cfendt@aip.de

Therefore, the similarities between jets from the different sources imply that the basic mechanism for jet formation should be the same. For protostellar jets, the observed mass and momentum fluxes exclude the possibility of a thermally or radiation pressure driven wind. The observed fluxes are much higher than the protostar could provide (DeCampli 1981; Königl 1986). The conclusion is that it is the magnetic field which is responsible for protostellar jet formation – acceleration and collimation of the initial stellar or disk wind (Pudritz & Norman 1983; Camenzind 1990). This magnetic field can be generated by some dynamo process either in the central young star itself, or the surrounding accretion disk, or it could be provided by the interstellar medium as a "fossil" field. What kind of mechanism turns the in-flowing matter of the accretion disk into an outflow from the disk (or the star) is still not really known, although it seems to be clear that magnetic fields play a major role (Ferreira 1997).

Examples of time–dependent MHD simulations of the jet formation include models of collimating disk winds, where this disk is taken as a boundary condition for the outflow (Ouyed & Pudritz 1997, hereafter OP97), models that consider the interaction of a stellar dipolar magnetosphere with the accretion

disk as well as the disk structure itself (Miller & Stone 1997), or some combination of both approaches (Fendt & Elstner 1999, 2000, hereafter FE00).

In this paper, we are interested in a time–dependent simulation of the *resistive* MHD equations for the corona above the accretion disk around a young star. The underlying disk provides a fixed boundary. The presence of a large scale poloidal magnetic field provided by the disk is assumed. After a brief theoretical introduction in Sect. 2, we describe our model and the numerical approach in Sect. 3, with emphasis on the effect of magnetic diffusion. For the numerical approach, we introduced magnetic diffusion in the ZEUS-3D MHD code. Tests of our code are included in Appendix. The results for protostellar jets are discussed in Sect. 4. We compare our diffusive MHD simulations of jet formation with the non–diffusive case.

2. Magnetic jets from accretion disks

Despite a tremendous amount of work concerning the formation of magnetic jets (e.g. Blandford & Payne 1982; Pudritz & Norman 1983; Lovelace et al.1987; Heyvaerts & Norman 1989; Pelletier & Pudritz 1992; Li et al. 1992; Contopoulos 1994; Fendt et al. 1995; Kudoh & Shibata 1997a, 1997b; Fendt & Memola 2001) the mechanism which actually launches the jet from the disk remains unclear. Most of the papers dealing with the theory of magnetized accretion disks driving jets have been following the principal approach of Blandford & Payne assuming stationarity, axisymmetry and self-similarity (Königl 1989; Wardle & Königl 1993; Li 1995; Ferreira 1997). After all, it is clear now that the launching of a jet from the accreting disk can be described as a purely *magnetic* process. Ferreira (1997) has derived trans–Alfvénic, stationary self-similar jet solutions with a smooth transition from a resistive disk, where the Lorentz forces are actually responsible for lifting the accreting gas in vertical direction.

Progress has been achieved, too, in the simulation of the time-dependent MHD jet formation from accretion disks. Two major, distinct approaches in order to deal with the complexity of the jet formation process have been undertaken so far. One approach is to take the rotating disk as a fixed boundary condition for the simulation of the jet. Depending on the choice of the initial setup (magnetic field, density and pressure) and the choice of the gravitational potential, the numerical results differ in the degree of collimation and the velocity of the resulting jet flow. From an initially split-monopole magnetic field configuration, collimated, non-stationary outflows were obtained (Ustyugova et al. 1995). In this simulation non-equilibrium initial conditions and a softened gravitational potential were used. For the same configuration, but for a stronger magnetic field, Romanova et al. (1997) again obtained stationary but only weakly collimated flows. Ouyed & Pudritz (1997) studied the jet formation embedded in a disk corona initially in hydrostatic equilibrium and in pressure balance with the disk surface. Essentially, after 400 disk rotations, a stationary collimated jet flow emerges. Similar results were obtained by another recent study taking into account also the time-dependent behavior of the disk boundary condition (namely the field inclination) due to the evolution of the disk wind (Krasnopolsky et al. 1999). The main advantage of the approach of a fixed disk boundary condition is the numerical stability of simulation over a long time scale. The jet launching itself – the process of diverting accreting matter in the disk into an outflow – cannot be treated this way.

The other approach was therefore to include the simulation of the disk structure in the simulation. The first step in this direction was made by Uchida & Shibata (1985) and Shibata & Uchida (1985, 1986) in their pioneering work considering time-dependent jet formation. Essentially, the authors show that the magnetic twist of the magnetic field induced by the rotation of the disk gives rise to Lorentz forces pushing the disk material upwards. The back-reaction of the magnetic field on the disk (magnetic braking) may lead to a sub-Keplerian disk rotation. These results have been confirmed by Stone & Norman (1994). MHD simulations considering the diffusive accretion disk in interaction with a stellar dipolar magnetosphere reveal the collapse of the inner disk after a few rotations (Hayashi et al. 1996; Goodson et al. 1997; Miller & Stone 1997). At the same time, episodic ejection of plasmoids are generated in outer parts of the disk wind. A collimated axial jet feature is observed. However, probably because of numerical reasons, these simulations could be performed only for a few or tens of Keplerian periods of the inner disk. Therefore, the results may depend strongly on the initial setup. The assumption of constant diffusivity in the disk and the corona is probably not very realistic.

The long-term evolution of such models has been investigated by FE00, however without treating the disk structure in the simulation. They find that the axial jet feature observed by Goodson et al. (1997) disappears on longer time-scales. A two-component quasi-stationary outflow (from disk and star) evolves after thousands of rotational periods. This flow is uncollimated on the spatial scales investigated, in agreement with the observations indicating a jet radius 100 times larger then the grid size of the numerical simulations discussed above.

Recent MHD simulations of the jet formation from accretion disks by Matsumoto et al. (1996), Kudoh et al. (1998, 2002b, 2002a), and Kato et al. (2002) investigate the disk-jet *interrelation* and may probably explain the time-dependent ejection mechanism in the jets. However, as we have pointed out above for the model setup of a magnetic dipole surrounded by a disk, these simulations also were carried out for several rotation periods only. The question remains as to how the system under consideration behaves on a long time scale. Further, the simulations apply the approach of *ideal* MHD, an approximation, which is most probably not strictly valid for accretion disks, especially for protostellar accretion disks. In this respect, the work by Kuwabara et al. (2000) is of particular interest as the authors extend the ideal MHD approach and include *resistivity* in the jet formation process. Comparing their simulations to the close environment of a supermassive black hole, Kuwabara et al. derive a *critical value* for the strength of magnetic diffusion. A normalized magnetic diffusivity below 0.05 may explain the observed activity in active galactic nuclei. In this case, the mass accretion and jet launching takes place intermittently. The paper also demonstrates the difficulty of carrying out such simulations, as gravity has been treated applying a softened

potential. On the other hand, this simplification allows for a simulation lasting up to 5 rotations of the accretion torus.

Again, we note that it is just the limitation in the time evolution which lead us to the decision to take into account the accretion disk only as a boundary condition. In this paper, we are mainly interested in the jet formation process (acceleration and collimation) and not in the jet launching mechanism from the accretion disk. In particular, we think it is essential to investigate whether a jet actually survives also on long time scales.

3. Model setup and equations

The paradigm accepted in this paper is the jet launched from a diffusive, turbulent accretion disk around a young stellar object. We may expect that the turbulence pattern in the disk may also enter the disk corona and the jet, and that the jet flow itself is subject to turbulent diffusion. We will discuss this idea of a diffusive protostellar jet below. Despite the fact that we take into account the effect of magnetic diffusion for the jet formation, our model setup is similar to the models in OP97 and FE00.

3.1. Resistive MHD equations

In order to model the time-dependent evolution of jet formation, the set of resistive MHD equations to be solved is

$$\frac{\partial \rho}{\partial t} + \nabla \cdot (\rho \boldsymbol{v}) = 0 \tag{1}$$

$$\rho \left[\frac{\partial \boldsymbol{u}}{\partial t} + (\boldsymbol{v} \cdot \nabla)\, \boldsymbol{v} \right] + \nabla(p + p_A) + \rho \nabla \Phi - \frac{\boldsymbol{j} \times \boldsymbol{B}}{c} = 0 \tag{2}$$

$$\frac{\partial \boldsymbol{B}}{\partial t} - \nabla \times \left(\boldsymbol{v} \times \boldsymbol{B} - \frac{4\pi}{c} \eta \boldsymbol{j} \right) = 0 \tag{3}$$

$$\rho \left[\frac{\partial e}{\partial t} + (\boldsymbol{v} \cdot \nabla)\, e \right] + (p + p_A)(\nabla \cdot \boldsymbol{v}) - \frac{4\pi}{c^2} \eta \boldsymbol{j}^2 = 0 \tag{4}$$

$$\nabla \cdot \boldsymbol{B} = 0 \tag{5}$$

$$\frac{4\pi}{c} \boldsymbol{j} = \nabla \times \boldsymbol{B}. \tag{6}$$

For the gas law we apply a polytropic equation of state, $p = K\rho^\gamma$ with a polytropic index $\gamma = 5/3$. Hence, we do not solve the energy Eq. (4). Instead, the internal energy of the system is defined with $e = p/(\gamma - 1)$. Such a simplification is not expected to affect the result of our simulations much, as the resistive dissipation term in the energy equation is negligible compared to the other terms because of the factor $1/c^2$ (see also Miller & Stone 1997). The magnetic diffusivity is denoted by the variable η (see Sect. 3.3). Additional to the hydrostatic pressure p, an Alfvénic turbulent pressure $p_A \equiv p/\beta_T$ with $\beta_T = \text{const.}$ (see OP97, FE00) is included. Alfvén waves from the highly turbulent accretion disk are expected to propagate into the disk corona, providing the perturbations for some degree of turbulent motion also in the jet. As shown by OP97 the additional Alfvénic turbulent pressure is able to support a *cold* corona above a protostellar accretion disk as suggested by the observations.

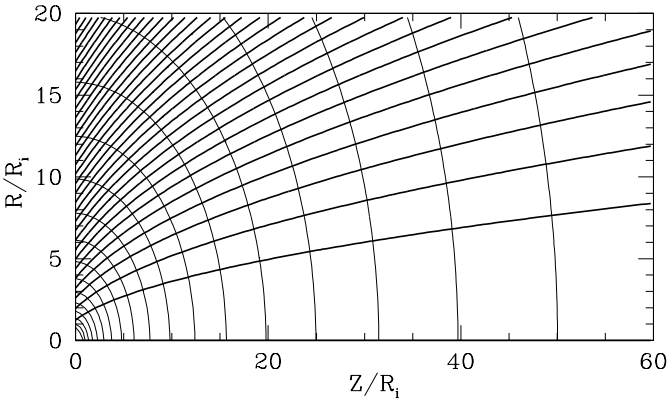

Fig. 1. Initial setup for the jet simulation. Shown is the part of the computational box close to the origin (the part of the "inner jet"). The initial hydrostatic density distribution is indicated by the *thin* concentric isocontours. *Thick* lines denote the initial poloidal field lines of a force-free potential field.

We solve the equations above using the ZEUS-3D code (Stone & Norman 1992, 1992) in the 2D-axisymmetry option for cylindrical coordinates (r, ϕ, z). We apply a point mass gravitational potential $\Phi = -1/\sqrt{r^2 + z^2}$ located in the origin. A finite physical magnetic resistivity is added to the original ZEUS-3D ideal MHD code. Tests of our now diffusive ZEUS code are presented in the Appendix.

For our computations we normalize the variables to their value measured at the inner disk radius r_i (see OP97, FE00), e.g. $\rho \rightarrow \rho/\rho_i$. The subscript "i" assigns that the variables are taken at this radius. The time is measured in units of a Keplerian rotation at the inner disk radius. The normalized equation of motion eventually being solved with the code is

$$\frac{\partial \boldsymbol{v}'}{\partial t'} + (\boldsymbol{v}' \cdot \nabla')\, \boldsymbol{v}' = \frac{2\, \boldsymbol{j}' \times \boldsymbol{B}'}{\delta_i \beta_i \rho'} - \frac{\nabla'(p' + p'_A)}{\delta_i \rho'} - \nabla' \Phi'. \tag{7}$$

The coefficients $\beta_i \equiv 8\pi p_i / B_i^2$ and $\delta_i \equiv \rho_i v_{K,i}^2 / p_i$ with the Keplerian speed $v_{K,i} \equiv \sqrt{GM/r_i}$, correspond to the plasma beta and the Mach number of the gas at the inner disk radius. For a "cold" corona with $p'_A > 0$, it follows $\beta_T = 1/(\delta_i(\gamma - 1)/\gamma - 1)$. In the following we will omit the primes and will discuss only normalized variables if not explicitly declared otherwise.

3.2. Initial and boundary conditions

As the numerical simulation of a magnetized disk is still a difficult task and is not yet fully resolved, we chose to study the formation of the jet flow independent of the evolution of the accretion disk. A precise *disk*-wind theory would predict the amount of angular momentum and energy carried away from the disk. Here, we prescribe the disk as a fixed, time-independent boundary condition for the jet.

One may question the combination of a magnetically diffusive disk corona and a steady-state disk magnetic field distribution. Naturally, the time scales of the disk evolution are definitely longer than those for the jet flow (except for the unknown mechanism responsible for the jet knots). Also, for a disk jet, the disk is acting as a source for magnetic flux.

This can be achieved either by a dynamo process working in the disk generating the magnetic field or just by advection of the interstellar magnetic field by the disk towards the central star. The time scale for both processes is longer than the jet time scale and, thus, we may safely assume a fixed magnetic flux as accretion disk boundary condition.

As initial condition we choose the same setup as OP97. The initial poloidal magnetic field is defined by the current-free potential field configuration of the ϕ-component of the vector potential, $A_\phi = \left(\sqrt{r^2 + (z_\mathrm{d} + z)^2} - (z_\mathrm{d} + z) \right) / r$. The dimensionless disk thickness z_d satisfying $(z_\mathrm{d} + z) > 0$ for $z < 0$ is introduced in order to avoid any kinks in the field distribution. The initial coronal density distribution is in hydrostatic equilibrium, $\rho = (r^2 + z^2)^{-3/4}$. The initial corona is defined by two free parameters δ_i and β_i.

The disk itself as a boundary condition for the jet flow is in centrifugal balance and penetrated by a force-free magnetic field. As the disk boundary condition is time-independent, the initial potential field magnetic flux from the disk is concerned. The toroidal component of the magnetic field in the ghost zones ($z < 0$) is chosen as $B_\phi(z < 0) = \mu_\mathrm{i}/r$, where μ_i is another free parameter. The mass flow rate from the disk surface into the corona is defined by the injection velocity and the density of the injected material. With the launching angle $\Theta_0(r, z = 0)$ (measured from the jet axis), the velocity field in the ghost zone is $\boldsymbol{v} = (v_r, v_\phi, v_z) = v_\mathrm{inj}(v_\mathrm{p} \sin\Theta_0, v_\mathrm{K}, v_\mathrm{p} \cos\Theta_0)$ for $r \geq 1$ with v_inj as a free parameter. For $r \leq 1$ the inflow velocity is set to zero, which actually defines the inner edge of the disk. The inflow density is given as $\rho_\mathrm{d} = \kappa_\mathrm{i} r^{-3/2}$, with κ_i as a free parameter.

Besides the disk "inflow" boundary condition, the boundary condition along the symmetry axis is set as "reflecting", and along the two remaining boundaries as "outflow" (see also Stone & Norman 1992, 1992; OP97; FE00). Figure 1 shows the initial setup of a hydrostatic density distribution together with the potential magnetic field for the part of the computational box close to the origin (the region of the "inner jet").

Our choice for the free parameters is the following. We have $\delta_\mathrm{i} = 100$, $\kappa_\mathrm{i} = 100$, $\mu_\mathrm{i} = -1.0$, and $v_\mathrm{inj} = 0.001$, similar to OP97 and FE00 in order to allow for a comparison of the results. For the plasma-β we choose $\beta_\mathrm{i} = 0.282$ (which is equivalent to OP97, but is based on the original ZEUS-3D normalization) or a lower value $\beta_\mathrm{i} = 0.141$ which has some numerical advantages[1]. The lower β_i does not change the general behavior of the jet. The jet evolution is faster (in physical time, not in CPU time) and the Alfvén surface is slightly shifted in z-direction, but the jet internal structure remains very similar.

3.3. Magnetic diffusion in jets

Most of the models of MHD jet formation deal with the collimation and acceleration of a plasma flow in the case of *ideal* MHD. However, it seems to us quite possible that magnetic diffusivity may play an important role in protostellar jet formation. There are (at least) two reasons which may account for that.

[1] See also Appendix A in FE00 for the different choice of β_i in OP97 (equal to unity) and here and in FE00.

The first reason may be the fact that the jet material of young stellar objects is not fully ionized, in difference from the case of relativistic jets in AGN or microquasars. The fraction of ionization (the ratio of ion to neutral particle density) derived from optical observations is about 0.5−0.01 with the tendency to decrease along the jet (Hartigan et al. 1994; Bacciotti & Eislöffel 1999). From this it can be expected that diffusive effects may indeed affect the MHD configuration. Theoretical studies on this topic have just started recently. We refer to Frank et al. (1999) who investigated the asymptotic MHD jet equilibria under the influence of ambipolar diffusion, showing that the initial MHD configuration of the jet changes due to ambipolar diffusion at least on the parsec scale. Another reference is Ferreira (1997) who showed the essential role magnetic diffusion plays for the launching mechanism of the jet from the accretion disk.

The other reason for the existence of turbulence in the jet formation region is the fact that the jet launching object itself – the accretion disk – is highly turbulent. While turbulence is an intrinsic property of accretion disks (and *necessary* for the accretion process itself), turbulence can further be driven in the disk corona by the differential rotation of the disk, which winds-up the coronal magnetic loops leading to powerful reconnection processes (see Miller & Stone 2000).

It seems to be natural to expect that the turbulent pattern being definitely present in the disk-jet interaction region becomes also advected with the jet/wind flow into the domains at greater height above the disk. We just note that additionally the interaction of the jet with the ambient medium leading to various kinds of instabilities increase the turbulent pattern in the jet (however, we do not expect that the latter process does affect the jet collimation region).

In Faraday's law (3), the ratio of the first to the second terms in the brackets is the magnetic Reynolds number. It can be represented by $R_\mathrm{m} = v\,L/\eta$, where L is a typical length scale and v is a typical velocity. Due to the large length scales in the astrophysical context, R_m based on the microscopic diffusivity is very large compared to unity. For a fully ionized hydrogen plasma the microscopic diffusivity is $\eta_\mu \sim r_\mathrm{e} c (v_\mathrm{th}/c)^{-3}$, where $r_\mathrm{e} = e^2/(m_\mathrm{e} c^2)$ is the classical electron radius, and $v_\mathrm{th} = \sqrt{k_\mathrm{B} T / m_\mathrm{e}}$ is the electron thermal speed. For $T = 10^4$ K, $v = 100\,\mathrm{km\,s^{-1}}$, and $L = 100$ AU we obtain $R_\mathrm{m} = v\,L/\eta_\mu \approx 10^{15}$.

It is clear that the relevant diffusivity in the protostellar disk and jet is most probably "anomalous" determined by macroscopic MHD instability phenomena (see above), with the resulting magnetic Reynolds number being much smaller. This *magnetic turbulence* we may parameterize the same way as in a Shakura-Sunyaev model for the hydrodynamical viscosity. We can define a *turbulent* magnetic diffusivity $\eta_\mathrm{T} = \alpha_\mathrm{m} v L$, where $\alpha_\mathrm{m} \leq 1$. As a characteristic velocity for the dynamical change of the system we might choose the poloidal Alfvén speed, $v_\mathrm{A} = B_\mathrm{p}/\sqrt{4\pi\rho}$. If we choose the size of our computational box r_max as a typical length scale and $\alpha_\mathrm{m} \approx 0.1$, we obtain $R_\mathrm{m} = v_\mathrm{A} r_\mathrm{max}/\eta_\mathrm{T} \approx 10$ as the typical magnetic Reynolds number for the *global* jet evolution. In difference, typical length and time scales are different if we are interested in the evolution of the local jet structure (as needed for example for the definition of the numerical time stepping in the code).

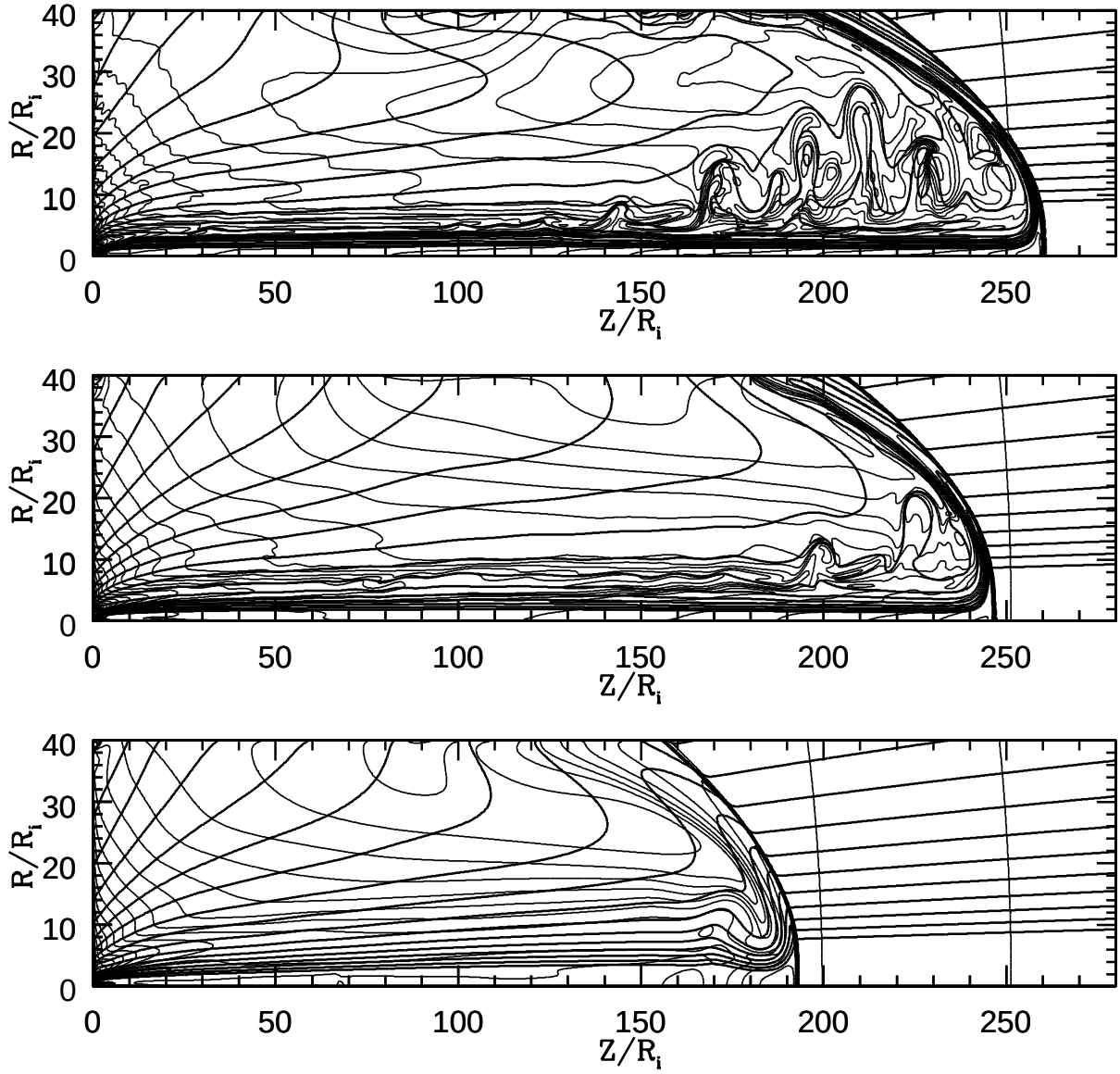

Fig. 2. Global evolution of the jet on a grid of $(z \times r) = (280 \times 40) r_{\rm i}$ with a resolution of 900×200 elements. Shown is the state of evolution after $t = 400$ rotations of the disk inner radius for different magnetic diffusivity, $\eta = 0$ (*top*), $\eta = 0.01$ (*middle*), and $\eta = 0.1$ (*bottom*). *Thin* lines denote 30 logarithmically spaced isocontours of density. *Thick* lines denote 20 and twenty linearly spaced magnetic flux surfaces (or poloidal field lines). The parameters are $\delta_{\rm i} = 100$, $\kappa_{\rm i} = 100$, $\mu_{\rm i} = -1.0$, $\beta_{\rm i} = 0.282$, and $v_{\rm inj} = 0.001$. Note the preserved initial hydrostatic density and force-free field distribution in front of the bow shocks. The figure demonstrates that the bow shock advances slower with increasing diffusivity.

It might be expected that the diffusivity throughout the jet and the disk corona differ considerably. However, it seems natural to expect the diffusivity in a corona close to the disk surface not to differ much from the value in the outer part of the disk. For simplicity, and since we are first interested in the general effect, our simulations are performed with a constant diffusivity parameter. To introduce a non-constant diffusivity is straight forward.

The local magnetic Reynolds number is also described by the ratio of the dynamic to the diffusive time scale $R_{\rm m} = \tau_{\rm diff}/\tau_{\rm dyn}$. Here we may define $\tau_{\rm diff} = \min(l^2/\eta)$ and $\tau_{\rm dyn} = \min(l/v_{\rm A})$, where l is the size of the numerical grid cell. Because of the internal structure of the jet, these minimum values can sometimes be well below the actual *global* magnetic Reynolds number described above, which is determined by the characteristic length scale of our simulation $L = r_{\rm max}$.

It is interesting to note that in the model of OP97 a *turbulent Alfvén pressure*, $p_{\rm A}$, has been introduced in order to establish a pressure equilibrium of a *cold* corona (or jet) above the (hot) accretion disk. Although this turbulence effect was taken into account for the pressure balance, OP97 did not consider it as a reason for a turbulent *magnetic diffusivity*. However, it is straight forward to relate the Alfvénic turbulent pressure $p_{\rm A}$ to a turbulent magnetic diffusivity $\eta_{\rm T}$. In order to derive such a relation, we now choose the turbulent velocity field $v_{\rm T}$ instead of the local Alfvén speed as the typical velocity for the turbulent diffusivity,

$$\eta_{\rm T} = \alpha_{\rm m} v_{\rm T} L. \qquad (8)$$

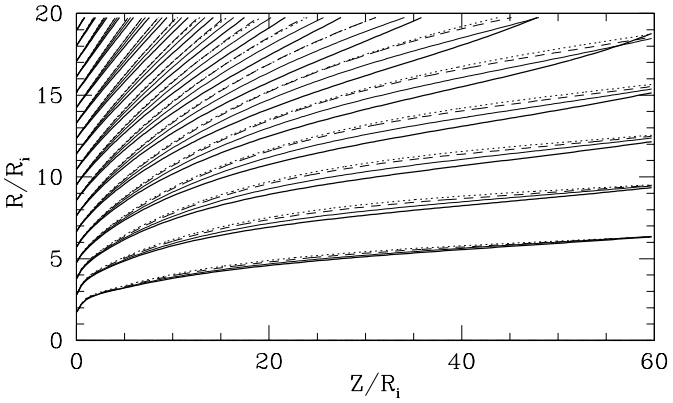

Fig. 3. The evolution of the inner jet approaches the quasi-stationary state. Shown are poloidal magnetic field lines in the case of $\eta = 0.1$ for different time steps, $t = 250, 300, 350, 400$ (*thick solid, thin solid, dashed* and *dotted* lines). Same parameter setup as in Fig. 2, except $\beta_i = 0.141$. Grid size 280×80 elements for a physical size of $(140 \times 40) r_i$. The picture shows how the poloidal magnetic field lines diffuse outwards but approach a (quasi)-stationary state after 400 rotations (see the dashed and dotted lines almost coinciding).

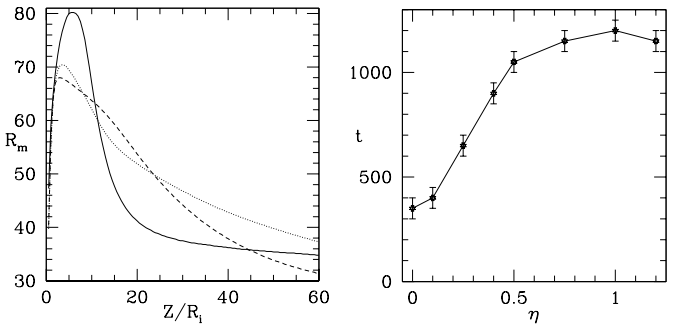

Fig. 4. Magnetic diffusivity and global time scales. *Left* Global magnetic Reynolds number as defined from the scale of the computational box of the inner jet $L = 20, v = v_A$. Shown is the R_m-profile along slices in z-direction at $r = 7, 13, 20$ (*solid, dotted, dashed* line, respectively), for the simulation run with $\eta = 0.1, \beta_i = 0.141$. The plot shows the variation of the typical velocity v, for which we have chosen the local Alfvén speed. *Right* Time of stationarity. This plot shows for different magnetic diffusivity the time period when the inner jet reaches a quasi-stationary state. This time is estimated from the evolution of the poloidal magnetic field lines (see Fig. 3) and the error bars indicate our uncertainty.

With the definition $\beta_T \equiv (c_s/v_T)^2$ and taking into account the fact that $c_s^2 = \gamma p/\rho$ for an adiabatic or polytropic gas law, we obtain

$$v_T^2 = \frac{\gamma}{\beta_T}\frac{p}{\rho}. \tag{9}$$

The normalization gives

$$v_T'^2 = \frac{p'}{\rho'}\frac{c_{s,i}^2}{v_{K,i}^2}\frac{1}{\beta_T}, \qquad \text{or} \qquad v_T'^2 = \rho'^{\gamma-1}\frac{\gamma}{\delta_i \beta_T}. \tag{10}$$

With the condition of sub-Alfvénic turbulence OP97 derived $\beta_T = 0.03$. With a typical value for $\delta_i \simeq 100$ and a "mean" value for the normalized density $\rho' \simeq 10^{-2}$ we obtain for the normalized magnetic diffusivity

$$\eta' \simeq 0.015\left(\frac{\alpha_m}{0.1}\right)\left(\frac{L'}{1.0}\right). \tag{11}$$

Since the diffusivity changes only weakly with the density, $\eta \sim \rho^{1/3}$, this provides a good estimate on the strength of magnetic diffusion. A self-consistent simulation would take into account the relation between diffusion and density as in Eq. (10). For comparison, we run a few of simulations with such a setup. So far, we find no significant difference to the computations with $\eta = \text{const}$.

4. Results and discussion

We now discuss the results of our numerical simulations considering the MHD jet formation under the influence of magnetic diffusion. For this, we have run simulations with a different parameter setup. The simulations were performed (i) in domains of different physical size in order to investigate the influence of boundaries and to obtain information about the large-scale flow, and also (ii) with different numerical resolution.

We detected numerical artifacts (a spurious velocity pattern) in the corners of the grid where outflow boundary conditions meets the other (inflow, reflecting) boundary conditions. In general, this artifacts remain localized close to the corners of the grid over many hundred of disk rotations. All the results discussed in this paper are not affected by these effects as we mainly concentrate on the inner part of the jet flow. We performed one reference set of global simulations with high resolution (numerical mesh of 900×200 grid points, physical grid of $(z \times r) = (280 \times 40) r_i$). In order to investigate effects which concern only the gross behavior the jet flow and not its structure in detail, we run another set of simulations with lower resolution (numerical mesh of 280×80 grid points, physical grid of $(z \times r) = (140 \times 40) r_i$). The much faster computation of the low resolution simulations allowed us to follow the jet evolution for a very long time even in the case of a high magnetic diffusivity (up to 4000 disk rotations). The computational domain was a factor 2 shorter in direction of propagation. All other parameters were the same as for the high resolution runs.

4.1. Formation of the global jet

The first point to be noted when comparing the large-scale evolution of the diffusive with the non-diffusive flow, is the different speed of the bow shock. With increasing magnetic diffusivity, the bow shock propagates slower. The bow shock pattern velocity is about $0.38, 0.35, 0.28$ for $\eta = 0, 0.01, 0.1$, respectively (Fig. 2). We will later see that, in apparent contrast, the jet velocity increases with η.

As in the case of ideal MHD simulations, before the bow shock front builds up, torsional Alfvén waves propagate from the disk surface into the corona slightly modifying the initial hydrostatic equilibrium. The super-Alfvénic flow catches up with and passes this wave front.

As the bow shock propagates through the corona it leaves behind a cavity of matter with dilute density and high velocity. The initially purely poloidal magnetic field becomes more and more helical. The toroidal magnetic field component is first generated by winding-up the initial poloidal field due to differential rotation between the disk and the static corona but later comes out as a natural result of the MHD flow due to the inertial forces of the matter.

The internal structure of the jet behind bow shock layer is smoother in the case of a non-vanishing magnetic diffusion (see Fig. 2). We note that also the "wiggly" structure in the density distribution close to the disk in the case of $\eta = 0$ is less prominent in the case of diffusive simulations. These "wiggles" seem to be a numerical artifact probably due to the density jump between the disk and the jet, however, the density variations are only of the order of some percent.

Here, we note another important point. In this paper we were interested in the cases of a typical MHD jet flow starting as a sub-Alfvénic (but super-slow magnetosonic) flow from the disk surface, being accelerated to super Alfvénic and super-fast magnetosonic speed, as e.g. described in the paper by Blandford & Payne (1982). This case often described as a *magneto-centrifugally driven* disk wind/jet differs from the case where matter is injected into the disk corona already with super Alfvénic speed. The latter case applies in the case of a relatively weak disk poloidal magnetic field as for example in the case of a central dipolar field with a strong gradient in radial direction. These winds are initially driven by the (toroidal) magnetic field pressure gradient in vertical direction (Lovelace et al. 1987; Contopoulos 1994; Fendt & Elstner 2000).

In this paper we are interested only in the classical case of MHD jet formation. However, in our simulations we note that the Alfvén surface moves as a function of time until the quasi-stationary state (see below) is reached. For a smaller than moderate magnetic diffusivity ($\eta = 0, ..., 0.5$), the location of the Alfvén surface is always within the active zones well above the accretion disk boundary. For higher diffusivity the Alfvén surface may advance into the disk for small radii and the character of the MHD flow is changed. We do not consider these cases in our discussion.

4.2. Inner jet

In the following we discuss the evolution of the inner substructure of the global jet close to the jet axis and the accretion disk. The size of this region is $60 \times 20 r_i$ and is comparable e.g. to the full grid in OP97. This part of the jet is not influenced from any outflow boundary condition or the jet evolution on the global scale. Note that the major part of the global jet is super fast magnetosonic, hence, there is no (physical) way to transport information from this part in upstream direction into the inner jet.

4.3. Quasi-stationary nature of the (inner) jet

As a major outcome of OP97 and FE00 it has been found that under a certain choice of boundary conditions the disk outflow

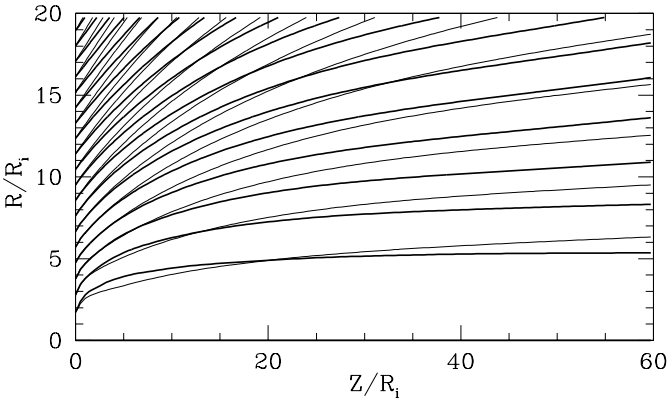

Fig. 5. The de-collimation of the stationary state poloidal magnetic field due to magnetic diffusivity. Same parameter setup as in Fig. 3. Shown is the poloidal magnetic field line distribution of the inner jet in the state of quasi-stationarity ($t = 400$) for vanishing diffusivity $\eta = 0$ (*thick*) and for $\eta = 0.1$ (*thin*).

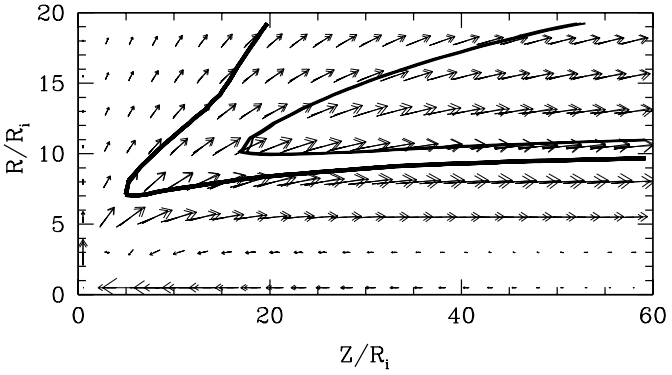

Fig. 6. Comparison of poloidal velocity vectors. Shown are the poloidal velocity vectors at the time of quasi-stationarity. Over-plot of the velocity field for the $\eta = 0$ simulation at $t = 350$ with the $\eta = 0.1$ simulation at $t = 400$. The de-collimation visible in the poloidal magnetic field lines (see Fig. 5) is *not* present here. The thick line indicates the Alfvén surface for $\eta = 0.1$, the thin line the fast magnetosonic surface.

may evolve into a stationary state after several hundreds of disk rotations. Such a stationary state solution provides an ideal test bed for investigation of the internal forces acting in the jet, since the well known equations of axisymmetric ideal MHD and its conservation laws may be used for interpretation of the jet flow.

In our present simulations considering the MHD jet formation under the influence of magnetic diffusion, we also find such stationary states. We denote them as *quasi-stationary* since – due to the large computational domain – such a behavior can be seen only in the inner region within reasonable computational time. The outer regions surrounding the (inner) stationary jet flow will further evolve in time. For the area of the inner jet the stationary state is reached after approximately $t = 350$ disk rotations in the case of ideal MHD. This time scale can be quite different in the case of a non-vanishing magnetic diffusion and also depends on the plasma-beta parameter β_i. Note that in spite of considering magnetic diffusivity, we use the same parameter setup as OP97 and FE00.

Figure 3 shows an over-plot of poloidal magnetic field lines resulting from our simulations at the time steps of $t = 250, 300, 350, 400$ disk rotations, respectively, in the case of relatively large magnetic diffusion $\eta = 0.1$. It can clearly be seen how the poloidal magnetic field lines first diffuse outwards from their position at $t = 250$ (which is close to the non-diffusive field distribution, see also Fig. 5). After some hundred of rotations more, the field distribution approaches the quasi-stationary state (note the dotted lines almost matching the dashed ones).

First, we note that the existence of such a quasi-stationary state might not necessarily be expected in the case of magnetic diffusion and instead one might think that the magnetic field will just decay forever. The reason, why a stationary state is possible in the case of a jet flow, is that with such a setup a loss of magnetic energy in the jet caused by diffusion can be replenished by the constant Poynting flux rising from the disk. This energy reservoir can be thought of as established constantly by the disk rotation and accretion and eventually by the gravitational potential of the central star. Note that also in the ideal MHD case the jet flow carries energy out of the computational box. Also this energy loss is balanced by the same way. The additional effect due to magnetic diffusivity is small compared to the total energy flow in the jet.

In general, our simulations show that with increasing η the flow reaches the quasi-stationary state at a *later* time. For a smaller than moderate magnetic diffusivity ($\eta = 0, ..., 0.5$), we find an approximately linear relation between this time and the diffusivity (Fig. 4, right panel). This is also the range where the jet flow is a classical MHD jet like the Blandford-Payne solution, starting as a sub-Alfvénic flow from the disk surface and crossing the Alfvén surface at some height above the disk. For higher diffusivity the Alfvén surface has been advanced into the disk for small radii and the character of the MHD flow is changed. We do not consider these cases in particular, however, we show the time of quasi-stationary state for completeness.

For comparison, the local time step accounting for magnetic diffusion and the Alfvén time step, together with the *global* magnetic Reynolds number R_m (defined by the jet size and a mean value for the jet Alfvén speed, see Sect. 3.3) and the related α_m are given in the Appendix in Table B.1 for the time when the quasi-stationary state is reached. In Table B.1 we have chosen a "typical" value for the Alfvén speed within the grid of the inner jet. That this is feasible, is shown in Fig. 4 (*left*) where we plot the variation of R_m along the jet in the case $\eta = 0.1$. As R_m does not change along the jet by more than a factor of two (this is similar for other diffusivity), this value provides a good estimate for the global jet dynamical behavior.

4.4. Jet velocity and collimation

The most interesting, since directly observable, quantities of a jet are its velocity and degree of collimation. In Fig. 6 we show the poloidal velocity vectors in the inner jet for a simulation without and with considering magnetic diffusion ($\eta = 0$ and $\eta = 0.1$), taken at that time step, when the flow has reached the quasi-stationary state.

The general point to mention is that the figures clearly show the self-collimating property of the MHD flow as the velocity vectors become more and more aligned with the jet axis as we go along the flow. However, there exists also a region of low collimation close to the disk where the velocity vectors point in radial direction (with $\simeq 45°$ half opening angle).

For the low magnetic diffusivity ($\eta < 0.05$) simulations we have observed an interesting feature. The apparent de-collimation of the poloidal magnetic field structure (Fig. 5), which is already present for a weak magnetic diffusivity ($\eta = 0.01$), is, however, not visible in the poloidal velocity (Fig. 6). In both cases, the flow evolution has reached a quasi-stationary state ($t = 400$). In contrast to ideal MHD, in the case of diffusive MHD, a miss-alignment between v_p and B_p is possible. Up to $\eta = 0.5$ the mismatch between the poloidal velocity and magnetic field vector is relatively weak for large z and about $5°-10°$ at intermediate heights above the disk. That means that we generally get a collimated stream along the axis, however, the mass load distribution varies implying a variation of the mass flow rate through the r and z-boundaries with η. If a larger magnetic diffusivity ($\eta > 0.1$) is applied, we observe also a de-collimation of the *mass flow* (see below).

In general, both the poloidal and toroidal velocity increase with increasing diffusivity. At the same time, the magnetic field components decrease with the increasing diffusivity. This is shown in Fig. 7 where we plot the velocity and field components along jet at a distance of 15 r_i from the jet axis. Thus, as a conclusion, the diffusive jet becomes faster. We discuss that point below in the context of the Lorentz forces acting in the jet.

However, two points should be mentioned concerning Fig. 7. The first is the *decrease* of toroidal velocity just above the disk surface. As the field line foot points rotate with Keplerian speed and the matter is corotating with the field lines, one would actually expect an increase of toroidal velocity, if the magnetic field is dominated by the poloidal component. In our case, we find at a certain radius along the disk surface that $B_\phi = B_\mathrm{p}$. Thus, the matter may substantially *slide along the field*. Just above the disk, the toroidal field strength first increases with height[2], and the slide along the field line becomes larger.

The second point is the fact that – unlike the poloidal velocity – the magnetic field strength and the toroidal velocity do not seem to match the given boundary condition along the disk surface for the case of non-vanishing diffusivity. The reason is the jump in diffusivity between the disk (boundary condition) and the disk corona (active zones of the grid). The magnetic field lines are frozen-in the accretion disk, but when leaving the disk surface, they are immediately affected by magnetic diffusion. Thus, the magnetic field strength in the active zones of the grid (which are shown in Fig. 7) deviates from the boundary value in the case of a non vanishing diffusivity. In the stationary state solutions shown in Fig. 7 an equilibrium state has been reached between magnetic field diffusion and advection. We see that at this radius ($r = 15$) the field strength has increased for the region immediately above the disk.

[2] This feature can be also observed in the simulations of OP97 (see their Fig. 4).

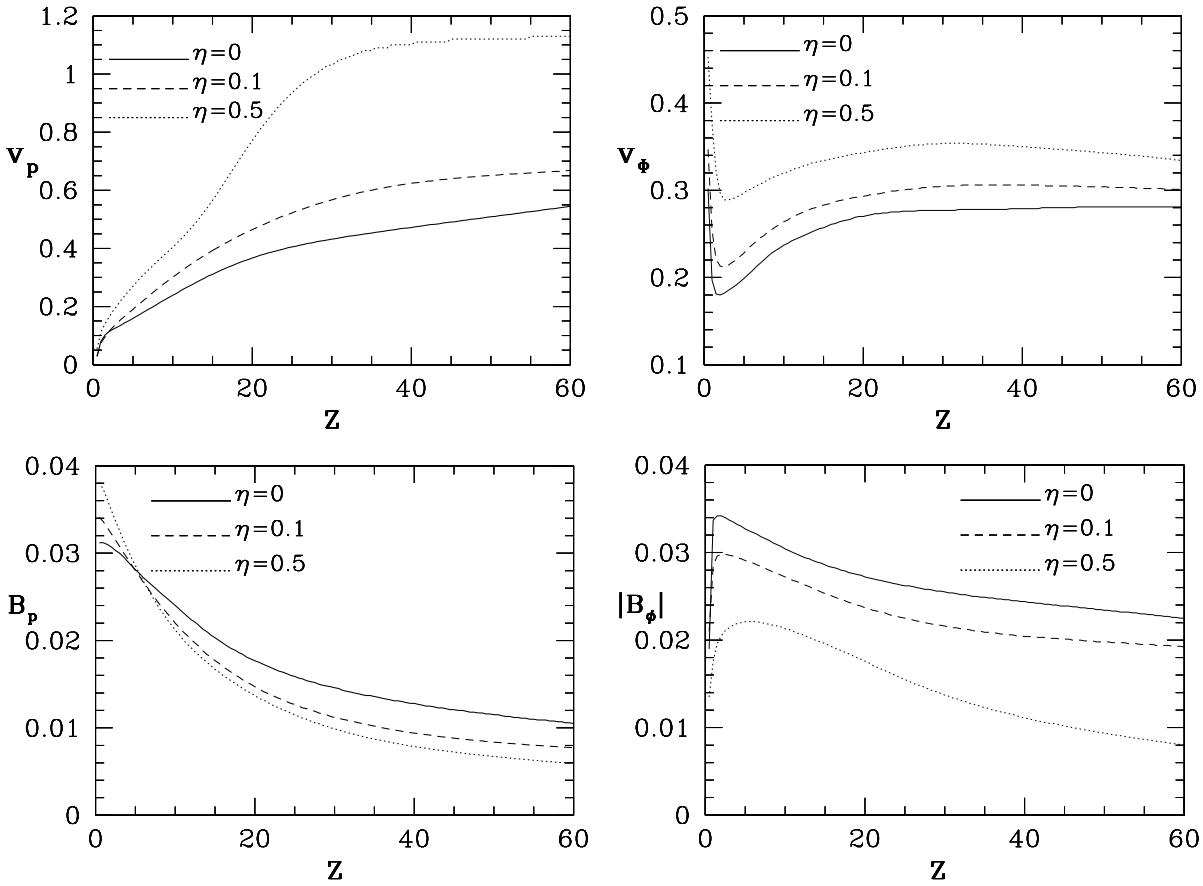

Fig. 7. Variation of the jet velocity and magnetic field with different magnetic diffusivity, $\eta = 0$ (*solid*), $\eta = 0.1$ (*dashed*), $\eta = 0.5$ (*dotted*). Shown is the profile of the poloidal (*left*) and toroidal (*right*) components of the velocity (*top*) and the magnetic field (*bottom*) in z-direction at $r = 15$ at the time of quasi-stationarity. The velocity components increase, while the magnetic field strength decreases with increasing η. Note the different scales for v_p and v_ϕ. The boundary value for the toroidal velocity is the Keplerian value $v_\phi = 0.258$ at $r = 15$.

The observed de-collimation of the matter flow with increasing diffusivity is most evident if we plot the mass and momentum fluxes across the boundaries of the inner jet region. We define the fluxes across surfaces parallel to the accretion disk boundary by

$$\dot{M} = \int_0^{r_\mathrm{max}} 2\pi r \rho v_z \mathrm{d}r\,, \quad \dot{M}v_z = \int_0^{r_\mathrm{max}} 2\pi r \rho v_z^2 \mathrm{d}r. \tag{12}$$

These are the mass flux and the kinetic z-momentum (i.e. momentum in z-direction) flux along the jet axis. For the inner jet $r_\mathrm{max} = 20$ and the integration is along $z_\mathrm{max} = 60$. The flux away from the jet axis (thus, in r-direction[3]) is defined correspondingly by the integration along the r_max-boundary from $z = 0$ to $z = z_\mathrm{max}$. The corresponding flux into the jet (thus, prescribed by the disk boundary condition) has to be integrated along the $z = 0$ axis. Signature of a good degree of collimation would be the fact that most of the mass and/or momentum flux is directed along the jet axis.

Figure 8 shows how the mass and momentum fluxes for different diffusivity evolve in time. We show the mass flux across the r and the *z-boundary* and the kinetic momentum flux in r and the *z-direction* integrated along both outflow boundaries.

The large mass and momentum fluxes for the outflow during the first 100–200 rotations result from the fact that at these stages the initial hydrostatic corona is being pushed out of the grid of the inner jet. After the the bow-shock has left the inner grid, this initial coronal mass reservoir has been swept out and the remaining mass flow in the jet is given purely by the mass injection rate from the disk boundary condition.

In the stationary state the mass inflow from the disk boundary into the jet must be equal to the mass loss across the boundaries in r- and z-direction. That this is true in our simulations can be seen in Fig. 8 on the long time scale if we compare the solid line (inflow condition) to the sum of the dotted (radial outflow) and the dashed lines (axial outflow). The analytical value for the mass rate as integrated from the given inflow boundary condition is $\dot{M} = 1.41$ which is in good agreement with the numerical result. Note that for the momentum flux a similar analytical integration gives a momentum flux from the disk into the jet of $\dot{M}v_z = 1.8 \times 10^{-4}$, which is much below the numerical value at the first active zone. As the momentum flux is not conserved as the matter becomes accelerated in the jet, this shows the tremendous gain of kinetic energy of the MHD flow.

[3] Note that we define the momentum flux in z-direction across the r_max-boundary as $\dot{M}v_z = \int_0^{r_\mathrm{max}} 2\pi r \rho v_z v_r \mathrm{d}r$.

As a good estimate, the kinetic momentum flux in z-direction across the $z = z_{\rm max}$ boundary is just the integrated mass flow rate $\dot{M}$ times the mean v_z-velocity at this position. In the case of vanishing diffusivity we have $\dot{M} v_z \simeq 1.5 \times 0.6 = 0.9$ which is similar to our numerically integrated momentum flux[4].

Now we compare the fluxes for simulations with different magnetic diffusivity. For the simulation run with $\eta = 0.5$ (Fig. 8, bottom panel) we have a mass inflow rate of 1.5 (in dimensionless units). The mass loss rate across the grid boundaries is about 0.45 in z-direction and 1.05 in r-direction. Compared to the corresponding values in the case of $\eta = 0$, where about 70% of the mass flow leaves the box in z-direction, this clearly shows that the mass flow for $\eta = 0.5$ is less collimated. This situation is even more evident for the simulations with higher diffusivity $\eta = 1.0$, where, however, the mass injection from the disk boundary is partly super-Alfvénic (not shown). Thus, even if the velocity vectors have more or less the same direction for diffusivity up to $\eta = 0.5$, the mass load along the stream lines is different due to the fact the matter, driven by centrifugal forces, may diffuse outwards across the magnetic field lines enhancing the mass flow rate in radial direction.

At this point it might be interesting to discuss the results of recent diffusive MHD simulations of the jet formation out of the accretion disk (Kuwabara et al. 2000). These authors find that the jet launching from the disk critically depends on the strength of the magnetic diffusivity. For small diffusivity, mass accretion in the disk and jet formation take place occasionally. For intermediate diffusivity the disk-jet system may reach a steady state. For high diffusivity the accretion rate and outflow rate decrease with diffusivity and may even vanish. In respect to our results, these results imply that the only way to launch a stationary MHD jet is indeed to allow for a reasonable amount of magnetic diffusion. Further, as we find less collimation for higher diffusivity or, equivalently, a weaker *jet*, such a state of stationary jet formation may become less important as the mass flow rates in the disk and the outflow decrease substantially. It would therefore be of great importance to follow the simulations of Kuwabara et al. (2000) for longer time scales comparable to our runs.

If we eventually define the *degree of jet collimation* by the *mass flux* across the jet boundaries, our simulations reveal the existence of a *critical value* of the magnetic diffusivity in this respect. In Fig. 9 the ratio of the mass flux leaving the grid in z-direction to that in r-direction is shown for different magnetic diffusivity for the time when the bow shock has left the inner box. This figure shows directly that for a high diffusivity mass flux ratio exceeds unity, indicating a weakly collimated mass flow. Figures 8 and 9 clearly show that for our model setup there exists a *critical value of the magnetic diffusivity*, $\eta_{\rm cr}$. In the simulations with $\eta \leq \eta_{\rm cr}$ the MHD flow evolves into a collimated stream. In contrary, for $\eta \geq \eta_{\rm cr}$ the flow remains only weakly collimated. The actual value for the critical η depends on the plasma beta $\beta_{\rm i}$. In our standard setup chosen for Figs. 8 and 9, we find $\eta_{\rm cr} \simeq 0.3$,

[4] Almost no kinetic momentum flux in r-direction leaves the inner box across the z-outflow boundary.

We note that the momentum flux gives somewhat different picture. The momentum flux in z-direction is always larger than that in r-direction. For our setup we obtain a ratio of about 5–8 when we compare the momentum fluxes in each direction. This demonstrates first the very high efficiency of rotating MHD flow in converting rotational kinetic energy into poloidal kinetic flux. In this respect, if we would define the degree of collimation by the momentum fluxes, our jets would perfectly collimated also for higher diffusivity. This leaves the question of how the degree of jet collimation is properly defined. Clearly, for diffusive MHD jets the field structure is *not* an accurate measure of propagation. What concerns the observational appearance, the mass flow distribution (or actually the density distribution) would be the theoretical equivalent to the observed intensity (as long as no emission maps can be provided by the simulations).

In summary, we propose that the mass flux gives the best measure of the degree of collimation. In our simulations we see a strong indication for the existence of a critical value of the magnetic diffusivity beyond which such a collimation cannot really be obtained.

4.5. Lorentz forces in the jet

Here, we deal with the question how the jet internal structure is modified by the effect of magnetic diffusivity as a result of our numerical simulations. Compared to the ideal MHD simulation (OP97) our results of (i) a de-collimation of the poloidal magnetic field structure for any value of magnetic diffusivity, (ii) a de-collimation of the hydrodynamic flow for strong diffusion and (iii) an increase of the jet velocity with increasing diffusivity are obtained purely by adding a physical magnetic diffusivity to the originally ideal MHD code.

As the flow evolution in the MHD simulation results from a combination of various physical effects – magnetic and inertial forces, pressure and gravity – it is not straight forward to distinguish between these contributions.

However, it seems to be clear that magnetic fields are the main driver for the flow acceleration and self-collimation and that, consequently, the addition of magnetic diffusion will modify the MHD structure of the jet. Therefore, investigating the Lorentz forces in the quasi-stationary state may provide some insight into the physical mechanisms at work.

At this point it might be instructive to recall in brief the basic mechanisms of MHD jet formation. Following the standard model (e.g. Blandford & Payne 1982; Ferreira 1997), a jet is launched as a sub-Alfvénic disk wind (by some unspecified – but also unknown – process) and becomes accelerated by magneto-centrifugal forces in a strong poloidal magnetic field at first hand. As the flow approaches the Alfvén surface, a toroidal magnetic field component is induced ("wound-up") due to the inertial back-reaction of the matter on the field. The toroidal field may lead to (de-) accelerating Lorentz forces $\boldsymbol{F}_{\rm L,\parallel} \sim \boldsymbol{j}_\perp \times \boldsymbol{B}_\phi$ and (de-) collimating forces $\boldsymbol{F}_{\rm L,\perp} \sim \boldsymbol{j}_\parallel \times \boldsymbol{B}$ where, here, the perpendicular and parallel projection is made with respect to the poloidal magnetic field (which, only in the case of ideal stationary MHD is parallel to the poloidal velocity).

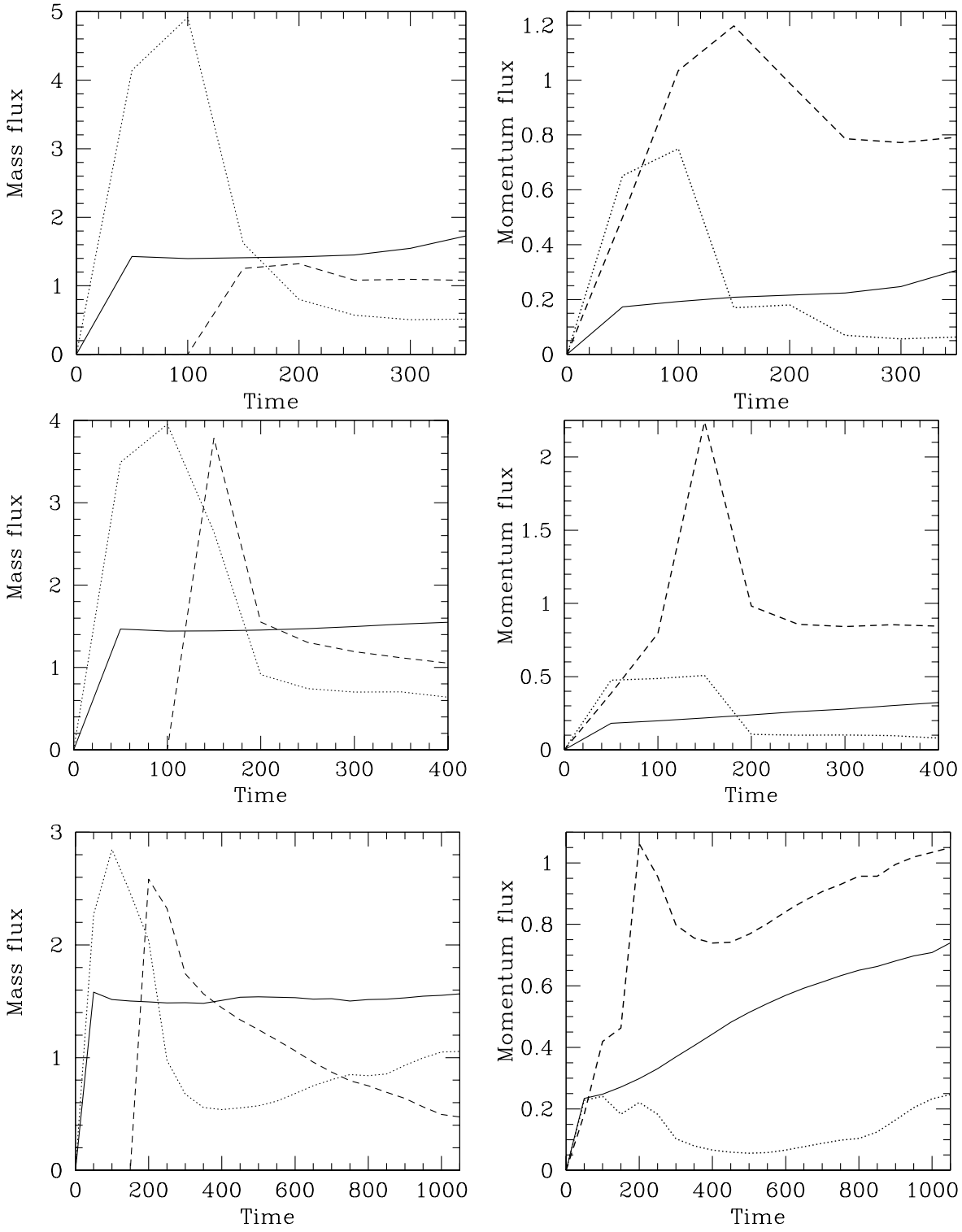

Fig. 8. Time evolution of the mass flux and kinetic momentum flux for different magnetic diffusivity, $\eta = 0, 0.1, 0.5$ (*top*, *middle* and *bottom* figures, respectively), in the inner part of the jet, $(z \times r) = (60 \times 20) r_{\rm i}$. The final point of each line corresponds to the end of the simulation when the (quasi-) stationary state has been reached. Shown is the mass flux (*left*) across the different boundaries. The mass inflow across the first active grid cells along the ($z = 0$)-boundary (*solid*), across the outer ($z = z_{\rm max}$) axial boundary (*dashed*), and across the outer ($r = r_{\rm max}$) radial boundary (*dotted*). Also shown is the kinetic momentum flux across the boundaries (*right*). Poloidal kinetic momentum flux across the first active grid cells along the ($z = 0$)-boundary (*solid*). Note that this is already evolved from the value of the boundary condition. Momentum flux in z-direction integrated along the outflow boundaries (*dashed*). Momentum flux in r-direction integrated along the outflow boundaries (*dotted*).

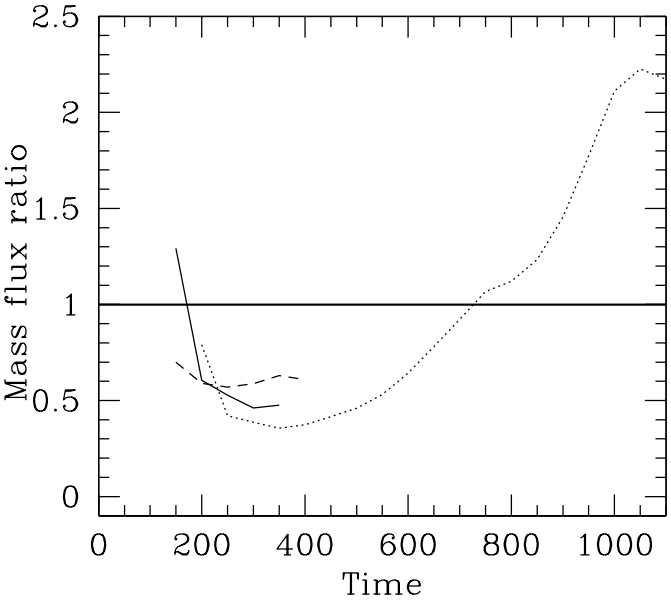

Fig. 9. Time evolution of the mass flow ratio between the radial outflow boundary (mass flow in r-direction) and the axial outflow boundary (mass flow in z-direction) for different magnetic diffusivity, $\eta = 0, 0.1, 0.5$ (*solid*, *dashed* and *dotted* line, respectively), in the inner part of the jet, $(z \times r) = (60 \times 20) r_{\rm i}$. The final point of each line correspond to the end of the simulation when the (quasi-) stationary state has been reached. For higher diffusivity, the mass flux ratio in the quasi-stationary state increases indicating a decrease in degree of collimation.

The toroidal Lorentz force $\boldsymbol{F}_{\mathrm{L},\phi} \sim \boldsymbol{j}_{\rm p} \times \boldsymbol{B}_{\rm p}$ affects the angular velocity of the matter, disturbing the centrifugal balance and, thus, give rise also to a poloidal motion.

Therefore, a change in the jet acceleration and collimation might be explained by the interplay of two mechanisms. First, the winding-up of the poloidal magnetic fields is less efficient since magnetic diffusion leads to a slip of matter across the field. As a consequence, the induced toroidal magnetic field is weaker leading to a less efficient acceleration by Lorentz forces but also to a de-collimation. This effect applies predominantly in the super-Alfvénic regime. Second, as a de-collimation of the poloidal magnetic structure also implies a smaller launching angle for the sub-Alfvénic flow, the magneto-centrifugal acceleration mechanism may work more effective. As a consequence, the resulting fluid velocities in the jet should be larger, as indeed suggested by our simulations (Fig. 7).

In Fig. 10 we show for different magnetic diffusivity the Lorentz force components along a field line (or, respectively, along the corresponding magnetic flux surface) leaving the numerical grid of the inner jet at $(r = 20, z = 60)$. Note that due to the magnetic field de-collimation with η, we compare *different magnetic flux surfaces*. These flux surfaces have their foot point between $r = 5$ and $r = 8$ along the disk surface and the Alfvén point at about $z = 25, 15, 5$ ($\eta = 0, 0.1, 0.5$). The figure shows the Lorentz force components $F_{\mathrm{L},\perp}$, $F_{\mathrm{L},\parallel}$, $F_{\mathrm{L},\phi}$ and the corresponding acceleration of the fluid $F_{\rm L}/\rho$.

The first point to mention is that the magnitude of the Lorentz force generally increases with increasing magnetic diffusivity. This is interesting insofar as the magnetic field strength decreases with increasing diffusion (Fig. 7). The Lorentz force has its maximum in that region *before* the Alfvén point where the curvature of the poloidal field is largest. Thus, *magnetic acceleration* mainly works in this regime.

This picture of an acceleration purely by magnetic forces is complementary to the above mentioned picture of an enhanced magneto-centrifugal effect. For the parallel component this may directly lead to the observed increase in the poloidal velocity with increasing magnetic diffusivity (see Fig. 7). Additionally, the higher velocity also leads to stronger inertial forces and, for moderate heights above the disk, the diffusive plasma flow will tend to maintain its (radial) direction even if the field lines bend in direction of the jet axis. This will re-distribute the mass flow distribution along the field line. The parallel component decreases rapidly with increasing z as it can be expected when the jet flow becomes more and more collimated. The same holds for the toroidal Lorentz force component. This component accelerates the plasma in toroidal direction leading to an additional centrifugal effect which drives the matter in radial direction diffusing across the magnetic field. This is the reason for the increase of the mass flow rate along the outer stream lines with increasing diffusivity.

While the curves for the three Lorentz force components look quite similar at a first glimpse, we see that the corresponding components for the *acceleration* are somewhat different. The perpendicular (collimating) component[5] of the acceleration remains on a rather high level throughout the (inner) box. That means that also in the asymptotic regime of the collimated jet these forces continue to collimate the jet flow.

On the other hand, compared to the perpendicular component, the parallel and the ϕ components of the corresponding acceleration have a steeper maximum and decrease to an only marginal strength beyond the Alfvén point. This is what one would expect also from the standard MHD jet model.

For $\eta = 0$ and $\eta = 0.1$, we see only a slight difference for the strength of the perpendicular components of force and acceleration at the large distances. Therefore, the degree of local flow collimation should be similar, as it is indeed visible in the poloidal *velocity* vectors, which are well aligned for the diffusivity considered (Fig. 6). However, we note the larger deviation of the perpendicular components for $\eta = 0.5$, which mirrors the fact that in this case we are above the *critical value* $\eta_{\rm cr}$ concerning the mass flow collimation (Fig. 8).

In summary, our discussion of the Lorentz forces and its associated acceleration gives a self-consistent picture of what we have observed in our numerical simulation. The perpendicular Lorentz force is essential for the collimation throughout the entire (inner) flow. The increase of the parallel Lorentz force for higher magnetic diffusivity gives rise to the higher velocities in the jet flow. The toroidal Lorentz force leads to an additional centrifugal effect enhancing the mass flow rate in the outer (yet un-collimated) parts of the jet flow.

[5] We note that the sign for $F_{\mathrm{L},\perp}$ is defined positive for the force vector pointing radially outwards. Thus, the increase of $|F_{\mathrm{L},\perp}|$ indicates an increase of the collimating Lorentz force on the matter.

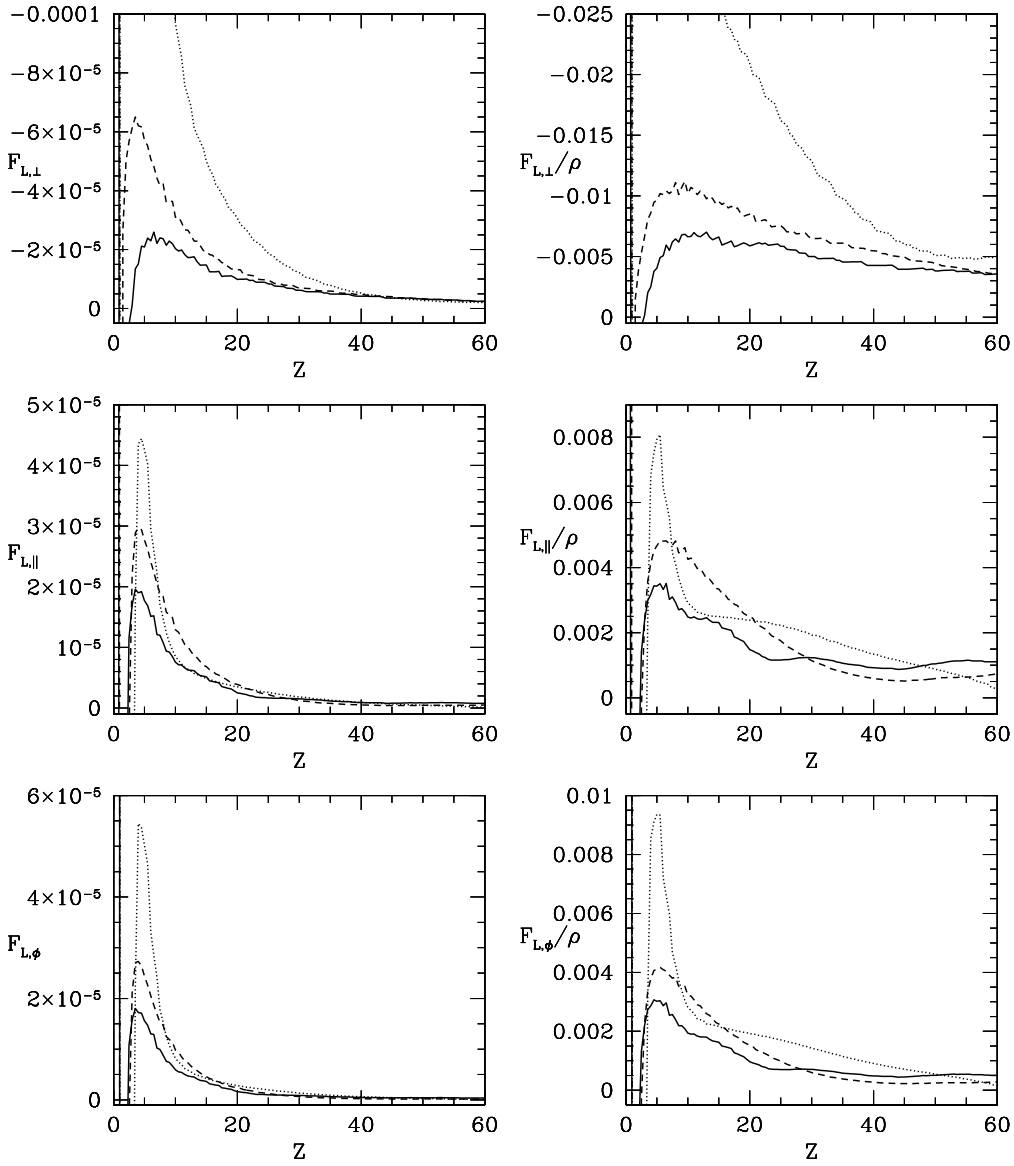

Fig. 10. Lorentz forces in the jet for different magnetic diffusivity $\eta = 0, 0.1, 0.5$ (*solid, dashed, dotted* lines). *Left* (Normalized) values of the force component perpendicular (*top*) and parallel (*middle*) to the field line and the toroidal component (*bottom*), $F_{\mathrm{L},\perp}$, $F_{\mathrm{L},\parallel}$, $F_{\mathrm{L},\phi}$, along a flux surface leaving the box of the inner jet close to $(R = 20, Z = 60)$-corner (see Fig. 3 or Fig. 5). For $F_{\mathrm{L},\perp}$ the positive sign denotes the r-direction (de-collimating force). For $F_{\mathrm{L},\parallel}$ the positive sign denotes the z-direction (accelerating force). For $F_{\mathrm{L},\phi}$ the positive sign denotes the ϕ-direction. *Right* Corresponding values of the magnetic acceleration $(F_{\mathrm{L},\perp}/\rho)$, $(F_{\mathrm{L},\parallel}/\rho)$, $(F_{\mathrm{L},\phi}/\rho)$.

5. Summary

In this paper we presented time–dependent simulations of the formation of axisymmetric protostellar MHD jets. In particular, we were considering the effects of *resistive* MHD on the collimation and acceleration of the jet flow. Similar to recent simulations considering the ideal MHD case (Ouyed & Pudritz 1997; Fendt & Elstner 2000), the accretion disk has been taken as a fixed boundary condition during the simulation, prescribing the mass flow rate and the magnetic flux distribution. Our initial condition is a force-free magnetic field in a hydrostatic corona. Our simulations were performed on a grid of $(z \times r) = (280 \times 40)$ inner disk radii with 900×200 grid elements or on a grid of 140×40 inner disk radii with 280×80 grid elements. We find that in general the low resolution simulations were sufficient to cover all physical effects observed in the higher resolution runs. In our discussion we mostly concentrate on the structure of the *inner jet* which is the region of 60×20 inner disk radii close to the star. We summarize our results as follows.

(1) We have successfully implemented the physical magnetic diffusivity into the ZEUS-3D code.
(2) We have discussed some analytical estimates about the strength of magnetic diffusivity in protostellar jets. We derive the distribution of magnetic diffusivity self-consistent to the turbulent Alfvénic pressure which is underlying our simulations and also present in the simulations of other

authors. Our simulations, however, are performed with a constant diffusivity. Our main results do not depend on the actual distribution of magnetic diffusivity.

(3) In the global scale of our simulation, the jet bow shock advances slower through the initial hydrostatic corona for the diffusive jets. The reason is the lower mass flux in the direction along the jet axis in these jets. As expected, the internal structure of the jet is less disturbed in the case of diffusion. The Alfvén surface comes closer to the disk surface.

(3) For our model setup we find that, similar to the case of ideal MHD jets (Ouyed & Pudritz 1997; Fendt & Elstner 2000), also resistive MHD jets can reach a quasi-stationary state. With increasing magnetic diffusivity, the quasi-stationary state of the jet is reached later.

(4) With increasing diffusivity the jet velocity increases. The direction of the velocity vectors does, however, only change weakly. At the same time the poloidal magnetic field distribution becomes increasingly de-collimated.

(5) As a proper measure of the degree of collimation we suggest the mass flux. If we compare the mass flow rates through the grid boundaries for different diffusivity we find strong indication for the existence of a *critical value* for the magnetic diffusivity $\eta_{\rm cr}$ concerning the jet collimation. Beyond this value we still find an almost cylindrically collimated stream along the jet axis, however, the bulk mass flow is in radial direction. For our setup, the critical (normalized) diffusivity is about $\eta_{\rm cr} \approx 0.3$.

(6) We discuss a self-consistent picture where these effects of jet de-collimation and acceleration are explained in the context of Lorentz forces. The perpendicular Lorentz force is essential for the collimation throughout the entire flow along the jet axis. The parallel Lorentz force increases for increasing magnetic diffusivity and gives rise to the higher velocities in the jet flow. The toroidal Lorentz force accelerates the plasma in toroidal direction. This leads to additional centrifugal forces re-distributing the mass flow rates across the magnetic flux surfaces towards the outer (yet uncollimated) parts of the flow. The latter two components play no role for larger distances along the flow.

With our results we have shown that magnetic diffusivity plays indeed a role for the jet formation process. Turbulence as a natural (and necessary) property of accretion disks will naturally enter the disk wind and will be further advected into the jet. As we see in our simulations only a weak collimation for a high magnetic diffusivity, a hypothetical, and for sure exaggerated, conclusion might therefore be that highly turbulent disks cannot drive a collimated jet mass flow. Such a claim may eventually be tested by the astronomical observation and may also give some hint to answer the question why some disks have jets and some do not.

Our present study should be understood as a first step in the right direction. Future work may improve the numerical resolution and the grid size but may also consider e.g. an additional central stellar magnetosphere as a boundary condition. The most interesting (but also most difficult) prospect would be to include the evolution of the disk structure in the simulation.

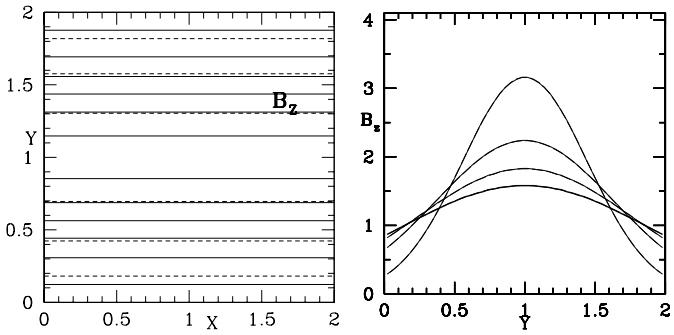

Fig. A.1. Numerical test of magnetic diffusion. Grid size 50×50 elements for a normalized physical grid 2.0×2.0. *Left*: Isocontours of the magnetic field strength $B_z(x, y)$ (normalized units) for different time steps $t = t_0 + \Delta t$, $\Delta t = 0.0$ (*solid line*), $\Delta t = 0.1$ (*dashed line*). *Right*: Normalized intensity profile of the magnetic field strength across the two-dimensional box along $x = 1$ for different time steps $t = t_0 + \Delta t$ with $\Delta t = 0.0, 0.1, 0.2, 0.3$ (*top* to *bottom* curve). Comparison between the analytical solution *solid lines* and the numerical simulation (*dashed lines*).

Acknowledgements. We thank the LCA team and M. Norman for the possibility to use the ZEUS-3D code. We acknowledge helpful discussions with D. Elstner, U. Ziegler and R. Ouyed. This work was partly financed by the German science foundation in the DFG Schwerpunktprogramm "Physik der Sternentstehung" (FE490/2-1). The referee, Takahiro Kudoh, is acknowledged for useful advice concerning the presentation of our results and for drawing our attention to some very recent papers in the literature.

Appendix A: Numerical tests

As we have introduced the effect of physical magnetic diffusivity into the ideal MHD ZEUS–3D code, careful tests were necessary to prove our implementation. In particular we checked the time scales introduced by magnetic diffusion and the behavior along the boundaries. The boundary conditions for an axisymmetric jet ("outflow", "inflow "and "reflecting") are quite different from what is e.g. needed in box simulations used for other scientific questions.

We defined two numerical tests for our diffusive code. In both cases the code basically solves the diffusion equation. We obtained this limit by setting the initial density in the simulation to arbitrarily large values (here the normalized $\rho \simeq 10^9$) effectively reducing any fluid motions in our simulations. The first test example is the analytical solution of the diffusion equation in Cartesian coordinates, the second example an axisymmetric torus of purely toroidal magnetic field in cylindrical coordinates.

A.1. Analytical solution to the diffusion equation

In Cartesian coordinates (x, y, z) the solution of the one dimensional diffusion equation for infinite space is

$$B_z(y, t) = \frac{1}{\sqrt{t}} \exp\left(-\frac{(y - y_0)^2}{4\eta t}\right), \tag{A.1}$$

with the magnetic diffusivity $\eta = c^2/(4\pi\sigma)$.

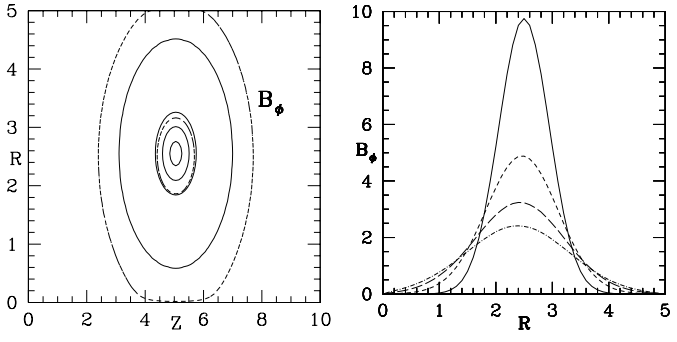

Fig. A.2. Numerical test of magnetic diffusion in cylindrical coordinates. Grid size 100×50 elements for a normalized physical grid 10.0×5.0. *Left*: Isocontours of the toroidal magnetic field strength for different time steps $t = t_0 + \Delta t$, $\Delta t = 0.0$ (*solid line*), $\Delta t = 0.1$ (*dashed line*). *Right*: Normalized intensity profile of the magnetic field strength across the two-dimensional box along $z = 5$ for different time steps $t = t_0 + \Delta t$ with $\Delta t = 0.0, 0.1, 0.2, 0.3$ (*top* to *bottom* curve).

As a test for our code, we choose as initial condition the magnetic field $B_z(x, y) = B_z(y)$ for a certain time $t = t_0$ from Eq. (A.1). For the two-dimensional numerical grid we prescribe "free" (i.e. outflow) boundary conditions in x-direction and a time-varying field for the boundaries in y-direction.

Figure A.1 show the result of our simulations for the time steps $t = t_0 \Delta t$ ($\Delta t = 0.1, 0.2, 0.3, 0.4$) for a magnetic diffusivity $\eta = 1.0$ in comparison with the analytical results. As result, we obtain a perfect agreement between the numerical simulation and the analytical solution.

A.2. Toroidal field torus

Here, our aim is to check how our code treats magnetic diffusion in cylindrical coordinates, along the outflow boundary in r-direction and along the symmetry axis. As initial condition, we define a torus of toroidal magnetic field

$$B_\varphi(r, z, t_0 = 0.1) = \frac{1}{t_0} \exp\left(-\frac{(r - r_0)^2 + (z - z_0)^2}{4\eta t_0}\right). \qquad \text{(A.2)}$$

Figure A.2 show the result of our simulations for the time steps $t = t_0 \Delta t$ ($\Delta t = 0.1, 0.2, 0.3, 0.4$) for a magnetic diffusivity $\eta = 1.0$ in comparison with the analytical results. The simulation shows how the peak of the field distribution moves slightly inwards from its initial central position as the field diffuses. Note that as the field diffuses outwards the volume over which the toroidal field is distributed increases. Therefore the decrease in field strength in outward direction. Along the symmetry axis the field strength remains zero, whereas the field strength along the outflow boundaries increases. No boundary condition is prescribed here.

Although there is no analytical solution to compare with, this simulation gives again convincing evidence that we properly incorporated the magnetic diffusion in the ZEUS-3D code.

Table B.1. Typical numbers for our simulations for different magnetic diffusivity η. Diffusive time step τ_η, Alfvén time step τ_A, the global magnetic Reynolds number R_m and the magnetic turbulence parameter α_m.

η	τ_η	τ_A	R_m	α_m
0	∞	0.258	∞	0
0.1	0.625	0.293	40	0.025
0.15	0.417	0.084	30	0.033
0.25	0.25	0.136	20	0.05
0.5	0.125	0.080	10	0.1
1	0.063	0.183	8	0.125
2.5	0.025	1.394	4	0.25

Appendix B: Time scales in the simulation

Table B.1 shows the time scales and typical number values applied in our jet simulations for different magnetic diffusivity η. As an example we refer to the simulation runs with relatively low numerical resolution. The diffusive time step (i.e. the local time scale for magnetic diffusion) is $\tau_\eta = (\Delta x/\eta^2)$ with the size of the grid element Δx. For comparison we show the Alfvén time step $\tau_A = (\Delta x/v_A)$. The other two numbers consider the global evolution of the jet flow. For the magnetic Reynolds number $R_m = (v_A r_{max}/\eta)$ we have considered the global size of the jet and similar for the magnetic turbulence parameter α_m.

References

Bacciotti, F., & Eislöffel, J. 1999, A&A, 342, 717
Blandford, R. D., & Payne, D. G. 1982, MNRAS, 199, 883
Bridle, A. H., & Perley, R. A. 1984, ARA&A, 22, 319
Cabrit, S., Edwards, S., Strom, S. E., & Strom, K. M. 1990, ApJ, 354, 687
Camenzind, M. 1990, Magnetized disk-winds and the origin of bipolar outflows, in Rev. Mod. Astron. 3, 234 (Springer, Heidelberg)
Contopoulos, J. 1994, ApJ, 432, 508
DeCampli, W. M. 1981, ApJ, 244, 124
Edwards, S., Cabrit, S., Strom, S. E., et al. 1987, ApJ, 321, 473
Fendt, C. 1997, A&A, 319, 1025
Fendt, C., Camenzind, M., & Appl, S. 1995, A&A, 300, 791
Fendt, C., & Elstner, D. 1999, A&A, 349, L61
Fendt, C., & Elstner, D. 2000, A&A, 363, 208 (FE00)
Fendt, C., & Memola, E. 2001, A&A, 365, 631
Ferreira, J. 1997, A&A, 319, 340
Frank, A., Gardiner, T. A., Delemarter, G., Lery, T., & Betti, R. 1999, ApJ, 524, 947
Goodson, A. P., Winglee, R. M., & Böhm, K.-H. 1997, ApJ, 489, 199
Hartigan, P., Morse, J. A., & Raymond, J. 1994, ApJ, 436, 125
Hayashi, M. R., Shibata, K., & Matsumoto, R. 1996, ApJ, 468, L37
Heyvaerts, J., & Norman, C. A. 1989, ApJ, 347, 1055
Kato, S. X., Kudoh, T., & Shibata, K. 2002, ApJ, 565, 1035
Königl, A. 1986, Can. J. Phys., 64, 362
Königl, A. 1989, ApJ, 342, 208
Krasnolpolsky, R., Li, Z.-Y., & Blandford, R. 1999, ApJ, 526, 631
Kudoh, T., & Shibata, K. 1997a, ApJ, 474, 362
Kudoh, T., & Shibata, K. 1997b, ApJ, 476, 632
Kudoh, T., Matsumoto, R., & Shibata, K. 1998, ApJ, 508, 186
Kudoh, T., Matsumoto, R., & Shibata, K. 2002, PASJ, 54, 121
Kudoh, T., Matsumoto, R., & Shibata, K. 2002, PASJ, 54, 267

Kuwabara, T., Shibata, K., Kudoh, T., & Matsumoto, R. 2000, PASJ, 52, 1109
Lada, C. J. 1985, ARA&A, 23, 267
Li, Z.-Y., Chiueh, T., & Begelman, M. C. 1992, ApJ, 394, 459
Li, Z.-Y. 1995, ApJ, 444, 848
Lovelace, R. V. E., Wang, J. C. L., & Sulkanen, M. E. 1987, ApJ, 315, 504
Matsumoto, R., Uchida, Y., Hirose, S., et al. 1996, ApJ, 461, 115
Miller, K. A., & Stone, J. M. 1997, ApJ, 489, 890
Miller, K. A., & Stone, J. M. 2000, ApJ, 534, 398
Mirabel, I. F., Rodrigues, L. F., Cordier, B., Paul, J., & Lebrun, F. 1992, Nature, 358, 215
Mundt, R., Buehrke, T., Fried, J. W., et al. 1984, A&A, 140, 17
Ouyed, R., & Pudritz, R. E. 1997, ApJ, 482, 712 (OP97)
Padman, R., Lasenby, A. N., & Green, D. A. 1991, in Beams and Jets in Astrophysics, ed. P. A. Hughes (Cambridge Univ. Press)
Pelletier, G., & Pudritz, R. E. 1992, ApJ, 394, 117
Pudritz, R. E., & Norman, C. A. 1983, ApJ, 274, 677
Ray, T. P., Mundt, R., Dyson, J. E., Falle, S. A. E. G., & Raga, A. C. 1996, ApJ, 468, L103
Romanova, M. M., Ustyugova, G. V., Koldoba, A. V., Chechetkin, V. M., & Lovelace, R. V. E. 1997, ApJ, 482, 708
Shibata, K., & Uchida, Y. 1985, PASJ, 37, 31
Shibata, K., & Uchida, Y. 1986, PASJ, 38, 631
Stone, J. M., & Norman, M. L. 1992a, ApJS, 80, 753
Stone, J. M., & Norman, M. L. 1992b, ApJS, 80, 791
Stone, J. M., & Norman, M. L. 1994, ApJ, 433, 746
Uchida, Y., & Shibata, K. 1985, PASJ, 37, 515
Ustyugova, G. V., Koldoba, A. V., Romanova, M. M., Chechetkin, V. M., & Lovelace, R. V. E. 1995, ApJ, 439, L39
Wardle, M., & Königl, A. 1993, ApJ, 410, 218

Astron. Astrophys. 334, 750–755 (1998)

ASTRONOMY AND ASTROPHYSICS

Possible bending mechanisms of protostellar jets

Christian Fendt and Hans Zinnecker

Astrophysikalisches Institut Potsdam, An der Sternwarte 16, D-14482 Potsdam, Germany

Received 17 November 1997 / Accepted 4 March 1998

Abstract. Observations of several bipolar jet flows from young stellar objects reveal a slight difference in the apparent direction of propagation for jet and counter jet.

In this paper, possible mechanisms leading to such a jet deflection are investigated. We discuss various effects, such as the motion of the jet source within a binary system, gravitational pull due to an asymmetric external mass distribution, dynamical pressure of the external medium, inertial effects due to proper motion of the jet source, an inclined interstellar magnetic field, and the coupling between a magnetic jet and an external magnetic field.

We find that for typical protostellar jet parameters the most likely mechanisms leading to a bent jet structure are *Lorentz forces* on the magnetic jet and/or motion of the jet source in a *binary system*. *Dynamical pressure* of a dense external medium or a stellar wind from a companion star cannot be excluded as source of jet bending.

Key words: MHD – ISM: jets and outflows – galaxies: jets – stars: magnetic field – stars: mass loss – stars: pre-main sequence

1. Protostellar jets with counter jets

There is now quite a number of cases for protostellar jets/counter jets, where the observed direction of propagation for jet and counter jet is not exactly $180°$.

Zinnecker et al. (1996, 1997) find that in the otherwise perfectly collimated, symmetric jet/counter jet system HH 212 the direction of propagation for jet and counter jet deviates by an angle of about 2° from 180°. In the case of HH 111, Gredel & Reipurth (1993) find a difference of 1°between the two lobes; however, the other bipolar jet originating in the same source region, HH 121, shows a rather large angle difference between its lobes of 15°- 20°. Another case is HH 24, where the flow directions are misaligned by 6°for jet and counter jet (Mundt et al. 1991).

In addition, many of the observed jets do not propagate in a straight motion, but form a curved or bent jet structure. Eislöffel & Mundt (1997) observed Herbig-Haro flows on a parsec-scale, and report changes in the flow direction (up to $\sim 10°$). They point out possible mechanisms for such changes, in particular precession and Lorentz forces. Mundt et al. (1990) observed several cases, i.e. the HH 30 jet and the HL Tau jet/counter jet, where they derived curvature radii from 0.6 to $3\,10^{18}\,\mathrm{cm}$. They were first to point out that the jet transverse displacement from a straight motion of a protostellar jet may be due to Lorentz forces. There are several examples known, where the jet/counter and jet form an S-shape structure (Eislöffel & Mundt 1997).

For HH 30 López et al. (1995) derive a P.A. for the jet propagation of 30°and 217°for the outer jet and counter jet, respectively. They point out a 'mirror symmetry' of jet and counter jet, ruling out Lorentz forces as the driving force of the jet deflection, unless a complex structure of the ambient magnetic field is supposed (see below).

Bent jets are observed also for extragalactic jet sources. Eilek et al. (1984) investigated several bending models for 3C 465, which exhibits a drastic bending of about 30°-50°despite being a very well collimated jet/counter jet system initially. They conclude that either Lorentz forces or interaction with cool clouds may account for the bending.

In this paper we compare and discuss several physical mechanisms possibly responsible for a change of propagation direction for protostellar jets. Their effectiveness is estimated for typical protostellar jet parameters.

2. Formation and propagation of magnetic jets

We briefly outline the general aspects and conditions of protostellar jet formation. It is now almost accepted that protostellar jets are *magnetically* driven jets (Pudritz & Norman 1986; Camenzind 1990, 1997; Shu et al. 1994). Recently, these theoretical ideas received direct support by radio observations, which, for the first time, detected large-scale magnetic fields in the outflow from a young stellar object (Ray et al. 1997).

Following current jet models the jet originates in the innermost part of a magnetized star-disk system (Camenzind 1990; Shu et al. 1994; Fendt et al. 1995; Fendt & Camenzind 1996). Whether the jet field is basically anchored in the accretion disk or in the stellar surface, is, however, not yet clear.

Send offprint requests to: C. Fendt, (cfendt@aip.de)

The principal mechanisms of jet formation can be summarized as follows. The underlying hypothesis is that jets can only be formed in a system with a *high degree of axi-symmetry*.

- *Magnetic field* is generated by the star-disk system.
- The star-disk system also drives an *electric current*.
- Accreting *matter* is ejected as a plasma wind (either from the stellar or disk surface) and couples to the magnetic field.
- The plasma becomes *accelerated magnetically*, i.e. by conversion of Poynting flux to kinetic energy.
- Plasma inertia leads to bending of the poloidal field (i.e. the field along the meridional plane including the jet axis). The pinching forces of the generated toroidal component (i.e. the field component winding around the jet axis) eventually collimate the wind flow, forming a collimated jet structure.
- The plasma velocity subsequently exceeds the speed of the magnetosonic waves. In the fast magnetosonic regime the flow is causally decoupled from outer boundary conditions.
- Where the jet front meets the interstellar medium (ISM), a *bow shock* develops, thermalizing the jet energy. Also, the electric current is closed via the bow shock, and the jet net current returns to the source of the current via the ISM.

3. Possible mechanisms leading to a jet deflection

A general point concerning the deflection of a jet from its original path of motion is that it can only be caused by some *acceleration/deceleration* mechanism. It cannot be caused by e.g. a steady, proper motion of the jet together with the jet source, since in this case the jet will have the same tangential velocity as its source. Thus, *forces* must be involved, either acting on the jet itself or on the jet source.

In the following we basically suppose the general model of jet formation outlined in Sect. 2. The jets are ejected as straight axisymmetric magnetosonic flows. The possible mechanisms leading to a change in the direction of jet propagation could be generally classified in three groups:

- *Internal effects* on small scales such as acceleration of the jet source (by e.g. a binary component), or precession of an accretion disk in a binary system.
- *Mixed effects* such as the interaction between intrinsic and external properties, such as a Lorentz force due to a jet net current and an external magnetic field.
- *External effects* on large scales such as a gravitational potential of a source outside the star-jet structure or a pressure /magnetic field of the ambient medium.

In general, we assume that the jet/counter jet with a length scale $L_{\rm jet}$ follows a *curved* trajectory with the corresponding curvature radius R_κ. This assumption is consistent with the observations, although a straight jet trajectory in the case of a small angle of deflection can not be excluded. Usually, the deflection angle α is small and of the order of some degrees, $\alpha \simeq \tan(\alpha) = 0.5\, L_{\rm jet}/R_\kappa$, (see Fig. 1).

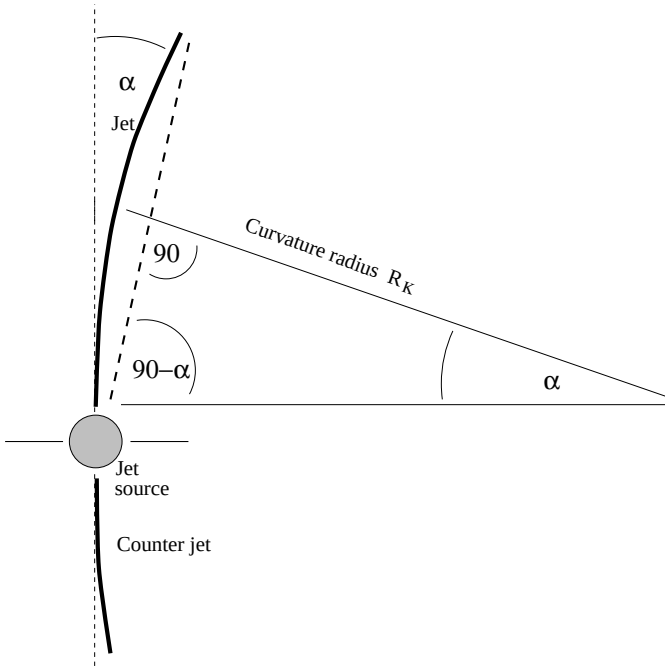

Fig. 1. Model geometry in a deflected jet/counter jet system (solid line) with an angle of deflection α. The corresponding curvature radius is R_κ. The direction of deflected jet propagation is approximated by the chord (thick dashed line). The jet source is represented as a star-disk-system.

3.1. Binary (multiple) system

Could an orbital motion of the jet source in a binary system account for the jet deflection? Binary systems are very common among main-sequence stars, and there is evidence that the binary frequency among protostars and PMS stars is at least as high as among main-sequence stars (see Mathieu 1994; Zinnecker & Brandner 1997).

To date, there are only few examples known of a jet source being member of a multiple systems. Among them is T Tau (Herbst et al. 1996) and RW Aur (Hirth et al. 1997). However, the separation of the components in T Tau and RW Aur is rather large. In turn, this may be the reason why jet motion occurs at all, since the formation of a jet requires a system with a high degree of axisymmetry, which would be disturbed by a close companion.

Here we assume a scenario of a young stellar binary system with one component emitting jets (see Fig. 2). The jet source moves a distance Δx while ejecting a series of different portions of the jet. The observed jet appears deflected, as the velocity components of the jet are different for different times t_1 and t_2.

We estimate a kinematic time scale $\tau_{\rm kin} \simeq 100\,{\rm yrs}$ for an observed jet length $L_{\rm jet} \simeq 10^{17}{\rm cm}$ and for a typical jet speed of $300\,{\rm km\,s^{-1}}$. This time scale might be larger, if the jet axis is inclined against the orbital axis.

In the case of a small ratio $\Delta x/L_{\rm jet}$, we define α as the angle between a straight jet propagation and the observed orientation, which for analytical reasons is approximated as straight line, $\sin\alpha = \Delta x/L_{\rm jet}$. With the assumption that this motion is due to

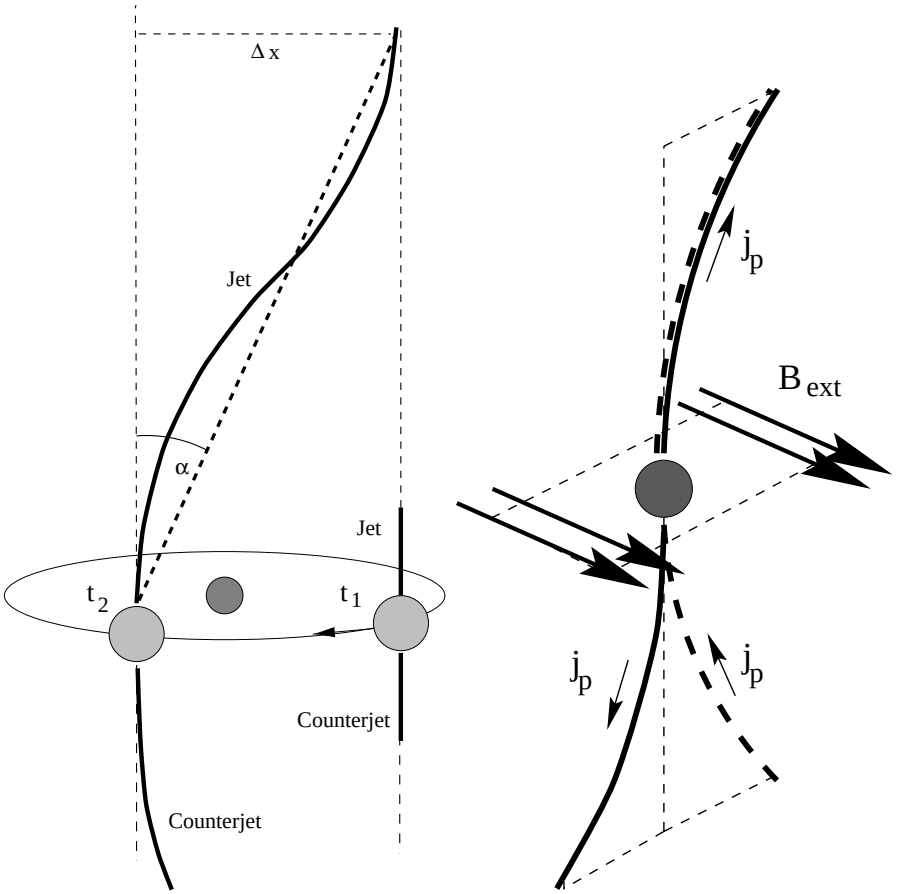

Fig. 2. Model geometries in deflected jet/counter jet systems. *Left:* Binary star - jet system. Shown is the jet source at different times t_1 and t_2. The observed jet is ejected between t_1 and t_2. The dynamical time of the jet motion is $\tau_{\rm dyn} = t_2 - t_1$. The angle of deflection α is approximated by a straight line (thick dashed line). *Right:* A poloidal current density $j_{\rm p}$ in the jet and an external magnetic field $B_{\rm ext}$ perpendicular to the jet axis give rise to Lorentz forces. The S-shape (solid line) and C-shape (dashed line) of the jet system depend on the direction of the current flow, as indicated.

acceleration by a companion star, the derived *minimum* binary separation is Δx. It might be larger because of two reasons. First, the binary system may not have completed half of its orbit. Second, the jet axis might be inclined against the orbital axis (different from Fig. 2).

In the case of HH 212 the angle of $\alpha = 2^\circ$ corresponds to $\Delta x = 120\,\mathrm{AU}$, if we assume a length scale $L_{\rm jet} \simeq 10^{17}\mathrm{cm}$ for the inner jet as observed (i.e. the series of the inner jet knots). Δx is a lower limit for the binary separation with regard to a detection of a jet bending within the kinematic time scale. In turn, the binary separation gives the maximum value for Δx.

Thus, there are two constraints on the binary period with regard to a detection of a jet bending: (i) If the period is too large, the low orbital speed of the jet source, $v_\star$, leads to an angle of deflection $\alpha \simeq \tan\alpha \simeq (v_\star / v_{\rm jet})$ too small for a detection, within the kinematic timescale. (ii) Similarly, a small period, equivalent to a small binary separation D, the jet deflection is too small, since $\Delta x \lesssim D$.

For the example of HH 212 from Kepler's Third Law follows an orbital period of the binary system of $P \gtrsim 500\,\mathrm{yrs}$, assuming a total mass of the system $M_{\rm tot} = 1\,\mathrm{M}_\odot$ and a minimum binary separation of $D = 0.5 \cdot 120$ AU.

This period is several times larger than the jet propagation time scale for $10^{17}\mathrm{cm}$, in other words, the jet bending time scale is shorter than the period of the orbit of the jet source. Therefore, jet bending would be observable within the kinematic time scale. (Note that, on the other hand, this implies that the formation the jets is just a short event along the path of the binary).

From the constraints (i) and (ii) it can be derived that the condition for an observation of the bending is $P \gtrsim \pi\tau_{\rm kin}$. The upper limit for P is given by the observational resolution for Δx. The ratio

$$\frac{P}{\tau_{\rm kin}} \gtrsim 25 \left(\frac{L_{\rm jet}}{10^{17}\mathrm{cm}}\right)^{\frac{1}{2}} \left(\frac{\sin\alpha}{\sin 2^\circ}\right)^{\frac{3}{2}} \left(\frac{v_{\rm jet}}{300\mathrm{km\,s^{-1}}}\right) \left(\frac{M_{\rm tot}}{\mathrm{M}_\odot}\right)^{-\frac{1}{2}} \quad (1)$$

does not strongly depend on the jet length and the total mass of the system.

The most likely main-sequence binary separation in the solar neighborhood is about $a \simeq 30\,\mathrm{AU}$ (Duquennoy & Mayor 1991). For pre-main-sequence binaries the semi-major axis follows roughly a $1/a$ distribution between 120 AU and 1800 AU (Reipurth & Zinnecker 1993; Köhler & Leinert 1997). These values are in agreement with the Δx estimated above for HH 212 as a requirement for a minimum binary separation in order to influence the shape of the jet.

Note that, although the binarity of the young stellar system breaks the axisymmetry on the large scale, the jet source itself must provide an axisymmetric geometry in order to produce a jet in the first place. The scenario of a 'stellar' jet formation might be preferred in close binary systems compared to a 'disk' jet formation. This is because tidal interaction between disk

and companion star may disturb the axisymmetry needed for jet formation and thus prohibit the jet formation.

Jet wiggling is observed for a number of protostellar jets. Examples are HH 30 (Burrows et al. 1996) and HH 83 (Reipurth 1989). It is, however, not yet clear whether this type of motion is due to precession or other effects. One should keep in mind that HH 30 is a very elongated, and thus presumably very stable jet structure, with a full length of about 2′(Mundt et al. 1990) or even 5′(López et al. 1995). For HH 83, Reipurth (1989) give a physical amplitude of the wiggling helical motion of 400 AU. This length scale would be identical to the binary separation, if we suppose that the wiggling arises not from tidal interaction, but from kinematic motion of the jet source in a binary system.

Evidence for tidal interaction and a precessing jet is found in the case of the famous SS 433 system (Margon & Anderson 1989). The precession amplitude is 5° with a period of 160 days. This jet is, however, relativistic and presumably highly magnetized, which is in difference to protostellar jets.

3.2. Gravitational/inertial effects

Could an external gravitational potential due to a mass asymmetry in the ISM account for a deflection of the jet? From comparison of gravitational to centrifugal forces on the jet,

$$G\frac{\rho_{\rm jet}\Delta M_{\rm ext}}{R_\kappa^2} = \frac{\rho_{\rm jet} v_{\rm jet}^2}{R_\kappa} \tag{2}$$

where $\Delta M_{\rm ext}$ is the external mass asymmetry (corresponding to an external attractor with mass $\Delta M_{\rm ext}$ at a distance R_κ), one calculates a deflection angle for typical jet parameters,

$$\alpha \simeq \tan(\alpha) = \frac{L_{\rm jet}\, v_{\rm jet}^2}{2\,G\,\Delta M_{\rm ext}} = \tag{3}$$
$$= 0.03 \left(\frac{L_{\rm jet}}{10^{17}\,{\rm cm}}\right)\left(\frac{v_{\rm jet}}{300\,{\rm km\,s^{-1}}}\right)^2\left(\frac{\Delta M_{\rm ext}}{10^7\,{\rm M_\odot}}\right)^{-1}$$

Thus, the deflection of the jet by a gravitational potential requires an unreasonably high mass asymmetry in the ISM. Therefore, these large scale gravitational/inertial effects can hardly account for the observed jet deflection.

Another possibility is that the star, or rather the jet source, becomes accelerated itself, while the jet remains in a steady motion. Since a large scale external gravitational potential attracts both star and jet, only internal, i.e. small scale, potential differences may account for a specific acceleration of the star. The most reasonable source for such a potential would be a binary companion (see Sect. 3.1)

3.3. Dynamical pressure of external medium

Suppose that the star-disk-jet system as a whole performs a steady motion. If it then penetrates a large cloud in the ISM, the 'light' jet flow will be deflected due to the dynamical pressure of the cloud, while the 'heavy' star will continue on its path. (Note that this scenario is different from that of a jet source at rest, where the jet bores a funnel through the ISM.)

For a system tangential velocity $v_\star$ and an external medium of constant density $n_{\rm ism}$, the stationary dynamic pressure exerted by the ISM is $P_D = n_{\rm ism} v_\star^2$. The force density is ∇P_D. If we assume that P_D drops on length scales of some jet radii $R_{\rm jet}$, comparison of centrifugal force with dynamical pressure force gives

$$\frac{n_{\rm jet} v_{\rm jet}^2}{R_\kappa} = \frac{n_{\rm ism} v_\star^2}{R_{\rm jet}}. \tag{4}$$

If we again define $\alpha \simeq \tan(\alpha) = 0.5\, L_{\rm jet}/R_\kappa$ as the angle of deflection, we find

$$\alpha \simeq \tan(\alpha) = \frac{1}{2}\frac{L_{\rm jet}}{R_{\rm jet}}\frac{n_{\rm ism}}{n_{\rm jet}}\left(\frac{v_\star}{v_{\rm jet}}\right)^2 = \tag{5}$$
$$= 10^{-3}\left(\frac{L_{\rm jet}/R_{\rm jet}}{20}\right)\left(\frac{n_{\rm ism}/n_{\rm jet}}{1}\right)\left(\frac{v_\star/v_{\rm jet}}{0.01}\right)^2.$$

This value for α is below the observed angles. The maximum deflection angle is observed if we look perpendicular to the motion of the star (but depends on the inclination of the jet axis). The observed deflection angle becomes larger if the jet axis is inclined.

The energy density involved in this stationary process is $m_p n_{\rm ism} v_\star^2$, being released in heating the jet and the ambient medium. The resulting jet luminosity due to this 'braking' process is of the order of

$$L_{\rm rad} \simeq 2 m_p n_{\rm ism} v_\star^3 L_{\rm jet} R_{\rm jet} = \tag{6}$$
$$= 8\,10^{-8} L_\odot \left(\frac{n_{\rm ism}}{10^3{\rm cm^{-3}}}\right)\left(\frac{R_{\rm jet}}{10^{15}{\rm cm}}\right)\left(\frac{L_{\rm jet}}{10^{17}{\rm cm}}\right)\left(\frac{v_\star}{\rm km\,s^{-1}}\right)^3.$$

In terms of the jet kinematic luminosity we calculate

$$\frac{L_{\rm rad}}{L_{\rm kin}} \simeq \frac{n_{\rm ism}}{n_{\rm jet}}\frac{L_{\rm jet}}{R_{\rm jet}}\left(\frac{v_\star}{v_{\rm jet}}\right)^3 \simeq \frac{1}{2}\,\alpha\left(\frac{v_\star}{v_{\rm jet}}\right), \tag{7}$$

which is very small for typical protostellar jet parameters, and therefore hardly observable.

Dynamical pressure of an external medium might however be important if the jet is propagating under the influence of a *stellar wind* from young stars in its vicinity (Mundt, 1997, private communication). This scenario of the protostellar jet environment is likely, since star formation produces groups of young stars.

In order to estimate this effect we have to rewrite Eq. (5), with the wind density $n_{\rm ism} \to n_{\rm wind}$ and velocity of the wind $v_\star \to v_{\rm wind}$. With the estimates $v_{\rm wind} \simeq 0.1 v_{\rm jet}$ and the density contrast $n_{\rm wind}/n_{\rm jet} \simeq 0.1$ we find $\alpha \simeq 0.01$, which is of the order of the observed angles.

3.4. Inclined strong external magnetic field

Without a detailed consideration, we mention another possibility of deflection of jets from their propagation direction. That is by strong external (poloidal) magnetic fields inclined against the jet axis. In a simple picture, this field acts like a wall for the conducting jet plasma (ideal magnetohydrodynamics, frozen in

magnetic field), and, depending on the field strength and on the inclination angle, the jet will tend to flow along this wall. Jet and counter jet are deflected in opposite direction, forming a S-shaped structure (see Fig. 2).

Currents are not considered here (but see Sect. 3.5). Estimation of the involved field and jet kinetic energy shows that a typical protostellar jet will clearly dominate the external field,

$$\frac{\rho_{\rm jet} v_{\rm jet}^2}{B_{\rm ext}^2/4\pi} = 4\,10^3 \left(\frac{n_{\rm jet}}{100{\rm cm}^{-3}}\right)\left(\frac{v_{\rm jet}}{100{\rm km\,s}^{-1}}\right)^2\left(\frac{B_{\rm ext}}{10\,\mu{\rm G}}\right)^{-2}. \quad (8)$$

This process is therefore unlikely for protostellar jet deflection. The 'magnetic wall' consisting of the interstellar magnetic field of typical field strength is too soft in order to deflect the jet motion.

3.5. Lorentz forces

Here we estimate the Lorentz forces between the current carrying jets and an external (interstellar) magnetic field. A net poloidal current along the jet is necessary in order to achieve a high degree of collimation (Heyvaerts & Norman 1989).

Comparison of the centrifugal force due to the curved jet motion and the Lorentz force due to jet current and external magnetic field gives

$$\frac{1}{c}\boldsymbol{j}_{\rm P} \times \boldsymbol{B}_{\rm ext} = \frac{\rho_{\rm jet} v_{\rm jet}^2}{R_\kappa}, \quad (9)$$

where $\boldsymbol{j}_{\rm P}$ is the poloidal current density and $\boldsymbol{B}_{\rm ext}$ the poloidal component of the external magnetic field (see Fig. 2). Integrating over the jet diameter, only the *poloidal* external magnetic field component which is *perpendicular* to the jet axis, $B_{\rm ext}\sin\delta$, gives a net Lorentz force perpendicular to the jet axis (with the angle δ between the jet and the poloidal field). The toroidal part of the external field does not contribute to the bending of the jet as a whole, it rather pinches and collimates the jet structure itself. The jet magnetic field $\boldsymbol{B}_{\rm jet}$ is responsible for the internal jet structure, i.e. the collimation and acceleration of the jet, and cannot bend the jet.

In Eq. (9), it was assumed that the external field is *homogeneous* on a large scale, at least on the scale of the jet length. Otherwise the bending effect will vary along the jet axis.

In particular, it was assumed that the external field is present also *within* the jet, after all in Eq. (9) $\boldsymbol{j}_{\rm P}$ and $\boldsymbol{B}_{\rm ext}$ have to be measured at the same physical position. This is a critical point if we consider highly conductive jets, where the jet plasma, as it flows along the jet, may potentially sweep any external field out of the jet funnel. In this case the Lorentz force in Eq. (9) would vanish and the problem is similar to that of Sect. 3.4.

From Eq. (9), it is straightforward to find an expression for small deflection angles,

$$\alpha \simeq \tan(\alpha) = \frac{I_{\rm jet} B_{\rm ext}\sin\delta}{c}\,\frac{L_{\rm jet}}{2\pi m n_{\rm jet} R_{\rm jet}^2 v_{\rm jet}^2} \quad (10)$$

with the jet particle density $n_{\rm jet}$, the jet radius $R_{\rm jet}$, the jet velocity $v_{\rm jet}$, and the particle mass m (in the following $m \sim 10^{-24}$ g). With typical jet parameters (see Camenzind 1990; Fendt et al. 1995) we find

$$\alpha \simeq 0.018\sin\delta \left(\frac{I_{\rm jet}}{10^{11}\,{\rm A}}\right)\left(\frac{B_{\rm ext}}{10\,\mu{\rm G}}\right)\left(\frac{L_{\rm jet}}{10^{17}\,{\rm cm}}\right) \left(\frac{R_{\rm jet}}{10^{15}\,{\rm cm}}\right)^{-2}\left(\frac{n_{\rm jet}}{100\,{\rm cm}^{-3}}\right)^{-1}\left(\frac{v_{\rm jet}}{300\,{\rm km\,s}^{-1}}\right)^{-2}, \quad (11)$$

which is of the order of the observed values ($1-2^\circ$),

We see from Eq. (10) that the deflection angle is rather sensitive to the jet parameters. The question arises, why only small deviations from the intrinsic direction of propagation have been observed? We suspect that a hypothetical larger deflection will just destroy the jet as such. Furthermore, it is not that plausible to change all the protostellar jet parameters in the brackets with a positive exponent in Eq. (11) by, say, an order of magnitude. Thus, Lorentz bending may change the direction of jet propagation only slightly.

However, considering the possibility of sweeping the external magnetic field out of the jet funnel (see above), the magnetic field in Eq. (11) may be strongly over-estimated concerning its strength *inside* the jet. In this case the deflection due to Lorentz forces would be much weaker. In turn, one may conclude that only jets with finite conductivity could be deflected.

The direction of the jet deflection is determined by the direction of the poloidal current, if we assume that the external field remains constant along the whole jet/counter jet structure (see Fig. 2). We expect an S-shape structure of the jets, if the poloidal current flows in opposite direction in the jet and counter jet. Similar shapes were observed (see discussion in Eislöffel & Mundt 1997). Alternatively, in a C-shaped jet/counter jet topology the poloidal current would flow in the same direction in both the jet and counter jet (see below). This scenario would be appropriate for e.g. the HH 212 jets, where jet and counter jet are deflected in the same (western) direction (Zinnecker et al. 1996).

In order to explain both types of jet bending, one may hypothesize that the physical parameters of the accretion disk play a role for the closure of the current system. In the case of the S-shaped topology the jet current system closes via the bow shock and the ISM to a *highly conductive* accretion disk (and possibly continues to the star), and the same holds for the counter-jet current. In the case of a C-shaped topology the jet current closes from the bow shock via the ISM to the counter jet, and does not penetrate the *weakly conductive* accretion disk. The difference in the disk conductivity could be caused by a different temperature, accretion rate, different composition of the disk material. These differences may develop at various stages during the lifetime of the accretion disk.

4. Conclusions

In this paper we have discussed several possible mechanisms providing a deflection of protostellar jets from their original direction of propagation.

Among these physical mechanisms, *gravitational* attraction of a mass external to the star-jet system, *inertial* effects of the jet

source and jet in an ambient medium, and an *inclined magnetic field* are probably irrelevant for the observed jet deflection of several degrees.

Dynamical pressure of the ambient medium on the jet cannot be ruled out, but requires lower jet velocities and a higher density contrast between jet and ambient medium than observed.

We find two physical processes, which are possible reasons for jet deflection. These are (1) the action of Lorentz forces between the jet and interstellar magnetic field, and (2) orbital motion of the jet source in a binary (or multiple) system. Mechanism (1) requires a net electric current flow in the jet, a realistic possibility in the case of a highly collimated jet. The conductivity of the accretion disk might play a role concerning the closure of the current system and the shape of jet / counter jet systems (S-shape vs. C-shaped). However, depending on how the interstellar magnetic field is distributed *within* the jet, the magnitude of jet bending due to Lorentz forces remains uncertain. Mechanism (2) requires a certain interrelation between the kinematic parameters of the jet and binary components. Otherwise the bending is too small (for high jet speeds or large binary separation). For typical jet speeds of $300\,\mathrm{km\,s^{-1}}$ the binary separation must be of the order of $\simeq 100$AU in order to obtain a jet deflection angle of several degrees. This is, indeed, what is observed as a typical separation in pre-main sequence binaries.

Although all processes discussed above imply non-axisymmetry of the jet source - jet system on large scale, we emphasize that the jet formation itself always requires an intrinsically axisymmetric topology. A high degree of non-axisymmetry would disrupt the jet. This might be the reason why protostellar jets show only small deflection angles.

Acknowledgements. We thank R. Mundt for discussions and valuable comments on the draft of this paper. Parts of Sect. 3.5. benefited from remarks of the referee F.H. Shu, for which we are grateful.

References

Burrows C.J., et al., 1996, ApJ, 473, 437
Camenzind M., 1990, in: G. Klare (ed.) Reviews of Modern Astronomy 3, Springer-Verlag (Heidelberg), p.234
Camenzind M., 1997, In: B. Reipurth and C. Bertout (eds.), Proc. IAU Symp. 182, Herbig-Haro flows and the birth of low mass stars, p.241
Duquennoy A., Mayor M., 1991, A&A, 248, 485
Eilek J.A., Burns J.O., O'Dea C.P., Owen F.N., 1984, ApJ, 278, 37
Eislöffel J., Mundt R., 1997, AJ, 114, 280
Fendt C., Camenzind M., Appl S., 1995, A&A, 300, 791
Fendt C., Camenzind M., 1996, A&A, 312, 591
Gredel R., Reipurth B., 1993, ApJ, 407, L29
Herbst T.M., Beckwith S.V.W., Glindemann A. et al., 1996, AJ, 111, 2403
Heyvaerts J., Norman C.A., 1989, ApJ, 347, 1055
Hirth G., Mundt R., Solf J., 1997, A&AS, in press
Köhler R., Leinert C., 1997, A&A, submitted
López R., Raga A., Riera A., Anglada G., Estalella R., 1995, MNRAS, 274, 19L
Margon B., Anderson S.F., 1989, ApJ, 347, 448
Mathieu R.D., 1994, ARA&A, 32, 465
Mundt R., Brugel E.W., Bührke T., 1987, ApJ, 319, 275
Mundt R., Ray T.P., Bührke T., Raga A.C., Solf J., 1990, A&A, 232, 37
Mundt R., Ray T.P., Raga A.C., 1991, A&A, 252,740
Pudritz R.E., Norman C.A., 1986, ApJ, 301, 571
Ray T.P., Muxlow T.W.B., Axon D.J. et al., 1997, Nature, 385, 415
Reipurth B., 1989, A&A, 220, 249
Reipurth B., Zinnecker H., 1993, A&A, 278, 81
Shu F.H., Najita J., Wilkin F., Ruden S.P., Lizano S., 1994, ApJ, 429, 781
Zinnecker H., McCaughrean M., Rayner, J., 1996. In: Beckwith S., Staude J., Quetz A. & Natta A. (eds.), Proc., Disks and Outlows around Young Stars, Lecture Notes in Physics 465, Heidelberg, Springer, p.236
Zinnecker H., McCaughrean M., Rayner J., 1997. In: Malbet F. and Castets A. (eds.), Proc. IAU Symp. 182, Low Mass Star Formation – from Infall to Outflow, p.182
Zinnecker H., Brandner W., 1997. In: Docobo et al. (eds.) Visual Double Stars: Formation, Dynamics and Evolutionary Tracks, Conf. Proc. Santiago de Compostella, Spain, in press

A&A 385, 1089–1094 (2002)
DOI: 10.1051/0004-6361:20020196

Astronomy & Astrophysics

Theoretical thermal X-ray spectra of relativistic MHD jets

E. Memola[1,⋆], Ch. Fendt[1,2], and W. Brinkmann[3]

[1] Astrophysikalisches Institut Potsdam, An der Sternwarte 16, 14482 Potsdam, Germany
e-mail: ememola@aip.de, cfendt@aip.de
[2] Universität Potsdam, Institut für Physik, Am Neuen Palais 10, 14469 Potsdam, Germany
[3] Centre for Interdisciplinary Plasma Science, Max-Planck-Institut für extraterrestrische Physik, Giessenbachstrasse, 85740 Garching, Germany
e-mail: wpb@mpe.mpg.de

Received 18 December 2001 / Accepted 4 February 2002

Abstract. Highly relativistic jets are most probably driven by strong magnetic fields and launched from the accretion disk surrounding a central black hole. Applying the jet flow parameters (velocity, density, temperature) calculated from the magnetohydrodynamic (MHD) equations, we derive the thermal X-ray luminosity along the inner jet flow in the energy range 0.2−10.1 keV. Here, we concentrate on the case of Galactic microquasars emitting highly relativistic jets. For a $5\,M_\odot$ central object and a jet mass flow rate of $\dot{M}_\mathrm{j} = 10^{-8}\,M_\odot\,\mathrm{yr}^{-1}$ we obtain a jet X-ray luminosity $L_\mathrm{X} \approx 10^{33}\,\mathrm{erg\,s}^{-1}$. Emission lines of Fe XXV and Fe XXVI are clearly visible. Relativistic effects such as Doppler shift and boosting were considered for different inclinations of the jet axis. Due to the chosen geometry of the MHD jet the inner X-ray emitting part is not yet collimated. Therefore, depending on the viewing angle, the Doppler boosting does not play a major role in the total spectra.

Key words. MHD – radiation mechanisms: thermal – X-rays: binaries – ISM: jets and outflows

1. Introduction

Microquasars (Mirabel & Rodríguez 1999) are Galactic X-ray binaries where the three basic ingredients of quasars are found – a central black hole, an accretion disk and relativistic jets. Jets are thought to be driven by magnetohydrodynamic (MHD) mechanisms (Blandford & Payne 1982; Camenzind 1986) triggered by the interaction of those three components, although the jet formation process is not yet fully understood (e.g. Fendt 1997). Some microquasars are superluminal sources, e.g. GRS 1915+105 at a distance of 7−12 kpc (Fender et al. 1999) with a central mass of about $14\,M_\odot$ (Greiner et al. 2001).

Fendt & Greiner (2001, FG01) presented solutions of the MHD *wind equation* in Kerr metric with particular application to microquasars. These solutions provide the flow dynamics along a prescribed poloidal magnetic field line. FG01 found temperatures up to more than 10^{10} K in the innermost part of the jet proposing that thermal X-rays might be emitted from this region. Here, we calculate the thermal spectrum of such an optically thin jet flow taking into account one of the solutions of FG01 and considering relativistic Doppler shifting and boosting as well as different inclinations of the jet axis to the line-of-sight (l.o.s.). A similar approach was undertaken by Brinkmann & Kawai (2000, BK00) who have been modeling the two dimensional hydrodynamic outflow of SS 433 applying various initial conditions. However, they do not consider relativistic effects such as Doppler boosting in their spectra.

Send offprint requests to: E. Memola,
e-mail: memola@asdc.asi.it

⋆ Current address: Italian Space Agency - Science Data Center, c/o ESA-ESRIN, via Galileo Galilei, 00044 Frascati, Italy.

2. The model

The axisymmetric, stationary and ideal MHD wind solution provides the density, velocity and temperature for each volume element along the field. Prescribing the jet mass flow rate $\dot{M}_\mathrm{j}$ together with the shape of the field line, these solutions give a unique set of parameters of the flow defined by the regularity condition across the magnetosonic points (see FG01 for details).

The calculated dynamical parameters are our starting point to obtain the X-ray spectra of the jet. Here, we refer to the solution S3 of FG01 obtained for a collimating field line $z(x) = 0.1(x - x_0)^{6/5}$, x being the normalized cylindrical radius, x_0 the foot point of the field line at the equatorial plane, and z the height above the disk. Length scales are normalized to the gravitational radius $r_\mathrm{g} = 7.4 \times 10^5\,\mathrm{cm}\ (M/5\,M_\odot)$. For completeness, we show the radial profiles of poloidal velocity, density, temperature, and emitting volume along the field line in Fig. 1.

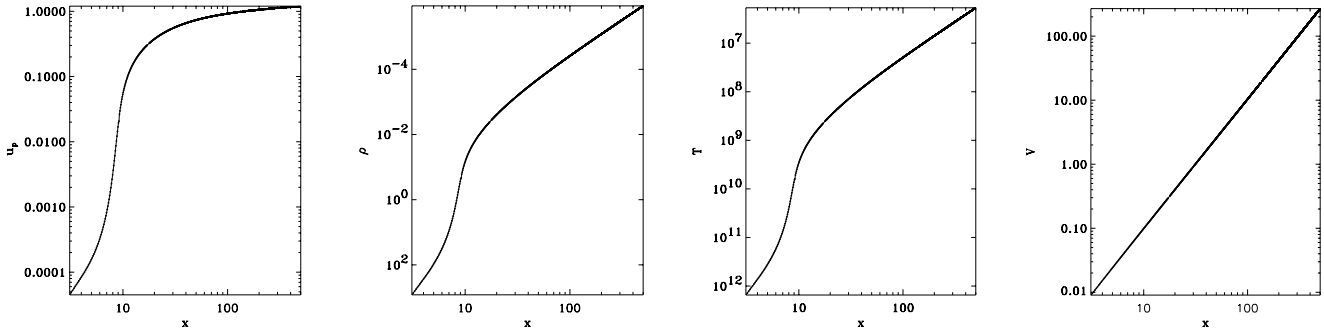

Fig. 1. Dynamical parameters of the MHD jet (see FG01). Shown is the radial dependence of the properly normalized poloidal velocities $u_{\rm p}(x) = \gamma v_{\rm p}/c$, particle densities $\rho(x)$, temperatures $T(x)$ (in K), and size of the emitting volumes $V(x)$ (from *left* to *right*) along the chosen magnetic field line. For the calculations in this paper we apply a central mass of $5\,M_\odot$ and a jet mass flow rate of $\dot{M}_{\rm jet} = 10^{-10}\,M_\odot\,{\rm yr}^{-1}$. The units are therefore $r_{\rm g} = 7.4 \times 10^5\,{\rm cm}$ for all length scales, $r_{\rm g}^3 = 4.1 \times 10^{17}\,{\rm cm}^3$ for the volumes, and $4.31 \times 10^{16}\,{\rm cm}^{-3}$ for the particle densities. Note that the jet injection point is located at $R_{\rm i} = 8.3\,r_{\rm g}$ with a gas temperature of $T_{\rm i} = 10^{10.2}\,{\rm K}$. In this solution for the MHD wind equation, the poloidal velocity saturates to a value of $u_{\rm p} = 2.5$ beyond $x \simeq 10^8$. The flow is weakly collimated reaching a half opening angle of 70° at about $x = 250$.

The jet geometry consists of nested collimating conical magnetic surfaces with sheets of matter accelerating along each surface. The sheet cross section becomes larger for larger distances from the origin. The distribution of the 5000 volume elements along the jet is such that velocity and density gradients are small within the volume. We have 63 volumes in ϕ direction defining an axisymmetric torus (i.e. 5000 tori along the magnetic surface).

We distinguish two parts of the inner jet flow. One is for a temperature range $T = 10^{6.6}$–$10^9\,{\rm K}$, where we calculate the optically thin continuum (bremsstrahlung) and the emission lines. The other is for $T = 10^9$–$10^{12}\,{\rm K}$, where only bremsstrahlung is important. Any pair processes are neglected and no (e^-e^-)-bremsstrahlung will be considered, although that might be dominant at the highest temperatures. Such unphysically high temperatures are to a certain degree caused by the use of a non-relativistic equation of state. Employing a relativistically correct equation of state (Synge 1957) one would expect gas temperatures an order of magnitude lower (Brinkmann 1980). These temperatures belong to the intermediate region between disk and jet. The injection radius,which is, in fact, the boundary condition for the jet flow, is located at $R_{\rm i} = 8.3\,r_{\rm g}$ and at a height above the disk (and the foot point of the field line) of $0.74\,r_{\rm g}$. For the chosen MHD solution the temperature at this point is $T_{\rm i} = 10^{10.2}\,{\rm K}$. With $R_{\rm i} \simeq 6 \times 10^6\,{\rm cm}\ (M/5\,M_\odot)$ we investigate a region of about $2.5 \times 10^{-5}\ (M/5\,M_\odot)\,{\rm AU}$.

Having determined the emissivities of single volume elements, these can be put together obtaining a rest-frame spectrum where any motion is neglected. However, the knowledge of the MHD wind velocities allows us to determine the Doppler shift of the spectral energies and the boosting of the luminosity for each volume. We finally obtain a total spectrum of the inner jet considering these effects in a *differential* way for each volume element. The final spectra of course depend also from the jet inclination.

We emphasize that our approach is not (yet) a *fit* to certain observed spectra. In contrary, for the first time, for a jet flow with characteristics defined by the solution of the MHD wind equation, we derive its X-ray spectrum. Our free parameters are the mass of the central object M defining the length scales, the jet mass flow rate $\dot{M}_{\rm j}$ and the shape of the poloidal field lines. In the end, from the comparison of the theoretical spectra with observations, we expect to get information about the internal magnetic structure of the jet close to the black hole and the jet mass flow rate.

3. X-ray spectra in the rest frame of the volumes

The computation of the continuum spectrum and the emission lines of an optically thin plasma takes into account free-free, free-bound and two-photon processes (Mewe et al. 1985; Kotani et al. 1996; BK00). Cosmic abundances given by Allen (1973) are used for a plasma in equilibrium at the local temperature.

3.1. Luminosities of the fast flow ($T = 10^{6.2}$–10^9 K)

Considering the size, density and temperature of each volume, the luminosities ($\rm erg\,s^{-1}(0.1\,keV)^{-1}$) of the jet-tori have been calculated in the energy range 0.2–10.1 keV (bin size 0.1 keV). Examples are shown for four temperatures in Fig. 2 (see also Table 1). With the increase of the temperature the luminosity range is compressed, therefore those spectra are flatter and the strong cutoff seen for lower temperatures disappears. The luminosity of hot gas volume elements ($T \simeq 10^9\,{\rm K}$), located above the injection point, is higher (factor 100) than the one of the cooler, but faster volume elements. Note that the luminosities shown in Fig. 2 are calculated for $\dot{M}_{\rm j} = 10^{-10}\,M_\odot\,{\rm yr}^{-1}$. This quantity is hardly known from observations and, in turn, the calculated luminosities may constrain its value. A mass flow rate 100 times higher increases the luminosity by a factor of 10^4, for the same magnetic field geometry.

For temperatures $T = 10^6$–$10^9\,{\rm K}$ many emission lines are present in the energy range 0.2–10.1 keV (Mewe et al. 1985). The 0.5–0.9 keV band contains O, N, Fe, Ne, S, Ca lines whereas lines of Ne, Fe, Mg, Ni, Si, S, Ar, Ca

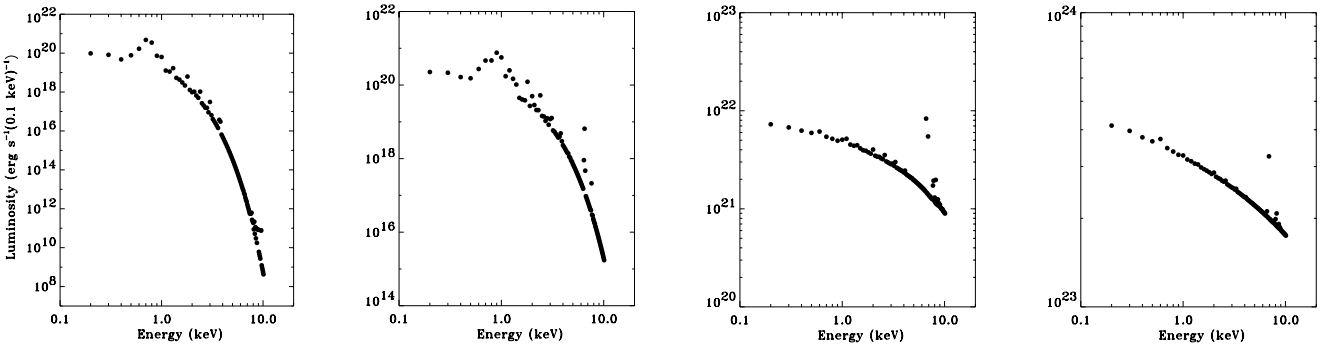

Fig. 2. X-ray luminosities of jet-tori of 63 volume elements with different temperatures: $T = 10^{6.64}$ K, $T = 10^7$ K, $T = 10^8$ K, $T = 10^9$ K (from *left* to *right*). The jet mass flow rate considered here is $\dot{M}_\mathrm{j} = 10^{-10}\,M_\odot\,\mathrm{yr}^{-1}$ for a $5\,M_\odot$ central object.

are found between 1.0−4.0 keV. From 6.6−7.0 keV mostly FeXXV (He-like) and FeXXVI (H-like) emission lines are present (BK00). For fully ionized plasma of $T \geq 10^9$ K the bremsstrahlung continuum emission is dominant.

The total rest-frame spectrum (neglecting the velocity of the volumes) of a conical sheet of the jet is the integrated luminosity of the single volumes along the field, taking into account also the number of volumes along the jet-tori (Fig. 3c). The emission lines at 6.6 and 6.9 keV can be identified as $K\alpha$ lines from He-like and H-like iron, while the one at 8.2 keV could be the $K\beta$ from the He-like iron.

3.2. The hot flow close to the disk ($T \geq 10^9$ K)

The thermal continuum of an optically thin fully ionized plasma follows from the formula of bremsstrahlung emission (Rybicki & Lightman 1979),

$$\varepsilon_\nu \equiv \frac{\mathrm{d}W}{\mathrm{d}V\mathrm{d}t\;\mathrm{d}\nu} = 6.8\times10^{-38}Z^2 n_\mathrm{e} n_\mathrm{i} T^{-1/2}\mathrm{e}^{-h\nu/kT}\bar{g}, \quad (1)$$

(in erg s^{-1} cm^{-3} Hz^{-1}), with the velocity averaged Gaunt factor $\bar{g}(T,\nu)$[1], the atomic number Z, the electron and ion number densities n_e and n_i, the Planck constant h and the Boltzmann constant k. Considering the calculated volume parameters for temperatures below 10^9 K, we obtain a bremsstrahlung luminosity L_br comparable to the results in Fig. 2 as expected, in fact, since bremsstrahlung is included in that calculation. Still considering $\dot{M}_\mathrm{j} = 10^{-10}\,M_\odot\,\mathrm{yr}^{-1}$, for $T \simeq 10^{10}$ K we obtain $L_\mathrm{br} \approx 10^{25}\,\mathrm{erg\,s^{-1}}(0.1\,\mathrm{keV})^{-1}$, for $T \simeq 10^{11}$ K we obtain $L_\mathrm{br} \approx 10^{27}\,\mathrm{erg\,s^{-1}}(0.1\,\mathrm{keV})^{-1}$, and when $T \simeq 10^{12}$ K the luminosity is $L_\mathrm{br} \approx 10^{30}\,\mathrm{erg\,s^{-1}}(0.1\,\mathrm{keV})^{-1}$. Therefore, we expect an increase of the X-ray luminosity due to the bremsstrahlung contribution of the hottest regions in the jet-disk system, if the optically thin condition is still satisfied there.

[1] For simplicity, the estimates in this subsection are obtained for a Gaunt factor set to unity. For the spectra shown in our paper this factor differs slightly from volume to volume.

4. Relativistic effects – Doppler shift and boosting

We now consider relativistic Doppler effects due to the motion of the jet volumes toward the observer. The relativistic Doppler factor is $D = (\gamma(1-\beta\cos\theta))^{-1}$, where γ is the Lorentz factor, β the plasma velocity in units of the speed of light and θ the angle between the trajectory of the volume and the l.o.s. The observed energies E_o and luminosities L_o of *each* volume element are shifted and boosted to the rest frame values (index e),

$$E_\mathrm{o} = D\,E_\mathrm{e} \quad \text{and} \quad L_\mathrm{o}(E_\mathrm{o}) = D^3\,L_\mathrm{e}(E_\mathrm{e}). \quad (2)$$

Note that the Doppler factor depends on both γ and θ (see also Urry & Padovani 1995) and is unity for $\theta = \arccos\left(\sqrt{(\gamma-1)/(\gamma+1)}\right)$. For larger angles, relativistic *de-amplification* takes place due to the time lapse in the moving frame of reference. This is the reason for $D < 1$ in our jet (Table 1). Also known as second order Doppler effect, this was first observed in SS 433 (Margon 1984). De-boosting is also present in the asymptotic radio jets (different from the collimation region investigated here) of GRS 1915+105 inclined by 70° to the l.o.s., actually providing a distance indicator (Mirabel & Rodríguez 1994).

4.1. Shifted and boosted spectra

Figures 3a,b show the effect of boosting and shifting of the rest frame spectra. For an angle between the l.o.s. and the jet axis of 40°, the maximum boosting $D^3 = D^3_{-40} = 6.7$ is obtained for the volume with $T = 10^{6.64}$ K (see also Table 1). The maximum de-boosting is for the volume at the opposite side of the cone, $D^3_{+40} = 0.15$. As in the rest frame, the "hot" spectra are flatter.

To obtain a total shifted and boosted spectrum we need to interpolate the single volume luminosity values since they are shifted to different energies. Considering the case where the jet axis is along the l.o.s. ($\theta_\parallel$, see Fig. 3c), we have only a weak effect of shifting, in fact, we are looking almost perpendicular to an uncollimated flow. For a larger jet inclination the Doppler effects become larger. In this case, one should take into account the fact that the angle between the velocity and the l.o.s. ($\theta_\parallel$) varies along the jet-torus. However, we have considered it reasonable

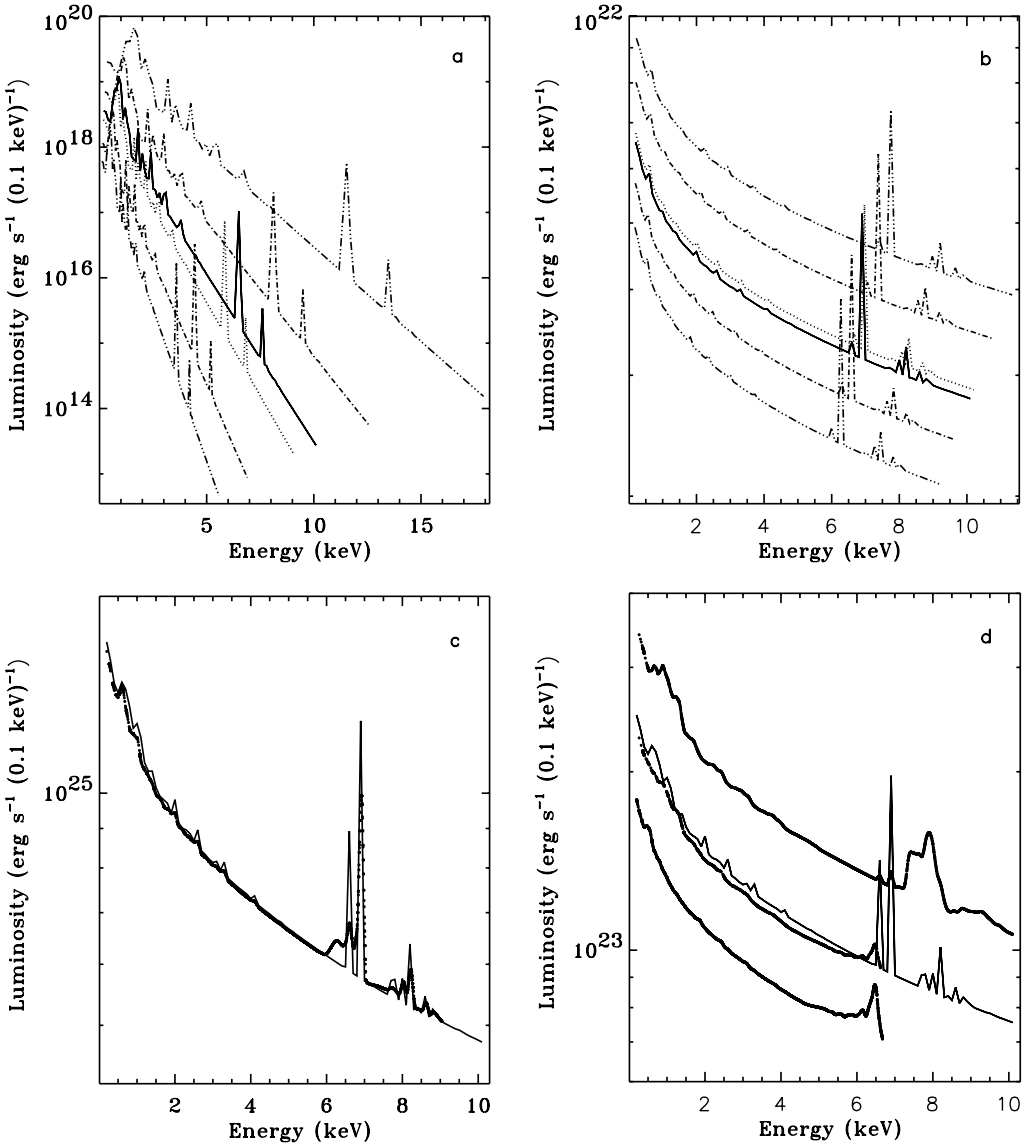

Fig. 3. Doppler shifted and boosted spectra. Spectra for a volume element with $T = 10^7$ K **a)** and $T = 10^9$ K **b)** for different jet inclinations. Doppler factor D_{-40} (triple dotted-dashed line, *top*), D_{-20} (dotted-dashed line, *top*), rest-frame (solid line), $D_{\|}$ (dotted line), D_{+20} (dotted-dashed line, *bottom*), D_{+40} (triple dotted-dashed line, *bottom*). **c)** Comparison of the total shifted/boosted spectrum $D_{\|}$ (thick dotted line) of a conical sheet with the rest-frame spectrum (thin solid line). **d)** Inclined jet, comparison of the boosted spectra D_{-20} (thick line *top*) and D_{+20} (thick line *bottom*) with the total spectrum (thick line *middle*) and the rest-frame spectrum (thin line *middle*).

to divide the jet-tori in two regions, one third containing volume elements for which the Doppler effect has been calculated using the minimum angle between the plasma velocity and the l.o.s., and two thirds containing volume elements for which the Doppler effect has been calculated using the maximum angle between the plasma velocity and the l.o.s.

The total spectra have been calculated by first considering the blue-shifted and red-shifted parts of the flow and then summing up all the luminosities in each energy bin, where blue *and* red shifted luminosities are available. The result is shown in Fig. 3d with the luminosity rescaled in order to compare the total spectrum with its components.

Note that the iron line features are considerably shifted also after the interpolation. The change in the line shape is due to the fact that for each of the 5000 volumes along the jet a different Doppler factor must be considered. For a larger jet inclination (D_{-40} , D_{+40}) the lines are spread out widely because of the larger Doppler shift (not shown). The de-boosting contribution of the receding counter-jet has not been taken into account.

5. Discussion

5.1. X-ray luminosities

We find a total rest-frame X-ray luminosity of the jet $L_{\rm X} = 3.8 \times 10^{31}\ (\dot{M}_{\rm j}/10^{-8}\,M_\odot\,{\rm yr}^{-1})\,{\rm erg\,s}^{-1}$. The total kinematic luminosity for this jet mass flow rate is $L_{\rm k} = \gamma\dot{M}_{\rm j}c^2 \approx 10^{39}\,{\rm erg\,s}^{-1} \gg L_{\rm X}$. This proves a posteriori that the assumption of a polytropic gas law used to obtain the

Table 1. Dynamical parameters for four example volume elements. Quoted are temperature T, mass M, particle density ρ and the Lorentz factor γ. The angle $\theta_\parallel$ is the angle between the plasma velocity and the l.o.s., *if* the l.o.s. is parallel to the jet axis. The corresponding Doppler factor is $D_\parallel$. If the l.o.s. is inclined 20° to the jet axis, the minimum (maximum) angle between the plasma velocity and the l.o.s. is $\theta_\parallel - 20°$ ($\theta_\parallel + 20°$) with a corresponding Doppler factor D_{-20} (D_{+20}) and similarly for an inclination of 40°.

T (K)	10^9	10^8	10^7	$10^{6.64}$
M (gr)	7×10^7	2×10^7	1.1×10^7	0.97×10^7
ρ (cm^{-3})	6×10^{13}	2×10^{12}	6×10^{11}	2×10^{11}
γ	1.014	1.179	1.428	1.494
$\theta_\parallel$ (°)	82	77	72	70
$D_\parallel$	1.010	0.960	0.898	0.899
D_{-20}	1.07	1.19	1.25	1.28
D_{+20}	0.96	0.79	0.68	0.67
D_{-40}	1.12	1.47	1.77	1.88
D_{+40}	0.91	0.68	0.55	0.53

MHD wind solution is consistent with the amount of radiation losses.

Considering the Doppler factor $D_\parallel$, the total X-ray luminosity of the jet is $L_\mathrm{X} = 6.4 \times 10^{32}\ (\dot{M}_\mathrm{j}/10^{-8}\,M_\odot\,\mathrm{yr}^{-1})\,\mathrm{erg\,s}^{-1}$. In the case of an inclined jet axis (D_{-20}, D_{+20}) we have $L_\mathrm{X} = 1.4 \times 10^{33}\ (\dot{M}_\mathrm{j}/10^{-8}\,M_\odot\,\mathrm{yr}^{-1})\,\mathrm{erg\,s}^{-1}$. For D_{-40} and D_{+40} we obtain $L_\mathrm{X} = 1.1 \times 10^{33}\ (\dot{M}_\mathrm{j}/10^{-8}\,M_\odot\,\mathrm{yr}^{-1})\,\mathrm{erg\,s}^{-1}$. These values can be increased by the contribution of bremsstrahlung from the high temperature ($T \geq 10^9\,\mathrm{K}$) volumes till about $L_\mathrm{X} \approx 10^{34}\,\mathrm{erg\,s}^{-1}$.

In comparison, the X-ray luminosity of GRS 1915+105 is $10^{38}\,\mathrm{erg\,s}^{-1}$ in low-state and $10^{39}\,\mathrm{erg\,s}^{-1}$ in high-state (Greiner et al. 1996), and larger than the one we obtain. Such a luminosity might be obtained from the jet for an increased mass flow rate. The jet inclination of 70° implies a maximum boosting of about 20 for some volumes. Further, also the accretion disk contributes to the X-ray flux. In SS433 we have $L_\mathrm{X} > 10^{35}\,\mathrm{erg\,s}^{-1}$ (Brinkmann et al. 1996) but no broad Fe-lines are observed. This might be either due to a very low mass flow rate (low jet luminosity) or to a very high mass flow rate (self-absorption of the emission lines).

Higher jet velocities ($\gamma > 2$) may increase the Doppler boosting. Such velocities can be easily obtained for a higher flow magnetization, i.e. for a stronger magnetic field strength or a lower jet mass flow rate (see FG01; Fendt & Camenzind 1996). However, for the same mass flow rate, a higher velocity implies a lower gas density, which may lead, instead, to a decrease of the luminosity. The interplay of these effects is rather complex. The *rest frame* emissivity depends on the density as $\sim\rho^2$ and is also proportional to the emitting volume. The maximum *Doppler boosting* increases with the Lorentz factor, $D^3(\cos\theta = 1) \simeq (2\gamma^2\,(1 + \sqrt{1-\gamma^{-2}}))^{3/2}$, whereas the real boosting parameter also depends on the inclination of the velocity vector to the l.o.s. Answering the question how these effects determine the observed X-ray luminosity, would require a detailed study of various MHD wind solutions and their derived spectra investigating different magnetic field geometries (degree of collimation), jet mass flow rates (the flow magnetization), and also possible masses of the central black hole. We will return to this important point in a future paper.

Markoff et al. (2001) have recently shown (for XTE J1118+480) that synchrotron emission from the jet may play a role also in the X-ray band. Their model differs from ours in some respects, especially the initial jet acceleration is not treated and the jet nozzle geometry is more concentrated along the axis with a jet radius of only 10 Schwarzschild radii (in our model the jet is much wider and collimates later). As a consequence, the densities become higher and it is questionable whether a more reasonable jet geometry will deliver the same amount of X-ray flux.

5.2. Jet plasma composition

At this point we should note that the fundamental question of the plasma composition in relativistic jets has not yet been answered. In the case of microquasars we do not really know whether the jet consists of a e^-p^+ or a e^-e^+ plasma (see e.g. Fender et al. 2000). It could be possible that these jets are "light" jets, i.e. made of a pair plasma only, and we would not expect to observe an iron line emission from such jets. Instead, the iron line emission would then arise from processes connected to the accretion disk or an accretion column. Such models were discussed for example in the case of XTE J1748−288 (Kotani et al. 2000; Miller et al. 2001).

On the other hand, the theoretical spectra derived in our paper provide an additional information needed in order to interpret the observed emission lines. A deeper understanding will, however, require a more detailed investigation of different jet geometries, viewing angles and mass flow rates. In the end, this might answer the question whether the line emission, or at least part of it, comes from the highly relativistic jet motion or from a rapidly rotating (i.e. also relativistic) accretion disk. For example, we expect the emission lines of a collimated jet being narrower, and probably shifted by a larger Doppler factor, due to the strong beaming. One should also keep in mind that the direction of motion of the jet material is inclined (if not perpendicular) to the disk rotation.

Evidently, if the observations would tell us that the Doppler shifted Fe lines which are visible in our theoretical spectra arise in the jet material, this would also prove the existence of a baryonic component in these jets.

Nevertheless, observations in the radio and shorter wavelengths give clear indication for synchrotron emission from highly relativistic electrons. Whether this non thermal particle population contributes to all of the observed emission is not clear, a hot thermal plasma may also exist besides the non thermal electrons.

A similar discussion concerning the plasma composition is present in the context of extragalactic jets (e.g. Mukherjee et al. 1997). The non thermal emission from blazars can be explained by inverse Compton scattering of low-energy photons by the relativistic electrons in the jet. However, two main issues remain unsolved: the source of the soft photons that are inverse Compton scattered, and the structure of the inner jet, which cannot be imaged directly. The soft photons can originate as synchrotron emission either within the jet (see e.g. Bloom & Marscher 1996) or nearby the accretion disk, or they can be disk radiation reprocessed in broad emission line clouds (see e.g. Ghisellini & Madau 1996). In contrast to these leptonic jet models, the proton-initiated cascade model (see e.g. Mannheim & Biermann 1989) predicts that the high-energy emission comes from knots in jets as a consequence of diffusive shock acceleration of protons to energies so high that the threshold of secondary particle production is exceeded.

Comparison of our calculated Fe emission lines to the observed ones potentially give some hints on the plasma composition ($e^- p^+$ or $e^- e^+$) in relativistic jets.

6. Summary

For the first time, theoretical thermal X-ray spectra were obtained for the dynamical parameters of a relativistic jet calculated from the MHD wind equation. The total spectra were derived as composition of the spectral contributions of the single volume elements accelerating along the jet with relativistic speed. Our results are the following.

1. We find X-ray emission from the hot inner part of the jet originating in a region of 2.5×10^{-5} AU diameter close to the center of a $5\,M_\odot$ jet source. The jet X-ray luminosity is $L_{\rm X} \sim 10^{33}\ (\dot{M}_{\rm j}/10^{-8}\,M_\odot\,{\rm yr}^{-1})\,{\rm erg\,s}^{-1}$.
2. Emission lines of Fe XXV and Fe XXVI are clearly visible in our spectra. Interestingly, the $K\alpha$ iron emission line has been probably observed in GRS 1915+105 (Ebisawa et al. 1998) and XTE J1748–288 (Kotani et al. 2000). The absence of broad Fe-lines in the spectrum of SS433 might tell us something on the "invisibility" of the acceleration region above the disk. Comparison of our calculated emission lines to observed ones may give some hints on the plasma composition in relativistic jets.
3. From the MHD jet underlying the spectra we find a maximum Doppler boosting of about 7. Minimum boosting is present along the opposite side of the jet cone (Doppler factor 0.53). The shift of the emission lines is always visible. The boosting, however, does not play a major role in the total spectra, because of the uncollimated geometry of the innermost part of the jet emitting the X-rays and the combined effect of boosting and de-boosting around the jet cone.

If jets from X-ray binaries indeed contain matter of baryonic composition, our model will have a broad application. Indication of that is probably given by the observation of iron emisson lines in some sources (see above). However, it is not yet clear, whether the line emission originates in the jet or in the accretion disk. Our calculated Fe emission lines may help to interpret the observed spectra and potentially give some clue on the plasma composition in relativistic jets.

This study will be extended in a future work investigating spectra of jets with different magnetic geometry, mass flow rates and central masses. In the end, this might also allow to constrain the intrinsic parameters of jet formation itself (such as mass loading or opening angle) from the observation of the large-scale, asymptotic jet.

Acknowledgements. This work was partly supported by the German Science Foundation (Deutsche Forschungsgemeinschaft) as project DFG/FE490. We thank an anonymous referee for useful comments.

References

Allen, C. W. 1973, Astrophysical Quantities, 3rd ed. (Athlone Press, University of London)
Blandford, R. D., & Payne, D. G. 1982, MNRAS, 199, 883
Bloom, S. D., & Marscher, A. P. 1996, ApJ, 461, 657
Brinkmann, W. 1980, A&A, 85, 146
Brinkmann, W., Aschenbach, B., & Kawai, N. 1996, A&A, 312, 306
Brinkmann, W., & Kawai, N. 2000, A&A, 363, 640 (BK00)
Camenzind, M. 1986, A&A, 162, 32
Ebisawa, K., Takeshima, T., White, N., et al. 1998, ASCA Observations of the Superluminal Jet Source GRS 1915+105, in The Hot Universe, Proceedings IAU 188, ed. K. Koyama, S. Kitamoto, & M. Itoh (Kluwer, Dordrecht), 392
Fender, R., Garrington, S., McKay, D., et al. 1999, MNRAS, 304, 865
Fender, R., Rayner, D., Norris, R., Sault, R. J., & Pooley, G. 2000, ApJ, 530, L29
Fendt, Ch., & Camenzind, M. 1996, A&A, 313, 591
Fendt, Ch. 1997, A&A, 319, 1025
Fendt, Ch., & Greiner, J. 2001, A&A, 369, 308 (FG01)
Ghisellini, G., & Madau, P. 1996, MNRAS, 280, 67
Greiner, J., Morgan, E. H., & Remillard, R. A. 1996, ApJ, 473, L107
Greiner, J., Cuby, J., & McCaughrean, M. 2001, Nature, 414, 522
Kotani, T., Kawai, N., Matsuoka, M., & Brinkmann, W. 1996, PASJ, 48, 619
Kotani, T., Kawai, N., Nagase, F., et al. 2000, ApJ, 543, L133
Mannheim, K., & Biermann, P. L. 1989, A&A, 221, 211
Margon, B. 1984, ARA&A, 22, 507
Markoff, S., Falcke, H., & Fender, R. 2001, A&A, 372, L25
Mewe, R., Gronenschild, E., & van der Oord, G. 1985, A&AS, 62, 197
Miller, J. M., Fox, D. W., Di Matteo, T., et al. 2001, ApJ, 546, 1055
Mirabel, I. M., & Rodríguez, L. F. 1994, Nature, 371, 46
Mirabel, I. M., & Rodríguez, L. F. 1999, ARA&A, 37, 409
Mukherjee, R., Bertsch, D. L., Bloom. S. D., et al. 1997, ApJ, 490, 116
Rybicki, G., & Lightman, A. 1979, Radiative Processes in Astrophysics (Wiley)
Synge, J. 1957, The Relativistic Gas (North Holland, Amsterdam)
Urry, C. M., & Padovani, P. 1995, PASP, 107, 803